Regulatory factors *gdf6a*, *tbx2b*, and *thr beta* in generation of multiple cone photoreceptor subtypes; and intersections of genetic factors *SOD1*, *TDP43*, and *gdf6a* in zebrafish models of amyotrophic lateral sclerosis

by

Michèle Genevieve DuVal

A thesis submitted in partial fulfillment of the requirements for the degree of

Doctor of Philosophy

in

Physiology, Cell and Developmental Biology

Department of Biological Sciences
University of Alberta

Abstract

The work within this thesis may be divided into two major foci with a unifying theme of understanding neurodegeneration and expanding the foundational knowledge necessary for treatment of two major degenerative diseases: macular degeneration and amyotrophic lateral sclerosis. To these ends the zebrafish served as a genetic, whole organism model of 1) tetrachromatic cone photoreceptor development and 2) of motor neuron pathology. Summaries of these foci are provided below.

First, the development of multiple cone photoreceptors, the specialized neurons required for bright light vision and colour discrimination, is explored. The roles of three genes in the cone subtype development network are interrogated: *gdf6a*, *tbx2b*, and *thrβ*. In this thesis the importance of *gdf6a*, a novel cone gene, toward blue- and red-sensitive cones, and its influence over *tbx2b*'s regulation of UV cones, is dissected using zebrafish mutants. The dynamic role of *thrβ* was elucidated with a combination of gene knock down and a newly-engineered dominant negative disruption model, revealing its developmental stage-dependent influence on promoting red and suppressing UV and blue cones. *Thrβ* and *tbx2b* were discovered to share an epistatic interaction in the development of UV cones, where reduction in *thrβ* expression can partially rescue the low abundance of UV cones in *tbx2b* mutants. Despite the overlapping roles of *gdf6a* and *thrβ* in red cone and opposing roles in blue cone development, their exact relationship in cone development could not be elucidated, however a novel retina lamination phenotype suggests that both factors also influence lamination. These interactions elaborate our understanding of the regulatory networks required to generate three or more types of cone photoreceptor.

Second, the roles of three genes in the pathology of amyotrophic lateral sclerosis are explored through a series of questions, utilizing zebrafish models of motor neuron pathology. *Gdf6a* is investigated as a novel modifier locus for neuromuscular junction maintenance in aging. Loss of *gdf6a* disrupts motor neuron function and neuromuscular junction morphology, and enhances neurodegenerative phenotypes in a genetic model of amyotrophic lateral sclerosis. Subsequent work focussed on novel mutations in the amyotrophic lateral sclerosis-linked gene *SOD1*, including W32S, A89R, and K128N. The relevance of these novel mutations to SOD1 toxicity were tested through cell culture, axonopathy and behavioural assays, and candidate therapeutics that act via the W32 region of SOD1 were evaluated. Finally, the toxic motor neuron phenotype of SOD1 was enhanced by co-expression with another disease-associated gene, *TDP43*. This enhanced toxicity depended on two specific tryptophan residues in TDP43, and was reduced with a candidate therapeutic drug. These findings highlight the genetic complexities of amyotrophic lateral sclerosis, and emphasize the necessity to explore for genetic and pathological intersections within ALS and with other neurodegenerations.

Preface

This thesis is an original work by Michèle G. DuVal, and the work presented was performed under ethics approval from the University of Alberta Animal Policy and Welfare Committee and in compliance with the Canadian Council on Animal Care (CCAC). The author has accomplished the mandatory training for animal users, as directed by the CCAC on the Care and Use of Animals in Research, Training, and Testing.

Published work is presented in accordance with permissions granted by the Creative Commons Attributions (CC BY). The text and figures in this thesis were originally drafted by the author, with the following exceptions: portions of text in Chapters 2 and 4 were originally drafted by W. Ted Allison; portions of text in Chapter 5 were originally drafted by Steven S. Plotkin; contributions to Figures are as follows: Figure 2.1 by W. Ted Allison and Neel Doshi; Figure 2.2 by A. Phil Oel; Figure 2.3 by A. Phil Oel; Figure 2.5 by W. Ted Allison; Figure 2.6 by A. Phil Oel; Figure 4.1 by W. Ted Allison; Figure 4.2 by Matthew Gilbert; Figure 4.3 by Daryn Ezekiel Watson; Figure 4.4 by Matthew Gilbert and Tanja Zerulla; Figure 6.2 by Richard Kanyo; Figure 6.3 by Vijaya Hinge and Nikolay Blinov; Figure 6.4 by Vijaya Hinge and Nikolay Blinov.

Chapter 1 includes content (with some modifications) from the following publications:
1) DuVal MG, Allison WT (2017) Impacts of the Retinal Environment and Photoreceptor Type on Functional Regeneration. Neural Regen Res. 2017 12(3):376-379. doi: 10.4103/16773-5374.202930 (DuVal and Allison, 2017) (manuscript writing was done by both authors); and
2) Allison WT, DuVal MG, Nguyen-Phuoc K, Leighton PLA (2017) Reduced Abundance and Subverted Functions of Proteins in Prion-Like Diseases: Gained Functions Fascinate but Lost Functions Affect Aetiology. Int J Mol Sci. 2017 18(10) pii:E2223. doi: 10.3390.ijms18102223 (Allison et al., 2017). Manuscript writing was performed primarily by WTA with contributions from MGD, KNP, and PLAL.

Chapter 2 comprises the publication of the same title: DuVal MG, Oel AP, Allison WT (2014) *gdf6a* Is Required for Cone Photoreceptor Subtype Differentiation and for the Actions of *tbx2b* in Determining Rod Versus Cone Photoreceptor Fate. PLOS ONE 9(3): e92991. https://doi.org/10.1371/journal.pone.0092991 (DuVal et al., 2014b). The questions, hypotheses, and experiments in this chapter were conceived and designed by

MGD, APO, and WTA. Contributions to experiments are as follows: measuring microphthalmia in *gdf6a* and *tbx2b* mutants by MGD and APO; expression of *tbx2b* via in situ hybridization by APO; cone subtype abundances in mutants by MGD and APO; validation of the 10C9.1 antibody by WTA; measuring the *lor* phenotype in mutants by MGD and APO; linkage analysis design and genotyping by APO. Histology shown in Fig. 2.4.1 was prepared by WTA, Arlene Oatway, and Neel Doshi. Data analysis was performed by MGD, APO, and WTA. Manuscript writing was performed by MGD and WTA, with editing contribution from APO.

Chapter 4 comprises the publication of the same title: DuVal MG, Gilbert MJH, Watson DE, Zerulla TC, Tierney KB, and W. Ted Allison (2014) Growth Differentiation Factor 6 As a Putative Risk Factor in Neuromuscular Degeneration. PLoS ONE 9(2): e89183. doi:10.1371/journal.pone.0089183 (DuVal et al., 2014a). The questions, hypotheses, and experiments in this chapter were conceived and designed by MGD, MJHG, KBT, and WTA. Contributions to experiments are as follows: survival curves and eye and skeletal morphology were performed and analyzed by MGD and WTA with assistance from Allison Murray, Bradley Scott, and Neel Doshi for microCT imaging; swim endurance and sprint testing and analysis were done by MJHG, TCZ, and KBT; immunohistochemistry and image analysis were done by MGD and DEW. Christine Beattie generously shared the os10 line. The manuscript was written by WTA and MGD, and edited by MGD, MHJG, DEW, TCZ, KBT, and WTA, with constructive feedback from Simonetta Sipione and Kelvin Jones.

Chapter 6 comprises the manuscript of the same title: Tryptophan 32 mediates SOD1 toxicity in a *in vivo* motor neuron model of ALS and is a promising target for small molecule therapeutics, by Michèle G. DuVal, Vijaya K. Hinge, Natalie Snyder, Richard Kanyo, Jenna Bratvold, Edward Pokrishevsky, Neil R. Cashman, Nikolay Blinov, Andriy Kovalenko, and W. Ted Allison (in review at Neurobiology of Disease, March 2018). MGD conceived of, performed, statistically analyzed, interpreted and presented all experiments involving zebrafish or drug applications, prioritized drugs to be tested, and was the principal author responsible for drafting the manuscript. VKH conceived of, designed, performed, analyzed and interpreted computational experiments, and wrote the associated portions of the manuscript. NB conceived of, designed, analyzed and

interpreted computational experiments, and wrote the associated portions of the manuscript. NS performed TEER experiments. RK performed and analyzed Western blot experiments. JB performed and interpreted aspects of axonopathy experiments and drug application. EP and NRC conceived of residue W32 being a potential therapeutic target and suggested experiments. AK wrote portions of the manuscript associated with computational experiments. WTA conceived of the experiments, interpreted data and participated in writing the manuscript. AK, NB, and WTA supervised, coordinated and funded the work.

Chapter 8 includes content (with some modifications) from the following publication: Allison WT, DuVal MG, Nguyen-Phuoc K, Leighton PLA (2017) Reduced Abundance and Subverted Functions of Proteins in Prion-Like Diseases: Gained Functions Fascinate but Lost Functions Affect Aetiology. Int J Mol Sci. 2017 18(10) pii:E2223. doi: 10.3390.ijms18102223 (Allison et al., 2017). Manuscript writing was performed primarily by WTA with contributions from MGD, KNP, and PLAL.

Dedication

“He was determined to discover the underlying logic behind the universe. Which was going to be hard, because there wasn’t one.”

-Terry Pratchett, *Mort*

Acknowledgements

This work would not have been possible without the support of many people. First, thank you to Dr. W. Ted Allison for his unwavering support, mentorship, and enthusiasm (even after the very long days). His guidance has been crucial both through difficult times and toward many successes. Many thanks to my committee members, Dr. Andrew Waskiewicz and Dr. Valerie Sim, who never turned down a request for advice or to chat, and shared their passions for scientific inquiry with enthusiasm. Thank you to my candidacy arm's-length examiners Dr. Yves Sauvé and Dr. David Eisentstat, and exam chair Dr. Dan Barreda for their support through a tough and significant milestone. I also want to thank the external examiners for my PhD defence, Dr. Ann Morris and Dr. Kelvin Jones, and the chair, Dr. David Pilgrim. To our collaborators Dr. Ordan Lehmann, Dr. Keith Tierney, Dr. James Fadool, Dr. Neil Cashman, Dr. Steve Plotkin, and their lab members, thank you for your hard work. As well, thank you to the Canadian Institutes of Health Research, Alberta Innovates Health Solutions, the Department of Biological Sciences, the Faculty of Graduate Studies and Research, and the Faculty of Medicine and Dentistry for funding support through my degree.

There are many members of the University of Alberta community who have helped me grow and made my graduate experience not just bearable, but incredibly fun! Thank you to the wonderful people I've met through GSA, fellow students in the Bio Sci department (Wednesday group, now meeting on Thursdays!), and the many Allison lab members over the years, especially Dr. Patricia (Trish) L. A. Leighton and Dr. A. Phil Oel, with whom I navigated this weird world called grad school, and whose hard work, creativity, and sharp minds keep me inspired. And of course the work presented here would not be possible without the animal model itself- thank you to the humble zebrafish and to the people who have worked hard over many years to keep them alive and happy, including Ted, Andrew, Dr. Richard Kanyo, Tad Plesowicz, and Dr. Toni Bayans.

Finally, thank you to my family, friends, and partner: my parents Monique and Doug for their support and (often tested) patience; my brothers Marc, Stephan, and Justin, sisters-in-law Sylvie and Jacquie, and nieces Pascale, Anna, Laurence, and Eveline for lifting my spirits; Emy, Sum, and Steph for being in my corner and helping me keep things

in perspective; and my partner Cody, whose love and encouragement has been steadfast through it all.

Table of Contents

List of Tables

List of Figures

List of Abbreviations

Gene and protein symbol conventions: human gene symbols are entirely capitalized and italicized, and human protein symbols are entirely capitalized; mouse gene symbols are italicized with first letter capitalized, and protein symbols are entirely capitalized; chick gene and protein symbols follow human symbol conventions; zebrafish and *Xenopus* gene symbols are lower case and italicized, and protein symbols have the first letter capitalized.

0.1M PO_4 – 0.1M phosphate buffer
5'-FUrd – 5'-fluorouridine
ALS – amyotrophic lateral sclerosis
ANOVA – analysis of variance
BMP – bone morphogenetic protein
ChAT – choline acetyltransferase
CNS – central nervous system
CRISPR/Cas9 – DNA cutting system, Clustered Regularly Interspaced Short Palindromic Repeats & Cas9 enzyme
CRX – gene, Cone-rod Homeobox (human)
DIG – digoxigenin
dpf – days post-fertilization
dnthrβ – dominant negative thyroid hormone receptor β
E3 media – standard embryo media for raising larval zebrafish
ER – endoplasmic reticulum
EtOH – ethanol
fALS – familial amyotrophic lateral sclerosis
FDA – United States Food and Drug Administration
FLR – fluorescein
FTD – frontotemporal dementia
GDF6 – gene, growth differentiation factor 6 (human)
gdf6a – gene, growth differentiation factor 6a (zebrafish)
GFP – Green Fluorescent Protein

hpf – hours post-fertilization

HTVS – high throughput virtual screening

inx – incross

IR – infrared

KOH – potassium hydroxide

LCA – Leber's congenital amaurosis

lor – gene mutation, *lots-of-rods* (allele p25bbtl), also phenotype, *lots-of-rods*

MO – morpholino

NGS – normal goat serum

NMJ – neuromuscular junction

NRL – gene, neural leucine zipper (human)

OMIM – database, Online Mendelian Inheritance in Man

PBS^{3+} – phosphate buffered saline, 1% DMSO, 1% Tween20, 1% Triton X, pH 7.4

PBSTw – phosphate buffered saline, 0.1% Tween20, pH7.4

PCR – polymerase chain reaction

PFA – paraformaldehyde, 4% in 0.1M PO_4

PKC – protein kinase C

PTU – 1-Phenyl-2-thiourea

qPCR – quantitative polymerase chain reaction

RA – retinoic acid

RAR – retinoic acid receptor

RFLP – restriction fragment length polymorphism

ROR – retinoic acid-related orphan receptor

RXR – retinoid X receptor

sALS – sporadic amyotrophic lateral sclerosis

SDF – structure fata file

SDS-PAGE – sodium dodecyl sulfate–polyacrylamide gel electrophoresis

SEM – standard error of the mean

SMAD – human homologue to Mad (*Drosophila*) & Sma (*C. elegans*); signal transducer of receptors of TGFβ superfamily

SNP – single nucleotide polymorphism

SOD1 – gene, [Cu, Zn] superoxide dismutase 1 (human)

$SOD1^{WT}$ – wildtype SOD1 protein

$SOD1^{W32S}$ – SOD1 protein with missense mutation (tryptophan #32 to serine)

T_3 – triiodothyronine, active thyroid hormone

TBST – tris-buffered saline with Tween20

TBX2 – gene, T-box factor 2 (human)

tbx2b – gene, T-box factor 2b (zebrafish)

TDP43 – gene, TAR-DNA binding protein 43 (human)

TEER – Touch-Evoked Escape Response

Tel – telbivudine

THRβ – gene, thyroid hormone receptor β (human)

thrβ – gene, thyroid hormone receptor β (zebrafish)

TGFβ – transforming growth factor β

U – Uridine

U_{crit} – sustained critical swimming speed

U_{max} – maximum sprint swimming speed

UV – ultraviolet

WT – wildtype

ZFIN – the Zebrafish Information Network

Chapter 1. Introduction

This chapter includes content (with some modifications) from the following publications:

1. DuVal MG, Allison WT (2017) Impacts of the Retinal Environment and Photoreceptor Type on Functional Regeneration. Neural Regen Res. 2017 12(3):376-379. doi: 10.4103/16773-5374.202930 (DuVal and Allison, 2017). Writing was performed by both authors.
2. Allison WT, DuVal MG, Nguyen-Phuoc K, Leighton PLA (2017) Reduced Abundance and Subverted Functions of Proteins in Prion-Like Diseases: Gained Functions Fascinate but Lost Functions Affect Aetiology. Int J Mol Sci. 2017 18(10) pii:E2223. doi: 10.3390.ijms18102223 (Allison et al., 2017). Manuscript writing was performed primarily by WTA with contributions from MGD, KNP, and PLAL.

1.1. Development of Cone Photoreceptor Diversity

1.1.1. Importance of diverse models of photoreceptor development for clinical research

The study of photoreceptor development and regeneration holds great clinical promise to combat degenerative disease. Vision loss from retinal degenerations is increasingly prevalent and currently incurable; these degenerations are characterized by loss of photoreceptors, specialized neurons that detect light. Photoreceptors are intimately connected to the rest of the retina through intercellular communication and cell support mechanisms. The two main photoreceptor types are rods, which are highly sensitive to light and are needed for vision in low light conditions; and cones, which are less sensitive to light and are utilized in the bright light of daytime. Cones are further divided into subtypes based on maximal wavelength sensitivity; combinations of inputs from multiple cone types enable colour discrimination. For vision restoration, the fovea is an important target- it is a region of human and other primate retinas containing exclusively cones, and is responsible for daytime, high acuity, and colour vision (Dowling, 2012). Therefore the ultimate goal is to restore or preserve function of the fovea and surrounding macula, which

requires not just a sufficient number of cones, but also their survival, integration, and function within this unique retinal environment. Hence in modeling vision development, disease, regeneration, and restoring function, more emphasis must be placed on the effects of 1) the surrounding retinal environment, and 2) the photoreceptor type, specifically cones and cone subtypes. In these endeavours, we suggest that diverse vision models would prove powerful complements to existing ones. The zebrafish retina especially can mimic the macula, because it contains a dense, even distribution of cones (Allison et al., 2010a; Raymond et al., 1995a) with ample cone-cone interactions (e.g. cone telodendria) (Noel and Allison, 2018). Zebrafish have numerous additional advantages such as conserved eye development, genetic tools, and robust regeneration (Bandmann and Burton, 2010; Bernardos et al., 2007; Bibliowicz et al., 2011; Bilotta and Saszik, 2001; Fadool and Dowling, 2008; Fleisch et al., 2011; Gemberling et al., 2013; Gorsuch and Hyde, 2014).

It is important to consider the retinal environment and how it affects photoreceptors. The retina is specialized to suit the unique visual environment of an organism, based on factors like circadian activity (e.g. diurnal, nocturnal) and vital visual stimuli (e.g. colour sensitivity, motion detection). The composition and connectivity of photoreceptor populations are complex and variable among vertebrates, necessitating the study of multiple models. In this regard the nocturnal rod-dominated mouse retina, a relevant system for mammalian genetics and retinal biology (but insufficient in cones), should be complemented with others such as the diurnal cone-dominated zebrafish retina, which mimics the human macula (Fig. 1). Furthermore, the retinal environment's response to photoreceptor loss is an emerging question relevant to photoreceptor biology, including disease. The murine and zebrafish retinas have several intriguing contrasts, including genetic regulation of photoreceptor specification (Kim et al., 2016) and responses to degeneration (Becker and Becker, 2008; Brockerhoff and Fadool, 2011; Fraser et al., 2013a; Kassen et al., 2007; Marc et al., 2007; Strettoi et al., 2002; Vihtelic and Hyde, 2000), and synaptic plasticity (Hagerman et al., 2016), which differentially influence rods and cones (Morris et al., 2008; Narayan et al., 2016; Waldron et al., 2018) during photoreceptor loss and re-introduction. Thus we are interested in how cone subtypes develop and regenerate, and how the retinal environment influences them. Indeed,

established and emergent data indicate the retinal environment influences photoreceptor fate and survival. The diversity of retinal responses to photoreceptor loss and/or introduction can be appreciated in the contexts of disease or damage, and through an organism's life history (Allison et al., 2006a; Hawryshyn, 2003; Raine et al., 2010; Veldhoen et al., 2006). In many of these cases the mechanisms are not well understood.

The mouse retina is biased to the survival and integration of primarily rods from donor precursors (Waldron et al., 2018), suggesting mechanisms to maintain a rod-dominated milieu. Implantation of *Crx*+ photoreceptor precursors (which have potential to become either rods or cones) into wildtype retinas results in the majority becoming rods. However, cone fate adoption is slightly higher when *Crx*+ precursors are implanted into cone-deficient *Gucy2e*$^{-/-}$ retinas, though not above cone:rod population ratios seen in wild type retinas (Lakowski et al., 2010). In other words, the murine retina strongly regulates photoreceptor populations toward a rod majority and a cone minority, suggesting, essentially, that environmental context matters. The zebrafish promises to expand on this hypothesis because zebrafish retinas have both a high density of cones and a large variety, as they possess tetrachromatic vision with four major cone types organized in a precise mosaic pattern (compared to two types in mice and three in humans) (Fig. 1.1). To better understand what is required for the generation of multiple cone subtypes, we therefore use the zebrafish, a retina model that generates four cone subtypes in tightly regulated proportions at both the larval and adult stages (Allison et al., 2010b). While larvae do not have the same row mosaic cone arrangement, cones of each subtype are regularly spaced and generated in consistent proportions. The nomenclature of vertebrate cone opsins and their orthologues among zebrafish, mice, and humans are provided in Table 1.1 for reference.

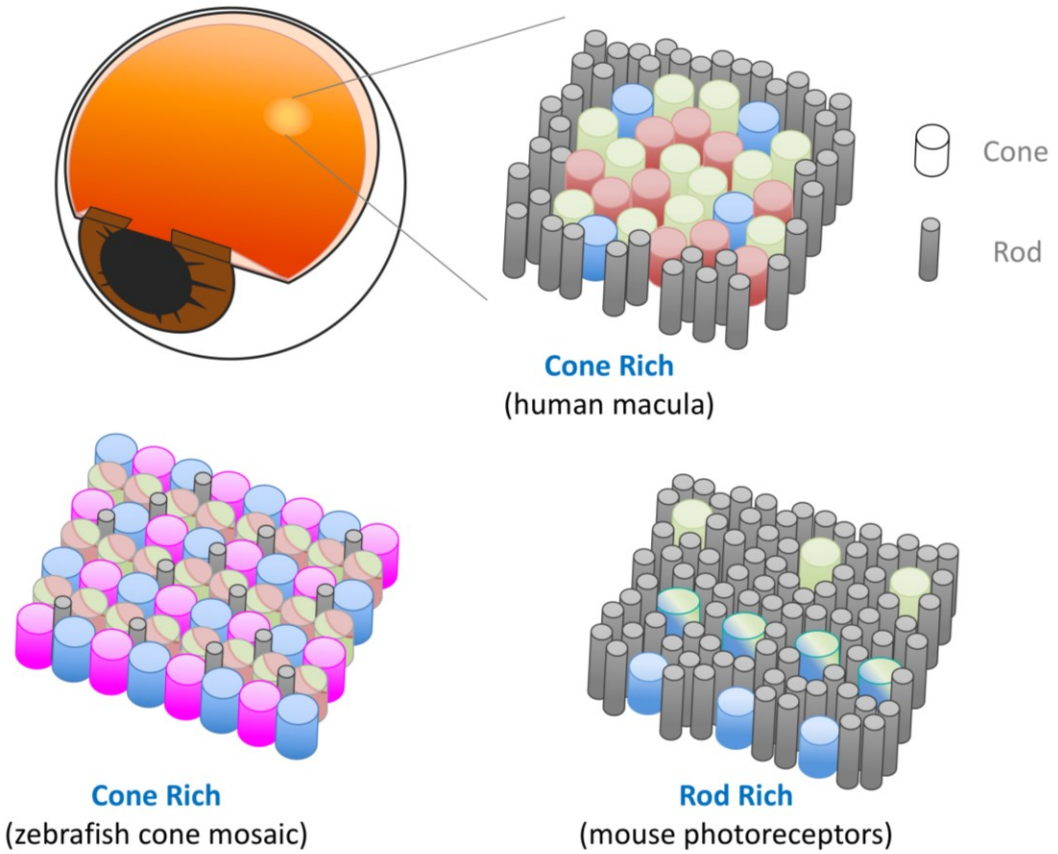

Figure 1.1. Diversity in photoreceptor composition among different retinal environments.

The retina is a thin neural tissue that lines the inside of the eye, as shown through a cutaway in a schematized eyeball. In humans, the macula is a region of the retina that is very rich in cones, including blue-, green-, and red-sensitive cone types. The cones of the macula are responsible for daytime photopic vision, colour discrimination, and visual acuity, thus the macula is an important target for vision restoration. The zebrafish and murine retinas are well-studied examples of cone rich and rod rich respectively, exemplary of a spectrum of retinal environments. Zebrafish have a high and even density of cones across the entire retina, with rods dispersed throughout.

Zebrafish cones are arranged in a row mosaic where rows of UV and blue cones (coloured purple and blue) alternate with rows of red and green cones (red and green, shown in double cone morphology). The mouse retina has a high density of rods and low density of cones. Mouse cones express green-sensitive opsin in the dorsal retina, blue-sensitive opsin in the ventral retina, and co-express both in the central retina. Rods are depicted as long grey bodies; cones depicted as stout bodies. In photoreceptor schematics, dorsal is towards the top.

Table 1.1. Summary of zebrafish, mouse, and human photoreceptor opsin orthologues.

Opsin	*D. rerio* Orthologue PhR type	*M. muscsulus* Orthologue PhR type	*H. sapiens* Orthologue PhR type
Long wavelength-sensitive LWS	*opn1lw1* **Red-sensitive cones**	*Opn1mw* **M-cones**	*OPN1LW* **Red cones**
	opn1lw2 **Red-sensitive cones**		*OPN1MW (gene duplication in primates)* **Green cones**
Short wavelength-sensitive SWS1	*opnsw1* **UV-sensitive cones**	*Opn1sw* **S-cones**	*OPN1SW* **Blue cones**
SWS2	*opn1sw2* **Blue-sensitive cones**		
Medium wavelength-sensitive RH2	*opn1mw1* *opn1mw2* *opn1mw3* *opn1mw4* **Green-sensitive cones**		
Rhodopsin RH1	*rho* **Rods**	*Rho* **Rods**	*RHO* **Rods**

Opsin gene orthologues are located in the same row. PhR- photoreceptor. Zebrafish have four major photoreceptor types: one long wavelength-sensitive cone, two short wavelength-sensitive cones, a medium wavelength-sensitive cone, and one rod. Mice have only two cone types, and the maximum sensitivity of the long wavelength-

sensitive opsin is shifted into the green spectrum. Human blue cones have short wavelength-sensitive opsin and red cones have a long wavelength-sensitive opsin; human green cones are a result of a gene duplication of the long-wavelength-sensitive opsin in the primate lineage. In the text, mouse opsins will be referred to as "M-opsin" and "S-opsin", and zebrafish cone types will be referred to by shorthand names, e.g. "red cones", "UV cones", etc.

1.1.2. Introduction to cone development

Below is a brief overview of several retinal development regulatory factors relevant for cone photoreceptor development. These factors are discussed in a general order from roles in unspecified retinal progenitor cells toward increasing photoreceptor fate specificity. The genes of interest in this thesis, *gdf6a*, *tbx2b*, and *thrβ*, are discussed in further detail together in subsequent paragraphs. Most knowledge of vertebrate retinal development and neural specification is derived from work in mice; many phenotypes involving changes to photoreceptors involve largely changes to the rod population, as rods comprise the vast majority of photoreceptors in mice. Therefore, at least some of the regulatory networks affecting mouse photoreceptors may not reflect regulatory processes of cone photoreceptors specifically. Where possible, knowledge from other retina models, notably *Xenopus*, zebrafish, and chick, is highlighted.

The eye field is established by a gradient of Wnt signaling, which establishes anterior-posterior patterning of the forebrain. Lower Wnt concentration anteriorly is required for eye field specification, as mutation or ectopic Wnt expression in *Xenopus* (Kiecker and Niehrs, 2001; Zuber et al., 2003), zebrafish (Erter et al., 2001; Heisenberg et al., 2001; Lekven et al., 2001), mouse, and chick results in failure to form an eye (Chow and Lang, 2001; Kim and Kim, 2012; Matsushima et al., 2011). The eye field is subsequently specified by *Pax6*, *Six3*, *Lhx2*, and *Rax*. These transcription factors are each necessary and sufficient, as mutation in any one leads to absent or abnormal eye

development, and ectopic expression can induce eye formation (Brown et al., 1998; Carl et al., 2002; Chow et al., 1999; Loosli et al., 1999; Martinez-De Luna et al., 2011; Mathers et al., 1997; Porter et al., 1997; Voronina et al., 2004). Fibroblast growth factor signalling (FGF1 and FGF2) from the surface ectoderm immediately adjacent the eye cup induces neural retina identity, as removal of this ectoderm results in conversion of the eye cup to retinal pigment epithelium in mouse (Nguyen and Arnheiter, 2000), and application of FGF1 and FGF2 in chick induces neural retina identity (Pittack et al., 1997; Spence et al., 2007).

Following this induction of neural retina (Grindley et al., 1995), *Pax6* then maintains multipotency of the retinal progenitor cell population; rat mutants, mouse conditional knockouts, and zebrafish morphants have microphthalmia, due to an unsustained progenitor pool (Hill et al., 1991; Li et al., 2000; Loosli et al., 2001; Matsuo et al., 1993; Schwarz et al., 2000). Pax6, one of the factors required for eye development, upregulates *Atoh7* and *neurogenin-2* in retinal progenitors, both of which are required for neurogenesis (Marquardt et al., 2001) as well as specification of the retinal ganglion cells (Riesenberg et al., 2009; Wang et al., 2001). However Pax6 downregulates expression of *Crx*, a photoreceptor-specific gene, thus contributing to the timing of photoreceptor specification. Conditional knock out of *Pax6* in retinal progenitors using Cre-lox dramatically changes retinal progenitor fates, with only amacrine cells produced (Marquardt et al., 2001). Thus *Pax6* is also required for maintaining multipotency of the progenitors. In the adult zebrafish regenerating retina, Müller glia are the latent stem cell population and are the primary source of new cells following retinal neuron loss. In retinal regeneration, *pax6b* is required for cell division in Müller glia-derived progenitors, whereas *pax6a* is required at later cell divisions (Thummel et al., 2010), suggesting that these paralogs have overlapping but timing-specific functions within regeneration. *Rax* is also required for maintenance and is sufficient for induction of retinal progenitors. Mouse knockouts of *Rax* and mutants of the zebrafish orthologue *rx3* (Loosli et al., 2003) do not develop eyes. Overexpression of *Rax* in *Xenopus* produces ectopic eyes (Furukawa et al., 1997a; Mathers et al., 1997; Terada et al., 2006; Zuber et al., 2003). *Rax* is known to upregulate expression of *Pax6*, *Otx2*, β-arrestin, and rhodopsin in *Xenopus* and zebrafish (Nelson et al., 2009; Pan et al., 2010). *Vsx2* (formerly *Chx10*) is also required for

proliferation in retinal progenitors, as loss of function due to a premature stop codon in the ocular retardation mouse leads to microphthalmia and a thin retina (Burmeister et al., 1996).

Notch signaling also maintains proliferation and the multipotency of the retinal progenitor pool in mouse (Wall et al., 2009), *Xenopus* (Dorsky et al., 1997), chick (Henrique et al., 1997), and zebrafish (in both embryonic development and regeneration) (Scheer et al., 2001). Its disruption early in retinal development produces excess cones (Jadhav et al., 2006) and reduced ganglion cells and horizontal cells (Yaron et al., 2006); disruption later leads to excess rods and fewer bipolar cells and Müller glia (Jadhav et al., 2006; Mizeracka et al., 2013). Zebrafish *rx3* mutants show reduced proliferation among retinal progenitors (Uribe et al., 2012), and in adult retina regeneration, Notch is exploited for the proliferation of dedifferentiated Müller glia (Elsaeidi et al., 2018; Taylor et al., 2015; Wan and Goldman, 2017; Wilson et al., 2016). Inhibition of Notch can successfully produce photoreceptors in cell culture (Lamba et al., 2008b; Nelson et al., 2008). Therefore it is thought that Notch limits cell cycle exit (Maurer et al., 2014; Nelson et al., 2006; Nelson et al., 2007), thereby limiting photoreceptor differentiation to balance cell type production.

Pbx2 and *pbx4* regulate progenitor transition and may initiate dorso-ventral patterning in the developing zebrafish retina, as their disruption leads to dorsal retina patterning defects. Combinations of mutant and MO knock down experiments show that loss of *pbx2* and *pbx4* causes aberrant expression of key retinal genes such as *rx3* (the expression of which persists beyond the normal developmental window) and *otx2* (which shows expanded expression). Expression of the dorsal retina marker *gdf6a* and its downstream targets *tbx5* and *aldh1a2* were reduced. Thus *pbx2* and *pbx4* are required for progression of retinal progenitors in specification and establishment of the dorsal retina via *gdf6a* (French et al., 2007).

The *Drosophila* gene orthodenticle (*otd*) is expressed throughout the developing nervous system, and acts in specification of the optic lobe (Schmidt-Ott et al., 1994; Schmidt-Ott et al., 1995), in rhabdomere morphogenesis (Fichelson et al., 2012; Johnston et al., 2011; McDonald et al., 2010a; Mishra et al., 2010; Tahayato et al., 2003; Vandendries et al., 1996); and subsequently activates Rh3 and Rh5 opsin expression

and represses Rh6 in the photoreceptors (McDonald et al., 2010b). Loss of *otd* leads to disorganization of the rhabdomeres, loss of opsins Rh3 and Rh5, and expansion of Rh6 opsin expression. The vertebrate orthologs to *otd* are *Otx1*, *Otx2*, and *Crx*, and these genes have each assumed functions homologous to those of *otd*. *Otx1* and *Otx2* in mice are expressed in developing sensory organs, including the optic vesicle (Acampora et al., 1998; Simeone et al., 1993). *Otx1* later is restricted to other tissues of the eye, such as the iris, ciliary process, and lachrymal gland; whereas *Otx2* is expressed in the precursors for bipolar cells, photoreceptors, and retinal pigment epithelium (Acampora et al., 2001; Bovolenta et al., 1997; Simeone et al., 1992; Simeone et al., 1993).

Mouse conditional knockouts of *Otx2* are microphthalmic and have an increased amacrine cell population and fewer photoreceptors (Sato et al., 2007); likewise overexpression of *Otx2* is sufficient to elicit excess photoreceptors and suppress amacrine cells (Wang et al., 2014). *Otx2* is a transcription factor that promotes expression of *Crx* (which is required for photoreceptor development) and *Prdm1* (formerly *Blimp1*). *Otx2* thus appears to be a cell fate switch between rod photoreceptors or bipolar cells, and amacrine cell fates (Koike et al., 2007; Nishida et al., 2003). Loss of one allele of *Otx2* is adequate to reduce the abundance of rods and bipolar cells, and conditional knockout of *Otx2* in maturing bipolar cells caused loss of bipolar markers and impaired function (Koike et al., 2007), suggesting *Otx2* has additional roles in bipolar cell maturation. *Otx2* is repressed by Hes/Hey proteins (Muranishi et al., 2011), which are expressed under Notch signaling as part of maintaining the progenitor pool.

CRX was discovered as a regulator of rhodopsin expression as well as a disease locus in cone-rod dystrophy and Leber congenital amaurosis (Chen et al., 1997; Freund et al., 1997; Furukawa et al., 1997). *CRX* belongs to the orthodenticle family of homeobox genes and is expressed in mature photoreceptors and pinealocytes (Furukawa et al., 1997a); during retinal development, *Crx* is expressed in the progenitors of photoreceptors and bipolar cells. Mouse knockouts of *Crx* develop photoreceptors, but these photoreceptors fail to develop outer segments, do not express required genes for transduction machinery, and are not functional as measured on electroretinogram (Furukawa et al., 1999). These photoreceptors subsequently degenerate, mimicking the associated retinal degenerative diseases. Gene targets of *Crx* for positive regulation in

the photoreceptors include *Nrl*, *Nr2e3*, *Thrβ*, rhodopsin, cone opsins (Corbo et al., 2010; Furukawa et al., 2002; Hennig et al., 2008), *Crx* itself, as well as similar genes for photoreceptors in the pineal gland (Rovsing et al., 2011). The transcription factor *Nrl* and its target *Nr2e3* drive rod fate and rhodopsin expression (Mears et al., 2001). Zebrafish *crx* also drives *otx5* expression, which also promotes photoreceptor identity in the retina and pineal gland (Asaoka et al., 2014; Gamse et al., 2002; Liu et al., 2001; Shen and Raymond, 2004a). *Crx* is thus necessary for photoreceptor maturation and function, though not fate assumption. As part of final differentiation, *Crx* represses *Otx2* in a negative feedback manner (Hennig et al., 2008; Nishida et al., 2003).

Zebrafish *cadherin2* (*cdh2*) and *cadherin4* (*cdh4*) mutants show photoreceptor development disturbances, with reduction in red/green double cone marker zpr-1 and reduced expression of rhodopsin, UV opsin, and mature photoreceptor genes (*gnat1*, *gnat2*, *irbp*). Double knockouts show a more severe phenotype, with lack of *crx* and *otx2* expression, followed shortly by degeneration. These observations point to *cdh2* and *cdh4* initiating and/or maintaining the Crx+ precursor population during development (Liu et al., 2007).

Onecut1 is involved in cone and horizontal fate, and possibly in their maturation as well. *Onecut* mutants fail to generate horizontal cells, and have fewer cones (Sapkota et al., 2014); ectopic expression during rod development caused expression of cone and horizontal cell markers, but not full maturation to these types. In chick and mouse, both *Otx2* and *Onecut1* regulate *Thrβ2* expression, and overexpression and dominant negative experiments show that *Onecut1* appears to regulate cone versus rod photoreceptor fates (Emerson et al., 2013).

In *Drosophila*, *sal* genes promote R7 and R8 photoreceptor differentiation; in *sal* mutants these precursors instead become R1-R6 photoreceptor types (Domingos et al., 2004; Mollereau et al., 2001). The homologue Spalt-like 3 or *Sall3* was found elevated in mouse *Nrl* knockouts (which lack rod photoreceptors) (Yoshida et al., 2004b); following this it was found that *Sall3* is expressed in S-cones and horizontal cells during retinal development; ectopic expression of Sall3 increased S-opsin and cone arrestin expression and produced excess horizontal cells. A *Sall3* mouse knockout confirmed this role with lack of S-opsin or arrestin expression, as well as reduction in expression of other cone

transduction genes. While *sal* in Drosophila is a fate switch gene, in mice *Sall3* may not be a simple fate switch, as it's not fully confirmed that S-cones become another photoreceptor type in the *Sall3* knockout (de Melo et al., 2011). Rather *Sall3* may have similar roles as *Crx* in S-cone maturation and function. In chicks, *SALL1* and *SALL3* expression was found in the photoreceptor layer and inner nuclear layer, suggesting a conserved expression pattern as in mice, though *SALL3* expression declined after hatching.

Prdm1 (formerly *Blimp1*), a transcription repressor, represses *Otx2* expression as part of rod differentiation (Wang et al., 2014). *Prdm1* fate-mapping (or lineage tracing) highlights subsets of interneurons and photoreceptors (Brzezinski et al., 2013). Through knock down and ectopic expression experiments, *Prdm1* was found to promote rod development and suppress bipolar fate via downregulating *Vsx2* (Brzezinski et al., 2013; Fossat et al., 2007; Wang et al., 2014). *Vsx2* is needed for bipolar cell development (Brzezinski et al., 2010; Brzezinski et al., 2013; Burmeister et al., 1996; Katoh et al., 2010), as it suppresses expression of photoreceptor-specific genes in bipolar precursors (e.g. S-arrestin, M-opsin) (Dorval et al., 2006; Livne-Bar et al., 2006).

Insulinoma-associated 1a (*insm1a*) in zebrafish regulates cell cycle progression early in retina development, but its loss of function causes photoreceptor phenotypes (Forbes-Osborne et al., 2013). *Insm1a* acts in cell cycle regulation and differentiation, including in the Müller glia during regeneration (Ramachandran et al., 2012) and in the rod progenitor cells of the adult retina (Morris et al., 2011). MO knock down of *insm1a* shows disrupted cell cycle kinetics in retinal progenitors, reduced final rod and cone abundances, signs of delayed bipolar and horizontal cell maturation, and areas of disrupted lamination in the outer nuclear layer and inner plexiform layer similar to that of Rb mouse mutants (Johnson et al., 2006). BrdU tracking and PH3 labeling determined that the rate of proliferation and cell cycle exit were slower in *insm1a* morphants (Forbes-Osborne et al., 2013). Expression of *Atoh7*, a marker of the first population to differentiate- ganglion cells- appeared to initiate and expand late. Expression of *crx*, *nr2e3*, and *neuroD* was reduced in morphants. *NeuroD* is required for cell cycle exit (Morrow et al., 1999; Ochocinska and Hitchcock, 2007; Ochocinska and Hitchcock, 2009) and also activates *Thrβ* in cone precursors (discussed below). Thus *insm1a* is thought to control timing of

progenitor progression through the cell cycle. *Her4* expression reduced *insm1a* promoter activity, so Notch-Delta signaling is implicated in regulating *insm1a*.

In mice, *Thrβ* drives M-cone fate and M-opsin expression (Ng et al., 2001a; Swaroop et al., 2010) and in dimers with RXRγ, Thrβ suppresses S-opsin expression (Pessoa et al., 2008; Roberts et al., 2006). The COUP-TF nuclear receptors, which require BMP signaling in early retina to establish their dorso-ventral patterning of expression, also regulate cone opsin expression in mice. In the dorsal retina, COUP-TFI and II suppress S-opsin while Thrβ and COUP-TFII promote M-opsin expression. In the ventral retina, COUP-TF I suppresses M-opsin, therefore allowing for S-opsin-dominant expression (Satoh et al., 2009). In zebrafish *nr2f1b* (formerly COUP-TFα-B) is detectable in the photoreceptor layer during late stage retinal development, and so may perform similar actions in regulating opsin expression (Bertrand et al., 2007). *NeuroD1*-deficient mice show a similar phenotype to *Thrβ* null mice: a pan-S-opsin expression and no detectable M-opsin. *Thrβ2* expression in *NeuroD*$^{-/-}$ mice was reduced, suggesting NeuroD1 positively regulates *Thrβ2* expression (Liu et al., 2008); *NeuroD1*$^{-/-}$ mice also develop a slow retinal degeneration (Pennesi et al., 2003). In zebrafish, levels of active thyroid hormone, T_3, must be tightly controlled in the developing retina, as knock down of T_3 activating enzymes deiodinases 1 and 2, or knock down of the T_3 inactivating enzyme deiodinase 3, lead to reduction in all photoreceptor types. Poor retinal lamination was also observed, which eventually recovered (Houbrechts et al., 2016). The zebrafish homologue *thrβ* is required and sufficient for red cone fate (orthologue to mouse M-cones) early in cone development, as ectopic expression of *thrβ* in cone precursors (under the *crx* promoter) appears to exert a red cone fate on most precursors. After cone differentiation, ectopic *thrβ* is sufficient to induce red cone opsin expression, but does not appear to change the cones' identities (Suzuki et al., 2013a). This same study identified asymmetric divisions of red cone progenitors that also produced horizontal cells which, along with cone and horizontal cell phenotypes in *Onecut1* and *Sall3* mouse mutants, showed that cone photoreceptors and horizontal cells have a closely-shared progenitor. Retinoic acid signaling also promotes LWS opsin expression in zebrafish (Mitchell et al., 2015a; Prabhudesai et al., 2005).

Pias3 encodes an E3 SUMO ligase that also has transcription modulating roles. In mice, Pias3 binds with Crx to promote expression of rod-specific genes. Pias3 SUMOylates Nr2e3, which then represses S-opsin expression in rods (Onishi et al., 2009). In developing cones, *Pias3* expression is induced in M-cones by Thrβ and RXRγ. While *ROR*□ was found to induce S-opsin expression in S-cones, in M-cones Pias3 SUMOylates RORα, which then dimerizes with Crx to suppress S-opsin expression. Pias3 also SUMOylates Thrβ2, an action that is required for Thrβ2 to induce M-opsin expression (Onishi et al., 2010). The zebrafish orthologue for *Pias3* is not confirmed, and as far as the author can ascertain, this gene has not been studied in chicken or *Xenopus* photoreceptors.

Retinoic Acid Receptor Related Orphan Receptor *β* (*RORβ*) has two isoforms. *RORβ2* is expressed in the retina and pineal gland (Andre et al., 1998; Jia et al., 2009b; Srinivas et al., 2006b), and *RORβ1* is more ubiquitous in the CNS (Jia et al., 2009a; Ng et al., 2001a; Swaroop et al., 2010). *RORβ2* serves many roles in retinal cell differentiation. In mice, RORβ2 binds the *Nrl* promoter in rod photoreceptors. Loss of *RORβ* causes a lack of rods, an excess of S-cones, many of which are not functional, and some persisting M-opsin expression (Jia et al., 2009a). This phenotype can be rescued with *Nrl* expression, demonstrating that *Nrl* is downstream of *RORβ*. *RORβ2* is also expressed in amacrine and horizontal cell progenitors; in combination with Foxn4, RORβ2 stimulates *Ptf1a* expression, which is necessary for both these neural types (Hafler et al., 2012; Liu et al., 2013). RORβ2 also dimerizes with Otx2 to stimulate *Prdm1* expression for rod production (Wang et al., 2014).

Retinoic Acid Receptor Related Orphan Receptor α (*ROR*□) is expressed in both S- and M-cones and some interneurons. *ROR*□ mutant mice called Staggerer (*sg*) only weakly express the S- and M-cone opsins, thus *ROR*□ is important but not necessary for cone opsin expression. In these *sg* mice, *Thrβ2* expression is slightly upregulated, thus *ROR*□ may partially suppress *Thrβ2* expression (Fujieda et al., 2009). Current models for *ROR*□ involve pulses of expression between *ROR*□, *RXRγ*, and *Thr2β* to create the pattern of S- and M-opsin in the mouse retina.

Retinoid X Receptor gamma (*RXRγ*) is expressed in the retina early and then later is restricted to the cone photoreceptors (Hoover et al., 1998). RXRγ dimerizes with Thrβ2

to suppress S-opsin (Roberts et al., 2005) and to induce expression of *Pias3*, which then enables Thrβ2 to promote M-opsin expression (Onishi et al., 2010). *RXRγ* mutant mice have a pan-cone S-opsin expression phenotype (Roberts et al., 2005). Lineage tracing with a *RXRγ* promoter sequence and Cre-lox reporter in the chick revealed that *RXRγ* is also expressed in the horizontal cells and cone precursors, supporting that cones and horizontal cells have a common progenitor.

In zebrafish, loss of *six7* results in nearly no green cone abundance and excess rods, mirroring the UV cone phenotype of *tbx2b* mutants (details in sections below). *Six7* larval mutants also had reduced blue cone abundance. In adulthood this lack of green cones persisted, whereas blue cone abundances recovered and relative expression levels of the two red opsins*, opn1lws1* and *opn1lws2*, were switched (Ogawa et al., 2015). Subsequent work implicates that most of the green cones are lost to cell death in development, and that the excess rods are likely not coupled to the green cone deficiency in a fate-switch fashion (Sotolongo-Lopez et al., 2016).

Neural Retina Leucine Zipper or *Nrl* is required for rod specification, as *Nrl* knockout mice lack rods and have excess S-cones (Jia et al., 2009b; Mears et al., 2001; Yoshida et al., 2004a), many of which differ from wildtype cones (and later degenerate) suggesting a fate switch had occurred in rod precursors (Daniele et al., 2005; Mears et al., 2001). *Nrl* is expressed in developing and differentiated rods and it dimerizes with Crx to promote rod-specific gene expression (Hao et al., 2012; Mitton et al., 2000b). Ectopic expression is sufficient to convert all *Crx+* photoreceptor precursors to rods, showing that *Nrl* is both necessary and sufficient for rod identity (Oh et al., 2007). Outside mice, *nrl* is expressed in the photoreceptor layer of zebrafish (Coolen et al., 2005; Nelson et al., 2008; Sun et al., 2018), and lipofection of *nrl* into *Xenopus* retinas enhanced rhodopsin expression (McIlvain and Knox, 2007), thus hinting at conserved roles in rod photoreceptor development. Recent work by a colleague, A. Phil Oel, has confirmed *nrl*'s critical role in zebrafish larval rod development via CRISPR/Cas9 knockout of zebrafish *nrl* (manuscript in preparation). In zebrafish, retinoic acid signalling promotes rod development through its receptor RARαb (Stevens et al., 2011).

1.1.3. A current lack of identified cone photoreceptor differentiation factors

At the beginning of the thesis research program, few genes impacting cone development genes had been identified, with knowledge mostly limited to the mouse, a model with dichromatic vision: while *Nrl* and *Nr2e3* defined rod photoreceptors, only one gene, *Thrβ*, strongly characterized cone subtype differentiation, inducing an M-cone fate. The other cone type, the S-cone, was thought to develop in progenitors lacking sufficient rod factors and *Thrβ* expression (Applebury et al., 2000; Mears et al., 2001; Ng et al., 2001a; Ng et al., 2011; Roberts et al., 2006). Based on the evidence available at the time, this model was sufficient to explain photoreceptor fate choices. However some of the underlying assumptions left much uncertainty, especially in comparison to photoreceptor development in other vertebrates. Because an S-cone inducing factor had not been found, it was assumed that there was not one, or that one was not needed (i.e. “default” implying a progenitor would assume S-cone identity without external influences), which was countered quickly upon the discovery of mutants (albeit in another organism) where the S-cone homologue is exclusively lost (Alvarez-Delfin et al., 2009). Additionally, if a cone fate were a “default” state for murine or mammalian photoreceptor progenitors, the notorious difficulty procuring cones in retina culture and transplant experiments (Gonzalez-Cordero et al., 2017; Lakowski et al., 2010; MacLaren et al., 2006; Nakano et al., 2012; Waldron et al., 2018; Zhou et al., 2015) becomes awkward to resolve. The spatial regulation of opsin expression is coordinated by *RORα*, *RORβ*, and *RXRγ* in the mouse, producing the dorsoventral gradient of S-opsin and M-opsin expression. *ROR* activates expression of both S- and M-opsins as well as *Arr3*, another cone gene (Fujieda et al., 2009). *RORβ* is required for maturation of S-cones and expression of S-opsin (Srinivas et al., 2006a), whereas *RXRγ* suppresses S-opsin expression in the dorsal retina (Roberts et al., 2005). Another important incongruity of mouse cone photoreceptors is the ubiquity of dual opsin expression; most of the cones in the mouse retina express both S- and M-opsin (Applebury et al., 2000; Ortin-Martinez et al., 2014), making the cone subtype differentiation pathways and final “identities” ambiguous (Glaschke et al., 2011; Nikonov et al., 2005). In the adult retina of most mammals, including humans, individual cones of do not express more than one opsin, and furthermore humans have one more cone type than mice, so making associations between human and mouse cone

development is problematic. In zebrafish, the list of known cone-specific genes was limited to *gnat2* (pan-cone expression) and the cone opsin genes, which encode phototransduction machinery and so provided a limited interpretation of cone differentiation and birth order. Photoreceptor phenotypes had been documented in several mouse and zebrafish loss-of-function models, including deiodinases 1, 2, and 3 (Houbrechts et al., 2016), *tbx2b* (Alvarez-Delfin et al., 2009; DuVal et al., 2014b), *rx1*, *rx2* (Nelson et al., 2009), *crx* (Chen et al., 1997; Freund et al., 1997; Furukawa et al., 1997b), *otx2* (Nishida et al., 2003), *neurod1* (Ochocinska and Hitchcock, 2009), *cdh2*, and *cdh4* (Liu et al., 2007), and *pob* (Brockerhoff et al., 1997; Taylor et al., 2005), but these phenotypes affected many if not all photoreceptor types, or were found critical for photoreceptor maintenance (in the case of *pob*). So while they are critical for photoreceptor differentiation, survival, and gene expression, they are not specific for any subtypes. The list of genes affecting assumption of cone subtype identity, or sets thereof, was thus quite short. In this thesis, we sought to identify factors regulating cone subtype outcomes and describe the roles of these factors using zebrafish: in this endeavour we examined the zebrafish genes *gdf6a*, *tbx2b*, and *thrβ*, described briefly below.

1.1.4. Introduction to TBX2

Brachyury (Abrahams et al., 2010; Chapman et al., 1996; Herrmann and Lehrach, 1988) was the first identified member of the T-box family of transcription factors, and it was first described for regulating the differentiation of mesoderm during gastrulation (Herrmann et al., 1990). The T-box DNA binding domain is the defining feature of this family, and was used to identify and classify more members (Bollag et al., 1994). Subsequent work established the TBX2 family (consisting of *TBX2*, *TBX3*, *TBX4*, and *TBX5*) as factors in proliferation and differentiation in a wide variety of contexts and tissues, often under the regulation of BMP signaling, including BMP4, BMP2, and GDF6. The TBX2 family is derived from two duplications, where *TBX2/3* and *TBX4/5* precursor genes arose from the first duplication, then the extant four arising from the second (Agulnik et al., 1996; Ruvinsky and Silver, 1997). The TBX2 family is related to the *Drosophila optomotor blind* (*omb*) gene (Pflugfelder et al., 1992).

TBX2 (and its orthologues *Tbx2* and *tbx2b*) is understood to play various roles throughout development and beyond, including neuron fate commitment (Gross and Dowling, 2005b; Snelson et al., 2008a; Snelson et al., 2008b) and regulation of cell cycle exit (Bilican and Goding, 2006; Harrelson et al., 2004; Jacobs et al., 2000; Ludtke et al., 2013; Sedletcaia and Evans, 2011a; Vance et al., 2005a).*TBX2* regulates cell cycle progression (Bilican and Goding, 2006; Mahlamaki et al., 2002; Packham and Brook, 2003; Vance et al., 2005a) and regulates apoptosis through p53 (Jacobs et al., 2000; Lingbeek et al., 2002; Prince et al., 2004). *TBX2* expression is often upregulated in cancers such as BRCA1 and BRCA2 breast cancers (Sinclair et al., 2002; Sinclair et al., 2003), melanoma, and pancreatic cancer (Mahlamaki et al., 2002). The consequences of *TBX2* overexpression include downregulation of tumour suppressor genes such as E-cadherin, a modulator of growth (Rodriguez et al., 2008), *PML* (Abrahams et al., 2010; Martin et al., 2012a), a tumour suppressor associated with cell senescence, and *NDRG1* (Redmond et al., 2010), which has roles in differentiation and apoptosis. By contrast, during development *TBX2* and its orthologues are best known for regulating cell differentiation and patterning. While *TBX2* often acts as a gene suppressor in development, it contains domains for both activation and suppression (Paxton et al., 2002; Sinha et al., 2000). The various conserved roles of *TBX2* include formation of the limbs, atrioventricular canal, and optic cup formation and patterning; the expression of *TBX2* is often subject to BMP4 signaling.

Tbx2 in mice is expressed in the heart (Harrelson et al., 2004), palate (Zirzow et al., 2009), optic vesicle (Behesti et al., 2009), and hind limbs (Gibson-Brown et al., 1996; Gibson-Brown et al., 1998a). *Tbx2* and *Tbx3* are targets of BMP signaling for hind limb digit patterning, heart patterning, and optic cup formation. Under Bmp4 signaling, *Tbx2* terminates Shh/FGF signaling to terminate limb outgrowth at the posterior limb margin for digit patterning; loss of *Tbx2* causes polydactyly (Farin et al., 2013; Harrelson et al., 2004; Yang et al., 2006). *Tbx2* null mice die from cardiovascular defects due to failure to form the atrioventricular cushions (Singh et al., 2012), resulting in a lack of atrioventricular canal formation and outflow tract septation. At the site of the future atrioventricular canal, *Tbx2* represses chamber differentiation, and in *Tbx2* mouse mutants the expression of chamber genes is expanded (Harrelson et al., 2004). No conditional knockouts with the

intent of examining *Tbx2*'s role in the eye have been examined, but *Tbx2* null mice have microphthalmia. *Bmp4* regulates expression levels of *Tbx2*, *Tbx3*, and *Tbx5* in the optic cup in a dose-dependent manner (Behesti et al., 2006; Koshiba-Takeuchi et al., 2000). *Tbx2* and *Tbx3* are also involved in secondary palate development, as homozygous *Tbx2* or compound heterozygous *Tbx2*/*Tbx3* mutants have cleft palate, likely due to impaired proliferation and survival in the palatal mesenchyme (Zirzow et al., 2009). *Tbx2* acts in the developing kidney to limit the expansion of the pronephric nephron. BMP signaling in the non-nephric mesoderm stimulates *Tbx2* expression, which then limits expression of *Hey1* and *Gremlin*, thereby regulating the size of the pronephros tissues (Cho et al., 2011).

In chick *TBX2* has roles in cardiogenesis, limb formation, and photoreceptor development. *TBX2* is induced in cardiogenesis by BMP2 (Gibson-Brown et al., 1998b; Yamada et al., 2000). *TBX2* is expressed in lateral mesoderm during limb development. Exogenous BMP4 induces *TBX2* expression in the limb bud; TBX2 then specifies the posterior digits by de-repressing Shh and suppressing *BMP2*. Overexpression of *TBX2* sufficiently enhances the posterior phenotype (Gibson-Brown et al., 1998b; Suzuki et al., 2004). *TBX2* is also implicated in chick UV cone development in RNAseq experiments, where *TBX2* expression was higher in UV cones compared to other cone types, suggesting a conserved role for *TBX2* in short wavelength-sensitive cones (Enright et al., 2015).

Xenopus tbx2 is expressed in the optic vesicles, otic vesicles, neural crest, cranial ganglia, notochord, heart, and limbs (Gibson-Brown et al., 1998b; Hayata et al., 1999; Showell et al., 2006; Takabatake et al., 2000). *Tbx2* and *tbx3* act together to modulate Shh in limb development (Takabatake et al., 2002). A similar pattern in hypothalamus development involves BMP signaling and the downstream Tbx2 suppressing *Shh* in order to induce a hypothalamic progenitor identity (Manning et al., 2006). In the dorsal retina, *tbx2* expression is conserved in *Xenopus* (Takabatake et al., 2000) and zebrafish (*tbx2b*) (Gross and Dowling, 2005b).

Zebrafish have two paralogs of *Tbx2*: *tbx2a* and *tbx2b*. *Tbx2a* is expressed in the tail bud, heart, pharyngeal arches, and pronephros. In conjunction with *tbx3*, *tbx2a* represses cardiac chamber formation pathways in the non-chamber myocardium, and limits proliferation to create the atrioventricular valve; this process is also critical for

correct looping of the heart in fish (Ribeiro et al., 2007). *Bmp4* is also expressed during atrioventricular canal formation, possibly upregulating *tbx2a* and *tbx2b* (Garrity et al., 2002). *Tbx2* in mice also regulates differentiation of the non-chamber myocardium for formation of the atrioventricular canal (Habets et al., 2002). In mice, *Bmp2* and *Tgfβ2* are also expressed in the atrioventricular canal (as well as the outflow and inflow tracts), contributing to non-chamber myocardium development (Bartram et al., 2001; Ma et al., 2005). Interestingly, among *Tbx2*$^{-/-}$ mice, only about 25% develop atrioventricular canal defects or outflow tract defects, suggesting other factors are able to compensate for loss of *Tbx2* (Harrelson et al., 2004). In zebrafish pharyngeal arch formation, *tbx2a* regulates morphogenesis of the endodermal pouches, mesenchymal condensation, and neural crest cell differentiation into the skeletal and connective tissue elements of the arches (Thi Thu et al., 2013). While positively regulated by BMP signaling, *tbx2a* (and *tbx2b*) is negatively regulated by retinoic acid signaling in the development of the pronephros (Drummond et al., 2017). Thus *tbx2a* and *Tbx2* are fairly well conserved in expression and function.

The second zebrafish paralog is *tbx2b*. Early in development, *tbx2b* acts in the specification of late notochordal precursors. *Tbx2b* is expressed in the developing dorsal eye field, otic vesicle, pectoral fin buds, tail bud, and heart (Dheen et al., 1999). Similar to *tbx2a*, *tbx2b* is also required for atrioventricular valve and outflow tract formation. Knock down of either *tbx2a* or *tbx2b* results in microcephaly and microphthalmia, in addition to cardiac defects. Knocking down both reveals additional roles in cardiomyocyte proliferation (Sedletcaia and Evans, 2011b). Wnt signaling works upstream of BMP signaling and *tbx2a* and *tbx2b* in atrioventricular canal specification by inducing *bmp4*, which induces *tbx2a* and *tbx2b* expression (Verhoeven et al., 2011).

Tbx2b has additional roles in neural plate development, liver regeneration, and parapineal cell migration. *Tbx2b* acts on neural plate development by mediating cell migration; this is also regulated by Wnt signaling (Fong et al., 2005). BMP signaling and *tbx2b* are also linked in the differentiation of hepatoblast-like stem cells in zebrafish liver regeneration (Choi et al., 2017). In the pineal gland, *tbx2b* is required for production of parapineal cells and their migration to their typical asymmetric location (Snelson et al., 2008b). These same parapineal cells are negatively regulated by *nr2e3*, which

suppresses parapineal fate in favour of other neuron fates. While suppressing *nr2e3* expression in *tbx2b* mutants can rescue the absolute number of parapineal cells, these cells still don't migrate to the left side, suggesting *tbx2b* is performing 2 separate actions in this process (inducing fate versus stimulating cell migration) (Khuansuwan et al., 2016). The opposing effects of *tbx2b* and *nr2e3* in parapineal development have interesting parallels in the retinal photoreceptors: *tbx2b* mutants show a lack of UV cones and excess of rods (described below). In mice, *Nr2e3* is a critical transcription factor in rod fate and rhodopsin expression, and there is reason to suspect the zebrafish orthologue *nr2e3* has a homologous role.

Finally, *tbx2b* is a marker of dorsal retina identity in zebrafish, regulating neuronal differentiation in the dorsal retina. Gdf6a signaling is upstream of *tbx2b* in the dorsal retina fate pathway; without Gdf6a signaling, *tbx2b* expression is reduced (French et al., 2009; Gosse and Baier, 2009). *Tbx2b* was thought to represses rod fate in favour of UV cone fate, based on the phenotypes of two mutations: 1) *fby*, a recessive allele in which homozygous mutants lack UV cones and have an overabundance of rods, and 2) *lor*, a recessive allele in which homozygous mutants have few UV cones and excess rods ("lots-of-rods") (Alvarez-Delfin et al., 2009). *Tbx2b*$^{+/-}$ heterozygous mutant zebrafish do not exhibit these photoreceptor phenotypes. Notably, despite being downstream of *gdf6a* in dorsal retina pattering, *tbx2b* mutants do not share the same anophthalmia, microphthalmia, or coloboma phenotypes as *gdf6a* mutants. Thus the regulatory relationship between these two genes is likely not direct and may even change through retinal development.

1.1.5. Introduction to THRβ

Thyroid hormone receptors are part of the steroid-thyroid receptor superfamily consisting of nuclear receptors, which also includes steroid, retinoid, melationin and vitamin D responsive receptors. The thyroid receptors are transcription factors that bind hormone response elements; active thyroid hormone or T_3 ligand binding instigates formation of a complex that activates the receptor to either increase or decrease gene expression (Aranda and Pascual, 2001; Cheng et al., 2010; Yen and Chin, 1994). Thyroid

hormone receptors can heterodimerize with retinoid X receptors (RXRs). Thyroid hormone receptors regulate gene expression in relation to development, differentiation, metamorphosis, growth, and metabolism (Cheng et al., 2010; Liu and Chan, 2002; Power et al., 2001).

In humans, mutations in thyroid hormone receptors cause hypothyroidism (*THR*α) or thyroid hormone resistance disorders (*THRβ*) (Ortiga-Carvalho et al., 2014). Clinical *THRβ* mutations are autosomal dominant and are suspected to create dominant negative receptors. These mutations cause metabolic and tissue-specific phenotypes like tachycardia, failure to thrive, hyperactivity, low IQ, low bone density (*THRβ1* isoform), or hearing and visual impairments (*Thrβ2* isoform) (Cardoso et al., 2014; Pazos-Moura et al., 2000; Refetoff et al., 2014; Refetoff and Dumitrescu, 2007). Most *THR* mutations occur in *THRβ*, and are characterized by elevations in thyroid hormone levels but fairly normal TSH levels (Refetoff et al., 2014). The few documented mutations in *THR*α cause delayed bone development, chronic constipation, heart defects causing slow heart rate, and impaired neural development (Moran et al., 2013; van Mullem et al., 2012). A lack of thyroid axis disturbance suggests *THR*α is not as involved in hormone axis regulation as *THRβ*.

During development in mice, *Thr*α is expressed in early neurogenesis, whereas *Thrβ* is generally inducted in later differentiation of tissues. Mouse *Thr*α1 is expressed in the adult heart and brain, whereas *Thrβ* is in predominantly the kidney, muscle, liver, retina, and pituitary gland. The first mouse *Thr*α knockouts had delayed intestine and bone maturation and died a few weeks after birth (Fraichard et al., 1997). Some mutations introduced to *Thr*α in mice are nonlethal, and these models have replicated several patient phenotypes, including variable delayed growth tied to slow bone development (O'Shea et al., 2005; O'Shea et al., 2003; Tinnikov et al., 2002) and delayed cerebellar development (Quignodon et al., 2007) with delayed granule cell differentiation. *Thr*α and *Thrβ* are both expressed in the cochlea, with *Thr*α in the cochlear and vestibular structures, and *Thrβ* in the Organ of Corti and cochlear duct (with stronger *Thrβ*1 isoform expression than *Thrβ2*). *Thrβ* loss caused shortening and thickening of the tectorial membrane (Griffith et al., 2002), delayed organ of Corti remodeling, disorganized support cells and eventual degeneration of the hair cells, leading to deafness (Ng et al., 2015).

Even heterozygous mutations of *Thrβ* can be detrimental, causing cerebellar defects and learning defects (Hashimoto et al., 2001; Kaneshige et al., 2000), which illustrates the significance of binding partners and context of tissue-specific actions.

Zebrafish have orthologues to *THR*α and *THRβ*, including two paralogues for *thr*α: *thrα**a*** and *thrα**b***. *Thrα**a*** is the more similar orthologue to human *THR*α and has two splice variants (Darras et al., 2011). *Thr*α is expressed in the blastula and gastrula stages, and may inhibit retinoic acid signaling. *Thrα**a*** is expressed in the embryonic brain (Bertrand et al., 2007; Kakizawa et al., 2007; Thisse and Thisse, 2008). *Thrβ* is expressed in the retina, midbrain, and hindbrain. *Thr*αa and *thrβ* expression begin very early (before 6hpf), drop between 6-18hpf, then rise significantly. Later in development, expression patterns in zebrafish and chick are highly similar: *thrα**a*** is found in the developing kidney, CNS, neuromast cells, heart, and pectoral fins; and *thrβ* is expressed in the embryonic pituitary, otic vesicle, and retina (Darras et al., 2011). In adult zebrafish *thrα**a*** is found in brain, heart, kidney, gastrointestinal tract, gill, and liver, whereas *thrβ* is in the eyes, brain, gill, intestine, and muscles, and both are found in the swim bladder, pectoral fins, and gonads (Liu et al., 2000). Knock down of *thrα**a*** caused microcephaly, dilated brain ventricles, and disrupted deiodinase II expression. The differences in expression during development, but also differential binding sites (Chatonnet et al., 2013) and effects on the thyroid axis (Gauthier et al., 1999) suggest *thrα**a*** and *thrβ* largely do not share roles.

Thyroid signaling is important in craniofacial development, and congenital hypothyroidism or hyperthyroidism (Hirano et al., 1995) can cause facial defects (Gamborino et al., 2001; Sperber, 1992). Thyroid hormone and retinoic acid (RA) signalling act together to regulate rostral and caudal neural crest cell development toward craniofacial development: *thrα**a*** knockdown caused failure of the neural crest to migrate, inhibited cartilage and muscle formation in the pharyngeal arches; and caused defects in anterior eye structures. *Thrα**a*** knockdown also disrupted expression of RA synthesis and degradation genes *raldh2* and *cyp26c1* in select regions, suggesting thyroid hormone signaling regulates RA availability. RA signaling was found to have opposing effects that suggests a balance of thyroid hormone and RA is required to balance anterior and posterior pharyngeal arch formation, and RXR is a likely mediator between the two in caudal pharyngeal arch formation. *Thrα**a*** knock down reduces proliferation, showing that

thyroid hormone signaling is needed to maintain neural crest cell proliferation, but also prevents differentiation if levels are too high (Bohnsack and Kahana, 2013). Like regulation of available active T_3, regulation of thyroid hormone receptor expression and activity is crucial. For example, *thrα* overexpression in zebrafish causes defects in the midbrain and hindbrain, including a disrupted midbrain-hindbrain border (Essner et al., 1999).

Currently the role of *thrαb* in zebrafish is largely unexamined. A considerably large portion of the N-terminal domains (which encode transactivation domains that enable interaction with other transcription factors) is missing, which might mean this receptor has more limited functions. *Thrαb* expression is detected starting at 4dpf, and at low levels in adult tissues: eye, liver, testis, and ovary (Takayama et al., 2008).

THRβ includes three isoforms with different expression patterns that are largely conserved among mammals, birds and amphibians: *THRβ1* is expressed in the brain, cochlea, pituitary, liver, kidney, lung, and heart (Davey et al., 1994; Forrest et al., 1990; Jones et al., 2002; Marchand et al., 2001; Murray et al., 1988; Showers et al., 1991; Weinberger et al., 1986; Wood et al., 1994; Yamano and Miwa, 1998; Yaoita et al., 1990); *THRβ2* is in the retina, cochlea, pituitary, and hypothalamus (Hodin et al., 1989; Sjoberg et al., 1992; Wood et al., 1991); and *THRβ3* is expressed in the lung and kidney (Williams, 2000). Specific deletion of the *Thrβ2* isoform in mice causes loss of M-cones. When bound by the T_3 ligand, the *Thrβ* receptor may exert either activating or suppressing effects on target genes (Santos et al., 2006; Sasaki et al., 1999; Shibusawa et al., 2003).

Mutations in *THRβ* in humans and mice cause defects in vision, hearing, and hypothalamic-pituitary-thyroid axis regulation. In mice *Thrβ1* acts in regulating the thyroid axis, as loss causes resistance to thyroid hormone (Abel et al., 1999a; Abel et al., 1999b; Ng et al., 2001b). *Thrβ2* is expressed in the inner ear of mice (Barros et al., 1998; Flamant and Samarut, 2003; Richter et al., 2011). Both *Thrβ1* and *Thrβ2* are tied to cochlear development; deletion of both isoforms causes early deafness, though isoform 1 is also important for maintenance of cochlear hair cells, as single knock outs show degeneration and resultant hearing loss (Ng et al., 2015).

Thrβ2 and *RXRγ* are required for correct opsin expression in mice. Without *Thrβ2*, M-opsin is not expressed (Ng et al., 2001a). Without *RXRγ* to dimerize with Thrβ2, S-

opsin is mis-expressed in M-cones and therefore appears in all cones (Roberts et al., 2005). *Thrβ2* and *RXRγ* also induce *Pias3* expression, which then enables Thrβ2 induction of M-opsin expression via SUMOylation (Onishi et al., 2010). *NeuroD1*-deficient mice show a similar phenotype to *Thrβ2* null mice: pan-S-opsin expression and no M-opsin. In these mice *Thrβ2* expression was reduced. Use of reporter cell lines showed increased *Thrβ2* expression with transfection of *NeuroD1*, and a *NeuroD1* responsive region was identified in an intron control region of *Thrβ*; mutation at this site reduced responsivity to NeuroD1 (Liu et al., 2008). The *Thrβ1* and *Thrα1* (Billon et al., 2002) isoforms are also expressed in mouse eye development, implying that thyroid hormone signaling has more effects in the retina that are not yet fully characterized.

The *thrβ2* isoform of zebrafish has a longer N-terminal domain and is expressed in similar patterns to mammalian *Thrβ*, including in the optic and otic vesicles, jaw cartilage, and pituitary (embryos); and the retina, gonads, and to a lesser degree, the brain, swim bladder, liver, muscle, and pectoral fins (adults) (Kaneshige et al., 2000; Marelli et al., 2016; Shibusawa et al., 2003). Thyroid hormone signalling is critical for zebrafish retinal development and function, as interference with T_3 levels or deiodinase function disrupts eye size and lamination (Baumann et al., 2016). Morpholino blocking of *thrβ* upstream intron-exon junctions caused delayed retinal lamination, incomplete development of the semicircular canals and otoliths, hypopigmentation, and kinked notochords (Marelli et al., 2016).

Importantly for this thesis, *Thrβ* and *thrβ* are expressed in the retinas of mice and zebrafish and is implicated in the development of medium wavelength-sensitive cones (or M-cones) in mice. Phenotypes in mouse knockouts of *Pax8* and *Thrβ2* indicate that Thrβ activity induces medium wavelength-sensitive cone (M-cone) fate and suppresses short wave-sensitive cone (S-cone) fate (Glaschke et al., 2010; Glaschke et al., 2011; Ng et al., 2011; Ng et al., 2010). In rainbow trout, high thyroid hormone signaling induces apoptosis in UV-sensitive cones (homologous to mouse S-cones); when thyroid signaling levels are reduced to pre-apoptotic levels, UV cones are regenerated and functionally integrated into the retinal network (Allison et al., 2006a; Raine et al., 2010). This correlation strongly implies that thyroid hormone signaling, and specifically *Thrβ* and its orthologues, has a conserved role in suppressing short wavelength-sensitive cone differentiation, maturation,

or survival (Allison et al., 2006a; Allison et al., 2006b; Hawryshyn, 2003; Raine et al., 2010; Veldhoen et al., 2006).

1.1.6. Introduction to GDF6

GDF6 is a member of the growth differentiation factor family, which belongs to the TGFβ superfamily. The transforming growth factor β (TGFβ) superfamily of regulatory proteins regulates patterning during embryogenesis (Herpin et al., 2004), and includes the TGFβ subfamily, growth and differentiation factors (GDFs) and bone morphogenetic proteins (BMPs) (related to the *Drosophila* morphogen *decapentaplegic* or *dpp*), activins, and inhibins. GDFs and BMPs are morphogens that regulate tissue patterning via gradients in multicellular organisms. For example, the *Drosophila* orthologue *dpp* is produced in a gradient along the anterior/posterior axis during wing development. GDF and BMP ligands have diverse roles in cell proliferation, survival, and differentiation. These and other TGFβ superfamily protein ligands bind to BMP and/or TGFβ receptors, which comprise heteromeric receptor complexes with type I and II serine/threonine protein-kinase receptor subunits. Ligand binding instigates SMAD phosphorylation, oligomerization, and translocation to the nucleus, where the activated SMADs regulate transcription of target genes (Derynck and Zhang, 1996; Graff et al., 1996; Hoodless et al., 1996; Macias-Silva et al., 1996; Massague, 1996).

GDF6 was first identified for its role in bone and cartilage formation in the limbs (Storm et al., 1994). *Gdf6* knockout mice have fused wrist and ankle joints, and deformities involving the inner ear cartilages (Settle et al., 2003). Mutations in *GDF6* can occur in some cases of Klippel-Feil Syndrome (Tassabehji et al., 2008) and in ocular anomalies such as microphthalmia, anophthalmia, and coloboma (Asai-Coakwell et al., 2007a; Asai-Coakwell et al., 2009). *GDF6* and its orthologues regulate patterning and cell division (Varga and Wrana, 2005; Watabe and Miyazono, 2009), and provide axon guidance cues (Augsburger et al., 1999; Butler and Dodd, 2003; Hocking et al., 2008; Sanchez-Camacho and Bovolenta, 2009; Wine-Lee et al., 2004). *GDF6* therefore plays a role in a variety of developmental processes, including dorso-ventral patterning of the neural tube, formation of the axial vasculature, limb and joint formation, neural crest differentiation, and growth

and patterning of the eye. During gastrulation in *Xenopus*, *gdf6* inhibits neural fate and induces epidermal fate (Chang and Hemmati-Brivanlou, 1999), but then later is required for the survival of the neural tube cells and retina progenitors, as well as neural differentiation in the eye and CNS (Hanel and Hensey, 2006). *Gdf6* in *Xenopus* appears to contribute to formation of the neural crest, and in rats *Gdf6* also acts in neural crest cells' development by stimulating their differentiation (Gajavelli et al., 2004).

There are two *GDF6* paralogues in zebrafish: *gdf6a* and *gdf6b* (Bruneau and Rosa, 1997; Hall et al., 2002; Rissi et al., 1995). These paralogues share 89% identity at the amino acid level (Bruneau and Rosa, 1997), and have some overlap in expression. *Gdf6a* has been more thoroughly interrogated and shares many functions with *Gdf6* orthologues in mice and *Xenopus*.

Gdf6a (formerly *radar*) shares many regulatory elements with *GDF6*, *BMP2*, and *BMP4*. Further, conservation of *cis* regulatory elements within the *gdf6a*/*radar* locus suggests that *gdf6a* and *GDF6* are highly conserved. *Gdf6a* was first identified in zebrafish as a member of the TGFβ superfamily with high homology to *GDF6*, and is implicated in establishing dorso-ventral polarity of the neural plate, dorso-ventral polarity of the retina, neural crest differentiation, and erythrocyte differentiation (Rissi et al., 1995). *Gdf6a* is expressed in parallel lines along the neural plate (which will form the dorsal neural tube and neural crest cells), in the hypochord, posterior endoderm, and ventral tail mesenchyme. Expression of *gdf6a* along the neural plate promotes dorsal neural tube identity and generation of the neural crest cells (Rissi et al., 1995). *Gdf6a* is also expressed in the primitive gut endoderm, dorsal fin, and optic cup (Hall et al., 2002; Rissi et al., 1995). Expression in the primitive gut endoderm and hypochord made *gdf6a* a candidate gene for vasculogenesis; knock down experiments revealed that while initial formation of the axial vasculature was normal, the integrity of the vessels was weakened shortly after, causing hemorrhages (Crosier et al., 2002; Hall et al., 2002). Knock down experiments to remove maternal *gdf6a* RNA contribution (Sidi et al., 2003), as well as mRNA overexpression experiments (Goutel et al., 2000), showed that *gdf6a* acts even earlier, initiating a ventralizing pathway by stimulating expression of *bmp2b* and *bmp4*, thereby contributing to the establishment of dorso-ventral patterning of the embryo. Knock down of *gdf6a* resulted in reduced *sox10* expression, a marker of neural crest cells, thus

gdf6a is necessary for specification of the neural crest cells during neurulation (Reichert et al., 2013). Like its mammalian orthologue, *gdf6a* regulates bone and joint formation; it is expressed in the pharyngeal arches, specifically in the joints and perichondrium of the hypobranchials (Reed and Mortlock, 2010). Like other BMP signaling genes (*bmp4*, *bmp2b*), *gdf6a* expression is maintained by Wnt signaling (Veien et al., 2008).

In early somitogenesis, GFP expression under a BMP responsive element (specific to BMP signaling) is detected in the dorsal and ventral edges of the myotome, with less at the midline. The muscle pioneer precursors form at the midline, and so may be negatively regulated by BMP signaling. Nguyen-Chi et al. found that knock down or mutation of *gdf6a* (*radar*) leads to reduced GFP expression and expansion of the muscle pioneer precursor domain at the midline, as well as increased numbers of differentiated muscle pioneer cells (Nguyen-Chi et al., 2012). These findings illustrate how BMP signaling plays different roles in muscle and neuron development, implying that a balance of signaling is critical for correct muscle patterning and neuromuscular junction formation.

In the retina, *gdf6a* signaling initiates dorsal identity by activating *tbx5* and *tbx2b* (Behesti et al., 2006; French et al., 2009; Gosse and Baier, 2009; Koshiba-Takeuchi et al., 2000); establishment of this dorsal identity is important for establishing the correct projections to the optic tectum, i.e. retinotectal mapping. The link between *gdf6a*'s role in zebrafish retinal development and microphthalmia in patients was first established with the *out of sight* mutant (den Hollander et al., 2010). Subsequent work with the mutant *radar* served to answer questions about the consequences of *gdf6a* loss in the developing retina.

The role of *GDF6* in retinal patterning is conserved, as loss of *gdf6a*/*Gdf6* in zebrafish, mouse, or *Xenopus* causes increased ocular apoptosis (Asai-Coakwell et al., 2007a; Asai-Coakwell et al., 2009; Asai-Coakwell et al., 2013; French et al., 2009; Gosse and Baier, 2009; Hanel and Hensey, 2006). In zebrafish this apoptosis has been linked to increased p38 MAP kinase activation and to increased expression of pro-apoptotic proteins *baxa* and *baxb*; this apoptosis can be rescued via knock down of *baxa* and *baxb*, suggesting Gdf6a signaling may prompt pro-survival mechanisms against the intrinsic apoptotic pathway. However *baxa* and *baxb* knock down did not stop photoreceptor degeneration, suggesting a separate role for *gdf6a* in photoreceptor maturation or survival

(Pant et al., 2013). This finding also leaves open the possibility that not all retinal cell types are affected equally by *gdf6a* loss.

Gdf6b (formerly *dynamo*) is expressed in the ventral posterior neural plate and then in the dorsal region of the neural plate and neural tube (Bruneau and Rosa, 1997), partially overlapping in expression with *gdf6a* (and *Xenopus gdf6*) during early embryo development. Knock down of *gdf6b* does not show an overt ocular phenotype like *gdf6a* (Asai-Coakwell et al., 2007a), indicating the two do not fully overlap in function. To date there has been considerably less investigation into the role(s) of *gdf6b*.

Gdf6 mutant mice share a similar joint defect phenotype (Settle et al., 2003) as *Tbx2* mutants. However there is no current evidence that Gdf6 signaling regulates *Tbx2* in limb development. It has been determined that Gdf6a signaling acts independently of Bmp4 in establishment of zebrafish dorsal retina fate, as *gdf6a* knock down was sufficient to eliminate phosphorylated SMAD in the retina, and knock down of *bmp4* showed no detectable retina phenotype (French et al., 2009). Zebrafish *gdf6a* mutants and morphants show reduced *bmp4* and *tbx2b* expression, suggesting Gdf6a signaling may regulate *tbx2b* both directly and possibly in conjunction with Bmp4. This is possible because BMP ligands often act in heterodimers- for example, Gdf6 is suspected to act in conjunction with Bmp2 to initiate ectoderm fate in the *Xenopus* embryo (Chang and Hemmati-Brivanlou, 1999). In contrast, in the mouse optic cup, *Bmp4* upregulates *Tbx2* directly (Behesti et al., 2006). It is not known why the role of Bmp4 in retinal patterning is not conserved between zebrafish and mice. Mutation of *Gdf6* in mice and *Xenopus*, and mutation and morpholino knock down of *gdf6a* in zebrafish lead to anophthalmia, microphthalmia and coloboma with varying penetrance (Asai-Coakwell et al., 2007a; Asai-Coakwell et al., 2013; DuVal MG, 2013; French et al., 2009; French et al., 2013; Gosse and Baier, 2009; Hanel and Hensey, 2006). The contribution of *GDF6* to photoreceptor development and survival, as well as identification of *GDF6* variants in patients with Leber's congenital amaurosis (characterized by early-onset photoreceptor degeneration) (Asai-Coakwell et al., 2013), compelled us to further examine the relevance of *GDF6* to photoreceptor development specifically.

In addition to Leber's congenital amaurosis, the potential role of *GDF6* in neurodegeneration was about to get wider. Preliminary, unpublished human genetics

data had hinted that *GDF6* is a novel disease locus in ALS, which prompted us to consider its possible contribution to neuromuscular degeneration.

1.2. Introduction to amyotrophic lateral sclerosis, SOD1, & TDP43

1.2.1. The complex genetics of ALS motor neuron degeneration

Amyotrophic lateral sclerosis (ALS) is a type of neuromuscular degeneration characterized by progressive death of the upper and lower motor neurons, and has an incidence of approximately 2/100,000. It is a complex disease that is not sufficiently explained by our current knowledge of genetics or environmental causes. The first described genetic component of ALS was mutation in [Cu-Zn] superoxide dismutase 1 (SOD1) in 1993 (Rosen et al., 1993). Since then, the genetics of ALS have expanded dramatically, with over 20 implicated genes in familial ALS (fALS) (including TDP43, FUS, C9ORF72, and UBQLN2)(Corcia et al., 2017) and candidate susceptibility loci identified in genome-wide association studies (e.g. (Du et al., 2018; Taskesen et al., 2017) and reviewed by Renton et al. (Renton et al., 2014)). The genetic components behind motor neuron degeneration and ALS in particular exceed the scope of this thesis. However while the contributions of gene variations toward motor neurons' susceptibility to degeneration, and toward the initiation and progression of numerous pathological processes that affect motor neurons in particular, is not understood, it appears significant. In fact, it is hoped that the contributions presented in this thesis will strengthen our understanding of the genetic heterogeneity behind ALS and other neurodegenerations. The sections below introduce the genes that will be the main topics of the motor neuron degeneration studies in this thesis.

1.2.2. SOD1 misfolding, toxicity, and investigations of prion-like properties

[Cu-Zn] superoxide dismutase 1 (SOD1) is featured in Chapter 4, and is a major focus of Chapters 5 and 6, thus a brief background is provided here. SOD1 is most well-known for protecting against oxidative stress, converting the superoxide anion O_2^- into O_2 or

H_2O_2, thereby clearing the free radical byproducts of cellular metabolism. But the oxidizing ability of SOD1 is utilized in other cellular processes, including activating proteins and producing peroxide to regulate signal transduction, gene expression, proliferation, differentiation, and cell death (Brown and Griendling, 2009; Rhee, 2006). SOD1 is ubiquitously expressed, acting in the cytoplasm and intermembrane region of the mitochondria (Bendotti and Carri, 2004); in cells with high energy demand including motor neurons, SOD1 activity at the mitochondria is especially critical to prevent oxidative stress and associated damage, including in the neuromuscular junction (NMJ). Extracellular SOD1 may also contribute to neuroprotection by raising intracellular calcium, possibly by activating the phospholipase C/PKC pathways (Bendotti and Carri, 2004; Harraz et al., 2008), as well as interacting with neighbouring glia and muscle tissue.

SOD1 is one of the most common genes implicated in ALS. To date as many as 185 mutations in SOD1 have been documented, primarily in cases of familial ALS (fALS) and in a minority of sporadic cases (ALS online genetics database, http://alsod.iop.kcl.ac.uk/home.aspx) (Abel et al., 2012; Brown, 1993; Corcia et al., 2017). These mutations are distributed approximately equally across the SOD1 coding sequence (Fig. 1.2), thus disruption in any region may cause disease. Based on clinical observations and modeling of in cell culture and mice, mutant SOD1 causes increased oxidative stress, ER stress, excitotoxicity, neuromuscular junction changes, mitochondrial dysfunction, disturbed axonal transport, denervation, and muscle atrophy (Boillee et al., 2006; Turner and Talbot, 2008). SOD1 function is important to motoneurons, and especially to the neuromuscular junctions, where its role is to mitigate oxidative stress (Fig. 1.3).

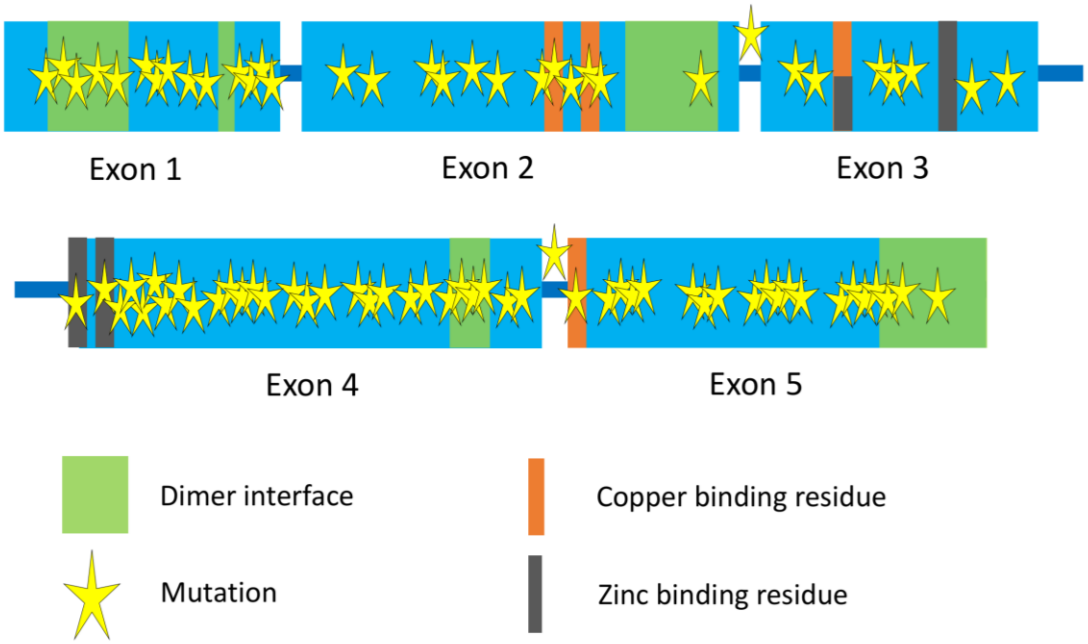

Figure 1.2. Illustrated distribution of mutations across the SOD1 peptide sequence.

Regions that form the dimer interface and metal binding sites shown. Mutations represented are non-comprehensive; sequence diagram not to scale. Diagram based on Figure 1 in Saccon et al., 2013.

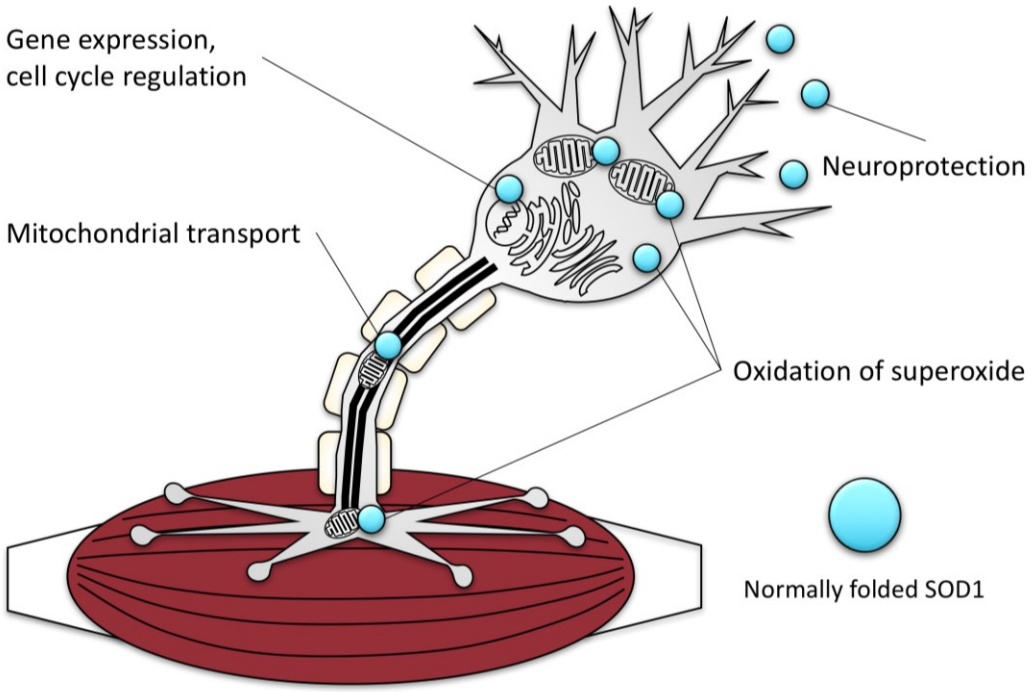

Figure 1.3. Functions of superoxide dismutase 1 (SOD1) in motor neurons. SOD1 is located in the cytoplasm, synapse and intermembrane space of mitochondria. SOD1's role is to oxidize free radicals, notably superoxide O_2^-, thereby mitigating oxidative stress. It is also secreted and thought to have neuroprotective effects extracellularly. SOD1 can change the activation states of other proteins, thereby regulating gene expression, proliferation, and differentiation. Loss of function studies have shown that SOD1 also participates in axonal trafficking of mitochondria to the synapse.

ALS, like other prion and prion-like diseases, is a proteinopathy characterized by accumulation of protein aggregates. Misfolding of mutant SOD1 protein has been interrogated in cell culture, transgenic mice, and tissues from patients with fALS (Bidhendi et al., 2016; Chia et al., 2010; Furukawa et al., 2013; Grad et al., 2015; Münch and Bertolotti, 2011; Sasaki et al., 2005; Sundaramoorthy et al., 2013a; Wang et al., 2002;

Yamagishi et al., 2007), and is suspected to play a significant role in pathology, including proposed prion-like spreading and possibly loss-of-function, though these mechanisms individually cannot fully explain motor neuron degeneration. Misfolded prions (or scrapie prions to distinguish from normally-folded prion proteins) (Prusiner, 1982) fulfill the strictest definition of prion behaviour: 1) the protein misfolds or assumes a different conformation that is detectable (historically measured via protease sensitivity or disease-specific epitopes) (Cohen and Prusiner, 1998; Fay et al., 1998); 2) critically, this conformation is capable of self-replication by exerting misfolding/conformation-altering effects on other proteins of the same type (Jucker and Walker, 2013; Petkova et al., 2005); 3) misfolded proteins can "infect" naïve cells by converting the proteins therein (termed seeding, often demonstrated *in vitro* (Bocharova et al., 2005) or by inoculating sensitized animals (Baker et al., 1994; Clavaguera et al., 2009; Kane et al., 2000; Luk et al., 2012)); and 4) misfolded protein can also spread *in vivo*, often cell to cell, and sometimes from animal to animal (Aguzzi and Calella, 2009; Caughey et al., 2009; Collinge, 2001; Jarrett and Lansbury, 1993; Prusiner, 1998) (usually considered true prion "infectivity"). The misfolded proteins characteristic of many neurodegenerations share some or most of these qualities, and so are often referred to as prion-like proteins.

It is strongly suspected SOD1 misfolding can spread in a prion-like manner. Evidence for and against prion-like mechanisms has been extensively reviewed by other colleagues (Grad et al., 2015), including observed seeded propagation *in vitro*, conformation changes (Grad et al., 2015) detected using antibodies and altered protease activity, and evidence that conversion hinges on a sequence specificity characteristic of a species barrier (Bidhendi et al., 2016; Grad et al., 2015; Munch et al., 2011). Whether this propagation is accomplished via template directed misfolding or nucleated polymerization (or perhaps both) is still to be elucidated (Grad et al., 2015; Munch et al., 2011; Prudencio et al., 2010; Witan et al., 2009). The spread of SOD1 aggregates in cell culture models strongly points to a prion-like behaviour. Uptake of mutant SOD1 in cultured neuronal cells causes aggregation of the endogenous (mutant) SOD1, which persists over cell divisions after the original seeds dissipate (Munch et al., 2011). There is evidence for mutant misfolded SOD1 inducing wildtype, normally-folded SOD1 to misfold, and misfolded wildtype SOD1 can also act as a seed in cultured cells, as aggregates of misfolded SOD1 spread from

cell to cell (Sundaramoorthy et al., 2013b). Though not yet rigorously tested, misfolded SOD1's spread *in vivo* is not inconceivable; misfolded proteins have been demonstrated to spread via macropinocytosis, exosomes, synaptic vesicles, or as dying cells release their contents (Grad et al., 2015; Munch et al., 2011). Neurons, astrocytes, and glia are known to exchange vesicle contents, and SOD1, a cytoplasmic protein, is commonly found in these. Seeding in transgenic mice that express large amounts of mutant SOD1 is currently the closest evidence for protein propagation of misfolded SOD1 *in vivo* (Bidhendi et al., 2016; Guest et al., 2011). It should be considered that delivery of misfolded SOD1 is not an accurate representation of the disease process, and seeding in this way might be accelerating disease (rather than, or in addition to, initiating misfolding). True prion-like infectivity (i.e., infection of a naïve host) has not been observed.

Though SOD1 does not currently meet the most strident definitions of being prion-like (i.e. whether or not misfolded SOD1 can induce disease in a naïve healthy individual, though there is some experimental evidence of tissue spread (Ayers et al., 2016b)), the literature supports that several mutant SOD1 proteins (including G93A (Brotherton et al., 2012), G127X (Cashman et al., 2007; Grad et al., 2011), and A4V (Ayers et al., 2017)) misfold, and misfolded SOD1 can induce template-directed misfolding of other SOD1 proteins in adjacent cells and tissues. SOD1 mutations do not occur in all cases of familial ALS (fALS), and fALS does not account for the majority of cases. If SOD1 is a primary agent of disease, the presence of misfolded wildtype SOD1 in sporadic ALS would further implicate a prion-like mechanism of spread. SOD1 inclusions have been detected in tissues of many ALS patients, including sALS with no SOD1 mutations, but whether misfolded SOD1 occurs in *all* cases of sALS is yet to be resolved (Bosco et al., 2011; Brotherton et al., 2012).

1.2.3. SOD1 models of ALS

In this section is a non-comprehensive overview of existing models of SOD1-associated ALS and insights therein regarding SOD1 behaviour in disease. Prominent

models discussed here include mice, rats, dogs, pigs, zebrafish, *Drosophila*, *C. elegans*, and a brief description of induced pluripotent stem cells (iPSCs).

SOD1 knockout mice were originally created to model ALS, and though they have a distal motor axonopathy, these mice do not develop symptoms of ALS (Reaume et al., 1996b). Knockout mice show slowly decreasing motor neuron unit counts with age, and mild increase in motor unit size; however there is no significant loss of neurons compared to wildtype mice (Shefner et al., 1999). In contrast, fALS-associated $SOD1^{G93A}$ transgenic mice show increased motor unit sizes, decline in the number of motor neuron units before onset of symptoms, and subsequently develop significant neuron loss. While there is no ALS-like pathology in SOD1 deficient mice, there is a vulnerability to motor neuron loss following axon injury; this has been attributed to susceptibility to oxidative stress (Reaume et al., 1996b). The $SOD1^{G93A}$ transgenic model also revealed variable vulnerability of the synapses. Slow-type synapses were resistant to denervation, while fast-type were more vulnerable and were lost early (interestingly, both fast and slow types showed vacuolization, suggesting pathology was ongoing in both types) (Frey et al., 2000). Further supporting that SOD1-associated ALS is a toxic gain-of-function disease, the overexpression of SOD1 WT can also cause disease or contribute to disease progression (Deng et al., 2006; Graffmo et al., 2013; Jaarsma et al., 2000).

The first transgenic mouse model expressing human mutant SOD1 was the $SOD1^{G93A}$ mouse (Gurney et al., 1994). Since then, many mouse models of SOD1 mutations replicate ALS findings such as protein inclusions, motor neuron dysfunction and loss, gliosis, and even learning deficits (G37R (Filali et al., 2011), G93A (Quarta et al., 2015)). The variability of phenotype character and severity is thought to be tied to the particular SOD1 mutation type, its expression levels, and location. One study comparing expression of SOD1 WT to $SOD1^{G37R}$ determined that the mutant line develops pathology and deteriorates faster than lines expressing SOD1 WT at higher levels (Wong et al., 1995). Some groups suggest there is a need for high expression of certain SOD1 mutants in order to induce phenotypes (e.g. SOD1 WT, G93A, D90A, G127X) (Gurney et al., 1994; Jonsson et al., 2006a), whereas other mutants perhaps not as much (e.g. G85R (Bruijn et al., 1997)). A study comparing high-expressing SOD1 mutant transgenic mouse models suggests that this high expression itself may contribute to phenotypes: excess

SOD1 may be lacking Cu^{2+} ions and are therefore inactive; excess SOD1, often misfolded, may strain protein clearance pathways above endogenous context; and levels of misfolded, detergent-resistant SOD1 remained similar between models despite large disparities in SOD1 expression level (Jonsson et al., 2006a). Limiting expression of $SOD1^{G93A}$ to neurons is sufficient to induce loss of grip strength, paralysis, neuromuscular denervation, ubiquitin and insoluble SOD1 inclusions, and increased expression of *Gfap* and *Hsp70*; but these phenotypes could only be elicited in homozygous transgenic mice, as mice with only one copy failed to develop signs of pathology (Jaarsma et al., 2008). In contrast, limiting a different mutant, $SOD1^{G37R}$, to the neurons fails to elicit a strong motor phenotype (Pramatarova et al., 2001). Expression of $SOD1^{G86R}$ in astrocytes is not sufficient to affect motor neuron function, but it does elicit an inflammatory response, which is proposed to modify disease progression (Gong et al., 2000). Deleting $SOD1^{G37R}$ from astrocytes using Cre-recombinase slowed progression, and production of inducible nitric oxide synthase, a measure of microglial activation, was reduced (Yamanaka et al., 2008). Thus specific expression of SOD1 mutants temporally or spatially have helped tease apart the roles of CNS cells outside the motor neurons. For the sake of brevity, some mouse models of human SOD1 pathology are briefly discussed below.

Overexpression of wildtype SOD1 itself in transgenic mice causes spinocerebellar axonal degeneration, mitochondrial vacuolization, gliosis, and SOD1 inclusions, but motor neuron loss occurs late, starting at 2 years of age (Graffmo et al., 2013). Co-expression of human wildtype SOD1 with SOD1 mutants appears to enhance phenotypes and speed progression, and wildtype SOD1 can be “recruited” to misfold (Deng et al., 2006; Jaarsma et al., 2000). SOD1 “dose” is important in this case as well, as experiments increasing WT SOD1 expression to match SOD1 protein levels in $SOD1^{G93A}$ transgenics caused ALS-like phenotypes and inclusions.

The $SOD1^{G93A}$ transgenic mouse replicates many disease symptoms and exhibits fairly fast disease progression, deteriorating in 17-26 weeks from symptom onset. Prior to onset of symptoms, motor neuron loss, SOD1 aggregates, and NMJ loss are detectable (Gurney et al., 1994). These mice showed motor neuron dysfunction, as measured by rotarod tests, hang wire tests, motor evoked responses, repetitive nerve stimulation tests for synapse function, nerve conduction velocity, and positive signs for spontaneous

activity (indicating denervated myofibres). These measures of dysfunction preceded motor neuron loss (Kennel et al., 1996), which was significant for demonstrating that disease is not necessarily caused by motor neuron death itself.

$SOD1^{G37R}$ and $SOD1^{D83G}$ mice show slower progression from symptom onset (25-29 weeks and 70-84 weeks respectively), and have additional phenotypes outside of motor neurons; $SOD1^{G37R}$ mice show somatosensory dulling and learning deficit, in addition to lower motor neuron signs and gliosis. $SOD1^{D83G}$ mice have sensory deficits, tremors, and both lower and upper motor neuron loss. The $SOD1^{D90A}$ mouse is interesting in that phenotypes are highly similar to those of patients. This mutation has a particularly slow progression (61 weeks) and bladder symptoms, mimicking clinical findings. This mutation also features motor neuron loss and SOD1 inclusions. $SOD1^{D90A}$ is nearly as stable as wildtype SOD1 under denaturing conditions. When human wildtype SOD1 was expressed at comparable levels to $SOD1^{D90A}$, disease symptoms were slightly lower and progression slightly slower, indicating that $SOD1^{D90A}$ is very mild and highly similar to wildtype SOD1. But wildtype SOD1 mice show more loss of ventral horn neurons compared to D90A mice, suggesting that wildtype SOD1 may have more toxicity in spinal cord (Jonsson et al., 2006b). $SOD1^{D90A}$ is thus considered less toxic than other mutations.

Other mutations modeled in mice include $SOD1^{A4V}$, which when expressed in combination with $SOD1^{WT}$, generated SOD1 inclusions, gliosis and motor neuron degeneration (Deng et al., 2006). Expression of $SOD1^{G85R}$ caused rapid disease progression and gliosis, and SOD1-ubiquitin inclusions were detectable in neurons & astrocytes (Bruijn et al., 1997). The H46R and G127X mutations also cause SOD1-ubiquitin inclusions and gliosis, with $SOD1^{G127X}$ causing rapid progression (Jonsson et al., 2004).

Work in rat models has also shown phenotypes similar to those in mice. Transgenic expression of SOD1 with the G93A mutation causes fast progression (17 weeks), vacuoles, SOD1-ubiquitin inclusions, motor neuron loss, and gliosis (Howland et al., 2002; Kashlan et al., 2015). $SOD1^{H46R}$ rats similarly had fast progression (24 weeks), motor neuron loss, SOD1-ubiquitin aggregates, Lewy-body-like hyaline inclusions, and gliosis (Nagai et al., 2001).

Dogs can develop degenerative myelopathy, a progressive neurodegeneration which is similar to human ALS (Nardone et al., 2016). Degenerative myelopathy is similar to upper motor neuron-dominant ALS, as it affects the upper motor neurons, features axonal degeneration, astrocytosis, and motor neuron phenotypes like fibrillation and electromyography signs (positive sharp waves), muscle atrophy, sensory impairment, and SOD1 inclusions. In fact, canine SOD1 mutations T18S (Awano et al., 2009) and E40K (Wininger et al., 2011) have been linked to degenerative myelopathy. Both are characterized by fast progression (21 months for T18S; 6 months-3 years for E40K), upper and lower motor neuron signs, sensory impairment, and SOD1 inclusions. It's not clear if motor neurons are lost over the course of disease, as evidence is conflicting and elective euthanasia is often performed (Morgan et al., 2013; Ogawa et al., 2014).

Deficiency in vitamin E or its related compounds in horses is detrimental to the photoreceptor outer segments, which are highly metabolically active and require robust free radical clearance; deficiency in alpha-tocopherol (α -TP) in particular is associated with pigment retinopathies in many species including mice, dogs, monkeys, horses, and humans (Davidson et al., 1998; Hayes, 1974; McLellan et al., 2003; Riis et al., 1999; Riis et al., 1981; Yokota et al., 2001; Yokota et al., 1996; Yokota et al., 1997). Vitamin E is also important for general neuron maintenance, as deficiency leads to neurological dysfunction as measured in electrophysiological studies and neuropathology, such as axonal dying back and demyelination (Muller, 2010). Specific to motor neurons, deficiency in vitamin E and/or α-TP may also cause degenerative myeloencephalopathy in foals that are genetically susceptible (Aleman et al., 2011; Finno et al., 2015; Finno et al., 2011). In older horses, prolonged vitamin E deficiency leads to equine motor neuron disease characterized by lower motor neuron weakness, which requires no genetic predisposition. These older horses show lipofuscin deposits in fundus examination and decreased B-wave amplitudes on electroretinogram, indicative of pigment retinopathy that was confirmed in horses affected by equine motor neuron disease (Finno et al., 2017; Riis et al., 1999). This is an uncommon example of retinal findings in a motor neuron disease, which is reminiscent of amyloid beta deposits detected upon funduscopy, suggesting, at the very least, that the retina is continuous with the rest of the nervous system and

susceptible to sharing pathologies. The above described neurodegenerations in dogs and in horses are the only known naturally-occurring non-human ALS-type diseases.

The neuroanatomy and physiology of the pig is closer to humans compared to rodents and more distantly related vertebrates, thus pigs can give additional, powerful context for disease progression and efficacy of possible therapeutics. Only $SOD1^{G93A}$ has been modeled thus far in pig. Much like in other animal models, G93A causes motor neuron loss, SOD1-ubiquitin inclusions, running deficits, muscle fibrillation potentials, and gliosis. However these pigs do not appear to die of disease, as they have been documented to live up to 2 years old (Yang et al., 2014).

Zebrafish are a useful model for *in vivo* screening for therapeutics, as the motor neurons are more accessible, the fish have fast generation time, and with the right tools, phenotypes can be screened quickly. Transgenic zebrafish expressing Sod1 with a G93R mutation show many typical motor neuron disease features, such as NMJ loss, motor neuron degeneration, and behaviours such as increased resting time and difficulty with respiration. Injection of mRNA encoding human SOD1 mutations causes phenotypes in the developing motor neurons. mRNA injection of $SOD1^{A4V}$ or $SOD1^{G37R}$ causes motor neuron axonopathy, including abnormal and excess branching and axonal tortuosity (Lemmens et al., 2007). Transgenic $Sod1^{G93R}$ zebrafish exhibit NMJ defects, progressive motor neuron loss, vacuolated mitochondria, and impaired swimming capacity (Ramesh et al., 2010; Sakowski et al., 2012).

Drosophila is a useful model to investigate the genetics of ALS, owing to its high tractability for gene manipulation, and for high-thoughput initial screening for therapeutics. Transgenic flies replicate some features of ALS. Transgenic expression of human $SOD1^{WT}$ elicits a Hsp70 response, and these flies show decreased synaptic transmission in the giant fiber pathway and climbing inability. $SOD1^{A4V}$ and $SOD1^{G85R}$ transgenic flies also show climbing inability (Watson et al., 2008). $SOD1^{D83S}$ transgenic flies express a SOD1 variant lacking Zn^{2+} binding, and show mitochondrial dysfunction (which can be ameliorated with NADH supplementation) and decreased locomotor activity (Bahadorani et al., 2013).

C. elegans are transparent, enabling direct visualization of motor neurons and the use of fluorescent markers *in vivo*; they also have rapid generation and high genetic

tractability, permitting rapid screening for therapeutics (Brignull et al., 2007). Expression of SOD1 WT in *C. elegans* causes a reduced thrash response and eventual paralysis. $SOD1^{G85R}$ expression also causes movement defects and paralysis, with SOD1 inclusions detectable (Wang et al., 2009a). Like $SOD1^{G85R}$, $SOD1^{G93A}$, $SOD1^{A4V}$, and $SOD1^{G37R}$ cause SOD1 inclusions and oxidative stress in the motor neurons, with $SOD1^{G93A}$ also associated with increased autophagy and axon guidance defects (Li et al., 2013; Oeda et al., 2001).

Induced pluripotent stem cells (iPSCs) have the potential to model a wide diversity of diseases while retaining individual genetic contexts, as they are derived from a patient's own cells (Han et al., 2011; Takahashi et al., 2007; Takahashi and Yamanaka, 2006). iPSCs have been used to model *SOD1*, *TDP43*, *FUS*, and *C9ORF72* mutations. iPSCs enable expression at realistic levels and gene modification to correct mutations can be tested (Kiskinis et al., 2014), as well as screening for effective therapeutics (i.e. use in personalized medicine) (Yang et al., 2013). These models can be used to interrogate disease mechanisms as well. For example, in an iPSC model with a $SOD1^{D90A}$ mutation, $SOD1^{D90A}$ protein was found to interact with neurofilament mRNA (*NF-1*), destabilizing it and altering ratios of neurofilament subunits, which lead to inclusions of neurofilament (Chen et al., 2014).

The current shortcomings of existing SOD1 ALS animal models include significant disparities between genetic models and sporadic ALS (sALS) and even other forms of fALS; while these models are accurate compared to SOD1 mutation-based ALS, it is difficult to extrapolate the findings beyond this. SOD1-related ALS features Lewy-body-like inclusions (which are infrequently documented in SOD1 models) (Tan et al., 2007), whereas other forms of ALS do not. Phenotypes that are common in both sALS and fALS are not often recapitulated in SOD1 ALS models, including TDP43 cytosolic inclusions (Robertson et al., 2007; Shan et al., 2009; Tan et al., 2007). Few studies interrogating interactions between genetics and environmental exposure (Powers et al., 2017) have been done to date, for SOD1 models or otherwise. One of the goals in Chapter 7 is to contribute to bridging this gap, by interrogating a recently described link between SOD1 and TDP43 in zebrafish.

1.2.4. Zebrafish as a model of motor neuron degeneration

Zebrafish have one gene encoding *sod1* with two splice variants, one of which is a non-coding RNA. The single zebrafish *sod1* mutant in the literature has a T70I missense mutation, which is predicted to disturb zinc binding. *Sod1* mutants have reduced enzymatic activity, resulting in increased susceptibility to oxidative stress, early NMJ phenotypes, interneuron stress, denervation of muscles (McGown et al., 2013), and adult-onset motor neuron defects such as reduced motor neurons in spinal cord and swim behaviour defects (Da Costa et al., 2014). Transgenic expression of zebrafish Sod1^{G93A} also causes NMJ defects, reduced swim capacity, muscle atrophy, loss of motor neurons (Ramesh et al., 2010), and interneuron hyperexcitability (Benedetti et al., 2016).

As a model organism of motor neuron disease, zebrafish have several advantages and drawbacks. The large range of gene editing tools, including gain or loss of gene function, transgenesis, and gene editing provides many ways to investigate genetic contributions to neurodegeneration. The ability to perform specific genomic editing with CRISPR/Cas9 can be used to model specific mutations or even edit a gene sequence to be similar to the human orthologue (i.e. “humanizing” a fish). In addition to genetic techniques, many behavioural assays are amenable to high-throughput screening (Kalueff et al., 2013; Wolman and Granato, 2012) for therapeutics and other disease modifiers (Kaufman et al., 2009; Murphey and Zon, 2006; Rihel and Schier, 2012). This screening approach was done using a SMN1 MO knockdown model, which identified axonotrophic compounds (Gassman et al., 2013; Wishart et al., 2014).

Some of the disadvantages of zebrafish for modeling motor neuron diseases involve differences in anatomy. While overall the spinal motor neurons between zebrafish and humans are similar in development and function, there are some anatomical differences. For example, there is an unclear human correlate to the zebrafish primary motor neurons (Lewis and Eisen, 2003). It is not fully known if the zebrafish fast and slow muscle types are truly comparable to human fast-twitch and slow-twitch muscles. Zebrafish slow fibers have electrophysiological similarities to the human tonic fibers in the extra-ocular muscles (Lewis and Eisen, 2003). Zebrafish fast muscle fibers are similar to human fast-twitch fibers in terms of heavy-chain myofiber isoform expression, but these features are far from comprehensive. Also, zebrafish do not have true upper motor

neurons (UMNs), as they lack a true rubrospinal tract (only a few fibers represent this) and they lack direct telencephalic projections to the spinal cord. In other words, there is no comparable corticospinal tract, thus zebrafish are not appropriate models for UMN-specific disease. In a way, the robust regenerative capacity of zebrafish may hinder the study of neuromuscular degeneration; zebrafish can regenerate neural circuitry following spinal injury (Reimer et al., 2013) and can regenerate brain cells (though genetic or environmental factors can interfere with this capacity) (Fetcho, 2007; Gemberling et al., 2013; Kizil et al., 2012; Schmidt et al., 2014).

In general, the usefulness of whole organism-based screening depends on the animal model being an accurate representation of the disease- to this end, current zebrafish models of motor neuron disease, which depend largely on mRNA overexpression or gene knockdown, are likely too simplistic or inaccurate. The use of transient genetic manipulation, notably mRNA and MO, in developing embryos risks confounding disruptions to development with relevant phenotypes. However gene knockout and other genome-editing techniques can circumvent these confounds and are not limited to the first few days of life, allowing for longitudinal study as fish age. These technologies will surely be utilized to create more robust zebrafish models of ALS in the near-future. Additional considerations for therapeutics, such as drug toxicity and interactions, can be identified in preliminary screenings with models such as zebrafish, but will require follow-up screening with models that are closer to humans in physiology, such as rats or non-human primates (which have their unique challenges as well, including higher sentience and susceptibility to stressors, thus only a shortlist of therapeutics can be considered for testing).

In this thesis, the toxic effects of SOD1 overexpression were measured in zebrafish embryos. This overexpression, especially of mutant SOD1, is known to be toxic in zebrafish models (Da Costa et al., 2014; Lemmens et al., 2007; McGown et al., 2013; Ramesh et al., 2010; Sakowski et al., 2012), though whether this toxicity is due to gain of function or loss of function (or both) remains unresolved. For the purposes of the experiments herein we assume that SOD1 has a capacity to misfold, and its propensity to misfold is modified by mutations. The misfolding of SOD1 in zebrafish has not been directly assessed, thus

modeling SOD1 misfolding in zebrafish remains an important goal, including towards better answering the questions herein.

1.2.5. TDP43 in ALS and FTD

TAR DNA-Binding Protein 43 (*TDP43*) encodes an RNA/DNA binding protein that has roles in RNA transcription, splicing, and stabilization. Mutation in *TDP43* is linked to both ALS (occuring in about 4% of fALS) (Gitcho et al., 2008; Van Deerlin et al., 2008). (Corcia et al., 2017) and frontotemporal dementia (FTD) (Cairns et al., 2007; Davidson et al., 2007; Huey et al., 2012; Neumann et al., 2006b). Inclusions of ubiquitinated, hyperphosphorylated TDP43 have been found in familial cases (Arai et al., 2006; Neumann et al., 2006a), and inclusions of wildtype TDP43 have also been detected in sporadic and non-*SOD1*/*FUS* ALS as well (Mackenzie et al., 2007; Shintaku et al., 2017; Tan et al., 2007), suggesting TDP43 may be a central component to both diseases. Surprisingly, FTD is uncommon in TDP43-ALS; one mutation, A382T, is found in ALS-FTD familial cases including in a Sardinian cohort (Floris et al., 2015), though this may be due to founder effects. Neuropathological findings in TDP43-fALS include TDP43 cytosolic inclusions in neurons and glia, often with ubiquitin and p62 (Okamoto et al., 2015).

Mislocalization of TDP43 from the nucleus to the cytoplasm may be a key step toward TDP43 pathology; aggregation of TDP43 in the cytoplasm leads to disrupted trafficking of RNA and proteins between the nucleus and cytoplasm, but aggregation in the nucleus does not cause this (Ritson et al., 2010; Woerner et al., 2016). Mouse models of mutant *TDP43* replicate many features of the diseases, including accumulation of ubiquitinated proteins (Akamatsu et al., 2013; Wegorzewska et al., 2009), progressive motor dysfunction, impaired memory, and premature death (Igaz et al., 2011a; Tsai et al., 2010). Even overexpression of wildtype human *TDP43* has been found to cause neurodegeneration and aggregation of ubiquitinated, hyperphosphorylated TDP43 in mice (Wils et al., 2010; Xu et al., 2010), and uncoordinated movement and abnormal motor neuron synapses in *C. elegans* (Ash et al., 2010a).

A large number of animal models has been created to investigate ALS and FTD. The models that recapitulate the most ALS features are discussed below. A comprehensive list is available in a review by Picher-Martel et al. (Picher-Martel et al., 2016).

Many mouse models expressing TDP43 mutations do not fully recapitulate ALS, especially motor neuron loss, subsequent paralysis, and TDP43 inclusions. What can be gleaned from these many models is that low expression of TDP43 is more correlated to cytosolic inclusions (Arnold et al., 2013; Swarup et al., 2011), whereas high TDP43 expression causes fast onset and progression, but not inclusions or motor neuron loss (Wegorzewska et al., 2009). Described below are the models that best recapitulate ALS features.

Under the *Prp* promoter, $TDP43^{WT}$ causes phosphorylated cytoplasmic inclusions, cytosolic ubiquitination, axonal degeneration, gliosis and rapid deterioration, but no motor neuron loss (Xu et al., 2010). Also under *Prp* promoter, $TDP43^{A315T}$ causes ubiquitin inclusions (these inclusions were not positive for TDP43), loss of upper and lower motor neurons, gliosis and a slower progression (Wegorzewska et al., 2009). However expression of $TDP43^{A315T}$ under the human *EP* promoter causes cytoplasmic inclusions positive for both TDP43 and ubiquitin as well as peripherin inclusions. These mice develop motor dysfunction but do not become paralyzed (Swarup et al., 2011).

Double transgenic mice for $TDP43^{WT}$ and $TDP43^{Q331K}$ under the mouse *Prp* promoter show moderate progression; cytosolic inclusions of TDP43, ubiquitin, and p62; gliosis; and significant motor neuron loss in the spinal cord anterior horn (Mitchell et al., 2015b). The findings of this double transgenic are intriguing because it has a more severe phenotype than either single transgenic. In addition, this double transgenic recapitulates most ALS features. The $TDP43^{G348C}$ transgenic mouse (under human *EP* promoter) also replicates many disease features, including inclusions of TDP43 and ubiquitin, peripherin inclusions, motor dysfunction without paralysis, and gliosis (Swarup et al., 2011).

Other animal models of TDP43 mutations include transgenic rats, *Drosophila*, *C. elegans* and zebrafish. Interesting findings from these models include a rat model of $TDP43^{M337V}$, which displays rapid onset and progression, and degeneration of the ventral root, dorsal root, and corticospinal tract. No TDP43 cytoplasmic inclusions were found, but ubiquitin inclusions were (Huang et al., 2012). Interestingly, overexpression of

TDP43^{WT} in *C. elegans* (Ash et al., 2010b; Liachko et al., 2010) or in zebrafish (Kabashi et al., 2010; Laird et al., 2010) does not cause overt phenotypes, whereas overexpression of TDP43 mutants does. Numerous other models have been created for other ALS-associated genes such as *C9ORF72* and *FUS*, and some models exist for less common mutations as well (*UBQLN2*, *OPTN*). For the sake of brevity these models will not be reviewed here.

1.3. Summary of Thesis Goals & Hypotheses

1.3.1. Elaborate the Cone Photoreceptor Development Regulatory Network

One of the primary goals in this thesis is to expand our knowledge of the regulation of cone photoreceptor subtype development. For the contents of Chapters 2 and 3, my research focuses on describing the roles of the following factors on cone photoreceptor subtype development: *gdf6a*, *tbx2b*, and *thrβ*. In the final discussion in Chapter 8, I will discuss future directions and re-visit the importance of understanding cone development to restoring lost vision in patients.

GDF6 was initially suspected to play a role in cone photoreceptors when mutations were identified in a panel of patients suffering from a photoreceptor degeneration: Leber's congenital amaurosis (Asai-Coakwell et al., 2013). When we had successfully raised homozygous *gdf6a* mutants to adulthood, we were able to determine that zebrafish *gdf6a* mutants, like their human and mouse equivalents, exhibited degeneration of the photoreceptor layer. Based on these findings, we hypothesized that *gdf6a* was required for cone photoreceptors to develop and/or survive. The UV cone and rod phenotypes in zebrafish *tbx2b* had also been published shortly before. Between *gdf6a* and *tbx2b*'s shared pathway in early dorsal retina formation, and their implicated roles in cone photoreceptor development, we hypothesized that these factors interact in cone development. We hypothesized that this relationship would be epistatic, where *gdf6a* acts upstream of *tbx2b* in promoting UV cones.

The requirement of *Thrβ* for M-cone development in mice and the thyroid hormone-induced loss of UV cones in rainbow trout lead us to hypothesize that *thrβ* would have

similar effects in zebrafish: promoting red cones (homologous to M-cones) and suppressing UV cones. An additional novel phenotype of increased blue cones in our dominant negative *thrβ* model prompted us to investigate if *thrβ* interacts with *tbx2b* in the development of UV cones or with *gdf6a* in development of UV, blue, or red cones. We hypothesized that *thrβ* and *tbx2b* have opposing effects in the same pathway of UV cone development, and that *thrβ* would act downstream of *gdf6a* in both UV and blue cone development.

1.3.2. Roles of gdf6a, SOD1, and TDP43 in ALS Motor Neuron Degeneration

The research described in Chapters 4, 5, 6, and 7 focuses on specific aspects of SOD1 and ALS that contribute to disease variability and complexity: 1) variations in function of disease modifier genes can influence motor neuron health and susceptibility to progressive dysfunction and degeneration; 2) predicting and testing amino acid changes in SOD1 that may alter protein stability and toxicity; and 3) describing intersections between known agents of ALS pathology (SOD1 and TDP43) in order to better understand the induction of SOD1 toxicity and the complex genetics of ALS, and to perform initial screening of test candidate compounds to alleviate SOD1 toxicity.

ALS is suspected to result from a complicated interplay of factors, and the roles of many genes are significant but difficult to deconstruct. *Gdf6a*, a gene already under our investigation in photoreceptor development, emerged as a candidate modifying gene in the maintenance of neuromuscular junctions, which are critical for motor neuron function. Because we were able to grow *gdf6a* mutants to adulthood and allow them to age, we could longitudinally investigate their neuromuscular condition. Based on evidence of BMP actions in neuromuscular junction growth and maintenance (including in *Drosophila* (McCabe et al., 2003; Ratnaparkhi et al., 2008), mice (Nakamura et al., 2008; Nakamura et al., 2013; Nakamura et al., 2012), and implicated in some cases of ALS (Bayat et al., 2011; Ruschke et al., 2012)), we hypothesized that *gdf6a*, a BMP receptor ligand, may have a modifying role in neuromuscular junction health (Chapter 4).

SOD1 remains one of the most prominent genes in ALS, and much evidence points to misfolded SOD1 protein being a culprit in motor neuron dysfunction. Both at the

beginning of the research program and currently, the mechanisms behind SOD1 misfolding continue to be contemplated. In conjunction with collaborators, we sought to create models for SOD1 that could predict and test the effects of mutations on protein stability (modeled *in silico*), on aggregation (as indirect measures of potential to misfold), and on motor neuron toxicity *in vivo*. We hypothesized that mutations that reduce protein stability would cause SOD1 to aggregate and would increase toxicity when expressed in zebrafish (Chapter 5). Previous work by our collaborators identified a specific amino acid in SOD1 that appeared critical for misfolding *in vitro*: the tryptophan W32. Based on this, we hypothesized that this tryptophan would also be important for SOD1 toxicity in zebrafish, and could serve as a target for candidate therapeutics identified by additional collaborators using *in silico* pharmacophore modeling (Chapter 6). Finally, we used zebrafish to investigate a novel interaction between SOD1 and TDP43 that had been documented in cell culture. We hypothesized that the toxicity of SOD1 may be mediated by TDP43 via the tryptophan W32 in SOD1 and one or more tryptophans in TDP43 (Chapter 7).

Chapter 2. *gdf6a* is required for cone photoreceptor subtype differentiation and for the actions of *tbx2b* in determining rod versus cone photoreceptor fate

This chapter comprises the publication of the same title: DuVal MG, Oel AP, Allison WT (2014) *gdf6a* Is Required for Cone Photoreceptor Subtype Differentiation and for the Actions of *tbx2b* in Determining Rod Versus Cone Photoreceptor Fate. PLOS ONE 9(3): e92991. https://doi.org/10.1371/journal.pone.0092991 (DuVal et al., 2014b).

The questions, hypotheses, and experiments in this chapter were conceived and designed by MGD, APO, and WTA. Contributions to experiments are as follows: measuring microphthalmia in *gdf6a* and *tbx2b* mutants by MGD and APO; expression of *tbx2b* via *in situ* hybridization by APO; cone subtype abundances in mutants by MGD and APO; generation and validation of the 10C9.1 antibody by WTA; measuring the *lor* phenotype in mutants by MGD and APO; linkage analysis design and genotyping by APO. Histology shown in Fig. 2.4.1 was prepared by WTA, Arlene Oatway, and Neel Doshi. Data analysis was performed by MGD, APO, and WTA. Manuscript writing was performed by MGD and WTA, with editing contribution from APO.

2.1. Summary

Functional vision restoration is within reach via stem cell therapy, but one of the largest obstacles is the derivation of colour-sensitive cone photoreceptors that are required for high-acuity daytime vision. To enhance progress made using nocturnal murine models, we instead utilize cone-rich zebrafish and herein investigate relationships between *gdf6a* and *tbx2b* in cone photoreceptor development. Growth/differentiation factor 6a (*gdf6a*), a bone morphogenetic protein family ligand, is an emerging factor in photoreceptor degenerative diseases. The T-box transcription factor *tbx2b* is required to specify UV cone photoreceptor fate instead of rod photoreceptor fate. Interactions between these factors in cone development would be unanticipated, considering the discrete phenotypes in their respective mutants. However, *gdf6a* positively modulates the abundance of *tbx2b* transcript during early eye morphogenesis, and we extended this conclusion to later stages of retinal development comprising the times when

photoreceptors differentiate. Despite this, *gdf6as327/s327* larvae possess a normal relative number of UV cones and instead present with a low abundance of blue cone photoreceptors, approximately half that of siblings ($p<0.001$), supporting a differential role for *gdf6a* amongst the spectral subtypes of cone photoreceptors. Further, *gdf6a*$^{s327/s327}$ larvae from breeding of compound heterozygous *gdf6a*$^{+/-}$;*tbx2b*$^{+/-}$ mutants exhibit the recessive *lots-of-rods* phenotype (which also shows a paucity of UV cones) at significantly elevated rates (44% or 48% for each of two *tbx2b* alleles, χ^2 $p\leq0.007$ for each compared to expected Mendelian 25%). Thus the *gdf6a*$^{s327/s327}$ background sensitizes fish such that the recessive *lots-of-rods* phenotype can appear in heterozygous *tbx2b*$^{+/-}$ fish. Overall, this work establishes a novel link between *tbx2b* and *gdf6a* in determining photoreceptor fates, defining the nexus of an intricate pathway influencing the abundance of cone spectral subtypes and specifying rod vs. cone photoreceptors. Understanding this interaction is a necessary step in the refinement of stem cell-based restoration of daytime vision in humans.

2.2. Introduction

The genetic regulation of cone photoreceptor differentiation from retinal progenitor cells is a critical knowledge gap hindering stem cell therapy as a feasible solution for clinical vision restoration. Such therapies promise treatment in patients with a breadth of retinal disease including retinitis pigmentosa and macular degeneration. Identifying pathways that promote cone photoreceptor fates, rather than rod photoreceptor fates, is particularly critical due to the reliance of the human visual system on cones for its most important functions: daytime vision, colour discrimination and high visual acuity.

Apart from this, current efforts to refine stem cell therapy more prominently include the identification of intrinsic genetic factors that regulate progenitor fate. Sorting of photoreceptor progenitor cells for implantation is the most efficient contemporary approach, employing expression of photoreceptor lineage-specific genes (e.g. *NRL, CRX*, and *NEUROD*) to facilitate the isolation of progenitor cells destined to develop into the photoreceptors of interest (Lakowski et al., 2010; Lakowski et al., 2011; MacLaren et al., 2006; Mansergh et al., 2010; Mears et al., 2001; Seko et al., 2012). From this perspective,

the current list of genes with roles in cone development remains too short for the purpose of development of functional cones that can integrate into an existing retinal structure, thereby sufficiently restoring functional daytime vision. This list consists largely of *TRβ*, *RXRγ*, *RORα*, *RORβ*, *COUP-TF,* (Fujieda et al., 2009; Roberts et al., 2005; Satoh et al., 2009; Seko et al., 2012; Srinivas et al., 2006a) and *tbx2b* (Alvarez-Delfin et al., 2009).

The functions of photoreceptor genes have largely been investigated in mice, especially in the context of degenerative disease (Mears et al., 2001; Milam et al., 2002; Ng et al., 2001b; Sharon et al., 2003), however the innately low cone photoreceptor density in murine models has meant that an understanding of cone photoreceptor specification has lagged behind that of rod photoreceptors. A complementary animal model promises to expand the list of genes and regulatory pathways in cone photoreceptor development: the zebrafish. The retina of zebrafish is structurally and functionally conserved to that of humans, and, due to the diurnal nature of zebrafish, it is cone-rich akin to the human macula. Zebrafish possess rods and four cone spectral subtypes (ultraviolet- (UV-), blue-, green- and red-sensitive cones), which are spatially arranged in a highly regular heterotypical mosaic (Allison, 2004; Allison et al., 2010a; Allison et al., 2004; Raymond et al., 1995b; Raymond et al., 1993a; Takechi and Kawamura, 2005; Vihtelic et al., 1999). In addition, zebrafish undergo external development, allowing for ease of observation and experimental manipulation, supported by a diverse genetic toolbox (e.g. mutants and transgenics). Of particular benefit to the study of stem cell therapy is the robust intrinsic regenerative capacity of the zebrafish CNS, which is the target of enthusiastic scrutiny (Becker et al., 1998; Becker et al., 1997; Easter and Hitchcock, 2000; Fausett and Goldman, 2006; Fleisch et al., 2011; Goldshmit et al., 2012; Kaslin et al., 2008; Kroehne et al., 2011; Lamba et al., 2008a; Matsukawa et al., 2004; Senut et al., 2004). In further pursuit of understanding this regenerative capacity, we have recently engineered conditional ablation of cone photoreceptors and argue that spatial cues of the remaining photoreceptor cells have substantial influence on the identity of regenerating photoreceptors (Fraser et al., 2013a).

Considering the great promise of zebrafish to become the premier model of photoreceptor regeneration, it is surprising that few regulatory factors in photoreceptor development are yet to be characterized in fish. One example is thyroid hormone, which

initiates UV cone death and regeneration in trout (Allison et al., 2006a; Allison et al., 2006b; Browman and Hawryshyn, 1994; Veldhoen et al., 2006) and modulates the maximal wavelength sensitivity of cones in zebrafish (Allison, 2004). Building on this, thyroid hormone receptor β has been shown to effect cone specification in mice (Ng et al., 2011; Ng et al., 2001b) and more recently in zebrafish (Suzuki et al., 2013a). We proposed that, during trout cone photoreceptor regeneration, thyroid hormone modulates a switch in progenitor specification very much akin to that described below, wherein UV cones are produced at the expense of rod photoreceptors (Allison et al., 2006a).

Another regulator of photoreceptor fate described in zebrafish is *tbx2b*, a transcription factor of the T-box family homologous to the mammalian gene *TBX2*. *Tbx2b* is required for neuronal differentiation in early retinal development and for maintaining dorsal retina identity during patterning of the dorsal-ventral axis (Gross and Dowling, 2005b). Mutation of *Tbx2* in mice results in microphthalmia (Behesti et al., 2009). This is in agreement with its position downstream of bone morphogenetic protein 4 (*BMP4*), mutations in which cause microphthalmia in humans and mice. Of great interest herein, *tbx2b* plays a role in promoting UV cone fate vs. rod fate late in zebrafish retinal development, as demonstrated by excess rods and few UV cones (denoted as the "*lots-of-rods*" phenotype) in *tbx2b* mutant fish (Alvarez-Delfin et al., 2009). One recessive allele, *tbx2b*^{fby} (also known as *tbx2b*^{c144}), is reasonably considered to be a null allele due to a nonsense mutation in the sequence encoding its DNA-binding T-box domain (Snelson et al., 2008b). Homozygous mutants of *tbx2b*^{fby} exhibit a severe form of the *lots-of-rods* phenotype, wherein few or no UV cones can be detected. A second recessive allele is *tbx2b*^{lor} (also known as *tbx2b*^{p25bbtl}), presumed to be a hypomorph because it generates a less severe form of the *lots-of-rods* phenotype, exhibiting a substantial reduction in the abundance of UV cones compared to wild type fish, but not to the degree observed in *tbx2b*^{fby} mutants. The location and nature of the *tbx2b*^{lor} mutation is unknown; however, based on linkage analysis and its failure to complement the *tbx2b*^{fby} allele, it is inferred to be near the coding region for *tbx2b*, but not within it (see (Alvarez-Delfin et al., 2009) and Results herein).

In recent studies, we and others identified *gdf6a* as a candidate regulator of cone photoreceptor development and disease (Asai-Coakwell et al., 2013; Gosse and Baier,

2009; Zhang et al., 2012). *Gdf6a* is a BMP gene in the transforming growth factor β (TGFβ) ligand super-family; *gdf6a* induces dorsal retina fate during ocular morphogenesis, lying upstream of other dorsal patterning genes. Disruption of human *GDF6* and homologs in mice, *Xenopus* or zebrafish produces anophthalmia, microphthalmia and coloboma with varying degrees of penetrance and severity (Asai-Coakwell et al., 2007a; Asai-Coakwell et al., 2013; DuVal MG, 2013; French et al., 2009; Gosse and Baier, 2009; Hanel and Hensey, 2006). The recessive *gdf6a* null allele used in this study, *gdf6a*^{s327}, causes microphthalmia in homozygous zebrafish mutants. Zebrafish knock-downs and mutants of *gdf6a* have down-regulation of *tbx2b* early in retinal development (French et al., 2009; French et al., 2013; Gosse and Baier, 2009), while over-expression of *gdf6a* likewise increases expression of *tbx2b* in the developing zebrafish retina (Gosse and Baier, 2009), indicating a tight regulation of *tbx2b* transcription by *gdf6a*. Based on this evidence, *gdf6a* is upstream of *tbx2b* in a pathway of dorsal retina patterning; however zebrafish mutants of *tbx2b* (*tbx2b*$^{lor/lor}$ and *tbx2b*$^{fby/fby}$) do not exhibit microphthalmia.

Mutations in *GDF6* were recently found to be associated with age-related macular degeneration and Leber's congenital amaurosis, both representing photoreceptor degenerative disease (Asai-Coakwell et al., 2013; Zhang et al., 2012). Further, we demonstrated that the retinas of zebrafish *gdf6a*$^{s327/s327}$ mutants exhibit photoreceptor deficits (Asai-Coakwell et al., 2013), together indicating that disruption of *GDF6* leads to photoreceptor degeneration, which marks *gdf6a* as a potential regulatory factor in the differentiation and/or maintenance of cone photoreceptors.

These commonalities between *gdf6a* and *tbx2b*, including both in early ocular morphogenesis and photoreceptor differentiation/maintenance, led us to hypothesize that *gdf6a* may also modulate *tbx2b* during the regulation of UV cone and/or rod photoreceptor fate specification. Establishing this type of genetic pathway in photoreceptor development would impact the direction of future studies by offering a much-needed springboard toward uncovering further signaling pathways and genetic interactions specific to cone photoreceptors. With such knowledge, stem cell therapy can be refined to procure more cone photoreceptors than using current methods, thereby enhancing functional, daytime vision restoration.

In this study we examined the relationship between the roles of *gdf6a* and *tbx2b* in photoreceptor development. We determined that these two genes do not share a genetic interaction in microphthalmia. Further, while disruption of *gdf6a* does not in itself lead to the predicted disruption of UV cone and rod abundances, *gdf6a* loss-of-function reduces the threshold for *tbx2b* mutations to manifest photoreceptor phenotypes.

2.3. Methods

2.3.1. Ethics statement

Fish care and protocols were approved by the Animal Care and Use Committee: Biosciences at the University of Alberta. Rat care and protocols were approved by the Animal Care Committee at the University of Victoria. In each instance protocols and care were in accordance with the Canadian Council on Animal Care.

2.3.2. Animal Care and Establishment of Mutant Crosses

Zebrafish (*Danio rerio*) were raised and maintained according to standard procedures (Westerfield, 2000b). Larvae were kept at 28°C in E3 media. *Gdf6a*$^{s327/+}$ (Gosse and Baier, 2009) (ZFIN ID ZDB-ALT-050617-10), *tbx2b*$^{p25bbtl/p25bbtl}$ (ZFIN ID ZDB-GENO-080920-2, referred in text and figures as *tbx2b*$^{lor/lor}$)(Alvarez-Delfin et al., 2009), and *tbx2b*$^{c144/+}$ (ZFIN ID ZDB-GENO-130130-6, referred in text and figures as *tbx2b*$^{fby/+}$) (Clanton et al., 2013; Snelson et al., 2008b) fish were gifted from Andrew Waskiewicz (University of Alberta), James Fadool (Florida State University), and Josh Gamse (Vanderbilt University) respectively. These lines were crossed to create [*gdf6a* $^{+/s327}$ *; tbx2b*$^{+/lor}$] and [*gdf6a* $^{+/s327}$ *; tbx2b*$^{+/fby}$] compound heterozygous mutants, which were subsequently in-crossed to acquire [*gdf6a* $^{s327/s327}$ *; tbx2b*$^{lor/lor}$] and [*gdf6a* $^{s327/s327}$ *; tbx2b*$^{fby/fby}$] compound homozygous mutants along with siblings of various genotypic combinations. The *gdf6a*$^{s327/s327}$ and *tbx2b*$^{lor/lor}$ lines were also crossed with transgenic lines: Tg(-5.5opn1sw1:EGFP)kj9 (Takechi and Kawamura, 2005) and Tg(-

3.5opn1sw2:mCherry)^{ua3011} (Duval et al., 2013; Fraser et al., 2013a) expressing fluorescent proteins in UV and blue cones, respectively.

2.3.3. Assessing Phenotypes, Genotyping and Linkage Analysis

Larvae from the above-described mutant lines were assessed for phenotype and, where noted, subsequently genotyped. *Gdf6a* $^{s327/s327}$ larvae were identified by their microphthalmic phenotype starting at 3dpf. Where relevant, eye size-to-body length ratios were calculated to check for an intermediate eye size phenotype (details below). To identify putative *tbx2b*^{lor} or *tbx2b*^{fby} homozygous mutants, larval retinas were removed from the heads, flatmounted, imaged on a Zeiss Axio Observer.Z1 microscope with AxioCam software (Carl Zeiss MicroImaging, Oberkochen), and thereby screened for the *lots-of-rods* phenotype, characterized by an abnormally large population of rod photoreceptors and a small population of UV cones, which is exacerbated in *tbx2b*$^{fby/fby}$ mutants (Alvarez-Delfin et al., 2009). Heterozygous mutant and wildtype *gdf6a* and *tbx2b* siblings, which do not have a phenotype, were identified by genotyping.

Genomic DNA was isolated as described by Meeker et al. (Meeker et al., 2007). Genotyping for *gdf6a*^{s327} was done by restriction fragment length polymorphism (RFLP) analysis. Primers designed by Gosse and Baier (Gosse and Baier, 2009) amplify a 280bp region including the *gdf6a*^{s327} locus. This PCR product was either digested with SfaNI restriction enzyme and run on a gel, or sequenced with a BigDye v3.1 kit (Invitrogen, Carlsbad, Cat. # 4337455) and submitted to Molecular Biology Services Unit at the University of Alberta. *Tbx2b*^{fby} was genotyped through RFLP analysis; primers used were designed by Snelson et al. (Snelson et al., 2008b) and amplify a 318bp region featuring the *tbx2b*^{fby} locus. The PCR product was digested with MseI restriction enzyme and run on a gel.

The lesion of the *tbx2b*^{lor} allele has been linkage-mapped to the region of *tbx2b* (Alvarez-Delfin et al., 2009), but has not yet been identified. Therefore, genotyping fish for *tbx2b*^{lor} required developing a single nucleotide polymorphism (SNP) genotyping assay, and inferring the *tbx2b* genotype. We explored six SNPs annotated in the zebrafish *tbx2b* gene in the *Ensembl* database; using Geneious software, we designed primers to

amplify each of the SNPs to genotype via sequencing (performed at Molecular Biology Service Unit, University of Alberta) (Table 2.2). Each SNP was amplified from representative adult male *tbx2b*$^{lor/lor}$ fish, and from representative adult female *gdf6a*$^{s327/s327}$ fish, and examined for homozygosity at each SNP. While several homozygous SNPs were identified, only two were different between the two populations, and one synonymous SNP (bold text in Table 2.2) was chosen based on the reliability of PCR amplification and sequencing (Fig. 2.6E). Thus, the presence of an "A" in this SNP implied inheritance of the parental *tbx2b*^{lor} allele, while presence of a "T" implied the parental WT allele (in fish with mutation in *gdf6a*). These adult fish were crossed, and all resulting [*gdf6a*$^{+/s327}$; *tbx2b*$^{+/lor}$] fish were confirmed to be heterozygous at the relevant SNP. In-crossing these compound heterozygotes and genotyping the resultant normophthalmic progeny confirmed that the SNP genotyping assay consistently predicts the *lots-of-rods* phenotypes.

Table 2.1. Primers used to identify single nucleotide polymorphisms (SNPs) for *tbx2b* genotyping.

SNP:	FWD primer	REV primer	Size (bp)
rs40785418	TGC GCT TGA ATG GAC ATC CGC A	AAG GCG AGA GCA GAC AGC GG	196
rs40952575	**CGG ACC ATA CCC TGG CCG GA**	**TGG TCC CAT AGA TCC TTC GCT TCC A**	160
rs41094432	CTG CCG ACG ACT GCC GCT AC	TCC CCA GTA GCT GGG CTA TCC G	115
rs41247043 rs40724179	CCG CAT TGC CAA GCG GCC TA	TGA CGA AGT CTC CCG CTG GCT	194

SNP names from http://www.ncbi.nlm.nih.gov/snp/, SNP ultimately used for genotyping in this study is in bold.

2.3.4. Generation of rat monoclonal against UV opsin

Generation of rat monoclonal antibodies against UV opsin was performed by Immunoprecise Antibodies Ltd (Victoria BC, Canada) using standard intraperitoneal injection method. Two F344 female rats were immunized with a recombinant antigen designed to mimic the N-terminus of trout UV opsin (NCBI accession NP_001117793.1) (Allison et al., 2003; Dann et al., 2004), see Appendix 1, Figure A1.1. Sera from hyperimmunized rats had been found to be specific against both trout and zebrafish UV opsin in immunohistochemistry and/or Western blots (Allison, 2004; Allison et al., 2006a). Lymphocytes were harvested from the spleen of the best responding rat and fused with rat myeloma YB2/0 to generate the hybridomas. Supernatants from a panel of clonal cells were screened for robust and specific labeling of zebrafish UV cones, and a successful clone was subcloned to generate line 10C9.1.

2.3.5. Immunocytochemistry and in situ hybridization

Immunocytochemistry was performed on larval zebrafish and retinal sections as previously described (Fraser et al., 2013a) to label relevant structures. Briefly, larvae were fixed in 4% paraformaldehyde with 5% sucrose made in PO_4, pH 7.4 (PFA) overnight at 4°C. Following fixation, washes of 1.0M PO_4/5% sucrose, 1% Tween/H2O (pH 7.4), and acetone were performed. Blocking was done for 90 minutes with 10% NGS/PBS^{3+} (PBS^{3+}— phosphate buffered saline with 1% Tween, 1% Triton-X and 1% DMSO, pH 7.4), followed by incubation in antibody in 2% NGS/PBS^{3+} overnight at 4°C. Primary antibodies and dilutions are as follows: 4C12 anti-rod opsin (ZFIN ID: ZDB-ATB-090506-2, 1:200) (Morris et al., 2005), zpr-3 anti-rod opsin (ZFIN ID: ZDB-ATB-081002-45, 1:200); zpr-1 anti-arrestin3a labels double cones (ZFIN ID: ZDB-ATB-081002-43); and 10C9.1 anti-UV opsin (generated herein as described above, 1:100). Larvae were then incubated in secondary antibody in 2% NGS/PBS^{3+} overnight at 4°C. Secondary antibodies used are as follows: Alexafluor anti-mouse 555 (Invitrogen, Carlsbad, Cat. #A-31570) (1:1000), Alexafluor anti-rabbit 488 (Invitrogen, Carlsbad, Cat. #A-21441) (1:1000). Deviations from the above protocol include using PBS/0.01% Tween in lieu of PBS^{3+} and omitting the 1.0M PO_4/5% sucrose wash. Retinas were dissected from the head and flatmounted for imaging. Immunohistochemistry on retinal sections followed the same protocols applied instead to 10 μm cryosections of adult eyes prepared as described previously (Fraser et al., 2013a) (Duval et al., 2013).

In situ hybridization for photoreceptor opsins and *tbx2b* expression was performed as previously described (Allison et al., 2010a) using DIG- and FLR-labeled riboprobes against blue-sensitive cone opsin (opn1sw2, 1424bp, Accession No. AF109372, ZFIN ID: ZDB-GENE-990604-40), UV-sensitive cone opsin (opn1sw1, 1777bp, Accession No. NM_131319, ZFIN ID: ZDB-GENE-991109-25), rod opsin (1584bp, Accession No. NM_131084, ZFIN ID: ZDB-GENE-990415-271), or *tbx2b* (1144bp) (French, 2010) (2616bp, Accession No. NM_131051, ZFIN ID: ZDB-GENE-990726-27). Briefly, larvae were fixed in 4% PFA overnight at 4°C, then permeabilized in MeOH overnight at -20°C. Larvae underwent 30 minutes of digest in Proteinase K at 37°C and were incubated in Hauptmann's prehybridization solution at 65°C for between 2 hours and overnight, depending on the riboprobes used. Subsequently larvae were hybridized with riboprobe

for at least one night at 65°C. Blocking with Maleate Tw/2% DMSO/2% RMB was done for 2 hours prior to riboprobe detection using either 1:100 anti-digoxigenin-POD (Roche, Québec, Cat. # 11 207 733 910) or 1:100 anti-fluorescein-POD (Roche, Québec, Cat. #11 426 346 910) overnight at 4°C. Larvae were then incubated in tyramide-conjugated fluorochrome according to manufacturer's instructions (Invitrogen, Carlsbad, Cat. #T-20912; T-30954).

Imaging was performed with a Zeiss Axio Observer.Z1 microscope with AxioCam software (Carl Zeiss MicroImaging, Oberkochen). Images were manipulated for channel colour and brightness in AxioCam (Carl Zeiss MicroImaging, Oberkochen), Imaris x64 (version 7.4.0, Bitplane, Badenerstrasse), or Adobe Photoshop CS5 Extended (Adobe Systems Inc., San Jose).

2.3.6. Histology

Paraffin sections of adult zebrafish heads fixed in PFA were prepared using standard protocols. Staining of sections with hematoxylin and eosin occurred after dewaxing. Sections were imaged on an Axioscope A.1 microscope (Carl Zeiss MicroImaging, Oberkochen) using a 12-bit, 2 megapixel MacroFIRE colour camera (Optronics, Goleta CA).

2.3.7. Data Analysis

Photoreceptor abundance was measured in flatmounted retinas by counting labeled cells within a 100µm x 100µm area dorsal to the optic nerve head or, if this location was not obvious, sampling an area containing a minimum of 100 cells of each labeled photoreceptor type. Eye-to-body ratios were calculated using values from measuring the largest width of the eye, and the body length from nose to end of notochord. Cell counts and eye-to-body measurements were performed in ImageJ 1.45 (Wayne Rasband, National Institutes of Health, Bethesda; http://rsbweb.nih.gov/ij/index.html) and statistical analysis was performed in SYSTAT 12 (Systat Software Inc., Chicago) and R (Robert Gentleman and Ross Ihaka, University of Auckland; http://www.r-project.org).

2.4. Results

2.4.1. Gdf6a and tbx2b do not genetically interact in any apparent way regarding the microphthalmic phenotype.

Loss of function in homologues of *GDF6* induces microphthalmia in zebrafish, mice and humans (Asai-Coakwell et al., 2007a; Asai-Coakwell et al., 2009; den Hollander et al., 2010; Gonzalez-Rodriguez et al., 2010; Okada et al., 2011). Further, mutation of *Tbx2* in mice likewise causes microphthalmia (Behesti et al., 2009). Considering that *gdf6a* is upstream of *tbx2b* during early eye morphogenesis in zebrafish (Gosse and Baier, 2009), we hypothesized that simultaneous disruption of both these genes would interact to increase the rate or severity of microphthalmia. We had anticipated that establishing the nature of the genetic interaction between *gdf6a* and *tbx2b* in early eye morphogenesis might be important to provide direction to, or potentially confound, our investigations of *gdf6a* and *tbx2b* in cone photoreceptor differentiation, which occurs later in retinal development.

Microphthalmia is apparent in homozygous *gdf6a*$^{s327/s327}$ larvae by 3 days post-fertilization (dpf), but is not observed in mutants for *tbx2b*$^{lor/lor}$ or *tbx2b*$^{fby/fby}$ through any age (Fig. 2.1A, Fig. 2.2A). Microphthalmic eyes in *gdf6a*$^{s327/s327}$ fish persist to adulthood, exhibiting variably small eyes (or none at all), while eyes in *tbx2b* mutants develop normally. Paraffin sections demonstrate the microphthalmic eyes as they are positioned in the heads of *gdf6a*$^{s327/s327}$ adult fish, with developed but irregularly-shaped lens and a lack of retinal lamination (Fig. 2.1B, C, D), consistent with our recent studies [43].

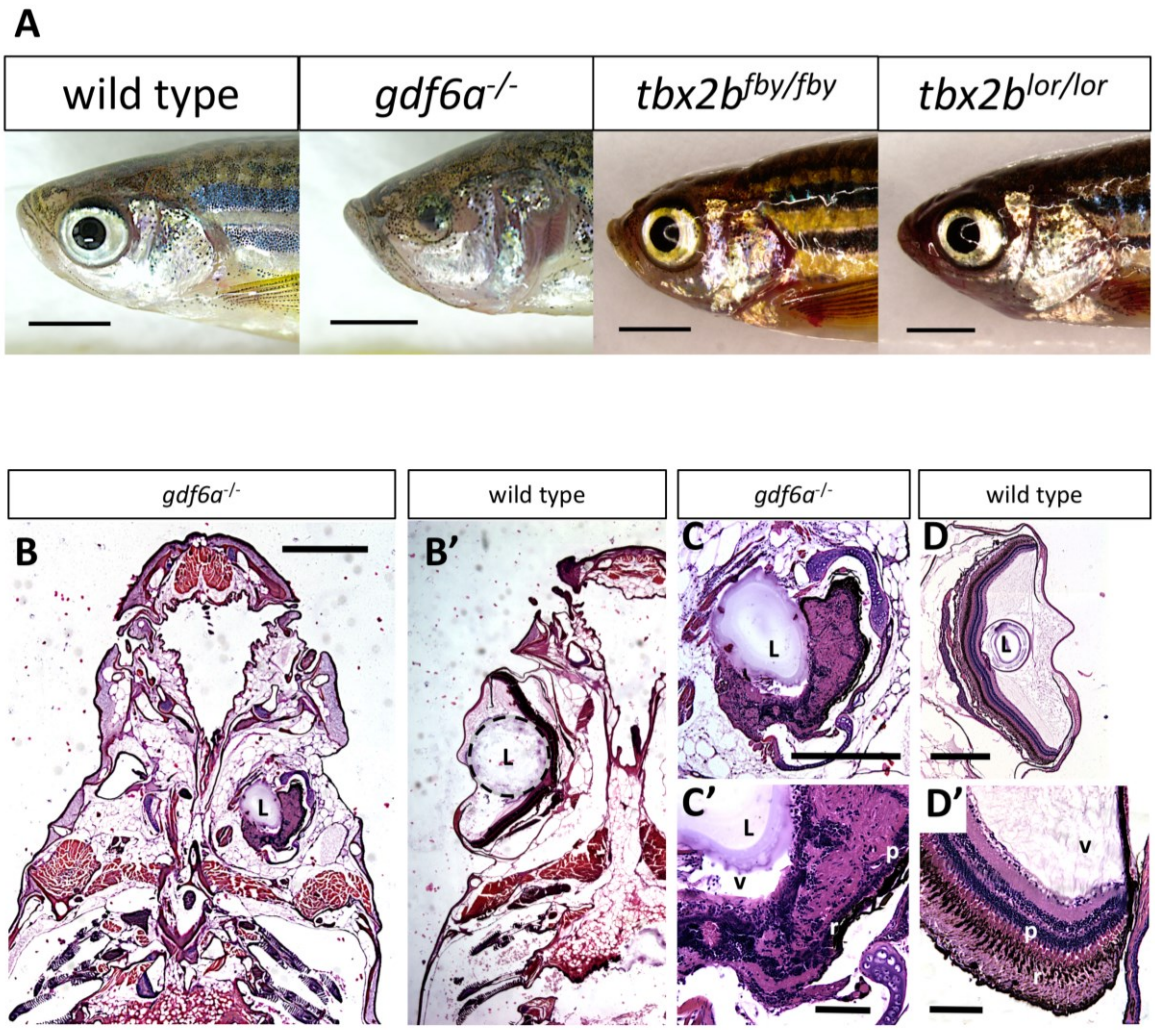

Figure 2.1. *gdf6a* and *tbx2b* mutants do not share the microphthalmic phenotype, despite a shared pathway in early eye development.

A. *gdf6a*$^{s327/s327}$ mutants (labeled *gdf6a*$^{-/-}$ in figures) exhibit microphthalmia to varying degrees of severity during development and throughout adulthood, unlike their wild type and heterozygous siblings. *tbx2b* mutants do not exhibit microphthalmia, and their eyes develop normally. Scale bars 2mm. **B, C, D.** Coronal sections of adult zebrafish heads, comparing microphthalmic *gdf6a*$^{s327/s327}$ (B) and wildtype fish (B′). Microphthalmia and anophthalmia present variably in *gdf6a*$^{s327/s327}$ fish (e.g. right and

left eyes in B, respectively) and eyes are often noted to possess a lens (L), though in this instance the right eye is inverted such that the anterior segment is oriented towards the midline. RPE (r) and a thin layer of photoreceptors (p) are discernable in *gdf6a*$^{s327/s327}$ fish (C′), though other retinal layers are not recognizable due to multiple tissue infoldings. In panel D, the lens was presumably displaced away from the iris during dissection/fixation. Note C is at higher magnification compared to D. Scale bar in B 1 mm; C, D is .5 mm; C′, D′ is .1 mm. L, lens; v, vitreous; r, RPE layer; p, photoreceptor layer.

Concerted disruption of both genes is the most sensitive test of the hypothesis that *gdf6a* and *tbx2b* share a genetic interaction in the early stages of eye development. *Gdf6a*$^{s327/s327}$ and *tbx2b*$^{lor/lor}$ (or, where noted in figures, *tbx2b*$^{fby/fby}$) mutants were crossed to produce compound heterozygous, [*gdf6a*$^{+/s327}$;*tbx2b*$^{+/lor}$] mutants, which were then in-crossed to procure a full range of genotypic combinations, including compound homozygous mutants. The proportion of resulting offspring exhibiting microphthalmia did not significantly deviate from 25%, suggesting that mutation in *tbx2b* does not affect the rate of microphthalmia in a *gdf6a*$^{+/s327}$ background (Fig. 2.2B). Genotyping these fish revealed that every microphthalmic larva had a *gdf6a*$^{s327/s327}$ genotype, and all combinations of *tbx2b* alleles (*tbx2b*^{lor} and wildtype alleles) existed among these microphthalmic larvae, supporting the null hypothesis that *gdf6a* mutation independently causes microphthalmia in the compound mutants. The eye size-to-body ratio of this pool was assessed to detect possible changes in phenotype severity. Both a microphthalmic population and a normophthalmic population were present and distinct from each other (Fig. 2.2C). The values in the normophthalmic population were statistically normal in their distribution (Shapiro-Wilk Normality test, W=0.9888, p=0.6532), further arguing against multiple populations of eye size being present. For confirmation, the eye-to-body ratios were also measured in an in-cross of [*gdf6a*$^{+/s327}$;*tbx2b*$^{+/fby}$] mutants, with similar results

(Appendix 1, Fig. A1.1). Only a single population of eye size was observed in in-crosses of *tbx2b*$^{+/lor}$ mutants (Fig. A1.1B). We did not explicitly test if combined mutations affected the *severity* of the microphthalmic phenotype (though no such difference is obvious in the data), because the manner in which data was collected did not support that analysis (we lacked foresight whilst collecting data to anticipate comparing between clutches of fish, which would require identical husbandry and timing of dechorionation: eye and body length are not allometric), though the data regarding *rate* of phenotype (from within a clutch) is robust and similar between all genotypes. We conclude that although *gdf6a* regulates *tbx2b* expression during early eye morphogenesis (Gosse and Baier, 2009), they do not genetically interact to cause microphthalmia in any obvious manner.

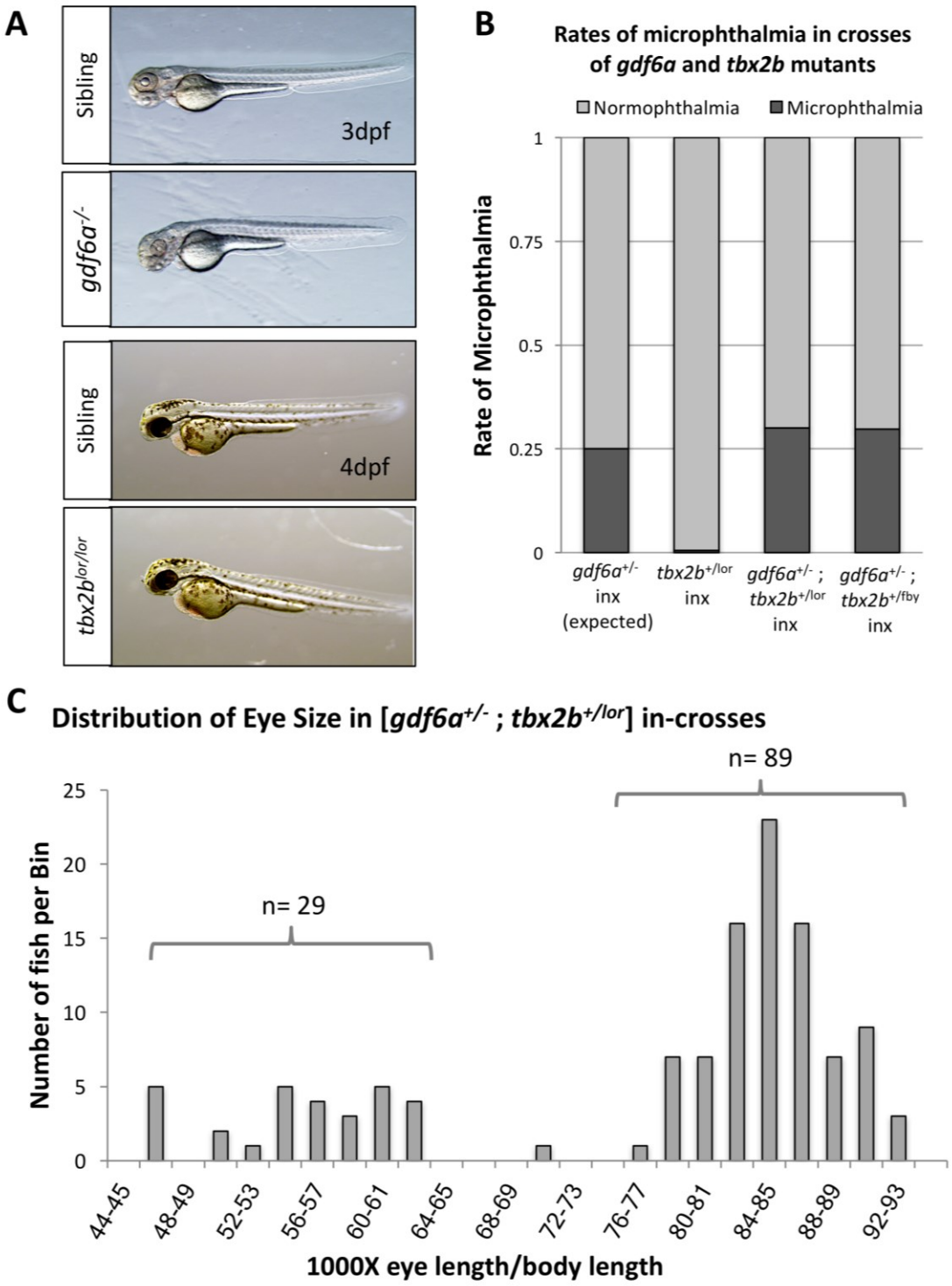

Figure 2.2. Disruption of *tbx2b* does not modify the *gdf6a* microphthalmic phenotype.

A. *gdf6a*$^{s327/s327}$ mutants exhibit microphthalmia (observed at 3dpf) but *tbx2b*$^{-/-}$ mutants (*lor* and *fby*) do not, indicating that disruption of *tbx2b* does not interfere with identical pathways as *gdf6a* in early eye development. **B.** Microphthalmia is rarely observed in *tbx2b* mutant in-crosses (inx) alone (*tbx2b*$^{+/lor}$ in-cross shown, n= 220) compared to in-crosses of *gdf6a*$^{+/s327}$, which yield 25% with microphthalmia (following Mendelian ratios of inheritance and recessive phenotype). When [*gdf6a*$^{+/s327}$;*tbx2b*$^{+/lor}$] or [*gdf6a*$^{+/s327}$;*tbx2b*$^{+/fby}$] compound heterozygous mutants are in-crossed (n=121 and 195 respectively, both at 6dpf), rates of microphthalmia do not increase significantly from rates expected of in-crosses of *gdf6a*$^{+/s327}$ alone (X^2 p=0.873 and p=0.137, respectively). **C.** The eye size compared to body length (shown as ratio) of a [*gdf6a*$^{+/s327}$;*tbx2b*$^{+/lor}$] in-cross does not reveal a subset of intermediate eye sizes, but remains bimodal, with the normophthalmic curve (right curve) showing a normal distribution (Shapiro-Wilk Normality test, W=0.9888, p=0.6532) (n=118, 4dpf).

2.4.2. gdf6a regulation of cone differentiation differs from predictions derived from phenotypes of tbx2b mutants.

Tbx2b is proposed to regulate UV cone-versus-rod fate, based on homozygous *tbx2b*$^{lor/lor}$ and *tbx2b*$^{fby/fby}$ mutants which present with a paucity of UV cones and an excess of rod photoreceptors (Alvarez-Delfin et al., 2009). Because *tbx2b* is downstream of *gdf6a* during the previously examined stages of retinal development, we hypothesized that the two genes may share a genetic pathway in a likewise fashion during photoreceptor development. This hypothesis predicts that UV cone and rod development should be disrupted in *gdf6a*$^{s327/s327}$ mutants, similar to observations in *tbx2b*$^{-/-}$ mutants.

Abundance of *gdf6a* expression during early ocular morphogenesis correspondingly affect expression levels of *tbx2b* (Gosse and Baier, 2009). We investigated whether this direct relationship still held later on in development, when the eye is developed and photoreceptors are assuming their respective fates. At 72hpf *gdf6a*$^{s327/s327}$ mutants appear to have less *tbx2b* expression in their retinas compared to wild type siblings, similar to the apparently low *tbx2b* expression in *tbx2b*$^{lor/lor}$ mutants of the same age (Fig. 2.3). In wild type retina *tbx2b* expression was not excluded from any of the retinal layers, but was perceived to be most abundant in the ganglion cell layer and vitreal half of the inner nuclear layer. Qualitatively, the latter tissue layer was the one with the greatest reduction of *tbx2b* abundance in the *gdf6a*$^{s327/s327}$ mutants.

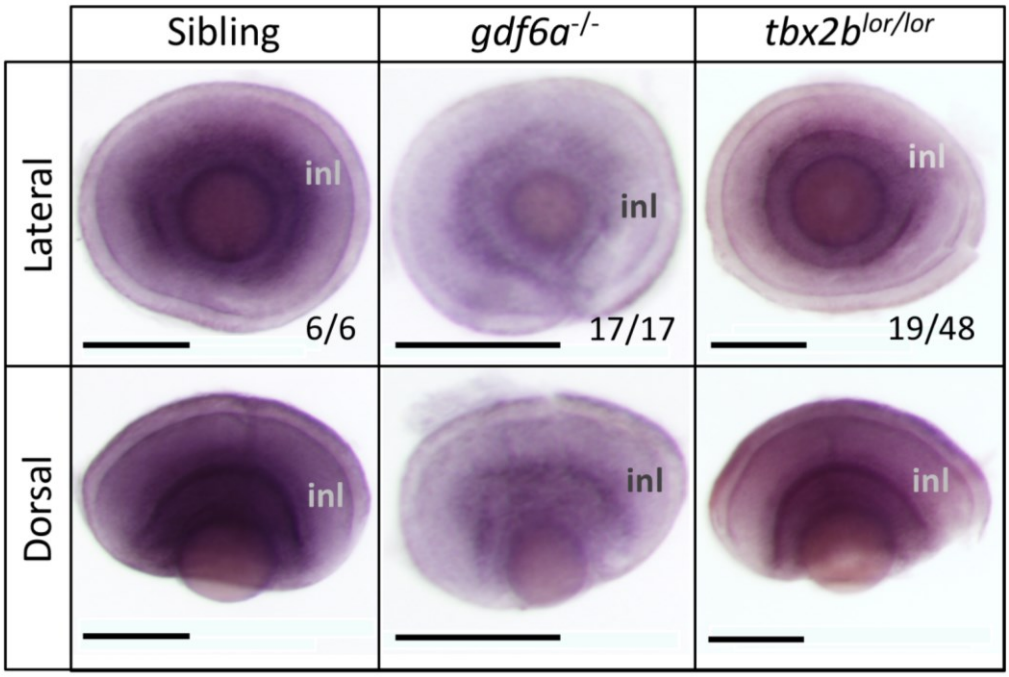

Figure 2.3. *gdf6a* positively modulates the abundance of *tbx2b* transcript during stages of retinal development when photoreceptors differentiate.

All panels show *in situ* hybridization using *tbx2b* riboprobe. *gdf6a*$^{s327/s327}$ mutants have less *tbx2b* expression at 3 days post-fertilization (dpf) compared to normophthalmic

siblings, akin to *tbx2b*$^{lor/lor}$ mutants. Fractions represent proportion of clutch represented by image shown. Scale bars 100μm; inl, inner nuclear layer.

We examined UV cone and rod photoreceptors in *gdf6a*$^{s327/s327}$ larvae and, contrary to our expectations, they did not show a *lots-of-rods* phenotype; UV cones and rods in microphthalmic *gdf6a*$^{s327/s327}$ eyes had normal relative abundance and distribution compared to wild type and to normophthalmic sibling eyes (Fig. 2.4A, B). Therefore, despite that *gdf6a* appears to regulate the abundance of *tbx2b* transcript during times of development when photoreceptors are specified (Fig. 2.3), disrupting *gdf6a* alone does not recapitulate phenotypes observed from disrupting *tbx2b* with regards to UV cone-versus-rod fate. This suggests that the downstream reductions in *tbx2b* resulting from mutation of *gdf6a* are insufficient in magnitude, or too different in their timing, to measurably produce effects upon UV cone or rod photoreceptor cell fate.

Assessing these phenotypes using a second metric was warranted because microphthalmia, a defect in early organogenesis, could have confounded potential differences in rod:cone ratios that are established later in development. Thus the abundance of UV cones in 6dpf *gdf6a*$^{s327/s327}$ larvae was also compared to the abundance of blue cones. We counted the number of UV and blue cones expressing GFP and mCherry, respectively, in transgenic fish (see Methods). This provided confirmation that UV cones were not reduced in abundance. However, the number of cones of the blue spectral subtype was dramatically reduced and often distributed in a patchy pattern in *gdf6a*$^{s327/s327}$ retinas compared to normophthalmic siblings (Fig. 2.4C, E). It was of interest to determine if this difference between genotypes was observable earlier in development, when cones are first detectable. Quantifying relative cone abundance in these transgenic fish at 4 dpf confirmed the difference between genotypes arises early (Fig. 2.4C). This was further confirmed at 3 dpf after identifying cones using UV and blue opsin riboprobes via *in situ* hybridization (Fig. 2.4C, D). This suggests that *gdf6a* signaling alone does not regulate cone-versus-rod development in the same fashion that *tbx2b* does, but instead appears to be acting in the differentiation of cone spectral subtypes.

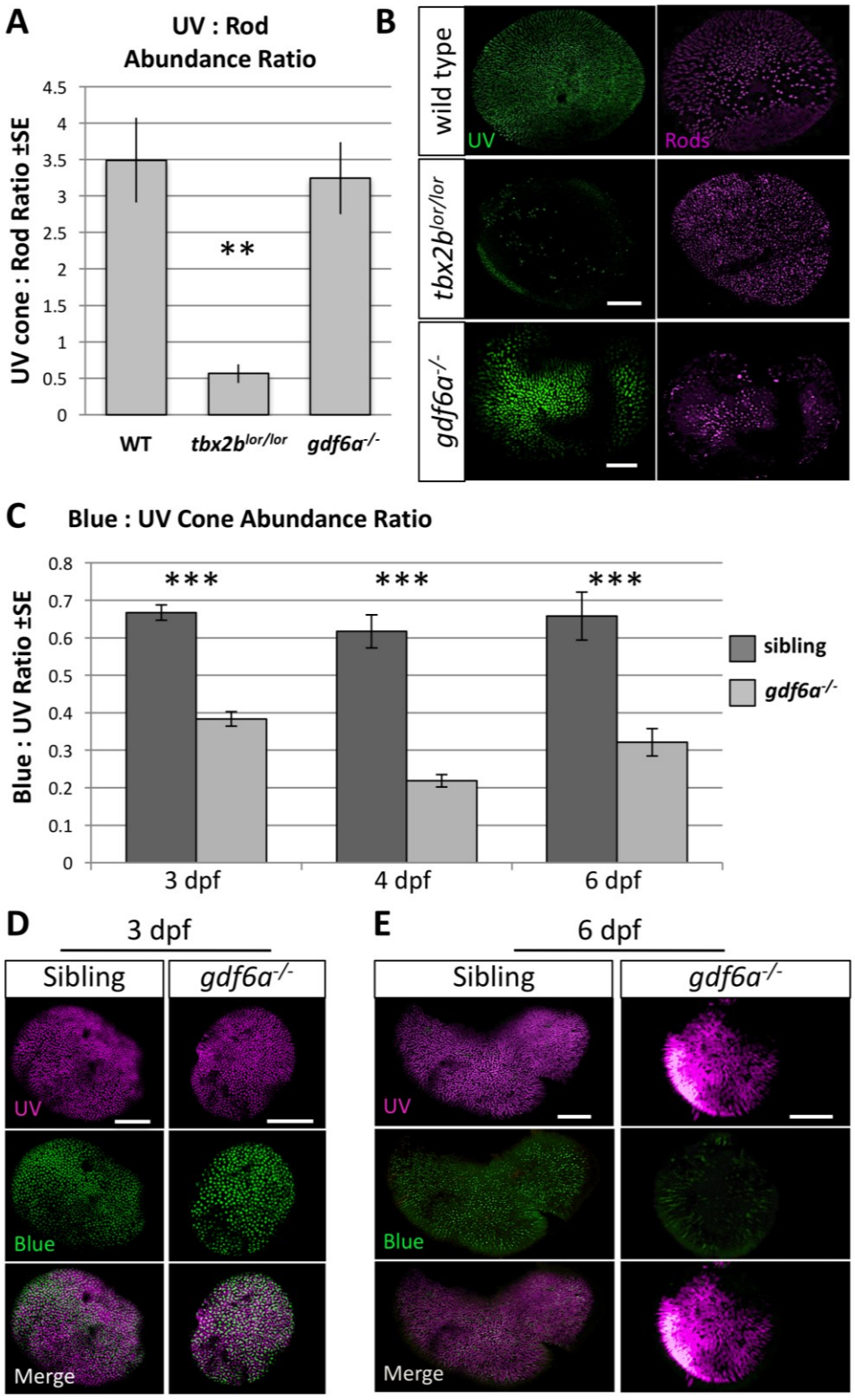

Figure 2.4. Mutation in *gdf6a* does not disrupt tbx2b function in UV-versus-rod photoreceptor specification, but *gdf6a* rather plays a role in blue cone specification.

A, B. *tbx2b*$^{lor/lor}$ mutants have fewer UV cones and more rods than wildtype fish (the *lots-of-rods* phenotype) (Kruskall-Wallis ANOVA, **p<0.005), but *gdf6a*$^{s327/s327}$ mutants have a normal abundance ratio and distribution of UV cones and rods (n= 10 wildtype, 8 *tbx2b*$^{lor/lor}$, and 7 *gdf6a*$^{s327/s327}$; UV cones expressing GFP and rods were labeled with antibody 4C12). Scale bars 30μm and 80μm, respectively. **C.** Larval *gdf6a*$^{s327/s327}$ mutants have a unique cone photoreceptor phenotype in which there are significantly fewer blue cones relative to UV cones at all ages examined (which is not observed in *tbx2b*$^{lor/lor}$ or *tbx2b*$^{fby/fby}$ mutants- not shown) (Kruskall-Wallis ANOVA, ***p< 0.001) Sample sizes at 3 days post-fertilization (dpf) are n=17 larvae per genotype quantifying cells visualized via opsin *in situ* hybridization (Panel D); at 4 dpf data are from n=9 wild type and n=13 mutants assessed via GFP and mCherry transgene expression in cones; at 6dpf data are from 2 replicates of n= 4+7 wild type and n= 5+6 mutants assessed via transgene expression in cones (Panel E). **D.** UV and blue cones identified in 3 dpf by *in situ* hybridization against their respective opsins (Scale bars are 100 μm). **E.** UV and blue cones identified in transgenic lines at 6dpf by expression of GFP and mCherry, respectively (Scale bars are 60 μm and 40 μm in sibling and mutants, respectively).

2.4.3. Specificity and utility of rat monoclonal antibody 10C9.1 for labeling UV cones

To better detect UV cones and phenotypes of interest, we isolated a novel monoclonal antibody raised in rat and characterized its ability to specifically detect UV-sensitive opsin (product of *opn1sw1*, ZFIN ZDB-GENE-991109-25). The clone giving rise to antibody 10C9.1 was derived from a rat injected with a peptide antigen equivalent to the 20 amino-terminal amino acids of trout UV opsin (Appendix 1, Fig. A1.2E), and polyclonal sera from this rat had previously been shown to label UV cones in trout (Allison et al., 2006a) and zebrafish [16]. 10C9.1 was isotyped to an IgG2c.

Application of 10C9.1 to cryosections of adult zebrafish retina, and counterstaining of lipid-rich material using BODIPY-TMR, revealed that 10C9.1 labels the outer segments of photoreceptors with a single cone morphology (Appendix 1, Fig. A1.2A, B). Restriction of the labeling to the cone outer segment is consistent with labeling of an opsin because in healthy eyes opsins are abundant only in this cellular compartment. Considering UV cones are one of only two spectral subtypes that exhibit a single cone morphology (along with blue cones, and in contrast to the green and red cones that are fused into a double cone morphology), the labeling also suggested that 10C9.1 was detecting either UV or blue cones. Simultaneous labeling using 10C9.1 and a well-characterized anti-blue opsin antibody (Vihtelic et al., 1999) demonstrated that 10C9.1 labels a population of single cone photoreceptors that is distinct from the blue cones (Appendix 1, Fig. A1.3). Further, the 10C9.1 labeling was localized to cone cells with a short single cone morphology with the outer segments in a more vitreal (basal) position than that of blue cone outer segments (Fig. 2.5A), and this is exactly consistent with the morphology of UV cones as identified via *in situ* hybridization (Raymond and Barthel, 2004; Raymond et al., 1995b; Stenkamp et al., 1996), immunohistochemistry (Vihtelic et al., 1999), and microspectrophotometry (Allison, 2004; Allison et al., 2004). Simultaneous labeling of 10C9.1 and zpr1 antibody that labels the entire plasma membrane of red/green double cones demonstrated no apparent overlap in labeling (Fig. A1.3).

The specificity of antibody 10C9.1 was assessed using two additional strategies. First, we noted that no such labeling was apparent when the 10C9.1 primary antibody was

excluded or when it was substituted by another rat IgG2c primary antibody (Appendix 1, Fig. A1.2C). Second, we noted that very few cells were labeled when 10C9.1 was applied to retinas that are known to have few UV cones, i.e. retinas from adult *tbx2b*$^{lor/lor}$ mutants (Fig. A1.2D), see also top row of Fig. 2.6B for the same approach on retinas from normophthalmic larvae).

We further confirmed that 10C9.1 is labeling UV cones by its co-localization with an established anti-UV opsin antibody raised in rabbit (Vihtelic et al., 1999) (Appendix 1, Fig. A1.3). Finally, we applied 10C9.1 to adult double transgenic zebrafish that we recently characterized as expressing GFP throughout their UV cones and expressing mCherry throughout their blue cones *Tg(-5.5opn1sw1:EGFP)kj9;Tg(-3.5opn1sw2:mCherry)ua3011* (Duval et al., 2013; Fraser et al., 2013a; Takechi et al., 2003). This labeling again revealed localization of 10C9.1 exclusively to the outer segments of UV cones (Fig. 2.5B).

In sum, the specificity of the antibody 10C9.1 for labeling UV cones was determined by its localization to the expected cellular compartment (photoreceptor outer segment) and only within the cone cells of the expected morphology (short single cones); this was complemented by co-localization of 10C9.1 with well-characterized antibodies and transgenes that label UV cones, and exclusion from similar markers that label other cones. Further, 10C9.1 labeling was greatly reduced when applied to retinas with few UV cones. The utility of 10C9.1 is enhanced by being a stable monoclonal source of reagent. Further, because the host animal was rat, 10C9.1 can be used in multi-label experiments with the large selection of available antibodies raised in rabbit and mouse. The latter includes that one can, for the first time we are aware of, simultaneously distinguish each of the cone subtypes of zebrafish using immunohistochemistry (Fig. 2.5A"). 10C9.1 is available from the corresponding author or from Immunoprecise Antibodies Inc. (Victoria BC, Canada www.immunoprecise.com; antibody name "UVop-10C9.1").

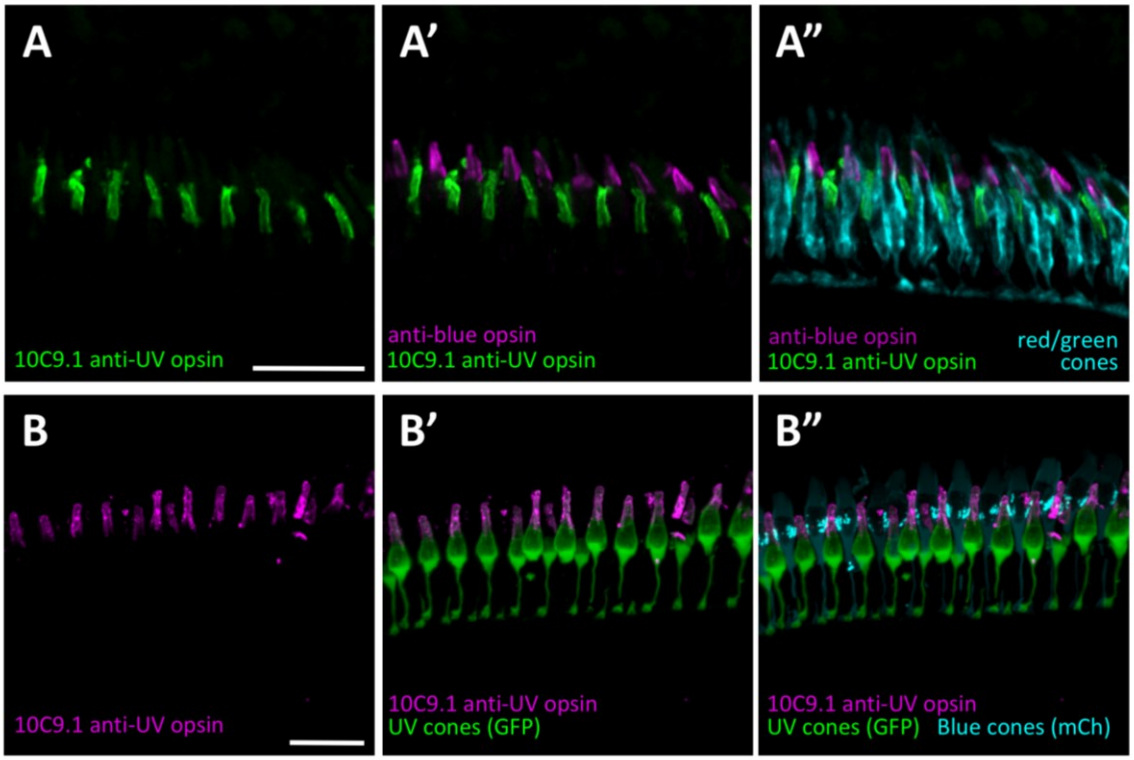

Figure 2.5. A monoclonal antibody raised in rat (10C9.1) labels zebrafish UV cone outer segments, allowing all cone subtypes to be simultaneously labeled by immunohistochemistry.

Antibody 10C9.1 specifically labels the outer segments of a class of short single cones in the adult zebrafish retina (Appendix 1, Fig. A1.2A). 10C9.1 specificity is supported (see Appendix 1, Fig. A1.2B-D), including by a dramatic decrease in number of cells labeled when 10C9.1 is applied to retinas from zebrafish mutants (*tbx2b*$^{lor/lor}$) that have a paucity of UV cones. **A.** The population of single cones labeled by 10C9.1 is the UV cones, because established antibodies against the other single cone class, the blue cones, labels a distinct cone population (A'). 10C9.1 enables an unprecedented combination of antibodies raised in different species that simultaneously label and distinguish all cone photoreceptor subtypes (A"). **B.** Further evidence that 10C9.1 labels

UV cone outer segments comes from its co-localization with UV cones filled with green fluorescent protein (GFP), and its exclusion from blue cones filled with mCherry (mCh) in transgenic zebrafish (*Tg(-5.5opn1sw1:EGFP)kj9;Tg(-3.5opn1sw2:mCherry)ua3011*). Scale bars 30μm.

2.4.4. A subtle interaction between gdf6a and tbx2b modulates the lots-of-rods phenotype

Based on the lack of a *lots-of-rods* phenotype in *gdf6a*$^{s327/s327}$ mutants (Fig. 2.4A, B), it had appeared that *gdf6a* might not regulate cone-versus-rod development. However, a more sensitive test to detect the presence of an interaction is concerted disruption of both genes. To determine whether *gdf6a* and *tbx2b* interact in photoreceptor development, we examined UV cone and rod photoreceptors in the progeny of compound heterozygous [*gdf6a*$^{+/s327}$;*tbx2b*$^{+/lor}$] in-crosses (and [*gdf6a*$^{+/s327}$;*tbx2b*$^{+/fby}$] in-crosses). We hypothesized that if there were a less linear, subtler interaction between *gdf6a* and *tbx2b*, disrupting both genes simultaneously would reveal it, by resulting in a synergistic phenotype or occurrence of phenotypes among larvae whose genotypes predict none.

Microphthalmic eyes from the aforementioned in-crosses showed an elevated rate of the *lots-of-rods* phenotype (48% of microphthalmic eyes showed a *lots-of-rods* phenotype among [*gdf6a*$^{+/s327}$;*tbx2b*$^{+/lor}$] in-crosses, a significantly greater proportion than the predicted 25%; X^2 $p < 0.001$). This contrasted eyes from normophthalmic siblings wherein the rate of the *lots-of-rods* phenotype (29%) did not statistically differ from the expected Mendelian rate (Fig. 2.6A, B). The elevation in *lots-of-rods* phenotypes among microphthalmic larvae also differed significantly from rates in *tbx2b*$^{+/lor}$ in-crosses (without *gdf6a* mutation), where 27% of embryos exhibited the *lots-of-rods* phenotype, which was also statistically consistent with predicted Mendelian inheritance (Fig. 2.6A).

To better define the genetics of this system, we repeated the in-crosses of *gdf6a*$^{s327/s327}$ and *tbx2b*$^{lor/lor}$ mutants in a fashion that allowed us to track genotypes via single nucleotide polymorphisms (SNPs) within the *tbx2b* gene. The use of SNPs was

necessitated by the fact that the *tbx2b*^{lor} mutation remains undefined. Screening a panel of potential SNPs (see Methods) on several fish of each genotype allowed us to identify homozygous *tbx2b*$^{lor/lor}$ and *gdf6a*$^{s327/s327}$ founders wherein each had a different homozygous SNP in the *tbx2b* gene (in the first exon, Fig. 2.6E). These were bred to generate compound heterozygous fish [*gdf6a*$^{+/s327}$;*tbx2b*$^{+/lor}$] within which we could reliably track the inheritance of the *tbx2b*^{lor} allele.

To test if the elevated rates of the *lots-of-rods* phenotype accords with a partial loss of *tbx2b* function, as predicted from a genetic interaction, 35 microphthalmic larvae from the aforementioned in-cross were genotyped. All larvae were *gdf6a*$^{s327/s327}$, as expected from their microphthalmic phenotype. Amongst these, we expected a 25% (i.e. 9/35 larvae) rate of the *lots-of-rods* phenotype based on a recessive pattern of inheritance (see "Expected" column in Table 2.2). We also expected all 9 of these larvae to have a *tbx2b*$^{lor/lor}$ genotype through SNP analysis. But we observed the previously mentioned increase in rate of the *lots-of-rods* phenotype – 13/35 or 37% of the larvae had the phenotype ("Observed" column in Table 2.2). Genotyping revealed that 4 of these 13 *lots-of-rods* phenotypic larvae were, in fact, heterozygous *tbx2b*$^{+/lor}$ (unexpected), whereas 9 were homozygous *tbx2b*$^{lor/lor}$ (matching the expected rate of homozygosity). This indicates that the *lots-of-rods* phenotype can occur in a subset of heterozygous *tbx2b*$^{+/lor}$ fish, but only when both copies of *gdf6a* are mutated. Genotyping also revealed that normophthalmic individuals with the *lots-of-rods* phenotype were all homozygous *tbx2b*$^{lor/lor}$. Therefore, the slightly elevated rate of the *lots-of-rods* phenotype (29%, not significantly different from Mendelian 25%, see above) in these normophthalmic eyes likely resulted from reduced survival of other genotypes. This might be expected if toxic mutations were not yet bred out following random chemical mutagenesis.

Table 2.2. Identification of compound [*gdf6a*$^{s327/s327}$; *tbx2b*] mutants with mismatched phenotype and genotype regarding *tbx2b*.

		EXPECTED				OBSERVED			
Phenotype:		wild type	*lots-of-rods*			wild type	*lots-of-rods*		
	Raw # /35 total	26	9			22	13		
	%	75%	25%			63%	37%		
			lots-of-rods				*lots-of-rods*		
tbx2b Genotype:			+/+	+/-	-/-		+/+	+/-	-/-
	Raw # /35 total		0	0	9		0	4	9
	%		0%	0%	**25%**		0%	**12%**	**25%**

Because the rate of *lots-of-rods* among microphthalmic larvae (48%) does not reflect any classical Mendelian ratio that may explain such elevated rates, we examined the effect of the stronger null *tbx2b*^{fby} allele in the same context with *gdf6a* mutation, with the suspicion that introducing a null *tbx2b* mutation may induce a more severe phenotype. An in-cross of [*gdf6a*$^{+/s327}$;*tbx2b*$^{+/fby}$] showed similar results to [*gdf6a*$^{+/s327}$;*tbx2b*$^{+/lor}$] in-crosses, with the *lots-of-rods* phenotype occurring in 44% of microphthalmic eyes again significantly (X^2 p=0.007) more than normophthalmic siblings (20.5%) (Fig. 2.6C, D).

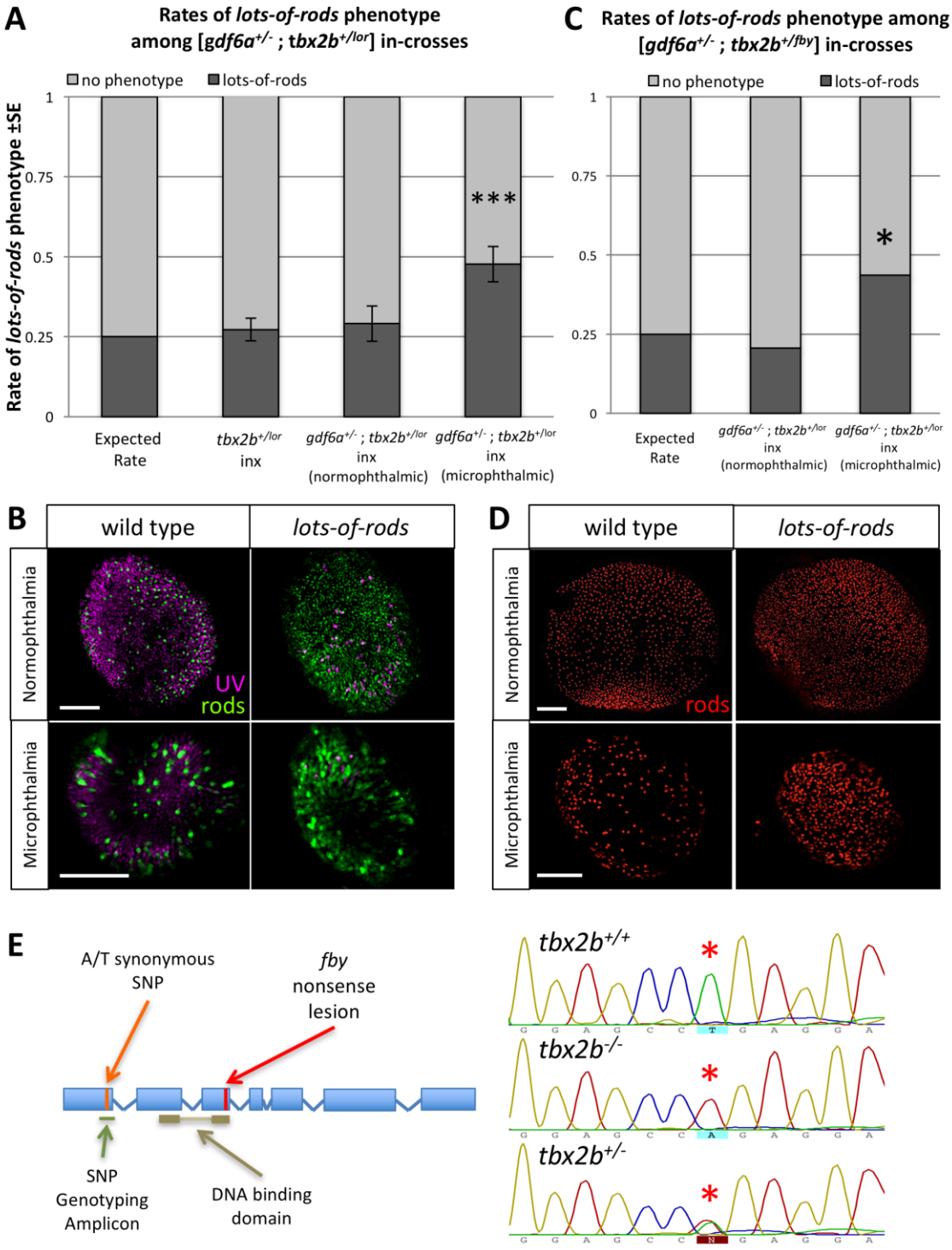

Figure 2.6. *gdf6a* modulates *tbx2b* regulation of UV cone and rod development.

A, B. When [*gdf6a*$^{+/s327}$;*tbx2b*$^{+/lor}$] compound heterozygous mutants are in-crossed (inx), a disproportionate fraction of microphthalmic offspring exhibit the *lots-of-rods* phenotype compared to normophthalmic siblings, *tbx2b*$^{+/lor}$ in-crosses, and to predicted Mendelian ratios of the recessive *lots-of-rods* phenotype (X^2 ***p< 0.001; 3 replicates of n= 17, 19, 35 microphthalmics; 6dpf). UV cones and rods were labeled using antibodies 10C9.1 and 4C12 displayed in magenta and green, respectively. A portion of microphthalmic larvae with the *lots-of-rods* phenotype has a *tbx2b*$^{+/lor}$ genotype (see Table 2.2). **C, D.** When [*gdf6a*$^{+/s327}$;*tbx2b*$^{+/fby}$] compound heterozygous mutants are in- crossed, the *lots-of-rods* phenotype is again observed at higher rates in microphthlamic eyes compared to normophthalmic eyes (X^2 *p= 0.007; 1 replicate, n= 39 microphthalmics, 6 dpf). Panel D shows rod opsin *in situ* hybridization (red). Scale bars are all 50 µm. **E.** Genotyping for the *lor* mutation was performed via linkage analysis using an A/T synonymous SNP located before the DNA binding domain of *tbx2b* in *lor* and non-*lor* alleles, respectively. *gdf6a*$^{s327/s327}$ mutants with a corresponding SNP of T were used in crossing of the mutant lines.

2.5. Discussion

Efforts to model vision regeneration using stem cells are stymied by the difficulties procuring progenitors for cone photoreceptors, the cells required for daytime vision, in established murine models. One of the obstacles in this respect is a limited knowledge of the genetic regulation of cone development from retinal progenitor cells. To complement and utilize our novel zebrafish cone regeneration model (Fraser et al., 2013a), we are

investigating candidate regulatory factors of cone and cone subtype development. In this paper, we explored the potential interaction between two genes with recently realized connections to photoreceptor development and degeneration. To this end we demonstrated that these genes, *gdf6a* and *tbx2b*, unexpectedly regulate development of spectral subtypes of cones and interact in the development of UV cones and rod photoreceptors specifically.

Tbx2b is one of the most recently recognized regulatory genes directing cone and rod differentiation (Alvarez-Delfin et al., 2009). *GDF6* (and its homolog *gdf6a)* was selected as a candidate regulator of cone development because deficits in its function cause photoreceptor degeneration, as identified through panels of LCA patients, complemented by murine and zebrafish models (Asai-Coakwell et al., 2013). These developments, in synergy with the established regulatory relationships between *gdf6a* and *tbx2b* in early retinal development (French et al., 2013; Gosse and Baier, 2009), led us to speculate that *gdf6a* signaling also regulates cone photoreceptor development.

2.5.1. Gdf6a signaling has a conserved role in ocular morphogenesis that does not appear to depend on tbx2b activity

The genetic interactions between *gdf6a* and *tbx2b* in zebrafish eye development are not as linear as we had assumed. Although *Tbx2* knockout mice display microphthalmia (Behesti et al., 2009), akin to *gdf6a* loss-of-function models in various vertebrate homologs [43,50,51,52,53]*,* and *gdf6a* signaling has been previously demonstrated to positively regulate *tbx2b* expression during ocular morphogenesis (Gosse and Baier, 2009), our data indicate that in zebrafish disruption of *tbx2b* is not sufficient to augment the pathology of microphthalmia observed upon *gdf6a* disruption. This was revealed both by the lack of a microphthalmic phenotype upon *tbx2b* loss of function, and the lack of change in rate or apparent severity of microphthalmia when *gdf6a* and *tbx2b* null mutations were combined. A lack of *tbx2b*-related microphthalmia ruled out an alternative explanation for the genetic interdependence we observed regarding photoreceptor development, demonstrating that alterations in microphthalmia cannot explain the increased rates of photoreceptor-related phenotypes we noted during concerted gene

disruption. Towards a broader relevance of this data, *gdf6a* and *tbx2b* have both been demonstrated to play roles in cell proliferation and establishing dorsal retina identity, though in different animal models (Behesti et al., 2009; Bilican and Goding, 2006; Chi et al., 2008; French et al., 2009; French et al., 2013; Gosse and Baier, 2009; Gross and Dowling, 2005b; Martin et al., 2012b; Snelson et al., 2008b; Vance et al., 2005b). Our observations of *tbx2b* disruption in zebrafish contrast that of the mouse homolog *Tbx2*, which is also downstream of ocular BMP signaling, and mutations in this pathway produce a microphthalmic phenotype in mice (Behesti et al., 2009). It may be that *tbx2b* and *Tbx2* do not share the same role in early retinal development, that *tbx2b* has different spatiotemporal kinetics, or that redundancy with other genes (*tbx2a*, *gdf6b* or others) can compensate in zebrafish.

2.5.2. Differential role for gdf6a amongst the spectral subtypes of cone photoreceptors

We had speculated that *gdf6a* mutants would present with phenotypes similar to *tbx2b* mutants (lots of rods and few UV cones). This speculation was borne upon observations that *tbx2b* specifies rod versus UV cone fate, and *gdf6a* is a positive upstream regulator of *tbx2b* expression. Instead, the data revealed that gdf6a mutants do not exhibit the anticipated phenotype; rather, our observations indicate that *gdf6a* signaling promotes development or maintenance of blue-sensitive cones. This is uniquely promising, suggesting a set of novel regulatory actions in a stage of photoreceptor development that has not been adequately explored in zebrafish before: that of cone opsin spectral *subtype* specification. It is not yet clear whether *gdf6a* serves a role in cone specification, differentiation and/or survival, but one avenue of investigation will be modulating *gdf6a* signaling during proliferation and cone photoreceptor differentiation as replicated in our regeneration model (Fraser et al., 2013a). Pursuing *gdf6a* effects in the regenerative context is especially intriguing since recent work shows that the proliferative response in Müller glia requires regulation of TGFβ signaling (Lenkowski et al., 2013).

It remains undetermined the extent to which the blue cone-specific requirement for *gdf6a,* established herein, is mechanistically similar to the apparent UV cone-specific

requirement of *tbx2b* (Alvarez-Delfin et al., 2009). At the cellular level, a notable difference in phenotypes is that *tbx2b* mutants present with an excess of rod photoreceptors (Alvarez-Delfin et al., 2009), which we did not observe in *gdf6a* mutants. With respect to cellular sites of action for these genes in determining cell fate, it is not clear whether UV and blue cones are products of a common pool of progenitor cells; although UV cones and blue cones are together the last photoreceptor types to differentiate during retinal development (based on the sequential appearance of detectable opsin transcript in goldfish (Stenkamp et al., 1997)), the terminal divisions seem to rely upon separate/dedicated progenitor pools (Suzuki et al., 2013a). Regardless, it is tempting to speculate that common molecular signaling pathways might lead to a low abundance of blue and UV cones, in *gdf6a* and *tbx2b* mutants respectively, especially considering the epistatic relationship of these genes during both early and late retinal development (see below).

2.5.3. Gdf6a and tbx2b genetic interdependence in UV cone and rod photoreceptor differentiation

Considering the disparate ocular phenotypes observed between their respective mutants, during both early and late retinal development, the genetic interaction between *gdf6a* and *tbx2b* is neither simple nor linear. But interpreting this relationship is made more complex by the low UV cone abundance and high rod abundance (the *lots-of-rods* phenotype) observed in high rates among compound mutant larvae. Some of these larvae were found to display the recessive *tbx2b* phenotype despite being genetically heterozygous for the *tbx2b* mutation (which alone does not yield the *lots-of-rods* phenotype). *Gdf6a* appears to modulate *tbx2b* indirectly, suggestive of a genetic interdependence in a UV cone fate decision. One hypothesis to this end is that *gdf6a* and *tbx2b* both promote a common activity, perhaps via being in the same pathway (as per Fig. 2.3). Thus a lack of *gdf6a* signaling would reduce the efficacy of *tbx2b* to promote a UV cone fate, causing the assumption of a *lots-of-rods* phenotype or a wild type phenotype to become more random. Alternatively, *tbx2b* expression may have a minimum threshold for activity that is sensitive to perturbations (including disrupted *gdf6a* signaling)

affecting *tbx2b* mRNA transcript levels. Alternatively, *gdf6a* signaling may alter the timing of cell cycle exit of photoreceptor progenitors, as has been established for *gdf11* (Kim et al., 2005); thus with altered *gdf6a* there may be increased probability that progenitors undergo specification/differentiation and invoke *tbx2b* expression at an inappropriate time, thereby shifting cell fates.

2.6. Conclusion

Further exploration into pathways utilizing *tbx2b* and *gdf6a* would clarify the order or pattern of photoreceptor specification, which will also provide insight into zebrafish cone mosaic formation and photoreceptor regeneration following injury. Zebrafish possess latent stem cells within the retina and have a robust neural regenerative capacity. Because of these properties, zebrafish are a promising *in vivo* model to study not just photoreceptor development, but also regulation of cone photoreceptor regeneration and integration. With zebrafish as an impressive model of functional regeneration, stem cell therapy for restoring daytime vision can become a reality.

Chapter 3. Photoreceptor progenitors depend upon coordination of *gdf6a*, *thrβ*, and *tbx2b* to generate precise populations of cone photoreceptor subtypes

The questions, hypotheses, and experiments in this chapter were conceived and designed by W. Ted Allison and Michèle G. DuVal. Experiments, including embryo injections, heat shocks, mutant genotyping, immunocytochemistry, imaging, analysis, and interpretation were performed by MGD; Hao Wang performed molecular work for creating the *Tg(hsp70:dnthrb.V2A.eGFP)*^{ua3113} line; Elizabeth Hodges, Quinton Schmidt, and Ramona Rosca assisted with heat shocks, genotyping, and immunohistochemistry. Zebrafish mutant lines were generously gifted by Andrew Waskiewicz and Josh Gamse. Writing for this chapter was done by MGD with editing and feedback by WTA.

3.1. Summary

Purpose: Replacing cone photoreceptors, the units of the retina necessary for daytime vision, depends upon successful production of a full variety of new cones from, for example, stem cells. Using genetic experiments in a model organism with high cone diversity, zebrafish, we map the intersecting effects of cone development factors *gdf6a*, *tbx2b*, and *thrβ*. **Methods:** We disrupted these genes of interest by employing genetic combinations of mutants, gene knockdown, and dominant negative gene expression, then quantified cone subtype outcomes (which normally develop in tightly regulated ratios). **Results:** *Gdf6a* mutants have reduced blue and, discovered here, reduced red cones. In combined *gdf6a*/*tbx2b* disruption, loss of *gdf6a* in heterozygous *tbx2b* mutants reduced UV cones. Intriguingly, when we disrupted *thrβ* in *gdf6a* mutants using a *thrβ* morpholino, their combined early disruption revealed a lamination phenotype. Disrupting *thrβ* via expression of a dominant negative *thrβ* (*dnthrβ*) at either early or late retinal development had differential outcomes on red cones (reduced abundance), versus UV and blue cones (increased abundance). Using *dnthrβ* in *gdf6a* mutants revealed that disrupting *thrβ* did not change *gdf6a* mutant cone phenotypes. **Conclusions:** *Gdf6a* loss directly affects blue and red cones, and indirectly affects UV cones by increasing sensitivity to additional

disruption, like reduced *tbx2b*, resulting in fewer UV cones. The effects of *thrβ* change through photoreceptor development, first promoting red cones and restricting UV cones, and later restricting UV and blue cones. The effects of *gdf6a* on UV, blue, and red cone development overlap with, but likely supercede, those of *thrβ*.

3.2. Introduction

Retinal degenerations are characterized by the gradual death of retinal neurons and become especially debilitating upon the loss of photoreceptors, the neurons that detect light. Cone photoreceptors, or cones, respond to high intensity light and are divided into subtypes based on maximal wavelength sensitivity, thus they are especially important for daytime visual function and colour discrimination. The human macula is populated exclusively by cones and is critical for daytime vision and visual acuity; thus when retinal degeneration occurs in the macula, functional vision is dramatically compromised. Restoring functional vision in humans demands strategies to replace lost cones, but how cones and their subtypes are produced remains poorly understood. Creating functional cone photoreceptors for therapeutic use, e.g. from stem cells, requires better knowledge and manipulation of the regulatory networks in cone development (Brockerhoff and Fadool, 2011; Lakowski et al., 2010; Lakowski et al., 2011; Morris et al., 2008; Ortin-Martinez et al., 2016; Pearson et al., 2016; Santos-Ferreira et al., 2016; Singh et al., 2016; Thummel et al., 2010; Zhou et al., 2015).

Much insight into photoreceptor development to date has come from the mouse, which has two cone types (M- and S-cones) typical of most mammals. Photoreceptor progenitors are characterized by *Crx* expression; from this pool, *Nrl* and its target *Nr2e3* direct rod photoreceptor fate (Mears et al., 2001). Mouse *Thrβ* and zebrafish *thrβ* are required for M-cones and red cones respectively (Ng et al., 2011; Suzuki et al., 2013a). In mice it is proposed that *Thrβ* drives the differentiation of M-cones, whereas S-cones are a default type (Forrest and Swaroop, 2012). ROR and RXR nuclear receptors can either negatively (*RXRγ*) (Roberts et al., 2005) or positively (*RORβ*, *ROR*□) (Fujieda et al., 2009; Liu et al., 2017; Srinivas et al., 2006a) regulate the expression of S-opsin in mice, which results in a dorso-ventral gradient pattern of S opsin expression. Overall, the

mouse retina is dominated by rods with a low density of cones and thus a paucity of cone-cone interactions. By contrast, the human macula is cone dominant and has three cone types, more than most mammals. How three (or more) cone subtypes can be created, and what conditions are required to build a cone-rich area like the macula, remain unanswered and demand a wider diversity of retina development models.

Non-mammalian vertebrates have a greater diversity of cones, and so offer insight into how multiple cone subtypes are generated. The zebrafish retina is dense with cones, with four subtypes based on maximal light spectrum sensitivity (UV, blue, green, and red), and these subtypes are produced in tightly controlled proportions in larvae and adults. Further, these four subtypes are arranged in a precise row mosaic pattern in the adult retina (Allison et al., 2010a; Duval et al., 2013; DuVal et al., 2014b; Fraser et al., 2013a; Hagerman et al., 2016; Raymond et al., 1995b; Raymond et al., 2014; Suzuki et al., 2013b; Tohya et al., 1999). The four major cone types are conserved in the vertebrate lineage, making zebrafish a highly useful model to study cone development. In zebrafish, *tbx2b* is required for early neuronal differentiation in the dorsal retina (Gross and Dowling, 2005b) and, specifically, UV cones (the homologue to mammalian S-cones and human blue cones); *tbx2b* appears to negatively regulate rod abundance (Alvarez-Delfin et al., 2009). *Gdf6a* is required for establishing dorsal identity in the early retina (French, 2010; French et al., 2009; Gosse and Baier, 2009), for regulating retinal cell proliferation (Valdivia et al., 2016), and for adequate blue cone abundance (DuVal et al., 2014b). *Gdf6a*$^{s327/s327}$ mutants are microphthalmic, and have reduced blue cone to UV cone abundance ratios. *Gdf6a* also enhances *tbx2b* for the correct production of UV cones and rods. *Six7*, a *sine oculis* homeobox transcription factor, is required for green cones (Ogawa et al., 2015; Sotolongo-Lopez et al., 2015; Sotolongo-Lopez et al., 2016).

In sum, while the murine retina contains 2 cone types with one developmental transcription factor complex discerning between them (Forrest and Swaroop, 2012; Ng et al., 2011; Swaroop et al., 2010), zebrafish have 4 cone subtypes produced in exact ratios (Allison et al., 2010a; Raymond and Barthel, 2004; Raymond et al., 1995b; Raymond et al., 2014; Salbreux et al., 2012; Tohya et al., 1999), so must employ a more complex system of progenitor fate choice. Much of the knowledge of zebrafish cone subtype production is expected to be directly relevant to the development of the human macula.

We sought to determine if the factors within this system interact to regulate the ratios, or relative abundances, of cone subtypes. In this study we examined *thrβ*, *gdf6a*, and *tbx2b*.

Our documentation of the cone phenotype in *gdf6a* mutants is expanded: *gdf6a* mutants have reduced blue and red cones but not UV cones, suggesting that *gdf6a* promotes blue and red cone development. In addition, the interaction between *gdf6a* and *tbx2b* is confirmed by quantifying cone abundances, showing that *gdf6a* loss increases sensitivity to insufficient *tbx2b* activity, which affects the UV cone population specifically. We find that *thrβ* has developmental stage-specific roles in i) red cone, and ii) UV and blue cone subtype specification, and iii) interacts with *gdf6a* to direct proper retina lamination.

3.3. Methods

3.3.1. Ethics Statement

All fish care and experiments were approved by the Animal Care and Use Committee: Biosciences at the University of Alberta under protocol AUP00000077 and were in accordance with the Canadian Council on Animal Care.

3.3.2. Animal Care and Embryo Injections

Zebrafish were raised and maintained according to standard procedures (Westerfield, 2000b). Embryos were kept in E3 media and at 28°C except where indicated in experimental procedures. Media with 0.003% PTU to prevent pigmentation was applied at 8-10hpf. Mutant lines were gifted as follows: *gdf6a*$^{+/s327}$ (ZDB-ALT-050617-10) (Gosse and Baier, 2009) from Andrew Waskiewicz (University of Alberta); and *tbx2b*$^{+/fby}$ (ZDB-ALT-070117-1) (Snelson et al., 2008a) (Clanton et al., 2013) from Josh Gamse (Vanderbilt University). Transgenic lines utilized were *Tg(-5.5opn1sw1:EGFP)*^{kj9} (ZDB-ALT-080227), *Tg(-3.5opn1sw2:mCherry)*^{ua3011} (ZDB-TGCONSTRCT-130819-1) (Duval et al., 2013; DuVal et al., 2014b; Takechi et al., 2003; Takechi et al., 2008), and Tg(-3.7rho:EGFP)^{kj2} (ZDB-ALT-060830-4) (Hamaoka et al., 2002). For *thrβ* knock down

experiments, embryos were injected with 10ng of either splice-blocking *thrβ* MO (5'-TCTAGAACTTGCAATACCTTTCTTA-3') (Suzuki et al., 2013a; Yoshimatsu et al., 2014) (ZFIN ID: ZDB-MRPHLNO-131114-1) or standard control MO (5'-CCTCTTACCTCAGTTACAATTTATA-3') (Kaiser et al., 2012) at the 1-2 cell stage, then were maintained as above.

3.3.3. Generating Transgenic dnthrβ Zebrafish

Dominant negative thyroid hormone receptor beta was generated by expressing a version of the cDNA modified to lack 12 amino acids from the C terminus, thereby removing the ligand binding and coactivator binding sites as previously accomplished in *Xenopus* (Schreiber et al., 2009) (Marsh-Armstrong et al., 2004). Primers utilized in construct creation were based upon *dnthrβ* mRNA NM_131340.1 and are: 5'-GGG GAC AAG TTT GTA CAA AAA AGC AGG CTC AGT ATG TCA GAG CAA GCA G- 3' (forward) and 5' -GGG GAC CAC TTT GTA CAA GAA AGC TGG GTG AGC TCT GTG GGA CAT TCC- 3' (reverse). Transgenic constructs were created using multisite Gateway cloning into vectors suitable for Tol2 recombination and transgenesis (Kwan et al., 2007). The sequence encoding dominant negative thyroid hormone receptor beta, or *dnthrβ*, was amplified from zebrafish cDNA and recombined with the hsp70 promoter sequence (allowing for conditional expression of the dominant negative receptor) and V2A.NLS.eGFP (for visualization of expression) to create the plasmid pDestTol2CG2.hsp70:dnthrβ.V2A.NLS.eGFP (Fig. 1). The V2A.NLS.eGFP sequence was kindly provided by Steven Leach (Provost et al., 2007). This construct was verified by sequencing and injected with Tol2 mRNA into zebrafish embryos at the 1-2 cell stage, and transient transgenic fish were raised to establish a stable transgenic line (line designation ua3113). Heat shock to induce transgene expression was performed at the ages indicated by placing Petri dishes (containing embryos in E3) in a water bath set to 37°C for two hours. Under these conditions the measured E3 media temperature reached 34°C. Transgene expression was confirmed through GFP expression visualized 4-6 hours following heat shock. To visualize the UV and blue cones, *Tg(hsp70:dnthrb.V2A.eGFP)*^{ua3113} fish were crossed to *Tg(-5.5opn1sw1: EGFP)*^{kj9} *; Tg(-*

3.5opn1sw2: mCherry)^{ua3011} carriers (Duval et al., 2013; DuVal et al., 2014b; Takechi et al., 2003; Takechi et al., 2008).

3.3.4. Genotyping for gdf6a and tbx2b mutations

Genotyping of adult and larval fish was performed via RFLP. Genomic DNA was extracted from fin clips from adults and whole larvae as previously described by Meeker et al. (Meeker et al., 2007), and regions containing the *gdf6a*^{s327} and *tbx2b*^{fby} loci were PCR amplified using the primers designed by Gosse and Baier for *gdf6a*^{s327} (forward 5'-ATGGATGCCTTGAGAGCAGTC-3'; reverse 5'-CTACCTGCAGCCACACTGTTC-3') (Gosse and Baier, 2009) and Snelson et al. for *tbx2b*^{fby} (forward 5'-TGTGACGAGCACTAATGTCTTCCTC-3'; reverse 5'-GCAAAAAGCATCGCAGAACG-3') (Snelson et al., 2008b). PCR products underwent restriction digest with BmsI (*gdf6a*) and SaqA1 (*tbx2b*) (FastDigest, FD2124 and FD2174) and were run on a 3% agarose gel. The *gdf6a*^{s327} mutation is detected by loss of a BmsI restriction site, such that wildtype product is digested into 170 and 110bp bands, and mutant product remains a single 280bp band. The *tbx2b*^{fby} mutation introduces a novel SaqA1 restriction site; wildtype product runs as a single 206bp band, and mutant product results in 169bp and 37bp products.

3.3.5. Immunocytochemistry and Imaging

Larvae were fixed at 4dpf in 4% paraformaldehyde overnight and wholemount immunocytochemistry was performed as previously described (Fraser et al., 2013a) (DuVal et al., 2014b). Briefly, larvae underwent washes in 0.1M PO_4/5% sucrose, then 1% Tween/H_2O (pH 7.4), then -20C acetone. Larvae were then blocked with 10% normal goat serum/PBS^{3+} and incubated overnight at 4°C in PBS^{3+} containing 2% NGS and antibody. Following incubation in primary antibody, larvae were washed with PBS^{3+} and incubated in secondary antibody overnight at 4°C.

Immunohistochemistry on cryosections was performed as follows: larvae were fixed at 4dpf in 4% paraformaldehyde overnight and dehydrated step-wise in 0.1M PO_4

with increasing concentrations of sucrose. Larvae were then embedded with frozen section compound (VWR, 95057-838) and the eyes cryosectioned (10µm/section) and mounted on Superfrost Plus slides (Fisher Scientific, 12-550-15). Sections were stored at -80°C until use, where they were re-hydrated with PBSTw, blocked in 10% NGS/PBSTw for 30-90 minutes, and incubated in primary antibodies diluted in 2% NGS/PBSTw overnight at 4°C. Slides were subsequently washed and incubated in secondary antibodies overnight at 4°C. All immunohistochemical steps were performed in a humid chamber.

Primary antibodies and dilutions used were: mouse 1D4 against zebrafish red cone opsin (1:500) (Abcam, ab5417) (ZFIN ID: ZDB-ATB-110114-2), rat 10C9.1 against UV opsin (1:100) (ZFIN ID: ZDB-ATB-140728-2) (DuVal et al., 2014b). Secondary antibodies/stains and dilutions used were: Alexafluor 647 chicken anti-mouse (Invitrogen, A-21463) (1:1000), Alexafluor 488 chicken anti-rat (Invitrogen, A-21470) (1:1000) or Alexafluor 647 chicken anti-rat (Invitrogen, A21472), and DAPI (Invitrogen, D1306) (1:1000). Retinas were then dissected and flatmounted. Imaging of wholemount and sectioned tissues was performed using a Zeiss LSM 700 confocal laser scanning microscope and Zen 2010 software (Carl Zeiss Imaging).

3.3.6. Image Analysis and Statistical Analysis

Images were analyzed in ImageJ or Fiji (Wayne Rasband, NIH, Bethesda, https://imagej.nih.gov/ij/index.html) (Schindelin et al., 2012) and data was analyzed in Stata/SE 14.1 for Mac (2015, StataCorp). For analysis of UV, blue, and red cones, abundances were counted within a 100µm x 100µm area just dorsal of the optic nerve head. For analysis of *tbx2b*^{fby} ; *thrβ* morphant retinas, rods were counted in a 50µm X 70µm box immediately dorsal of the optic nerve head, and UV cones were counted either in this same box (for retinas with wildtype UV cone distribution) or across the entire retina when there were few UV cones to count. Researchers were blinded to treatment group and genotype during photoreceptor counts.

3.4. Results

3.4.1. Gdf6a influences tbx2b in UV cone development

We had previously investigated the interaction of *gdf6a* and *tbx2b* in photoreceptor development, using the *tbx2b*^{lor} and *tbx2b*^{fby} mutants (hypomorphic and null alleles, respectively). *tbx2b*$^{lor/lor}$ mutants display the *lots-of-rods* phenotype with an overabundance of rods and a small number of UV cones, and *tbx2b*$^{fby/fby}$ mutants have lots of rods and a near-complete absence of UV cones (Alvarez-Delfin et al., 2009). While zebrafish heterozygous for *tbx2b*^{lor} or *tbx2b*^{fby} have typical rod and UV cone abundances, in a *gdf6a*$^{s327/s327}$ background (*gdf6a*$^{-/-}$ in Figures), some *tbx2b*$^{+/lor}$ or *tbx2b*$^{+/fby}$ embryos have an overabundance of rods (DuVal et al., 2014b). Here we re-examined the effects of this interaction and expanded upon it by assessing abundances of UV, blue, and red cones.

Quantification of cone abundances confirmed phenotypes that have been documented previously: homozygous *tbx2b*$^{fby/fby}$ mutants lack UV cones (Alvarez-Delfin et al., 2009), and *gdf6a* $^{s327/s327}$ mutants have a reduction in blue cones (39% fewer than wildtype, p= 0.003). Additionally, we found that *gdf6a* $^{s327/s327}$ mutant retinas have a novel phenotype of fewer red cones (29% reduction, p= 5.16x10^{-5}) (Fig. 3.1). In our previous publication, only the UV and blue cones were examined and quantified (DuVal et al., 2014b), so this red cone phenotype had not been appreciated. Cone abundances of fish heterozygous for either *gdf6a*^{s327} or *tbx2b*^{fby} were not different from wildtypes (Fig. 3.1). Absolute cone counts are available in Appendix 2, Fig. A2.1.

Fish heterozygous for *tbx2b*^{fby} but lacking *gdf6a* (*gdf6a*$^{s327/s327}$; *tbx2b*$^{+/fby}$) had a 23% reduction in UV cone abundance compared to wildtypes, a partial but statistically significant reduction (p=0.014) (Fig. 3.1). For *gdf6a*$^{s327/s327}$ mutants, blue cones were reduced further with *tbx2b*^{fby} mutation (81% reduction, p= 8.16x10^{-5} in *gdf6a*$^{s327/s327}$; *tbx2b*$^{+/fby}$ and 63% reduction, p= 6.49x10^{-6} in *gdf6a*$^{s327/s327}$; *tbx2b*$^{fby/fby}$). Red cone abundance remained low in all *gdf6a*$^{s327/s327}$ retinas, but interestingly this abundance was reduced further with sequential accumulation of *tbx2b* mutant alleles (51% reduction, p=8.16x10^{-5} in *gdf6a*$^{s327/s327}$; *tbx2b*$^{+/fby}$ and 64% reduction, p=2.37x10^{-6} in *gdf6a*$^{s327/s327}$; *tbx2b*$^{fby/fby}$).

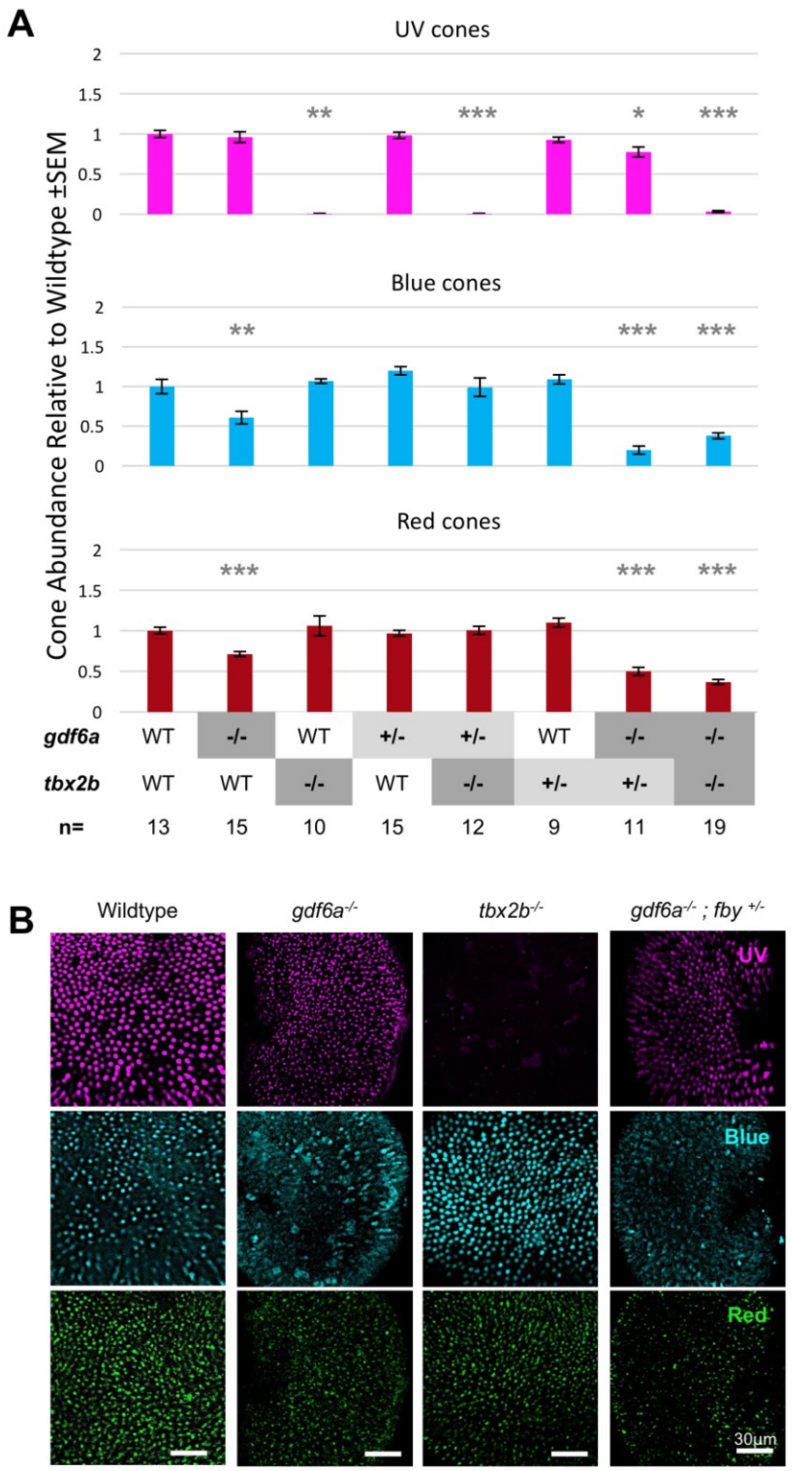

Figure 3.1. *gdf6a* loss in *tbx2b* heterozygous *fby* carriers reduces UV cone abundance.

A. Relative abundances of UV, blue, and red cones in compound *gdf6a*$^{+/s327}$; *tbx2b*$^{+/fby}$ in-crosses show near-complete loss of UV cones in *tbx2b*$^{fby/fby}$ mutants, and partial loss of UV cones in *tbx2b*$^{+/fby}$ mutants with *gdf6a*$^{s327/s327}$ background (labeled *gdf6as327/s327* or "-/-" in Figure) (compared to wildtypes (WT/WT), Kruskall-Wallis ANOVA, *p< 0.05, ** p>0.01, ***p>0.001). *Gdf6a* $^{s327/s327}$ mutants have reduced blue cones and a novel reduced red cone abundance phenotype, both of which appear either unaffected or slightly enhanced by *tbx2b* loss. Wildtype values shown are sibling controls. **B.** Representative retinal images depicting UV (magenta), blue (cyan), and red cones (green) in wildtype, *gdf6a* $^{s327/ s327}$, *tbx2b*$^{fby/fby}$, and compound *gdf6a* $^{s327/ s327}$; *tbx2b*$^{+/fby}$ mutants.

3.4.2. Thrβ knock down in tbx2b mutants partially rescues UV cones

Knock-down of *thrβ* causes a loss of red cones but also an increase in UV cone abundance; yet loss of *tbx2b* in null mutants (*fby* allele) causes complete loss of UV cones (with excess rods). We hypothesized that *thrβ* and *tbx2b* may act in the same UV cone development pathway, and so we utilized these tools to test if *thrβ* knock down could rescue the loss of UV cones in *tbx2b*$^{fby/fby}$ mutants. We injected 10ng of either *thrβ* MO or control MO into embryos of *tbx2b*^{fby} mutant incrosses with GFP in the rods [Tg(-3.7rho:EGFP)^{kj2}], and then labeled UV cones with antibody to assess the *fby* phenotype.

The *lots-of-rods* phenotype of *tbx2b*$^{fby/fby}$ mutants includes absence of UV cones and excess rods, and this was unaffected by injection of control MO. However injection of *thrβ* MO into these mutants yielded a small but significant UV cone population, the bulk of which is located across the middle of the retina's dorso-ventral axis (Fig. 3.2A, B). Interestingly, the excess rod phenotype was not diminished by the *thrβ* MO, rather the rod abundance also increased compared to control MO mutants (Fig. 3.2A). Examination

of one such *tbx2b*$^{fby/fby}$ thrb morphant retina for colocalization of UV and rod opsins (which would suggest an incomplete fate “switch”) had inconclusive results- while cells strongly labeled for 10C9.1 anti-UV opsin antibody showed some possible GFP expression in the cell body, this GFP signal was not as strong as neighbouring rods, leaving open the possibility of opsin co-expression.

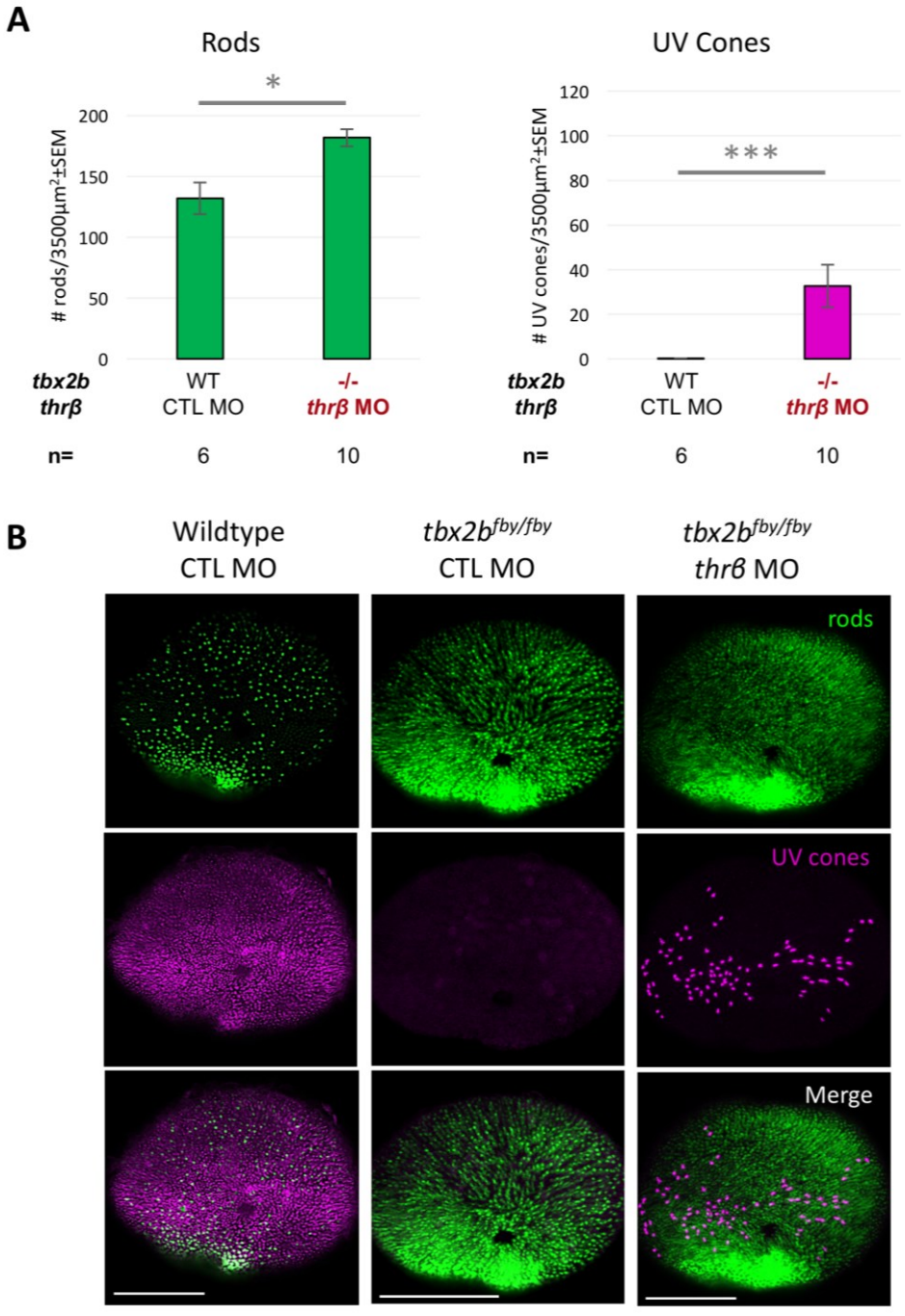

Figure 3.2. *thrβ* knockdown increases UV cones and rods in *fby* mutants.

A. Excess rods and absent UV cones are typical of *tbx2b*$^{fby/fby}$ mutants (labeled *tbx2b*$^{fby/fby}$ or "-/-" in Figure) this phenotype is not affected by control MO. UV cones are partially but significantly rescued when *thrβ* is knocked down in *tbx2b*$^{fby/fby}$ mutants (Kruskall-Wallis ANOVA with pairwise comparisons, * $p < 0.05$; ** $p < 0.01$; ***$p < 0.001$). **B.** Representative retinal images of rods and UV cones in control (CTL) MO-treated wildtype and *tbx2b*$^{fby/fby}$ retinas and *thrβ* MO-treated *tbx2b*$^{fby/fby}$ retinas. Scale bars 100µm.

3.4.3. Thrβ knock down in gdf6a mutants disrupts cone abundances and retinal lamination

Based on our cone quantifications in *gdf6a* mutants, Gdf6a signaling positively influences the red cone and blue cone populations. While loss of *gdf6a* alone does not alter UV cone abundances, it appears to increase sensitivity toward UV cone loss, as seen in *tbx2b* heterozygous mutants. *thrβ* is required for red cone specification, but it also negatively regulates UV cones, as *thrβ* morphants have a UV cone excess (Suzuki et al., 2013a). *Gdf6a* and *thrβ* have similar effects on red cone populations but differing effects on UV cone populations.

We wanted to resolve if *gdf6a* and *thrβ* act in shared or separate regulatory pathways toward UV cone fate. We generated two hypotheses: 1) *gdf6a* and *thrβ* act independently in UV cone development, where Gdf6a signaling promotes UV cones indirectly (possibly linked by *tbx2b*), and Thrβ suppresses UV cones separately from that; or 2) UV fate is regulated by *gdf6a* and *thrβ* in an epistatic fashion. For hypothesis 1, we would predict that lack of both factors, and lack of their opposing influences, would result in a wildtype abundance of UV cones. For hypothesis 2, we predict the lack of both causing either excess of UV cones (if *thrβ* knock down can override any sensitization to

UV cone reduction as caused by *gdf6a* loss) or a reduced abundance of UV cones (if *thrβ* knock down does not rescue sensitization). To test these predictions we knocked down *thrβ* in *gdf6a*$^{s327/s327}$ mutants with a *thrβ* splice-blocking morpholino which was previously used by others (Suzuki et al., 2013a).

Disruption of *thrβ* with 10ng of morpholino in *gdf6a*$^{s327/s327}$ mutants yielded a surprising set of results. When we examined wholemount retinas with antibody-labeled UV and red cones, *thrβ* morphants showed a consistent lack of red cone labeling regardless of *gdf6a* genotype, assuring us of the morpholino's efficacy (91% and 97% decrease in wildtype and *gdf6a*$^{s327/s327}$ respectively, p= 3.64×10^{-5}, p= 5.53×10^{-5}). In *gdf6a*$^{s327/s327}$ mutant retinas, the low blue cone phenotype persisted, and in fact dramatically worsened (98% decrease, p= 0.00005). In the UV cone channel, gaps or holes in the photoreceptor layer were apparent in *gdf6a*$^{s327/s327}$; *thrβ* morphants, which affected UV cone abundance counts (Fig. 3.3A, B). Absolute cone counts are available in Appendix 2 Fig. A2.2.

Radial sections of 4dpf *gdf6a*$^{s327/s327}$; *thrβ* morphant retinas revealed lamination defects impacting all retinal layers. Gaps in the photoreceptor layer were confirmed, and "bridges" of cells were found spanning the inner plexiform layer between the inner nuclear layer and ganglion cell layer (Fig. 3.3C). These lamination defects were not present when either *thrβ* or *gdf6a* were disrupted individually. This lamination phenotype suggests *thrβ* and *gdf6a* may be active in an early retinal development process, such that loss of one or the other has no overt effect, but loss of both interrupts lamination.

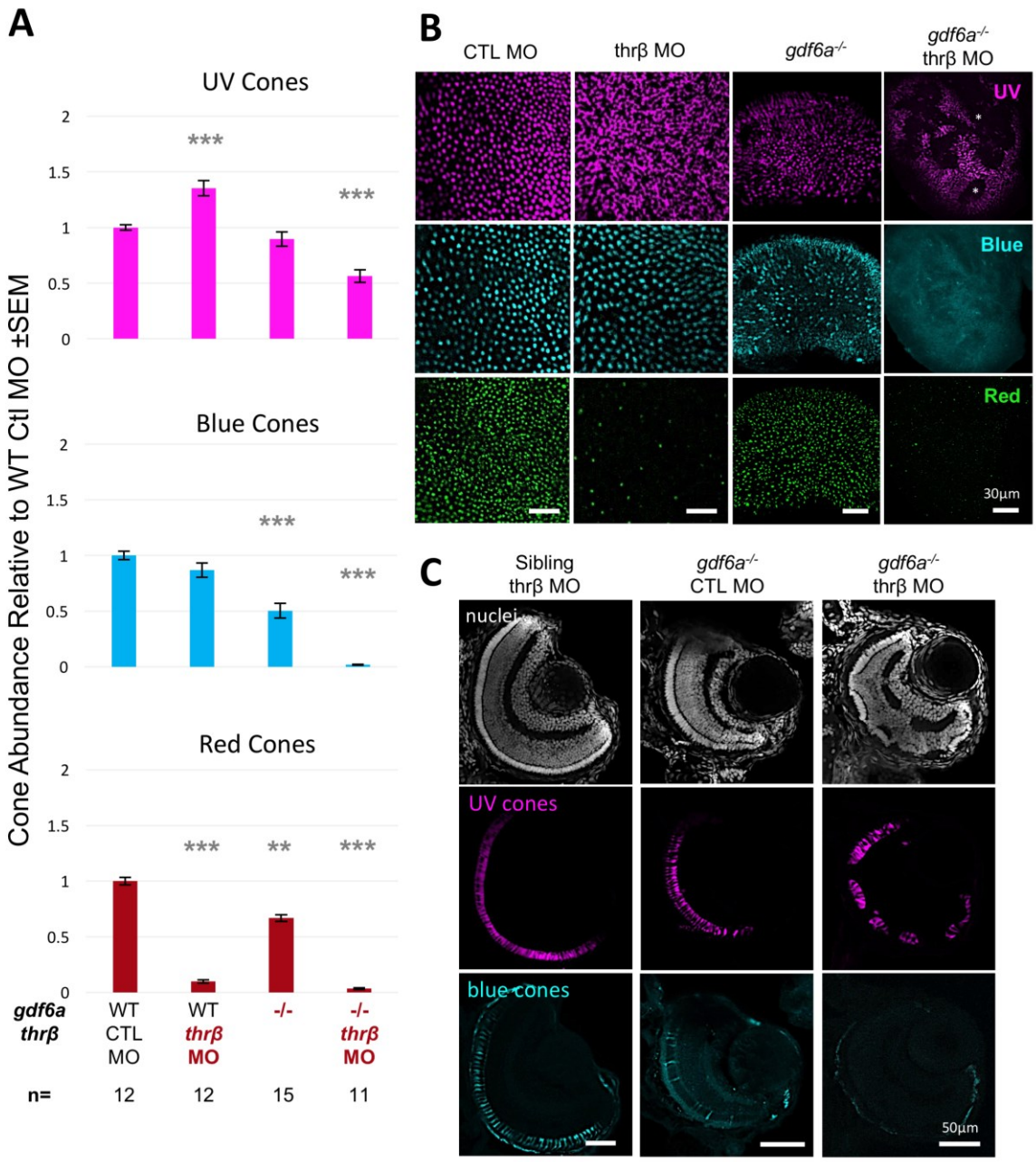

Figure 3.3. Knockdown of *thrβ* disrupts retinal lamination, including the photoreceptor layer, in *gdf6a*$^{s327/s327}$ mutants.

A. *Thrβ* knockdown with splice-blocking morpholino in *gdf6a*$^{s327/s327}$ mutants (labeled *gdf6a*$^{-/-}$ or "-/-" in Figure) fails to increase UV cone abundance, instead causing near-total loss of blue and red cones (compared to control MO injected wildtypes, Kruskall-

Wallis ANOVA, *p< 0.05, ** p>0.01, ***p>0.001). UV cone abundance decreased significantly, in contrast to *thrβ* knockdown in wildtype fish. **B.** Gaps or "holes" can be seen in the photoreceptor layer of *gdf6a*$^{s327/s327}$; *thrβ* MO-treated whole-mount retinas (two holes indicated by asterisks in UV image). These holes are not seen in control (CTL) MO-injected *gdf6a*$^{s327/s327}$ mutants, nor in wildtype or heterozygous morphants. **C.** Sections of 4dpf *gdf6a* $^{s327/ s327}$; *thrβ* MO-treated retinas show disrupted retinal lamination, with gaps in the photoreceptor layer that are occupied by cells of the inner nuclear layer, and cells disrupting the inner plexiform layer between the inner nuclear layer and ganglion cell layer (n=9 embryos examined per group).

3.4.4. Differential disruption of thrβ reveals new roles in cone development

The severity of the lamination defect limited our ability to quantify cone subtypes when *gdf6a* and *thrβ* are both disrupted, so to overcome this, we created a model of conditional Thrβ disruption via expression of a dominant negative receptor. It was determined through morpholino knock down that *thrβ* is required for red cone development (Suzuki et al., 2013a), however morpholinos must be introduced at the 1-2 cell stage, prohibiting manipulation of *thrβ* expression at later developmental stages. To further investigate *gdf6a* and *thrβ*, as well as actions of *thrβ* at different stages of cone photoreceptor development, we created a transgenic line with a construct created with Gateway recombination (Kwan et al., 2007) that enables expression of a dominant negative receptor predicted to disrupt endogenous receptor activity. Modeling after Ulisse et al.'s work expressing a dominant negative *thrβ* in *Xenopus* (Ulisse et al., 1996), we amplified the zebrafish *thrβ* sequence and removed nucleotide bases coding for the N-terminal 11 amino acids (which are necessary for ligand and coactivator binding). Without these binding sites, the receptor may dimerize and bind to DNA target sequences, but fail

to recruit the rest of the activation complex, and so transcription is not initiated. Expression of this dominant negative receptor (*dnthrβ* for short) was placed under the *hsp70* promoter to enable conditional induction upon heat shock, and is followed by eGFP (Fig. 3.4A). This construct was injected into 1-2 cell-stage embryos and a stable *Tg(hsp70:dnthrβ.V2A.eGFP*) line was established (designation ua3113). Heat shock induction allows us to temporally manipulate *dnthrβ* expression, thereby disrupting endogenous Thrβ proteins at specific developmental stages. It is important to note that the presence of a dominant negative stands in contrast to MO knockdown (in which receptor protein abundance is reduced), as it is predicted to create an incomplete complex that occupies promoter and enhancer regions to the exclusion of other complexes; therefore it is predicted to have negative transcriptional effects.

Upon heat shock, we observed zebrafish embryos show eGFP expression throughout the body (Fig. 3.4B). Without heat shock induction, eGFP expression is limited to the eye lens, which expresses *hsp70* during normal development (Blechinger et al., 2002).

We examined the effects of *dnthrβ* expression on cone photoreceptor subtype development in comparison to splice-blocking morpholino knockdown of *thrβ* (Suzuki et al., 2013a). Knockdown of *thrβ* causes near-complete loss of red cones and an increase in UV cone abundance (by approx. 35%, p=0.0003), whereas expression of *dnthrβ* via heat shock at 52hpf leads to increased UV (by 27%, p= 0.003) and blue cone abundance (by 36%, p=0.001) relative to heat shocked nontransgenic siblings (Fig. 4.4C). Absolute cone counts are available in Appendix 2, Fig. A2.3. Inducing *dnthrβ* expression at other time points, including 24hpf, 30hpf, and 36hpf, did not alter cone abundances as dramatically relative to controls (<20% change, data as normalized values available in Appendix 2, Fig. A2.4). This revealed an effect of *thrβ* that is limited to later in photoreceptor development: the endogenous receptor negatively regulates blue cone development, and the dominant negative receptor would dis-inhibit this process, allowing for more progenitors to assume a blue fate late in differentiation. In contrast, disrupting Thrβ either early (with morpholino knock down) or late leads to more UV cones.

Disrupting Thrβ protein activity via dnThrβ increased blue cone abundance (Fig. 3.4C, D), making *thrβ* only the second gene identified as affecting blue cone abundances

in zebrafish (or any animal), after *gdf6a* (DuVal et al., 2014b). Additionally, like morpholino knock down, the *dnthrβ* model has an excess UV cone phenotype, therefore we used this line to test whether Gdf6a signaling and Thrβ are epistatic in their regulation of UV cones (and/or blue cones). With the conditional activation of *dnthrβ* expression, we bypassed the *gdf6a*/ *thrβ* lamination phenotype by disrupting Thrβ activity after lamination. We heat shocked *gdf6a*$^{s327/s327}$*; hsp70:dnthrβ* embryos at 52hpf, as done previously. But instead of increasing UV and blue cone abundances, expressing dnThrβ in *gdf6a*$^{s327/s327}$ mutants yielded slightly reduced UV and significantly reduced blue populations (by 62%, p= $1.2x10^{-4}$); thus *dnthrβ* failed to rescue the *gdf6a* blue cone phenotype. *Gdf6a* $^{s327/s327}$ retinas also retained the phenotype of fewer red cones (up to 35% reduction compared to wildtype, p= 0.0001) regardless of *dnthrβ* expression (Fig. 3.5). Absolute cone counts are available in Appendix 2, Fig. A2.5.

Experiments with *dnthrβ* in *tbx2b*$^{fby/fby}$ mutants were not achievable as incrosses yielded very low recombination frequency between the *tbx2b fby* mutant allele and the *dnthrβ* transgene. It is therefore suspected that the transgene is inserted near the *tbx2b* locus.

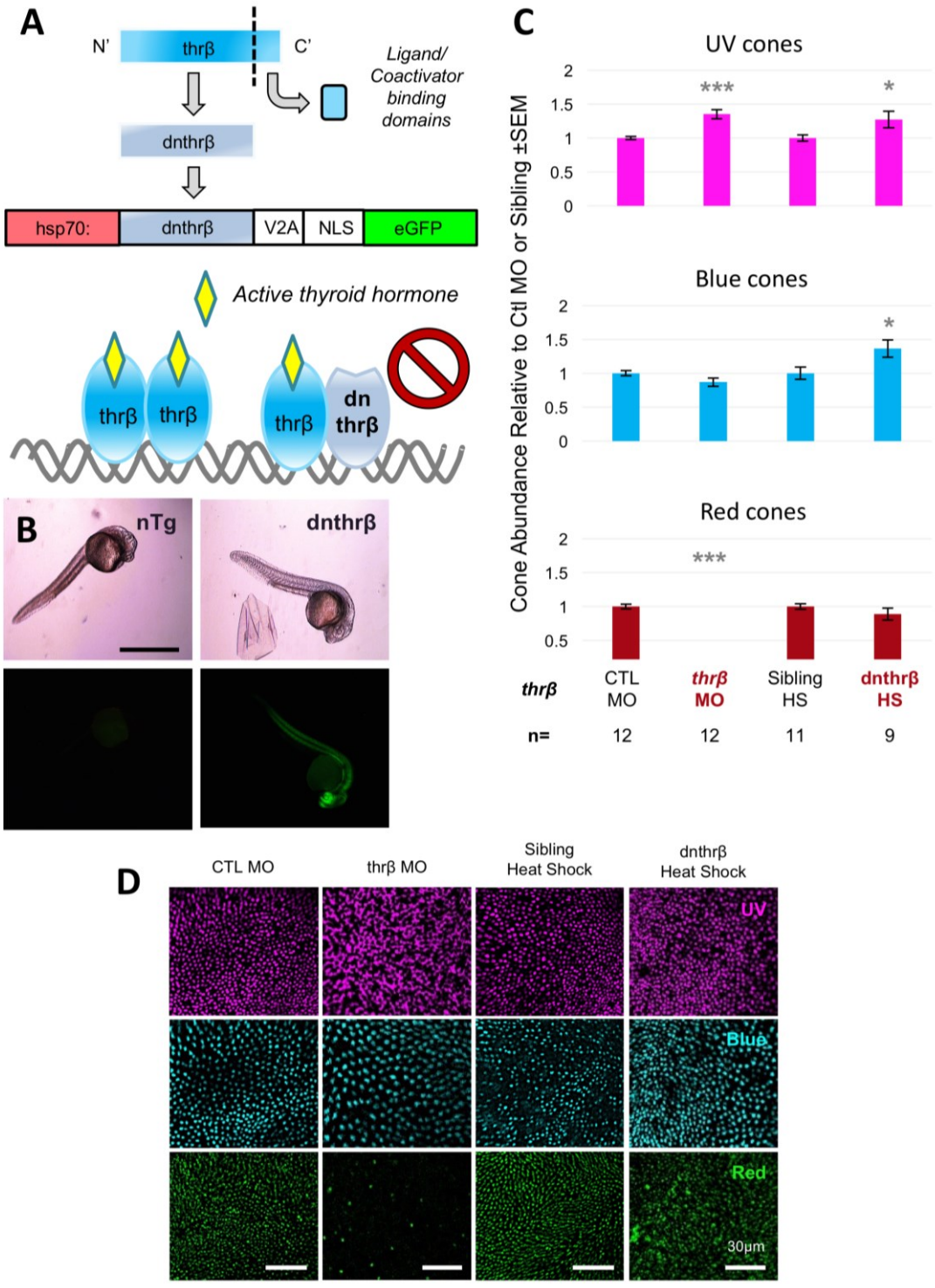

Figure 3.4. A transgenic zebrafish model of conditional Thrβ disruption reveals additional roles in cone development.

A. Generation of a dominant negative thyroid hormone receptor β was accomplished via an 11-amino acid C-terminal deletion, then cloned into a transgene encoding the dominant negative *thrβ* (*dnthrβ*) and eGFP under the hsp70 promoter. Endogenous Thrβ dimerizes and binds thyroid hormone to activate transcription (left), whereas dnThrβ would bind endogenous receptors but, lacking ligand and coactivator binding domains, would render dimers inactive (right). **B**. Transgenic embryos express the transgene, including GFP, throughout the body. Scale bar 1mm. **C.** *Thrβ* MO causes dramatic reduction in red cone abundance and increased UV abundance at 10ng dose. Our dominant negative model shows the same increase in UV cones but also a significant increase in blue cones (HS= heat shocked) (Kruskall-Wallis ANOVA, *p< 0.05, ** p>0.01, ***p>0.001). *Thrβ* MO data is normalized to control (CTL) MO data; *dnthrβ* HS data is normalized to sibling HS data.

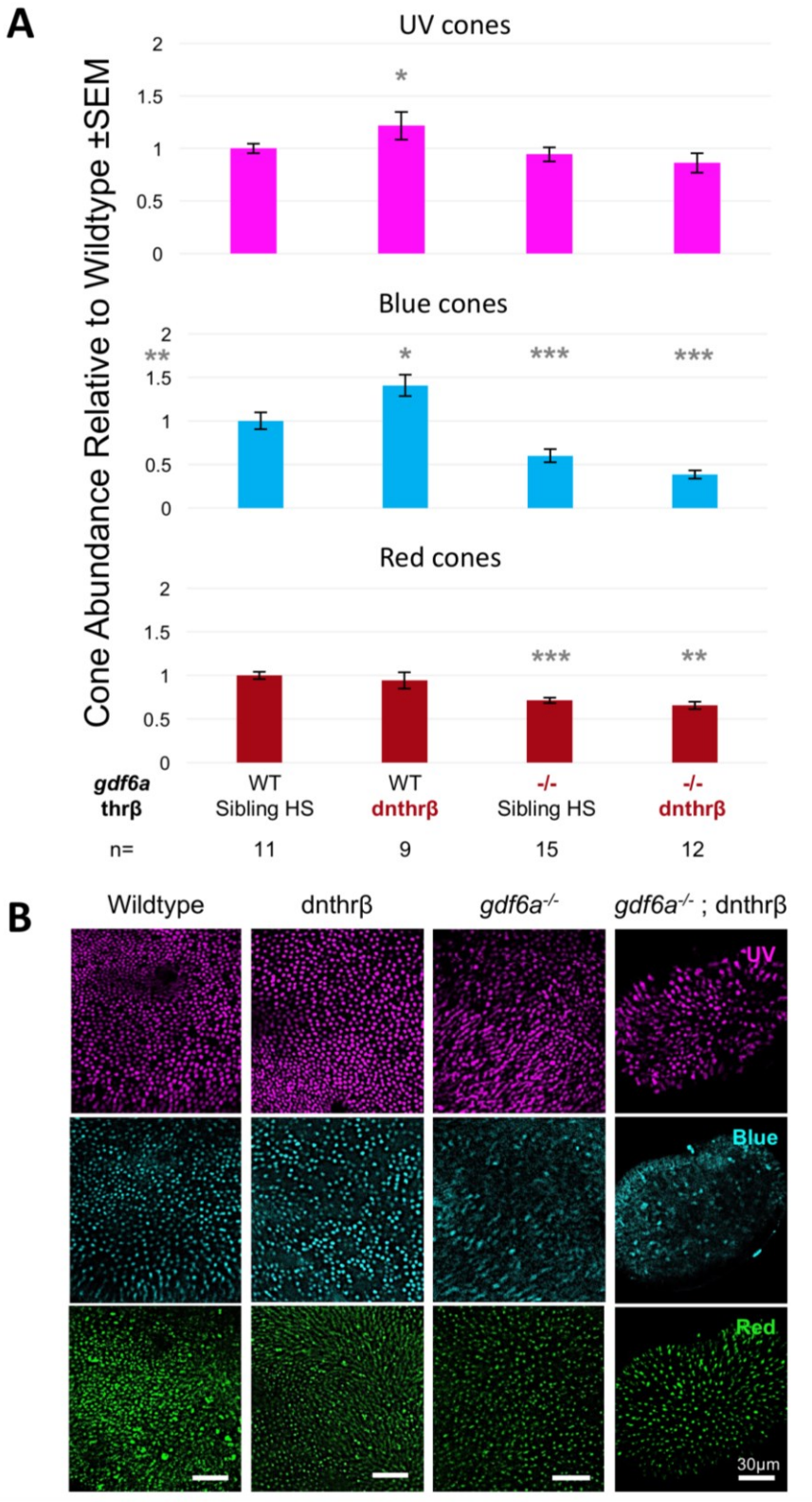

Figure 3.5. Thrβ disruption with dnThrβ does not rescue the *gdf6*$^{s327/s327}$ blue cone phenotype.

A. Expression of dominant negative *thrβ* (*dnthrβ*) increases UV and blue cone abundances, but in *gdf6a* $^{s327/\,s327}$ mutants (labeled *gdf6a* $^{-/-}$ or "-/-" in Figure) the low blue cone abundance is not changed and UV cones are not increased with *dnthrβ* expression. *Gdf6a* $^{s327/\,s327}$ mutants have reduced red cone abundance regardless of *dnthrβ* expression (compared to nontransgenic wildtype siblings, Kruskall-Wallis ANOVA, *p< 0.05, ** p>0.01, ***p>0.001) **B.** Representative retinal images of wildtype sibling, *gdf6a* $^{s327/\,s327}$, and *gdf6a* $^{s327/\,s327}$ with *dnthrβ* expression.

3.5. Discussion

In this work we describe novel genetic roles among *gdf6a*, *tbx2b*, and *thrβ* that impact cone differentiation, and which elaborate the cone differentiation regulatory network. We summarize the effects of *gdf6a*, *thrβ*, and *tbx2b* on cone development as found in our experiments here, and then explore the larger implications, including intersecting effects, of these factors on cone subtype development below.

3.5.1. Gdf6a signaling positively regulates tbx2b in UV cone development

Tbx2b is a downstream target of *gdf6a* in the early retina, contributing to dorsal identity and differentiation of dorsal retinal cells, as well as photoreceptor differentiation (DuVal et al., 2014b; French et al., 2009; French et al., 2013; Gosse and Baier, 2009; Gross and Dowling, 2005a). *Tbx2b* is required for UV cone identity during photoreceptor differentiation; homozygous *tbx2b* mutant retinas have few or no UV cones (*lor* and *fby* alleles are thought to be hypomorphic and null alleles, respectively) (Alvarez-Delfin et al., 2009). These mutants also present with an overabundance of rods (termed the *lots-of-rods* phenotype) (Alvarez-Delfin et al., 2009). The *lots-of-rods* phenotype can be elicited in some *tbx2b* $^{+/lor}$ heterozygous mutants if *gdf6a* is absent (i.e. *gdf6a* $^{s327/s327}$) (DuVal et

al., 2014b). Here, we crossed *tbx2b*^{fby} mutants to *gdf6a*^{s327} mutants to quantify the effects of the combined mutations on cone subtypes more comprehensively. A 23% reduction in UV cone abundance was observed in the *gdf6a*$^{s327/s327}$; *tbx2b*$^{+/fby}$ genotype compared to wildtypes, and this aligns with previous findings that these compound mutants are predisposed to excess rod generation (Alvarez-Delfin et al., 2009; DuVal et al., 2014b), thus *gdf6a* loss likely increases the sensitivity of progenitors to insufficient *tbx2b,* which affects both UV cone and rod abundance. Reduction in *tbx2b* wildtype gene dosage may also worsen *gdf6a* homozygous mutants' blue and red cone phenotypes, though the relevance of *tbx2b* to these cone types is less clear. In sum, *gdf6a* impacts upon both UV and blue cone development, plausibly via *tbx2b* for UV cones, and possibly via a different pathway for blue cones (Fig. 3.6).

3.5.2. Thrβ acts downstream of tbx2b in UV cone development

When the photoreceptors of *tbx2b* mutants were first studied, the paucity of UV cones and excess rods (Alvarez-Delfin et al., 2009) posited that *tbx2b* is necessary for UV cones in zebrafish (and without it, precursors become rods). This notion is now challenged by the data herein showing that, while *tbx2b* is important for UV cones, it is not absolutely required. *Thrβ* knock down in *tbx2b* mutants was sufficient to elicit a small number of UV cones, and so the regulation of UV cone development is more complex than previously thought. Based on the UV cone partial rescue, *thrβ* likely acts to suppress UV cones downstream of *tbx2b*. In the *tbx2b*-deficient retina, only some photoreceptor precursors respond to disinhibition from *thrβ* by becoming UV cones, and the majority of these are located along the midline of the dorsal-ventral axis. This patterning may indicate that a balance of additional factors (e.g. a signaling gradient) is necessary for this rescue, which occurs at midline. Additionally, the persistence and even enhancement of the rod overabundance in *tbx2b*$^{fby/fby}$; *thrβ* morphants uncouples the loss of UV cones from excess rods. These observations counter a hypothesis centered around a UV cone-rod fate switch that is proposed between S-cones and rods in mice (Forrest and Swaroop, 2012; Mears et al., 2001; Ng et al., 2011).

3.5.3. Thrβ promotion of red cones and suppression of UV and blue cones depends on photoreceptor development stage

Thrβ is required for long-wavelength-sensitive cone identity in mice, zebrafish, and likely chick as well (Ng et al., 2011; Sjoberg et al., 1992; Suzuki et al., 2013a); this represents a rare genetically and functionally shared node in vertebrate photoreceptor specification between these species and few other such commonalities have been experimentally demonstrated to date (i.e. beyond commonalities in gene expression) (Viets et al., 2016). Thus *thrβ* is of deep interest for comparative retinal development and we sought to extend the characterization of its role and position in the zebrafish photoreceptor regulatory network. With a *dnthrβ* conditional line we were able to discern that *thrβ* influences cone progenitors differently depending on developmental age. UV and blue cone abundances were both enhanced whereas red cones were unaffected when *dnthrβ* was expressed late in photoreceptor development. Thus we discovered that *thrβ* can negatively regulate zebrafish blue cone fate (mice, like all eutherian mammals, lack this sws2 cone subtype), in addition to regulating red cones and UV cones.

Loss of *thrβ* expression early in photoreceptor development (via MO knockdown) strongly affects red cone abundance (reduction) and UV cones (increase), but not blue cones. These differential and age-dependent responses to reduced Thrβ (in either availability or activity) suggest that the competency of cone progenitors regarding *thrβ* may change during retinal development. This interpretation of our data is consistent with observations of differential cone abundances when *thrβ* was ectopically expressed under various promoters with differential timing of expression (Suzuki et al., 2013a). Red cones appear to have a critical window of induction by *thrβ* shortly after initiation of *crx* expression, because in *thrβ* morphants the red cones can be rescued by *thrβ* expression driven by the *crx* promoter (i.e. as early as 19hpf), as described by Suzuki et al. (Suzuki et al., 2013a). In the same article, induction of *thrβ* after the final cell division resulted in cones that co-express red cone opsin with another cone opsin, an imperfect “rescue” (Suzuki et al., 2013a). Thus during the critical period for red cone differentiation, Thrβ induces red cone fate and suppresses UV cone fate, whereas after this period (in post-mitotic photoreceptors) Thrβ seems to merely activate red cone opsin expression (and

not change cone identity). Likewise, disrupting endogenous Thrβ with dnThrβ late in photoreceptor development, as done here, did not penalize the red cone population.

Using our model of conditional disruption of the Thrβ protein, we determined that Thrβ's effect on blue cones is limited to late photoreceptor development. We speculate that *thrβ*'s time-dependent effects on blue cone abundances may be a result of negative transcriptional actions, because this phenotype is not observed when *thrβ* expression is merely reduced by MO (see Fig. 3.2). Thrβ proteins are known to bind and occupy regulatory elements without activating transcription thereby preventing or reducing gene expression (Billings et al., 2010; Harvey and Williams, 2002), unless (or until) the requisite cofactors are present in adequate amounts, including active thyroid hormone T_3 and coactivators. Thus Thrβ may limit the number of cone progenitors assuming certain fates (UV cones, and blue cones later in development) and promote others (such as red cones) at the appropriate time. Modification of Thrβ's actions may occur through differential expression of co-repressors such as SMRT and/or dimerization with other thyroid receptors versus retinoid X receptors. As Thrβ is known to interact with RXRs and RORs in mouse development, and zebrafish cone differentiation initiates in the ventral retina where retinoic acid signaling is active (Harvey and Williams, 2002; Hyatt et al., 1996; Kelley et al., 1995; Marsh-Armstrong et al., 1994; Mitchell et al., 2015a; Stevens et al., 2011), these interactions are plausible. Expression of *dnthrβ* did not reduce red cone abundances significantly (check Appendix); we speculate that the timing of heat shock may have failed to capture red cone subtype generation, or the resultant dosage of *dnthrβ* was insufficient to reduce endogenous Thrβ activity below levels required for red cones. Based on observations, *dnthrβ* fish with two transgenic alleles largely do not survive to adulthood, thus embryos used in experiments were generated from crosses of single-allele fish; these embryos would more often have one transgene allele than two, which may have limited expression levels.

Interestingly, inhibition of Thrβ in the adult mouse retina enhances cone photoreceptor survival (Ma et al., 2014), which stands in contrast to its necessity for M-cone development and function in mice (Glaschke et al., 2011) and zebrafish (Suzuki et al., 2013a), and possibly similar roles in chicks (Enright et al., 2015; Trimarchi et al., 2008) and *Xenopus* (Cossette and Drysdale, 2004; Havis et al., 2006; Oofusa et al., 2001)

(though more studies are needed). Thus the role of *thrβ* is context-dependent: *thrβ* promotes specifically red cone identity within a specific window of development; outside this window, and outside of red cones, *thrβ* may have negative effects on cone development and survival.

3.5.4. Actions of thrβ in cone development are superceded by gdf6a

We next examined *gdf6a* and *thrβ*, as both are implicated in UV cone development. By knocking down *thrβ* in *gdf6a* mutants, we encountered a surprising disruption to lamination across all three retinal layers, as well as near-total lack of blue or red cones. This lamination defect is highly similar to the lamination defect in *insm1a* morphant zebrafish, which showed similar gaps in the photoreceptor layer with inner nuclear layer (INL) cells appearing to "invade" the photoreceptor layer (Forbes-Osborne et al., 2013). While the lamination defect in *insm1a* morphants is restricted to the INL and photoreceptor layer, our *gdf6a*$^{s327/s327}$; *thrβ* morphants had disruptions with bridges of cells between each layer. This overlap in lamination defects may hint at a process of lamination that is shared among *gdf6a*, *thrβ,* and *insm1a*. Each of these factors appears important for photoreceptor differentiation and maturation, and so the cells within the "bridges" may have defects in differentiation which disrupts their migration to the correct layer. If this were true, cells derived from the same shared progenitors that contained sufficient MO for disruption would almost all show the phenotype, and a single band of disturbed lamination would plausibly extend radially through the retina. We did not see this in any sections of *gdf6a*$^{s327/s327}$; *thrβ* morphants; instead areas of disturbed photoreceptor layer occurred in spatial independence of disturbances to ganglion cell layer (Fig. 3.3). Further work examining expression of *insm1a* under *gdf6a* disruption, as well as quantification of rods and the retina interneurons such as horizontal cells (which share a lineage with cones) and bipolar cells (which share a lineage with rods) is needed to determine if this shared phenotype is due to defects in differentiation.

To resolve whether *gdf6a* and *thrβ* are linked in terms of cone development, and to further understand the temporal nature of *thrβ* in cone differentiation, we created a

transgenic zebrafish with inducible dominant negative *thrβ* expression to disrupt endogenous Thrβ activity.

We then returned to the question of *gdf6a* and *thrβ* with the expanded question of whether they act in shared pathways toward UV or blue cone fate. Our new observation above that *thrβ* is required for suppressing blue cones is noteworthy in contrast to the requirement of *gdf6a* in promoting blue cone development. We thus expected to identify epistatic or other intersections between these factors using combinatorial genetic disruption. Intriguingly, neither the *thrβ* MO nor our *dnthrβ* transgene changed the *gdf6a* phenotype of low blue and low red cone abundances. While *thrβ* disruption in wildtype retinas increases UV cone abundance, UV cones were not increased in *gdf6a* mutants with *thrβ* disruption. Thus disrupting *thrβ* failed to rescue blue or red cones, or enhance UV cones, suggesting that the influence of *gdf6a* overrides that of *thrβ* in cone differentiation (Fig.3. 6).

Comparing the blue and red cone phenotypes seen in *gdf6a* mutants with either *thrβ* knock down or *dnthrβ* expression, it appears that disruption to both genes' functions negatively affects both types. Though *thrβ* knockdown in *gdf6a* mutants disrupted the photoreceptor layer, the remaining intact areas contained UV cones, but almost no red cones or blue cones (Fig. 3.3B). Thus the blue and red cone populations were more severely affected than UV cones. In *gdf6a* mutants expressing *dnthrβ*, the blue and red cone abundances were reduced in an additive fashion as well, though not as dramatically. These observations suggest that both *gdf6a* and *thrβ* promote red cones, but for blue cones the relationship is less clear- knock down of *thrβ* alone does not affect blue cones, but it does in combination with *gdf6a* loss. Along with the disrupted lamination phenotype, this near-complete loss of blue cones suggests *gdf6a* and *thrβ* may share other, unknown functions in retinal development that influence lamination and blue cone (and red cone) precursors.

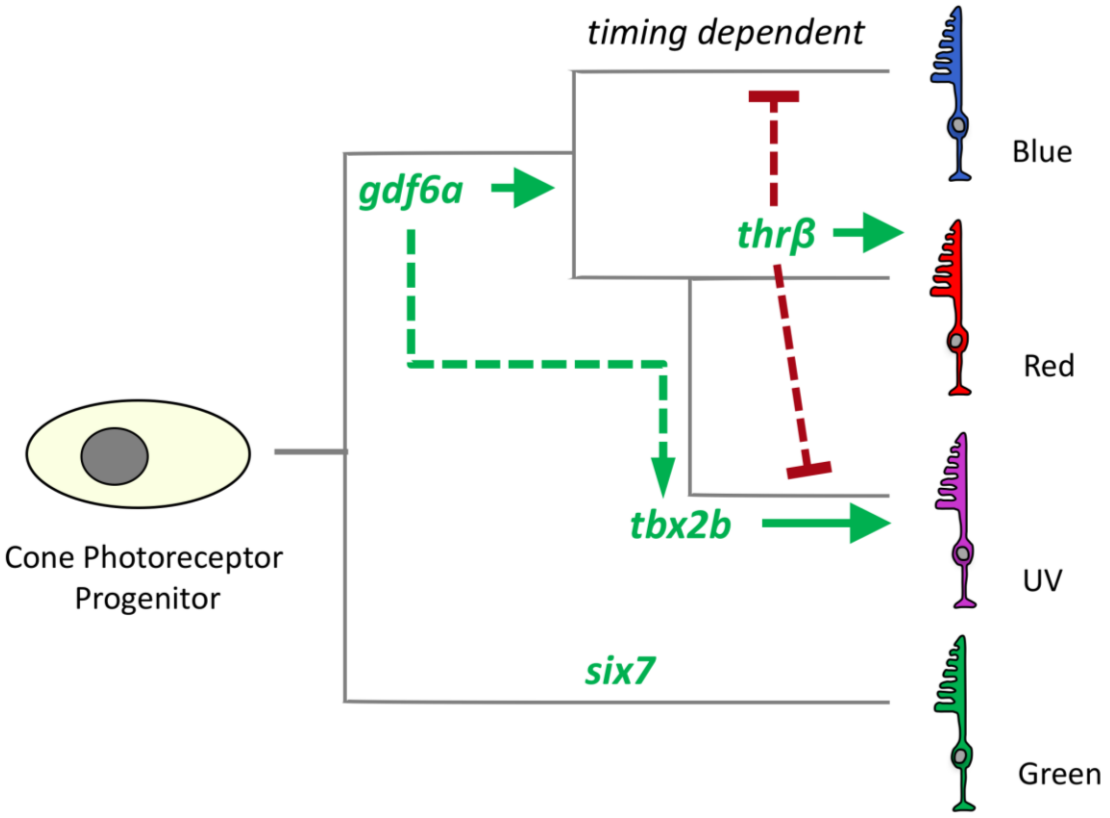

Figure 3.6. Regulatory actions of *thrβ*, *gdf6a*, and *tbx2b* in zebrafish cone photoreceptor differentiation.

The proposed pathway shown is a summary of the effects of the factors studied on cone subtype development, and does not represent order of expression, order of progenitor/precursor progression, or a chronological sequence of events. *Gdf6a* promotes blue and red cones (solid green arrows) and indirectly influences UV cones (dashed arrow), and *tbx2b* promotes UV cones. *Thrβ* stimulates red cone identity (solid green arrow) and inhibits UV cones and blue cones (red dashed lines), though its effects on blue cones appears limited to late photoreceptor development. *Gdf6a*'s regulation of blue and red cone abundances supercedes *thrβ*, thus its effects may be considered downstream of *thrβ*. Preliminary qPCR measurement of transcript

abundances for *gdf6*a, *tbx2b*, and *thrβ* showed increased (nonsignificant) *thrβ* expression in *gdf6a* and *tbx2b* mutants compared to wildtype embryos (Appendix 2, Fig. A2.6). *Thrβ* expression may thus be disinhibited in these mutants, which may contribute to the reduction/lack of UV cones in *tbx2b* mutants. Work by other groups established that *six7* is required for green cones, but it is not known whether the other factors, such as *gdf6a*, actively regulate green cones.

3.5.5. gdf6a loss disrupts retinal cell survival and proliferation, yet resulting cone subtype populations are not equally affected

Gdf6a$^{s327/s327}$ mutants exhibit numerous retinal phenotypes: increased apoptosis (Asai-Coakwell et al., 2013; French et al., 2013); a smaller progenitor pool (French et al., 2013), reduced markers of proliferation, and expanded expression of early-born neural progenitor markers *atoh7* (retinal ganglion cells) and *crx* (photoreceptors) (Valdivia et al., 2016); and we have found reduced blue and red cone abundances yet normal UV cone abundances (DuVal et al., 2014b), i.e. skewed cone populations and not simply a general reduction in all cone subtypes. We speculate here that these phenotypes may be interrelated, and that cone subtype outcomes may be differentially affected because of imbalances in cell survival and cell cycle in these mutants. Red cones are generated from a precursor population that also produces horizontal cells, and this type of precursor appears separate from that of other cone types (Suzuki et al., 2013a).

Beyond red cones we do not know whether the other types are derived from more than one precursor, but the *gdf6a*$^{s327/s327}$ cone phenotypes hint that cone types and possibly their precursors may not be affected equally by the dysregulation in cell cycle and survival. As red cones are reduced in *gdf6a*$^{s327/s327}$ mutants, an examination of horizontal cell abundance may offer insight into whether their shared precursor population is affected. Multiple observations point to UV cones deriving from a unique precursor type, as UV cones are uniquely affected in certain genetic paradigms: in zebrafish *tbx2b*

mutants, UV cones exclusively are reduced or lost (Alvarez-Delfin et al., 2009); UV cones are increased upon *thrβ* disruption both early and late in zebrafish retinal development (whereas other types show stage-dependent effects) ((Suzuki et al., 2013a) and here); and mouse *Nrl* mutants have excess S-cones (homologue to zebrafish UV cones), but not excess M-cones (Mears et al., 2001). If *gdf6a* loss skews precursor populations, then interventions to downstream processes may not rescue the affected cone daughter populations. These speculations await further testing.

3.5.6. Conclusion

The cone photoreceptor development relevant genes *thrβ*, *gdf6a*, and *tbx2b* interact in a fashion that is critical for the production of three cone types, and our work has found that their influences in cone subtype development intersect in intriguing ways, thereby adding new aspects to a model of vertebrate photoreceptor development. This and future work may provide new avenues to explore how the development of colour vision may be modified to suit the multitude of visual environments, including diverse colour environments, in which vertebrates live (DuVal and Allison, 2017). Further, a detailed model of vertebrate photoreceptor development, especially one featuring multiple cone subtypes, is a valuable framework for regenerative medicine. This framework, once established, will guide the modification of existing stem cell protocols and other therapeutic strategies toward higher cone production for restoring daytime vision.

Chapter 4. Growth Differentiation Factor 6 as a putative risk factor in neuromuscular degeneration

This chapter comprises the publication of the same title: DuVal MG, Gilbert MJH, Watson DE, Zerulla TC, Tierney KB, and W. Ted Allison (2014) Growth Differentiation Factor 6 As a Putative Risk Factor in Neuromuscular Degeneration. PLoS ONE 9(2): e89183. doi:10.1371/journal.pone.0089183 (DuVal et al., 2014a).

The questions, hypotheses, and experiments in this chapter were conceived and designed by MGD, MJHG, KBT, and WTA. Contributions to experiments are as follows: survival curves and eye and skeletal morphology were performed and analyzed by MGD and WTA with assistance from Allison Murray, Bradley Scott, and Neel Doshi for microCT imaging; swim endurance and sprint testing and analysis were done by MJHG, TCZ, and KBT; immunohistochemistry and image analysis were done by MGD and DEW. Christine Beattie generously shared the *os10* line. The manuscript was written by WTA and MGD, and edited by MGD, MHJG, DEW, TCZ, KBT, and WTA, with constructive feedback from Simonetta Sipione and Kelvin Jones.

4.1. Summary

Mutation of *Glass bottom boat*, the *Drosophila* homologue of the bone morphogenetic protein or growth/differentiation factor (BMP/GDF) family of genes in vertebrates, has been shown to disrupt development of neuromuscular junctions (NMJ). Here we tested whether this same conclusion can be broadened to vertebrate BMP/GDF genes. This analysis was also extended to consider whether such genes are required for NMJ maintenance in post-larval stages, as this would argue that BMP genes are viable candidates for analysis in progressive neuromuscular disease. Zebrafish mutants harboring homozygous null mutations in the BMP-family gene *gdf6a* were raised to adulthood and assessed for neuromuscular deficits. Fish lacking *gdf6a* exhibited decreased endurance (~50%, $p=0.005$) compared to wild type, and this deficit progressively worsened with age. These fish also presented with significantly disrupted NMJ morphology ($p=0.009$), and a lower abundance of spinal motor neurons (~50%, $p<0.001$) compared to wild type. Noting the similarity of these symptoms to those of

Amyotrophic Lateral Sclerosis (ALS) model mice and fish, we asked if mutations in *gdf6a* would enhance the phenotypes observed in the latter, i.e. in zebrafish over-expressing mutant Superoxide Dismutase 1 (SOD1). Amongst younger adult fish only bigenic fish harboring both the SOD1 transgene and *gdf6a* mutations, but not siblings with other combinations of these gene modifications, displayed significantly reduced endurance (75%, $p<0.05$) and strength/power (75%, $p<0.05$), as well as disrupted NMJ morphology ($p<0.001$) compared to wild type siblings. Bigenic fish also had lower survival rates compared to other genotypes. Thus conclusions regarding a role for BMP ligands in effecting NMJ can be extended to vertebrates, supporting conservation of mechanisms relevant to neuromuscular degenerative diseases. These conclusions synergize with past findings to argue for further analysis of *GDF6* and other *BMP* genes as modifier loci, potentially affecting susceptibility to ALS and perhaps a broader suite of neurodegenerative diseases.

4.2. Introduction

Development, growth and stabilization of neuromuscular junctions (NMJ) in larval *Drosophila* require the bone morphogenetic protein (BMP) gene *glass bottom boat (gbb)* (McCabe et al., 2003). Here we tested whether this same conclusion can be broadened to vertebrates, and extended this analysis to consider whether such genes are required for vertebrate NMJ maintenance in post-larval stages. *Gbb* is the *Drosophila* homolog of a family of vertebrate genes including the BMP and growth/differentiation factor ligands (BMP/GDF Family), which is itself a sub-family of the transforming growth factor β (TGFβ) genes (Baines, 2004; Kahlem and Newfeld, 2009; McCabe et al., 2003). Extending their role to encompass vertebrate NMJs would embolden speculation that mutations in BMP/GDF genes can sensitize patients to progressive late-onset neuromuscular disease. This affirmation would support the contended relevance of several intriguing cellular and molecular mechanisms of neuromuscular degeneration, derived from *Drosophila* studies (see Discussion), that are hypothesized to impinge upon the development of treatments or diagnostics of neuromuscular disease.

Indeed the synthesis of disparate literature by several authors has recently suggested that mutations in BMP/GDFs are good candidates for sensitizing patients to amyotrophic lateral sclerosis (ALS), if not representing causal instigators of disease etiology (Bayat et al., 2011; Ruschke et al., 2012). This suggestion was based not only on the aforementioned role of *Gbb* (Baines, 2004; McCabe et al., 2003), but also upon the requirement for the proteins constituting *Gbb* receptors in NMJ development (Eaton and Davis, 2005; Marques, 2005; Marques et al., 2003). BMP/GDFs have also been implicated in ALS progression via a separate line of inquiry, in that a *Drosophila* model of familial ALS8 demonstrates disrupted BMP signaling at their NMJs; Thus mutations in *VAPB* (vesicle-associated membrane protein B) cause ALS8 (Dion et al., 2009; Nishimura et al., 2004) and altering *VapB* disrupts BMP signaling at the *Drosophila* NMJ (Ratnaparkhi et al., 2008). A role for BMP/GDFs in other neuromuscular diseases has also been proposed, including Spinal Muscular Atrophy, Hereditary Spastic Paraplegias, Multiple Sclerosis and Huntington's Disease (Bayat et al., 2011).

BMPs are most widely recognized for their fundamental roles in development across vertebrates, including patterning the dorsoventral axis of the body, CNS and retina (Chang and Hemmati-Brivanlou, 1999; French et al., 2009; Gosse and Baier, 2009; Graff, 1997; Rissi et al., 1995; Sasagawa et al., 2002). BMP/GDF proteins heterodimerize or homodimerize to signal through BMP receptors, and canonically through phosphorylating SMAD proteins, though several other signaling cascades can be important in many instances (Miyazono et al., 2005).

ALS is a progressive neuromuscular disease caused by motoneuron loss, though the etiology of motoneuron death is unknown. Candidate causes include glutamate excitotoxicity, oxidative stress, and RNA processing defects. Symptoms in patients, recapitulated in animal models overexpressing mutant SOD1, include progressive muscle weakness and decreased endurance, altered gait, motor neuron death and progressive paralysis. Genetics of familial ALS (fALS) include lesions in TARDBP, FUS/TLS, C9orf72 and SOD1. Identification of misfolded SOD1 in sporadic ALS argues for a central role for SOD1 in ALS regardless of genetic or environmental initiators (Pokrishevsky et al., 2012b). *SOD1*^{G93A} mice are an indispensable staple in the ALS field because they exhibit many etiological similarities to, and present with disease progression that has fidelity to,

clinical ALS presentation. Zebrafish, with conserved CNS and motoneuron physiology/genetics, have proven very useful to study the genetic relationships between fALS genes via loss-of-function analyses (Hewamadduma et al., 2013; Kabashi et al., 2011; Laird et al., 2010; Lemmens et al., 2007; Metz et al., 2000; Schmid et al., 2013; Vaccaro et al., 2012; Van Hoecke et al., 2012). Furthermore, toxic gain-of-function zebrafish have been generated overexpressing mutant SOD1 and that recapitulate all hallmark attributes of fALS (McGown et al., 2013; Ramesh et al., 2010). A substantial percentage of fALS remains to be explained, and genes that modify such susceptibility have potential to be influential in late-onset disorders with complex interactions of genetics and/or environmental factors.

The proposed requirement for BMP/GDF6 family genes in vertebrate NMJs is supported by at least three previous lines of inquiry. First, disruption of intracellular trafficking led to NMJ deficits in zebrafish mutants of *atlastin*, and it was argued that this deficit was due to disrupted trafficking of BMP receptors (Fassier et al., 2010). Second, BMPs and BMP receptors are increased in expression at NMJs during recovery from experimentally induced traumatic injury in mice (Ruschke et al., 2012). Third, a role for TGFβ/BMP/GDF signaling in ALS progression is suggested by the increase in pSMADs in ALS inclusions observed in both patient pathology and mouse models (Nakamura et al., 2008; Nakamura et al., 2013; Nakamura et al., 2012). Although these lines of evidence are encouraging and suggestive, a role for BMP ligands in vertebrate neuromuscular degeneration remains unaddressed.

Our recent success in raising topical mutant zebrafish to adulthood (Asai-Coakwell et al., 2013) enabled us to address the questions above regarding a role for BMPs in the maintenance of vertebrate NMJs. Zebrafish harboring a null mutation in a homolog of *GDF6* were outcrossed, establishing a viable and fecund line of homozygous *gdf6a* mutants. Increased cell death in at least some CNS neurons was reported during early development of these mutants (Asai-Coakwell et al., 2013). This encouraged us to explore a potential role for *gdf6a* in neuromuscular degeneration, which would potentially implicate BMP/GDF6 genes as candidate loci in neuromuscular disease. We document progressive neuromuscular deficits in these mutants, including reduced muscle endurance, neuromuscular junction anomalies and loss of spinal motor neurons. Further,

this mutation in *gdf6a* increased disease severity in a zebrafish model of ALS that over-expresses mutant SOD1. These data integrate to compel *GDF6* as a candidate locus that increases susceptibility to or progression of ALS.

4.3. Methods

4.3.1. Ethics Statement

All fish husbandry and procedures were completed with approval of the University of Alberta Animal Care and Use Committee: Biosciences, in accordance with the Canadian Council on Animal Care.

4.3.2. Zebrafish husbandry and establishment of mutants and transgenic crosses

Zebrafish bearing *gdf6a*$^{s327/s327}$ (also known as *radar* $^{s327/s327}$ (Gosse and Baier, 2009), ZFIN ID ZDB-ALT-050617-10), referred to here as *gdf6*$^{-/-}$, previously identified as larval lethal, were recently acquired as viable adults through breeding of heterozygous mutants, preceded by backcrosses onto an AB background (Asai-Coakwell et al., 2013). Homozygous *gdf6a*$^{s327/s327}$ larvae were identified by the presence of microphthalmia at 3dpf and were raised separately from their siblings. Mutants and siblings were confirmed in several cases by genotyping from finclip derived DNA at adulthood (using primers 5'-TGTGAGACACGGCTCCACTT-3' and 5'-GCAGGACGAGAGCTTACCAA-3') and/or by examining the Mendelian frequency with which their progeny exhibited microphthalmia. At 9 and 18 months, *Gdf6a*$^{s327/s327}$ adults and WT siblings underwent a swim channel assay and were subsequently sacrificed for NMJ and spinal cord immunocytochemistry.

ALS model zebrafish, expressing mutant SOD1^{G93R} under control of the zebrafish *sod1* promoter (Ramesh et al., 2010), were generously provided by Christine E. Beattie. The fish, *Tg(sod1:sod1G93R,hsp70l:DsRed)os10* (ZFin ID: ZDB-GENO-101006-6), herein referred to as *os10*, can be readily identified from their expression of DsRed under a promoter that is independent of the *sod1* expression cassette, but linked immediately

contiguous to it in the construct. The *os10* line was crossed to *gdf6a*$^{s327/s327}$ fish, and screened for the presence of *os10* transgene following heat shock at 2dpf (Ramesh et al., 2010); the resultant compound heterozygous fish were inbred to acquire the combinations of *gdf6a*^{s327} and *os10* in the various combinations reported.

Zebrafish husbandry and breeding used standard methods (Westerfield, 2000a), with 14:10 L:D light cycle, 1300±100 μS conductivity at 28±1°C water temperature. Fish were fed a diet dominated by brine shrimp and trout chow.

4.3.3. Assessing primary motoneuron axonopathy in embryonic zebrafish

Zebrafish embryos were scored for abnormal primary motoneuron axonopathy, as previously described (Lemmens et al., 2007), in transgenic animals where primary motoneurons abundantly express GFP under control of the promoter *mnx1* (also known as *hb9,* ZFIN ID: ZDB-GENO-080606-250). Breeding created *gdf6a*$^{+/-}$*;Tg(mnx1:GFP)ml2* fish. These were bred to *gdf6a*$^{+/-}$*;Tg(sod1:sod1G93R,hsp70l:DsRed)os10* fish described above to generate genotypes including *gdf6a*$^{s327/s327}$ fish and siblings with labelled motoneurons and/or expressing mutant Sod1^{G93R}.

At 30hpf, larvae were visualized under a Leica MZ16F fluorescent stereomicroscope and axon branching was scored while the researcher was blind to genotype. As per established methods (Lemmens et al., 2007), branching of the GFP positive motoneurons was considered abnormal if it initiated at or above the ventral aspect of the notochord. Branching that was observed below this point was considered normal. The yolk sac extension was used as a landmark, and only the ten motoneurons immediately above it were scored for defects (Fig. S1). Subsequent to quantifying its axonopathy, each of the larvae was reared individually in 24 well plates until they were old enough to assess genotypes based on microphthalmia, and heat-shocked for one hour prior to screening for DsRed expression associated with *os10*. To assess the sensitivity of the axonopathy assay in our hands, *Tg(mnx1:GFP)ml2* fish were injected with 900 pg of mRNA encoding wildtype or G93A human SOD1. mRNAs were synthesized and delivered as per previous methods (Kaiser et al., 2012). Axonopathy scores per fish were analyzed using a Kruskall-Wallis ANOVA followed by a pairwise

Mann-Whitney U-test, calculated in SYSTAT 12. All p-values reported are two-tailed and significance was set at $p<0.05$.

4.3.4. Adult fish - assessing endurance in swim channel assay and activity in open field test

Individual fish were tested for their critical sustained swimming (U_{crit}), which was the maximum velocity at which they could swim for a set period in a 10L modified Brett-style swim tunnel (Loligo Systems, DK). Fish were placed in the swim tunnel under blackout hoods with infrared lighting (see below for characterization of lighting) and allowed to acclimate for 30 minutes to a low velocity current (5 cm/s). The flow rate was then increased every 10 minutes by 4 cm/s. Fish were monitored via infrared camera (SAV-CD120; Matco, QE) and Elgato video capture software (Elgato Systems, CA), and were considered to have reached maximum velocity when they were no longer able to maintain position in the current and fell into a screen at the back of the swim chamber. After fish fatigued the test was halted and the fish removed following a cool-down swimming period of 10 minutes at low velocity. The four month old fish were allowed to recover in the chamber at 5 cm/s for 45-minutes before completing a second test with shortened, one-minute steps to determine their maximum sprint swimming speed (U_{max}). The U_{crit} and U_{max} values were calculated using the Brett formula (Brett, 1964). All fish were measured for morphological traits that are potential covariates of swimming endurance (Gilbert et al., 2013; Plaut, 2000). Morphology measurements included: head length, muscle length, standard length, fork length, total length, body height, body width, caudal peduncle, and mass. Condition factor was determined using the standard formula from mass (g) and body length (BL; mm), calculated as $10^5 \bullet \text{mass}/\text{BL}^3$.

Open field tests on zebrafish were carried out on groups of three fish per tank under conditions nearly identical to their normal husbandry conditions regarding temperature, water chemistry, water flow rates and lighting (except that IR lights were used to enable video recording in the dark). Fish were transferred from their housing tanks to test tanks of the same dimensions and were acclimated for one hour prior to the start of testing (N=6 tanks with 3 fish each). Zebrafish motion was then recorded from

above for 10 minutes every hour for 24 hours, using IR-lit cameras (as above) and video surveillance software (Visio-soft; Matco, QE). Average swimming speeds were determined from video (15 measures per second) for each fish using behavioural analysis software (Ethovision XT8.5; Noldus, NL). Infrared lighting was characterized using a calibrated spectrophotometer (USB4000-UV-VIS Ocean Optics, Dunedin FL) connected to a 455 micron optical fiber (QP450-2-XSR, Ocean Optics) held at the approximate position that fish maintained during trials. Spectra were recorded to Spectra Suite software (Ocean Optics).

Differences in the day- and night-time swimming speed between *gdf6*$^{-/-}$ and wild-type fish were assessed using a two-way repeated measures analyses of variance with a Holm-Sidak post-hoc test. Differences in U_{max} (BL/s) and U_{crit} (cm/s) between genotypes were analyzed using one-way ANOVA's with Holm-Sidak post-hoc tests. Holm-Sidak adjusted p-values were reported. All swimming performance and open field test data were log transformed to achieve normality. All data were tested for normality (Shapiro-Wilk) and equal variance (Levene's test) prior to the use of parametric statistics. Multiple linear regression analyses were also performed using standard body length and genotype as explanatory variables of swimming performance to ensure that the detected differences were independent of fish size. The statistical analysis of swimming performance and activity was conducted using SPSS 20.0 (SPSS IBM, Chicago, IL) and Sigmaplot 11 (Systat Software, CA).

4.3.5. Adult zebrafish tissue preparation and immunocytochemistry

To assess neuromuscular junctions (NMJ), muscles from adult zebrafish were removed, cut transversely into quarters (anterior to posterior) and fixed in 4% paraformaldehyde/0.1M PO_4 for 24 hours at 4˚C. Samples were prepared for cryosectioning as per previous methods (Fraser et al., 2013b) by washing thrice in 5% sucrose/0.1M PO_4 (20 minutes), once in 12.5% sucrose/0.1M PO_4 (30 minutes), and overnight in 20% sucrose/0.1M PO_4. Samples were embedded and frozen in OCT media (Tissue-Tek 62550-12). 16 µm sections were serially placed on Superfrost Plus

microscope slides (Fisherbrand 12550-15). All sections used in immunocytochemistry were of the second-most anterior quarter of muscle.

NMJs were visualized by labeling pre-synaptic terminals and post-synaptic terminals as reported previously (Ramesh et al., 2010). Briefly, slides were blocked for 60 minutes in 10% NGS/PBSTw and incubated in 1:50 rabbit anti-synaptophysin (Invitrogen 180130) in 2% NGS/PBSTw overnight at 4˚C. Slides were washed with PBSTw and incubated in 1:500 AlexaFluor 488 chicken anti-rabbit (Invitrogen A21441)/1:100 AlexaFluor 555-tagged α-bungarotoxin (Invitrogen B35451)/2% NGS/PBSTw overnight at 4˚C. Sections were viewed with a Zeiss LSM 700 confocal mounted on a Zeiss Axio Observer.Z1 microscope and imaged with ZEN 2010 (version 6.0) software (Carl Zeiss MicroImaging).

To quantify motoneuron abundance, spinal cords were dissected whole and fixed in 4% paraformaldehyde/0.1M PO_4 for 24 hours at 4˚C. The spinal cords were then prepared for cryosectioning as previously described. Transverse sections (20μm) of each sample were serially placed on 6 Superfrost Plus microscope slides. Motor neurons were labeled as previously described (Ramesh et al., 2010). Briefly, slides were incubated in 0.003% H_2O_2/PBS for 20 minutes, blocked for 1 hour in 5% normal donkey serum (NDS)/1% DMSO/PBSTw, washed, and incubated in 1:100 goat anti-ChAT (Chemicon AB 144P)/2% NDS/1% DMSO/PBSTw for 3 days at 4˚C. Slides were rinsed and washed in PBSTw, and incubated in 1:500 Alexafluor 555 or Alexafluor 488 donkey anti-goat (Invitrogen A-21432 and A-11055)/2% NDS/1% DMSO/PBSTw overnight at 4˚C. Actin was labelled using phalloidin conjugated to AlexaFluor-488 (Invitrogen #A12379). Nuclei were stained with TO-PRO-3 (Invitrogen, #T3605). After three 30-minute washes with PBSTw, slides were coverslipped and imaged. Sections were viewed with a Zeiss LSM 700 confocal mounted on a Zeiss Axio Observer.Z1 microscope and imaged with ZEN 2010 (version 6.0) software (Carl Zeiss MicroImaging). Powerpoint 2008 for Mac (Microsoft) was used to assemble figures following being merged and/or linearly manipulated for brightness and contrast in Photoshop CS3, Zen confocal software (Zeiss), and/or Imaris x64 7.4.0 (Bitplane).

4.3.6. Histological analysis

NMJ volumes were measured using the voxel counter plugin for ImageJ 1.45 (Wayne Rasband, National Institutes of Health; http://rsbweb.nih.gov/ij/index.html) and colocalization was analyzed in Imaris x64 (version 7.4.0, Bitplane). Researcher was blinded to genotype prior to image analysis. Values were normalized to WT values (shown as either 100% or 1) and statistical analysis was performed with Kruskall-Wallis ANOVA (volume and colocalization measurements) and Mann-Whitney U test (colocalization measurements) on SYSTAT 12.

Motoneurons in spinal cord cross-sections were quantified as per established methods (Ramesh et al., 2010) by averaging the number of motoneuron cell bodies, identified as ChAT-positive objects greater than 10 μm, per section. Researcher was blinded to genotype during quantification and analysis. Statistical analysis was performed with Kruskall-Wallis ANOVA in SYSTAT 12.

4.3.7. Clearing and staining of skeletal elements

Clearing and staining of cartilage and bone was performed using established protocols (Taylor and van Dyke, 1985). Briefly, adult fish were fixed whole in 4% paraformaldehyde overnight, rinsed in distilled water and preserved step-wise in 30%, 70% and 95% ethanol. The fish were then placed in alcian blue stain (cartilage) (Sigma-Aldrich A5268) in 30% acetic acid/70% EtOH for 6 hours and placed in saturated sodium borate overnight. Depigmentation was performed using 15% peroxide/ 85% KOH for 25-50 minutes or until pigment was removed. Fish were partially cleared in 30% saturated sodium borate with 1:250 tissue culture grade trypsin (VWR, CA97061-708)(1/16 teaspoon/30mL). Bones were stained using a 1:1000 dilution of stock alizarin red dye (Sigma-Aldrich A5533) in 1% KOH for 1 hour, or until sufficiently pink. Afterward, fish were fully cleared in trypsin solution and preserved step-wise in 30% and 70% glycerin/ 1% KOH. Fishes were finally stored and imaged in 100% glycerin.

4.3.8. Imaging skeletal elements in zebrafish by microCT

Intact fish were fixed in 4% paraformaldehyde/5% sucrose in 0.1 M PO_4 buffer for 24 hours and washed in 0.1 M PO_4 pH 7.4. buffer 3-times for 20 minutes to remove fixative. Fish were incubated overnight in Lugol solution (Sigma-Aldrich; No. L-6146) with gentle agitation followed by three 20-minute baths in 0.1 M PO_4 buffer. Tissue was dehydrated in a graded ethanol series and kept at -20° C. To orient the specimen appropriately for scanning, it was partially embedded vertically in 2% agarose, caudal fin down, with the top half of a 15 mL Falcon tube serving as a mold. Imaging was performed on a SkyScan1174 (Bruker; Kontich, BE) compact Micro CT (50 kV x-ray source and inbuilt 1.3 MP cooled x-ray camera). Raw data obtained from the scanner was initially reconstructed using NRecon v. 1.6.6 (Bruker; Kontich, BE) and further processed to optimize viewing of structures of interest using Osirix v. 5.0.2 (Open-source DICOM Viewer). 360° rotating specimen videos were produced using Osirix v. 5.0.2 for viewing.

4.4. Results

4.4.1. Gdf6$^{-/-}$ zebrafish do not display motoneuron axonopathy in early development

Because *Gdf6*$^{-/-}$ mice are not viable beyond embryonic stages (Asai-Coakwell et al., 2013), we considered alternate animal models and asked if zebrafish deficient in a GDF6 homologue might present with neuromuscular deficits akin to ALS. Our recent work employed several generations of out-crosses to successfully isolate a viable line of homozygous null *gdf6a*$^{s327/s327}$ fish (ZFIN ID: ZDB-ALT-050617-10) that can be raised to adulthood (Asai-Coakwell et al., 2013). This nonsense mutation occurs in the pro-domain, at residue 55, abrogating production of mature Gdf6a ligand. These fish display microphthalmia (Asai-Coakwell et al., 2013), but are otherwise normal in development (Fig. 4.1A), adult morphology, and fecundity. A decreased longevity in *gdf6a*$^{s327/s327}$ fish compared to their siblings was noted, not reaching statistical significance in a small cohort (Fig. 4.1B).

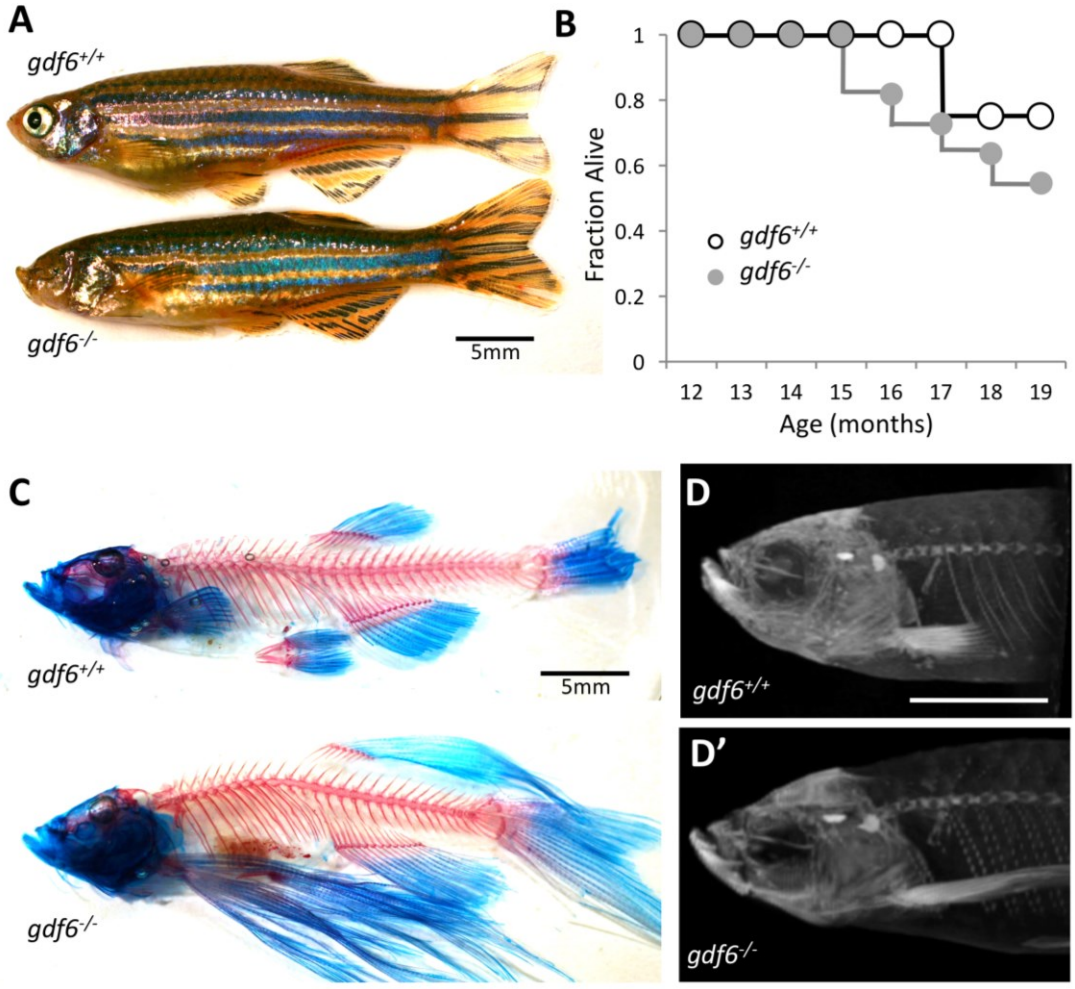

Figure 4.1. Zebrafish harboring homozygous mutations in *gdf6a* can be raised to adulthood and do not display overt skeletal defects.

A. *gdf6a*$^{-/-}$ or *gdf6*$^{-/-}$ fish are viable into adulthood, exhibit variably penetrant microphthalmia and normal body morphology. B. *gdf6a*$^{-/-}$ fish exhibit somewhat decreased survival compared to *gdf6a*$^{+/+}$ siblings (n= 11 gdf6-/- fish; n= 4 *gdf6a*$^{+/+}$ siblings). C, D. *gdf6a*$^{-/-}$ fish lack overt skeletal phenotypes, as revealed by (C) clearing and staining or by (D) microCT analysis. Scale bars are 5 mm. A variety of fin morphologies were present in the fish examined, but these were neither different

between experimental groups (genotypes) nor a significant covariant with swim performance (see Results).

To assess if *gdf6a*$^{s327/s327}$ embryos display motoneuron disease, we utilized sensitive assays of motoneuron disease/ALS that are deployed frequently in embryonic zebrafish, consisting of examining branching and pathfinding defects in GFP-positive primary motoneurons of transgenic fish (Hewamadduma et al., 2013; Kabashi et al., 2011; Laird et al., 2010; Lemmens et al., 2007; Schmid et al., 2013; Vaccaro et al., 2012; Van Hoecke et al., 2012). *gdf6a*$^{s327/s327}$ embryos did not display a significant increase in motoneuron pathfinding or axonopathies as determined in a transgenic background that enables sensitive detection of motoneuron morphology based on GFP fluorescence; both *gdf6a*$^{s327/s327}$ and siblings had a low rate of abnormalities in this scoring system (Appendix 3, Fig. A3.1; $p \geq 0.315$, $n \geq 9$ larvae per genotype). We confirmed that this assay was sensitive to ALS-related genetic lesions in our hands by delivering mRNA encoding human SOD1 with or without mutations associated with familial ALS (5.7 and 0.18 primary motoneurons affected per fish injected with $SOD1^{A4V}$ or $SOD1^{WT}$, respectively $p<0.05$), consistent with past results (Lemmens et al., 2007; Van Hoecke et al., 2012).

Considering ALS is a late-onset disease, it was of interest to characterize adult *gdf6a*$^{s327/s327}$ zebrafish with respect to ALS-like phenotypes. We examined fish at 9 to 18 months old (zebrafish are considered to be 'adult' at sexual maturity, ~3 months old and can thrive for 3-5 years of age) regarding muscle endurance, gait, motoneuron abundance and character of their neuromuscular junctions.

4.4.2. gdf6a loss in adult zebrafish leads to neuromuscular disease, including deficits in endurance

Deficits in muscle endurance are a hallmark of ALS progression consistently observed in murine and fish models (Ramesh et al., 2010). We quantified muscle endurance in *gdf6a*$^{s327/s327}$ and sibling fish by assessing their ability to swim against a strong, accelerating water current (Tierney, 2011b), from which we determined the critical

swimming speed (U_{crit}, the water flow velocity at which a fish can no longer maintain its position (Tierney, 2011b); See Methods). At 9 months of age, *gdf6a*$^{s327/s327}$ fish were found to have substantially reduced swimming endurance, with mean U_{crit} values approximately half those of *gdf6a*$^{+/+}$ siblings (Fig. 4.2A, B; p=0.005, n=12 and 9 fish, respectively). At 18 months of age, the same significant difference was observed between genotypes (Fig. 4.2B, p<0.0005, n=4 and n=3). Endurance was lower in the older fish within each genotype, though this difference between ages was not significantly different when comparing within genotypes.

The swim endurance (U_{crit}) values in the wild type fish above are within the range of values obtained in past studies, being higher than (Ramesh et al., 2010), lower than (McClelland et al., 2006; Plaut, 2000) or comparable to (Gilbert et al., 2013) previous results. Differences between studies are likely due to methodology, including duration of water velocity steps and flow chamber construction that can affect absolute values; thus comparisons between experimental configurations can be challenging, but the results are robust when compared within an experiment or laboratory.

An alternative interpretation of our endurance data is that fish were less able to perform the swimming test because of decreased availability of visual cues, due to microphthalmia. To rule out any confounding role for the visual deficits, swimming performance was assessed in a dark room under infrared light, which zebrafish are unable to detect (lighting conditions of the swimming endurance assay and zebrafish light sensitivity are characterized in Appendix 3 Fig. A3.2). A further alternative is that the fish have decreased endurance due to decreased activity patterns in their typical husbandry conditions, perhaps predicting decreased muscle fitness. Open field tests on groups of fish were performed in conditions closely mimicking the husbandry conditions in which these fish were raised, and conducted in multiple replicates during each hour through a full circadian cycle. No significant difference in activity was found, arguing against mean activity as a confounding factor in these fish (Fig. 4.2C, Fig. A3.2). The methods deployed were sensitive enough to detect lower average swim velocity in night vs. day (regardless of genotype, p<0.001), however no difference was detected between genotypes for average swim velocity during day (p=0.247) or night (p=0.814) (Fig. 4.2C).

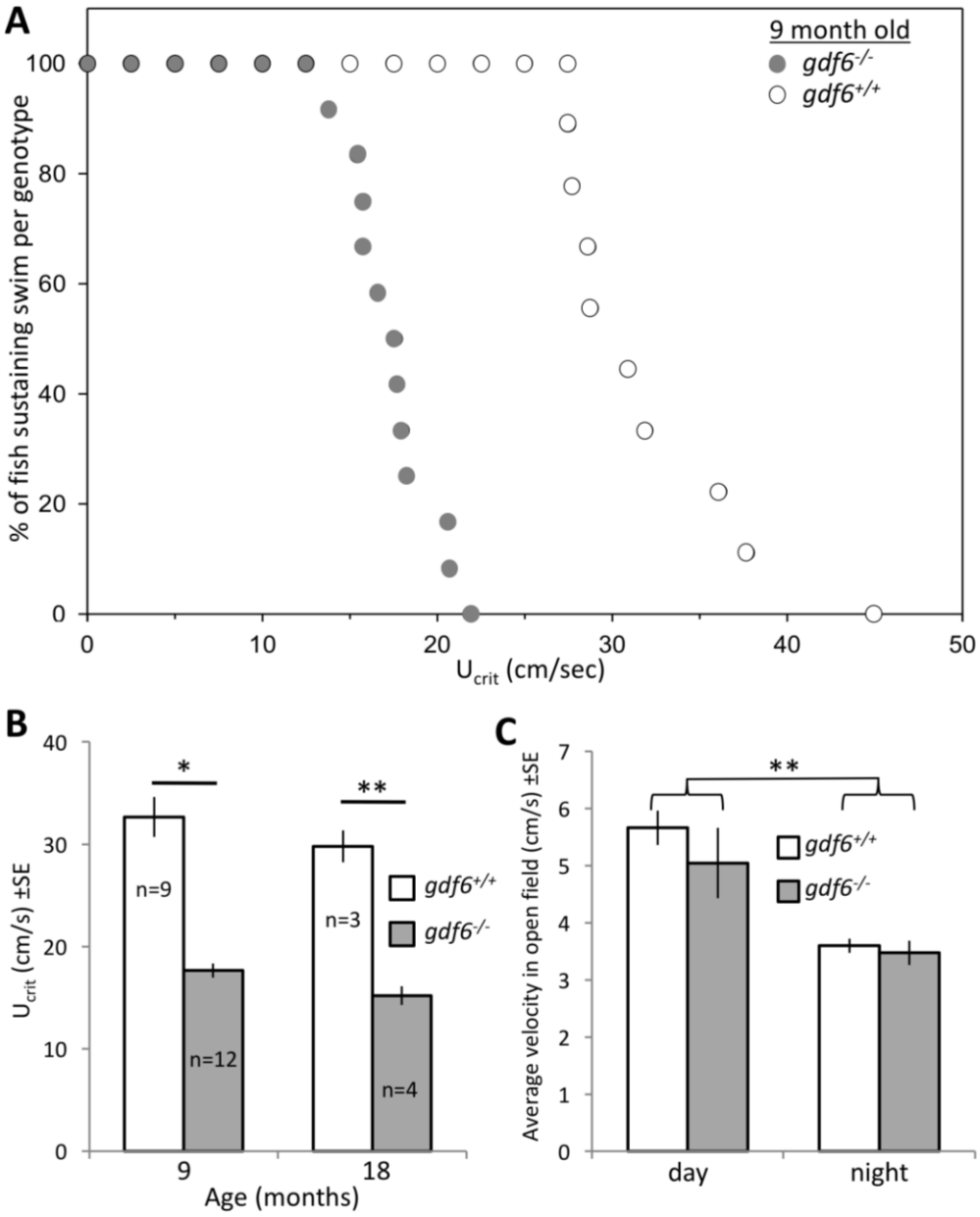

Figure 4.2. Zebrafish harboring homozygous mutations in *gdf6* exhibit decreased endurance.

A. *Gdf6a*$^{-/-}$ or *gdf6*$^{-/-}$ fish have a lower endurance compared to *gdf6a*$^{+/+}$ siblings as measured by increasing water velocity in a swim channel to determine the U_{crit} i.e. 'critical swimming speed' which is taken to be the highest speed that a fish can swim at for a period of several minutes before exhaustion. Each fish tested at 9 months is

plotted. **B.** The same data in A (9 month) plotted along with 18 month old siblings. *gdf6a*$^{-/-}$ fish have approximately 50% lower endurance compared to *gdf6a*$^{+/+}$ siblings at each age (*p =0.005, **p<0.01). Endurance trends towards being decreased in older fish of each genotype, but this difference is not significant. **C.** Open field tests of average swim velocity during 10 minutes of each hour through a circadian cycle, in tanks replicating lifetime husbandry conditions, show a lower mean movement at night (in either genotype, **p<0.01) but no difference between genotypes in any measure during day (p=0.247) or night (p=0.814).

A small difference was noted between genotypes in the open field test, only during mating activity at light onset (Appendix 3, Fig. A3.2), which accounted for the small non-significant decrease in overall activity of the *gdf6a*$^{s327/s327}$ fish. The difference observed during breeding is not relevant to the fish under consideration here, because they were raised and maintained in tanks that included sibling fish with normal eyes. When housed with normophthalmic siblings (our standard practice), *gdf6a*$^{s327/s327}$ fish had ample activity during breeding times and coordinately robust fecundity; this contrasts groups comprised solely of *gdf6a*$^{s327/s327}$ fish that had no breeding success. Thus the open field test we deployed under-represented the *gdf6a*$^{s327/s327}$ fish's activity during mating behaviour at light onset. In sum, the data argue against visual system deficits playing either an acute or long-term role in the muscle deficits of microphthalmic *gdf6a*$^{s327/s327}$ fish.

A further alternative explanation for deficits in swimming performance could be morphological changes resulting from long-term loss of *gdf6a*. Skeletal changes might be anticipated from BMP namesake functions in bone morphogenesis, from skeletal defects observed in patients with *GDF6* mutations (Asai-Coakwell et al., 2007b; Asai-Coakwell et al., 2009; Settle et al., 2003; Tassabehji et al., 2008) or past analysis of zebrafish *gdf6a* morphants (Ye et al., 2010). In adult zebrafish, skeletal deficits in the axial skeleton were not observed (Fig. 4.1). Body morphology was also assessed, and

no significant morphometric covariates of U_{crit} were observed, including condition factor (Appendix 3, Fig. A3.2). Caudal fin length was not different between experimental groups (One-way ANOVA $F_{5,31}$= 1.320 p =0.28) and was not a significant covariant in the relationship between experimental group and swimming performance (MLR: $F_{1,31}$=0.36 p= 0.55). Thus there was no evidence for a role of skeletal system malformation in the swimming deficits of *gdf6a*$^{s327/s327}$ zebrafish.

4.4.3. gdf6a loss in adult zebrafish leads to neuromuscular disease, including disruption of neuromuscular junctions

Histological hallmarks of ALS include neuromuscular deficits, comprising loss of motoneurons at the level of the spinal cord and abnormal structure of neuromuscular junctions (NMJ). Nine month old *gdf6a*$^{s327/s327}$ zebrafish were noted to have disrupted NMJ, including increased mean volume and greater variation of the presynaptic motoneuron compartment compared to wild type siblings (Fig. 4.3). This presynaptic motoneuron volume, when normalized to the post-synaptic volume, was nearly 3-fold greater in *gdf6a*$^{s327/s327}$ mutants (p= 0.009, n= 5 fish per genotype). Co-localization of pre- and post-synaptic compartments was not significantly different based on genotype (Fig. 4.3). Increased volume of pre-synaptic compared to post-synaptic NMJ compartments has also been observed in ALS model zebrafish overexpressing mutant SOD1 (Ramesh et al., 2010).

Further, *gdf6a*$^{s327/s327}$ fish at nine months of age were noted to have approximately 50% fewer spinal motoneurons compared to wildtype fish ($p<0.001$, Fig. 4.3D, E, F, $n>50$ sections from 4 fish per genotype), akin to changes observed in ALS model fish overexpressing mutant SOD1 (Ramesh et al., 2010).

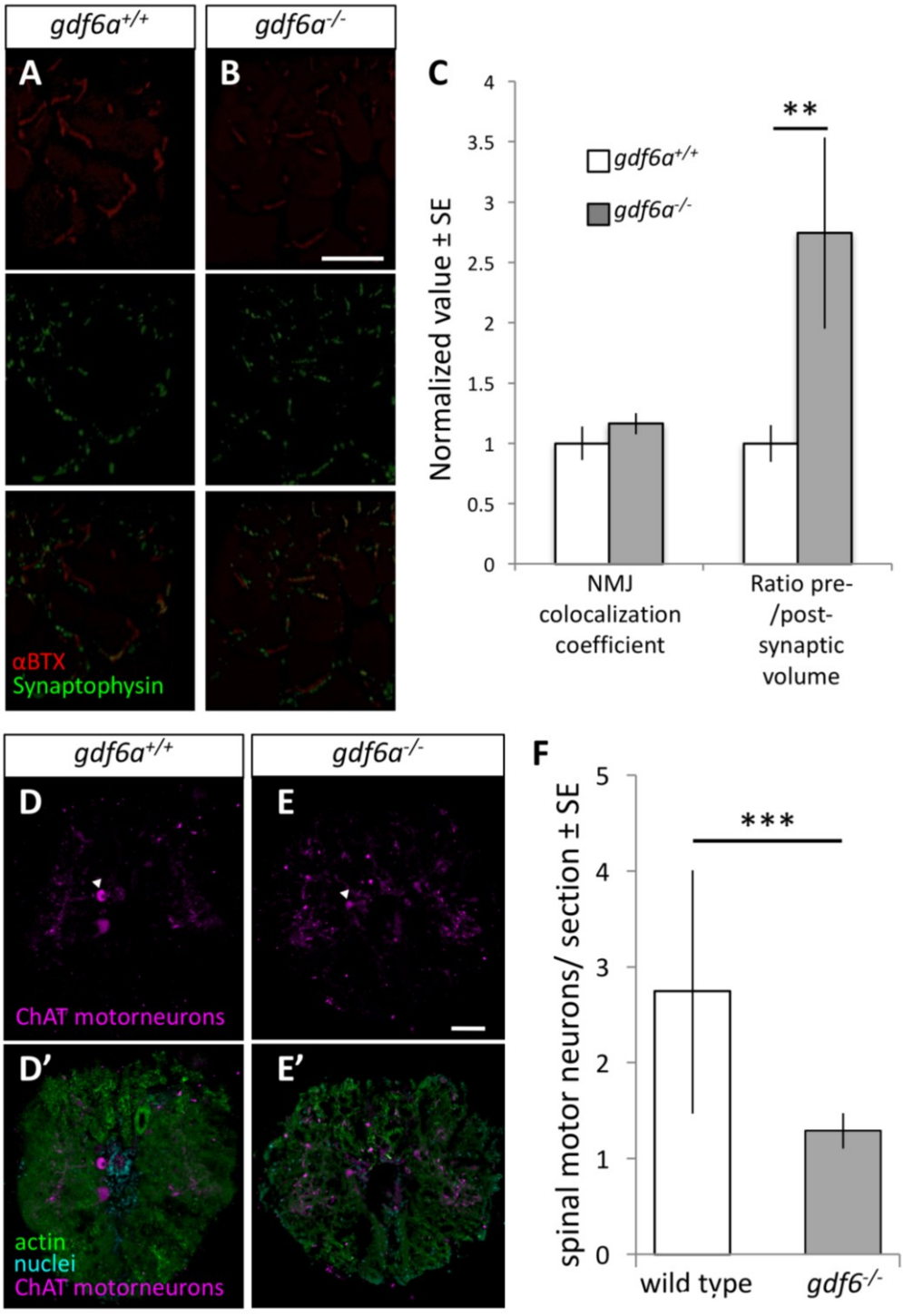

Figure 4.3. Zebrafish harboring homozygous mutations in *gdf6* exhibit altered neuromuscular junctions and fewer spinal motor neurons.

A-B. Assessment of neuromuscular junction (NMJ) morphology including presynaptic (synaptophysin) and postsynaptic (αBTX) compartments in 9 month old *gdf6a*$^{-/-}$ and *gdf6a*$^{+/+}$ siblings by immunohistochemistry. **C.** ALS-like increases in motoneuron pre-synaptic volumes are observed in *gdf6a*$^{-/-}$ fish when normalized to post-synaptic volumes (**p= 0.009, n= 5 fish per genotype). Coefficients of colocalization for pre- and post-synaptic compartments are not altered, as is expected in later-stage zebrafish ALS models. **D-E.** Motor neuron cell bodies were identified in cross-sections of spinal cord using immunohistochemistry against choline acetyl transferase (ChAT, e.g. arrowheads) in nine month-old *gdf6a*$^{+/+}$ and *gdf6a*$^{-/-}$ fish (panels A and B, respectively). ChAT-positive neuron bodies with a diameter of 10um or greater were counted as motor neurons, based on assays performed by other groups. Bottom panels affirm motoneuron cell body identification using actin and nuclear counter-stains. **F.** *gdf6a*$^{-/-}$ fish have approximately 50% the abundance of spinal motor neurons compared to sibling *gdf6a*$^{+/+}$ fish. (Mann-Whitney U Test, *** $p<0.001$, $n>50$ sections from 4 fish per genotype, researcher blinded to genotype during quantification). Scale bar = 60 μm in A,B and 50 μm in D,E.

4.4.4. Disruption of gdf6 hastens disease progression in a zebrafish model of ALS

We reasoned that if *gdf6a* mutation hastens disease progression, or increases susceptibility to ALS, then this should be recognizable in ALS animal models lacking *gdf6a* function. We bred *gdf6a* mutants to an established zebrafish model of ALS:

transgenic *os10* zebrafish that over-express zebrafish Sod1^{G93R} and develop symptoms of ALS very reminiscent of transgenic mice over-expressing human SOD1^{G93A} (Ramesh et al., 2010). Breeding *gdf6a*$^{+/-}$; *Tg(sod1:sod1*^{G93R}*;hsp70l:DsRed)*^{os10} fish generated six genotypes, consisting of three *gdf6a* genotypes (+/+, +/- or -/-), each with the *os10* transgene being present or absent. Herein we define 'bigenic' fish as those both homozygous null for *gdf6a* and possessing the *os10* transgene, i.e. *gdf6a*$^{s327/s327}$; Tg(sod1:sod1^{G93R};hsp70l:DsRed)^{os10}.

Similar to the observations on fish larvae with *gdf6a* lesions alone, no significant increase in axonopathy was noted in primary motoneurons when *os10* was also present in the larval genome (Figure A3.1). In older fish, amongst the six genotypes examined, it was apparent that a subset of bigenic *gdf6a*$^{s327/s327}$; *os10* fish failed to thrive. The time to reach 75% survival was approximately 6 months in bigenic ALS model zebrafish lacking normal gdf6a function, but more than 13 months in all other genetic combinations, including the same ALS model fish with at least partial *gdf6a* function (Fig. 4.4A).

Muscle endurance was assessed in bigenic *gdf6a*$^{s327/s327}$; *os10* fish and their siblings, using younger fish (4 months old) in an effort to capture any potential acceleration of disease progression. Deficits in swimming endurance attributable to gdf6a genotype alone were less dramatic at this young age: *gdf6a*$^{s327/s327}$ fish (lacking the *os10* transgene) had U_{crit} values approximately 75% those of their siblings but these differences were not statistically different (Fig. 4.4B). This smaller endurance deficit in young fish contrasts the significant reductions observed at 9 and 18 months of age (where U_{crit} was ~50% that of siblings, Fig. 4.2B), providing additional support for the contention that *gdf6a* loss of function leads to neuromuscular degeneration in a progressive manner.

Similarly, young *os10* fish consistently displayed decreased endurance within each *gdf6a* genotype, similar to what was observed previously for older *os10* animals (Ramesh et al., 2010), though in no case did this rise to the level of statistical significance (Fig. 4.4B). Only when the genetic lesions were combined were statistical differences attained, such that bigenic *gdf6a*$^{s327/s327}$; *os10* fish had U_{crit} values approximately 65% those of wild type fish (Fig. 4.4B, $p<0.05$ by MANOVA, sample size = 37, with 5-7 individuals per genotype as indicated on Fig. abscissa). Thus, in young adult fish, *gdf6a* and *os10* genotypes both imposed effects on muscle endurance that were consistent with

neuromuscular disease, but these deficits only reached statistical significance when both genetic lesions were combined.

Muscle strength/power was also assessed in these six genotypes, by documenting the ability of the fish to sprint against increasing velocities of water flow. This constant acceleration test was similar to the U_{crit} endurance test, but with water velocity increased at an accelerated rate such that fast-twitch white muscle became dominant, allowing the velocity at fatigue (U_{max}) to be calculated (Farrell, 2007; Tierney, 2011a). Neither the presence of the *os10* transgene nor loss of *gdf6a* function were individually potent in reducing swimming strength in these young fish (Fig. 4.4C). Only when the two genetic lesions were combined was any statistically significant deficit in swimming power observed, compared to wild type fish. Thus bigenic *gdf6a*$^{s327/s327}$; *os10* fish had U_{max} values approximately 75% those of wildtype fish (Fig. 4.4C, $p<0.05$ by MANOVA, sample size = 37, with 5-7 individuals per genotype as indicated on the Figure.).

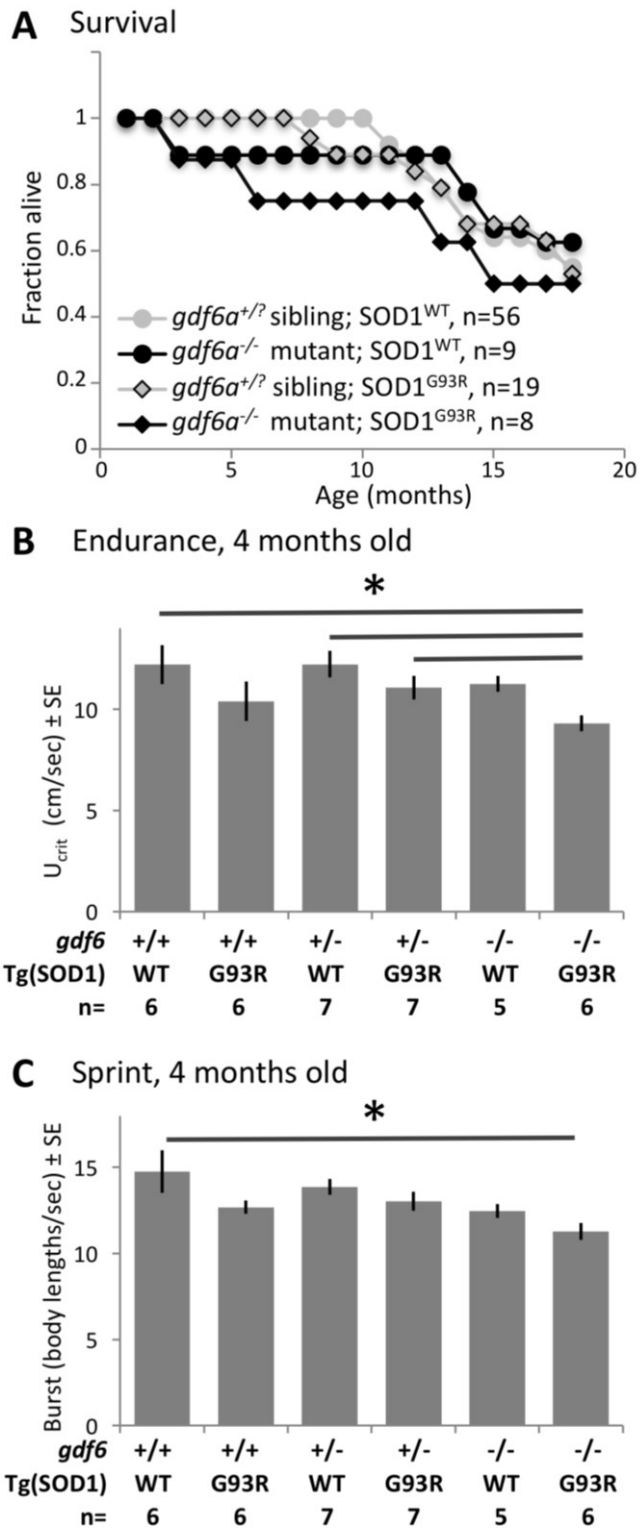

Figure 4.4. Mutations in *gdf6a* sensitize SOD1^G93R zebrafish to develop ALS-like symptoms.

Six genotypes combining *gdf6a*$^{-/-}$ alleles and SOD1^{G93R} alleles were examined in endurance and sprint tests, which primarily measure red and white muscle respectively. The SOD1^{G93R} fish mimic many aspects of ALS progression (Ramesh et al., 2010). Swimming performance was measured in all six genotypes (determined by outcrosses and examining progeny) at 4.5 months of age. **A.** bigenic fish, i.e. *gdf6a*$^{-/-}$ mutants expressing SOD1^{G93R}, had decreased survival compared to all other genotypes, i.e. their siblings (*gdf6a*$^{+/+}$ or *gdf6a*$^{+/-}$) with or without SOD1^{G93R}. **B.** bigenic *gdf6a*$^{-/-}$ mutants expressing SOD1^{G93R} had significantly lower endurance compared to heterozygous siblings also expressing SOD1^{G93R}, and to WT and heterozygous siblings without SOD1^{G93R}. **C.** Sprint test demonstrates a significant deficit in white muscle function only when SOD1^{G93R} and *gdf6a*$^{-/-}$ genotypes are combined (=25% deficit). (ANOVA and multiple linear regression, $p<0.05$; sample size indicated below graph).

These same bigenic *gdf6a*$^{s327/s327}$; *os10* fish and their siblings were subsequently examined for neuromuscular junction abnormalities. Both *os10* and bigenic *gdf6a*$^{s327/s327}$; os10 fish at 7 months of age had increased presynaptic/postsynaptic volume ratios compared to wildtype siblings, though the differences did not reach statistical significance (Fig. 4.5A, B. Kruskall-Wallis ANOVA $p=0.134$, n= 6 WT, 4 *os10*, 6 *gdf6a*$^{s327/s327}$; *os10*). Further, NMJs in bigenic *gdf6a*$^{s327/s327}$; os10 had significantly decreased overlap of synaptic compartments compared to either *os10* or wildtype siblings (Fig. 4.5B) (Kruskall-Wallis ANOVA, $p<0.001$). Mander's colocalization coefficients for the postsynaptic compartment were significantly lower for bigenic *gdf6a*$^{s327/s327}$; *os10* fish, implying loss of synaptic connectivity because postsynaptic compartments were less colocalized with presynaptic compartments despite the increase in presynaptic size (Fig. 4.5B) (Kruskall-Wallis ANOVA, $p<0.05$). Thus the *gdf6a*$^{s327/s327}$ genotype does not alter co-localization

of NMJ pre- and post-synaptic compartments on its own (Fig. 4.3C), but it further exacerbates the ALS-like NMJ abnormalities observed in bigenic fish expressing overexpressing mutant *SOD1*.

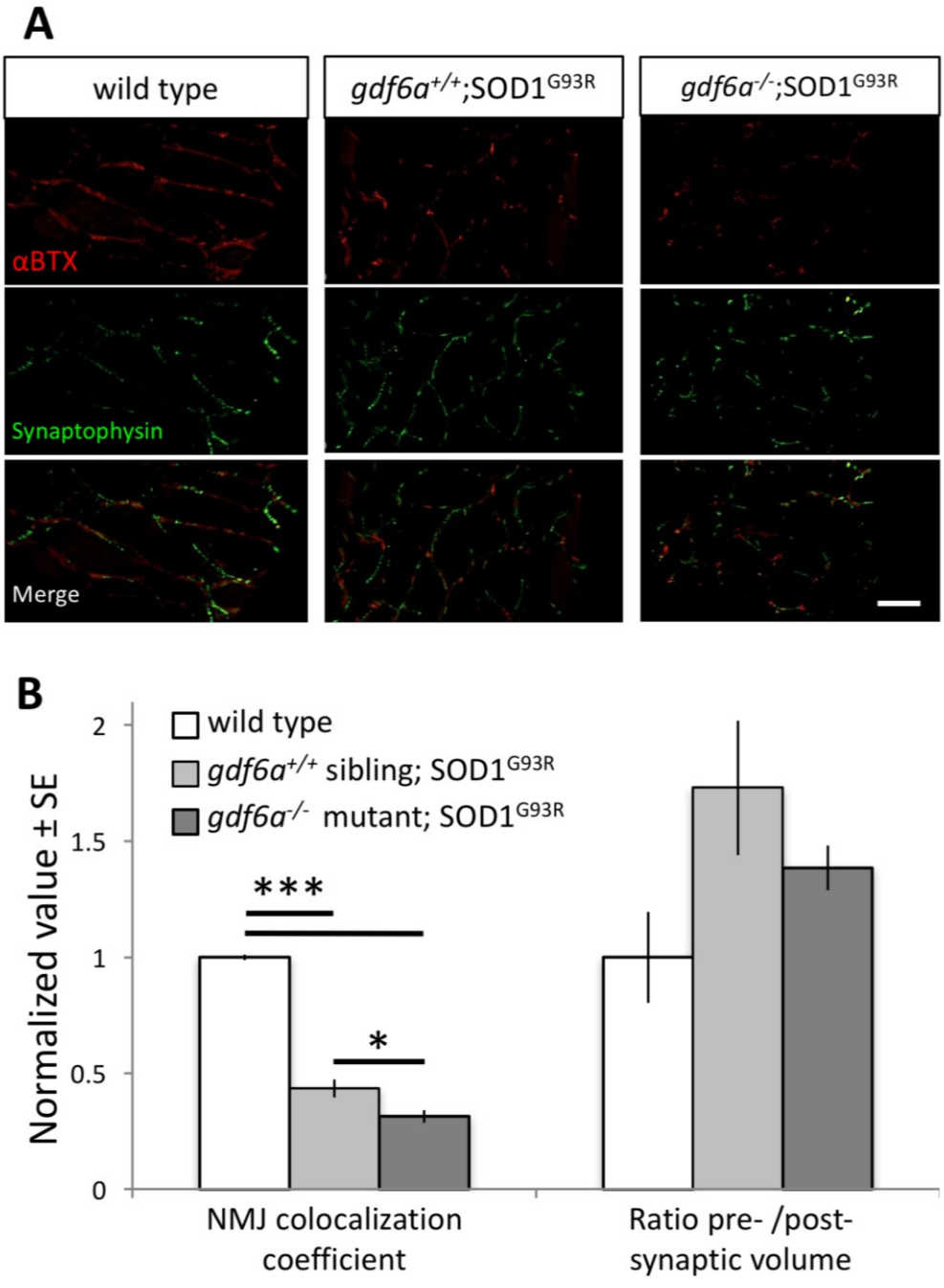

Figure 4.5. Disruption of *gdf6a* function exacerbates neuromuscular junction abnormalities in ALS model zebrafish.

ALS model zebrafish possess disruptions to neuromuscular junctions (NMJ), and loss of *gdf6a* function exacerbates this by 7 months of age. **A.** The presynaptic junctions (labeled with synaptophysin antibody) and postsynaptic junctions (labeled with fluorescently tagged αBTX) in ALS model zebrafish expressing the mutant SOD1^{G93R} show punctate morphology, deviations in presynaptic volume and less overall colocalization compared to WT sibling junctions. Some abnormalities are exacerbated in bigenic siblings expressing the mutant SOD1^{G93R} that are also *gdf6a*$^{-/-}$ (scale bar is 40 μm). **B.** Quantification of these NMJs suggests the presynaptic/postsynaptic volume ratios of SOD1^{G93R} and bigenic *gdf6a*$^{-/-}$; SOD1^{G93R} zebrafish are larger than those of WT siblings at this age, though these differences do not rise to statistical significance (Kruskall-Wallis ANOVA, p=0.134; n=6,4,6 for WT, SOD1^{G93R}, and bigenic fish respectively). Colocalization coefficients, that measure overall colocalization of presynaptic and postsynaptic junctions, are altered in these fish. The values for SOD1^{G93R} zebrafish are significantly lower than wild type sibling values, indicating that presynapses and postsynapses overlap less, as characterized previously for this transgenic ALS model (Ramesh et al., 2010). Bigenic SOD1^{G93R} zebrafish that are also *gdf6a*$^{-/-}$ have a dramatically lower coefficient than either sets of siblings, including being 30% lower than ALS model SOD1^{G93R} fish with normal *gdf6a* (*p< 0.05; ***p< 0.001. Kruskall-Wallis ANOVA with pairwise comparisons).

Overall, loss of Gdf6 function led to an acceleration of disease progression in this ALS animal model, as measured by longevity, integrity of neuromuscuslar junctions,

muscle endurance and muscle strength. These data are in good accordance with the hypothesis that deficits at the *GDF6* locus can sensitize animals to onset and/or progression of neuromuscular degeneration akin to ALS.

4.5. Discussion

Zebrafish harboring homozygous null mutations in a *GDF6* homologue were found to be viable, fecund and robust into adulthood, though exhibiting somewhat reduced longevity. Homozygous *gdf6a*$^{s327/s327}$ fish had progressively severe deficits in endurance, loss of spinal motoneurons and disrupted neuromuscular junctions compared to the wild type siblings, very much akin to ALS model zebrafish. Furthermore, progression of neuromuscular disease in ALS model zebrafish was accelerated when this homologue of *GDF6* was mutated: older zebrafish expressing mutant SOD1 exhibit ALS-like symptoms, but young fish only exhibited significant ALS-like neuromuscular deficits when on a *gdf6a*$^{s327/s327}$ background.

Regarding ALS and other neuromuscular diseases, support for BMPs' relevance is continuing to be revealed by genetic studies in *Drosophila*, including that a homologue of BMPs and homologues of BMP receptors are each required for normal NMJ development in flies (Aberle et al., 2002; Bayat et al., 2011; James and Broihier, 2011; McCabe et al., 2003), but suggestions of such functions for BMP pathway components rarely extend to vertebrates. Within vertebrates, BMP receptor type II has recently been localized to mouse NMJs, and one of its ligands BMP4 was found in close proximity (Chou et al., 2013). BMP4, BMP5 and their receptors have also been shown to have a role at some synapses in the CNS (Xiao et al., 2013). A role for BMPs in the vertebrate neuromuscular system has more frequently been suggested following motoneuron or spinal cord injury (Henriquez et al., 2011). Recent work has also demonstrated a role for proper trafficking, including that of BMP receptors, in primary motor axon outgrowth during zebrafish development (Fassier et al., 2010), instigating a search for which component of the BMP gene family might underpin this effect. A potential example may be *GDF15*, a member of the BMP subfamily with divergent properties and typically associated with macrophage recruitment and inflammation, in that *GDF15* disruption

causes loss of motoneurons in mice (Strelau et al., 2009). A link between BMP signaling and neuromuscular disease is suggested by the observation of phosphoSMAD proteins (downstream signaling components of TGFβ/BMP/GDF signaling) being enriched in pathological ALS inclusions (Katsuno et al., 2011; Nakamura et al., 2008; Nakamura et al., 2013; Nakamura et al., 2012). Human genetics suggests that loci associated with hereditary spastic paraplegia, including *ATL1*, can regulate BMP receptor trafficking and effect neuromuscular disease (Fassier et al., 2010; Henriquez et al., 2011). Despite this substantial level of interest, we are not aware of previously published data from vertebrate experiments or human genetics directly linking BMP/GDF gene family members (ligands or receptors) with ALS or any neuromuscular disease.

A substantial proportion of ALS susceptibility remains unexplained with respect to human genetics. Analyses herein support *GDF6*, a member of the BMP family, as worthy of further consideration. A role for *GDF6* homologues in progressive, late-onset neuromuscular disease was supported herein by muscle physiology, histopathology and behavioural assessment of zebrafish carrying mutations in *gdf6a*. Further, *gdf6a* loss of function accelerated disease progression in a zebrafish model of ALS. The synthesis of this data combines with recent reports of a role for *GDF6* in congenital and late-onset photoreceptor degenerations (Asai-Coakwell et al., 2013; Zhang et al., 2012) to compel a role for *GDF6* as a modifier gene in the etiology of disparate neuropathies.

4.5.1. BMPs in neurodegenerative disease

Inappropriate growth factor expression and signaling have been linked to inflammation and apoptosis in other neural diseases such as Alzheimer's, Parkinson's and, in one instance, Creutzfeldt-Jakob Disease, which are characterized by inappropriate accumulation of misfolded proteins, leading to neuron death via a multitude of proposed pathological pathways (Deininger et al., 1995; Li et al., 2011; Vawter et al., 1996). *TGFβ1* and *TGFβ2* expression are high in brains afflicted with Alzheimer's, causing inflammation, astrogliosis and neuron death through such pathways as NADPH oxidase-induced oxidative stress and caspases (Hashimoto et al., 2005; Wyss-Coray et al., 2000). *Xenopus* TGFβ1, a member of the same gene superfamily as *GDF6*, is

released from Schwann cells and can promote synaptogenesis at NMJ (Feng and Ko, 2008). TGFβ1 is an effector of motoneuron survival (references in (Galbiati et al., 2012)) and has been proposed as a mediator of increased ALS susceptibility in athletes abusing anabolic steroids (Galbiati et al., 2012). Based on these similarities, it is plausible that *GDF6* dysfunction could contribute to any of these pathways as they play out in ALS. Based on our data, we believe the expansion of ALS studies to the investigation of TGFβ signaling is warranted, beginning with *GDF6*.

4.5.2. Therapeutic implications

Application of BMPs as treatment has been investigated previously (Henriquez et al., 2011), especially following injury, suggesting that further knowledge of *GDF6* function could lead to strategies that replace BMP function. A number of TGFβ superfamily members are neuroprotective, such as *BMP7* in cerebral ischemia and *GDF5* in Parkinson's disease (Hurley et al., 2004; Perides et al., 1995). *GDF15* plays a role in the pathology of motoneuron loss, but is also required to effect the therapeutic effects of *GDNF* (Krieglstein et al., 2002; Strelau et al., 2009), illustrating how these signaling factors are able to participate in either neuroprotection or degeneration.

Therapeutic potential also exists in small molecules such as aminopropyl carbazoles and their derivatives. For example it has recently been demonstrated that P7C3 can ameliorate phenotypes in zebrafish *gdf6a* mutants (Asai-Coakwell et al., 2013), and P7C3 has also recently been shown to be efficacious in mouse models of ALS and Parkinsons Disease (De Jesus-Cortes et al., 2012; Tesla et al., 2012). Efficacy of P7C3 seems to be driven by a combination of pro-neural and neuroprotective signals, and identifying the mechanisms that underpin this could be aided by zebrafish models and/or by investigation of its etiological effects in diverse neurodegenerations.

Finally, *GDF6* may represent an entry-point into unexplored pathogenic mechanisms of vertebrate neuromuscular degeneration. In cases where such mechanisms have been identified, the etiology of ALS can be associated with a variety of cellular mechanisms. Ferraiuolo and colleagues (Ferraiuolo et al., 2011) review these to include oxidative stress, RNA processing, endosomal trafficking, protein degradation,

cytoskeletal integrity and glutamate excitotoxicity. It is conspicuous that, despite being a member of the BMP family with diverse functions, *GDF6* is not currently associated with any of these etiological categories.

Three mechanisms whereby BMP ligands and receptors affect NMJs can be suggested as potential routes to explore in the zebrafish system. First, retrograde signaling of BMP ligand from the muscle to the NMJ, and retrograde transport of receptors to activate transcription in the nucleus of motoneurons is important for motoneuron survival in *Drosophila* (Bayat et al., 2011; Henriquez et al., 2011). Second, BMP in *Drosophila* is required for stabilizing the NMJ through non-canonical signaling via LIM Kinase domain 1 (Bayat et al., 2011; Henriquez et al., 2011). Third, vertebrate BMP ligands have recently been revealed to bind Agrin (Banyai et al., 2010), and thus directly affect the clustering of acetylcholine receptors during formation and stabilization of the NMJ. In support of the latter we found that the NMJ morphology, as measured by α-bungarotoxin labelling of acetylcholine receptors, was disrupted in *gdf6a*$^{s327/s327}$ mutants (Figures 4.3, 4.5), suggesting one priority for future analysis.

4.5.3. Conclusion

In summary, past conclusions regarding a role for *Drosophila* BMP ligands in effecting NMJ can be extended to vertebrates, supporting conservation of mechanisms that may be of substantial import to degenerative neuromuscular diseases. Zebrafish present a tractable system for assessing the role of BMP/GDF ligands (data herein) and their receptors (Fassier et al., 2010) with respect to neuromuscular disease. The data also synergize to argue for further analysis of *GDF6* and other BMP genes as modifier loci, affecting susceptibility to ALS and perhaps a broader suite of neurodegenerative diseases. Further efforts to assess the role of vertebrate BMPs in motoneuron disease are warranted.

Chapter 5. Modeling novel aggressive and beneficial mutations of SOD1 in a zebrafish motor neuron axonopathy model

This Chapter comprises work in collaboration with Steven S. Plotkin. The questions and protein modeling experiments were conceived by Steven S. Plotkin. Preliminary inclusion assay experiments in cell culture were performed, imaged, and analyzed by Luke McAlary. Zebrafish experiments were conceived by W. Ted Allison and Michèle G. DuVal and were performed by MGD. Writing was initiated by SSP with significant contributions by MGD and WTA.

5.1. Summary

Patients expressing mutant SOD1 invariably develop ALS; they may live for over 20 years or less than one year once symptoms are expressed, depending on the mutation. The reasons for this variability have remained mysterious. Using arginine and alanine scans, we identified amino acid positions wherein mutation is predicted to significantly alter the stability of the SOD1 monomer. Following the scans, we tested several hits, including clinical mutants and novel variants, *in vitro* and *in vivo* in induced SOD1 aggregation and zebrafish motor neuron toxicity assays. Among the variants tested, the severity of aggregation and motor neuron toxicity by clinical variants was generally in agreement with disease progression. Both our predicted deleterious (A89R) and beneficial (K128N) novel variants showed phenotypes in concordance with their computational effects on monomer stability. K128N is an especially remarkable mutation, as it is a stabilizing variant that reduced the toxic axonopathy effect of the $SOD1^{A4V}$ mutant. The demonstrated success of these combined methods to predict the physical properties of SOD1 mutants, and their relevance to SOD1 toxicity *in vivo*, promises to enhance rationally designed therapies to counter the progression of ALS caused by SOD1 mutation and toxicity.

5.2. Introduction

Amyotrophic lateral sclerosis (ALS) is an invariably fatal motor neuron degenerative disease characterized by progressive loss of motor neurons (Cleveland, 1999), with a lifetime risk by age 70 of about 1/1000 (Rowland and Shneider, 2001). Though most cases are sporadic, over 180 mutations throughout the homodimeric antioxidant protein [Cu,Zn] superoxide dismutase (SOD1) have been found associated with a familial form of the disease (fALS), affecting about 1/5 of those with autosomal dominant inheritance (Deng et al., 1993; Rosen et al., 1993). While over 90% of ALS cases are sporadic (sALS) with no consistently identified genetic mutation, a growing body of functionally diverse genes has been implicated in the various biomolecular pathways leading to familial and sporadic ALS (Robberecht and Philips, 2013). These have included SOD1 (Deng et al., 1993; Rosen et al., 1993), fused in sarcoma/translocated in liposarcoma (FUS/ TLS) (Kwiatkowski et al., 2009; Vance et al., 2009), TAR-DNA–binding protein 43 (TDP43) (Neumann et al., 2006a), polyglutamine expansions in ataxin-2 (ATXN2) (Elden et al., 2010), and noncoding hexanucleotide repeat expansions in C9ORF72 (DeJesus-Hernandez et al., 2011; Renton et al., 2011). Intriguingly, both sALS and fALS patients display intraneuronal immunoreactivity to SOD1 misfolding-specific antibodies (Bosco et al., 2011; Brotherton et al., 2012; Forsberg et al., 2010; Gruzman et al., 2007), suggesting a common potential pathway involving the misfolding of SOD1. The ubiquity of disease-associated mutations throughout the primary sequence of SOD1 (http://alsod.iop.kcl.ac.uk/) suggests a shared physico-chemical origin for the familial disease, which is the subject of ongoing intensive protein modeling (Shi et al., 2016a).

Spatial and temporal restrictions on the progression of ALS (Ravits and La Spada, 2009), *in vitro* evidence of intracellular induction of SOD1 misfolding (Grad et al., 2011), evidence of misfolded and aggregated SOD1 in mouse models (Chia et al., 2010; Sasaki et al., 2005; Wang et al., 2002; Yamagishi et al., 2007) and fALS patient tissues , along with intracellular and intercellular transmission of misfolded wildtype (WT) (Grad et al., 2013; Sundaramoorthy et al., 2013a) and mutant (Bidhendi et al., 2016; Furukawa et al., 2013; Grad et al., 2015; Münch and Bertolotti, 2011; Munch et al., 2011) SOD1, all suggest a prion-like propagative role of misfolded SOD1 in ALS, reminiscent of the intermolecular induction of misfolding observed in prion and prion-like diseases (Bosco

et al., 2011; Desplats et al., 2009; Frost and Diamond, 2010; Soto et al., 2006; Tycko and Wickner, 2013; Walker et al., 2016). These observations inspired us to consider whether mechanisms that may accelerate the onset of misfolding or acquisition of toxic gain-of-function, such as monomerization or instability/partial loss of native structure, may be more likely for mutant SOD1 variants than for wildtype SOD1. To identify key amino acids toward monomer stabilization, we performed arginine and alanine mutational scans, as mutation toward arginine is common in fALS SOD1 mutations, and alanine scanning is an established method to estimate the contribution of individual amino acid residues to overall protein stability (Morrison and Weiss, 2001; Weiss et al., 2000).

We tested these predictions by co-expressing known SOD1 mutants, and these novel mutants, in a SOD1-GFP aggregation assay. While $SOD1^{A89R}$ induced aggregation of SOD1-GFP, $SOD1^{K128N}$ did not, which is in agreement with scans. We also tested these variants in a zebrafish model to test whether their predicted stability corresponds to motor neuron phenotypic severity *in vivo*; the novel variants proved extremely toxic (A89R) and non-toxic (K128N) to zebrafish motor neurons compared to wildtype SOD1 and to deleterious clinical variants, demonstrating the impact of these particular residues on the SOD1 protein's capacity to become toxic. Further, $SOD1^{K128N}$ rescued the motor neuron phenotype caused by the extremely toxic clinical variant $SOD1^{A4V}$. The novel K128N variant's rescue effect in zebrafish motor neurons opens new avenues to investigate how specific amino acid positions, including this unique mutant, may exert protective effects on the SOD1 protein.

5.3. Methods

5.3.1. Arginine and alanine scans to predict deleterious and protective mutants

Alanine and arginine scans were performed for all 153 residues in WT SOD1, and the approximate free energy change as reported by the Eris server (Yin et al., 2007) recorded. Alanine was chosen because of its small side chain, while arginine was chosen because it is statistically overrepresented in fALS mutations (i.e. 21 of 175 mutations on

alsod.org are Arg (12%), while the natural abundance of Arg is about 5.5% as estimated from the UniProt protein database [https://web.expasy.org/protscale/pscale/A.A.Swiss-Prot.html]). Scans were performed on SOD1 monomers and dimers with either fixed backbones or flexible backbones (and with Cu^{2+} and Zn^{2+}, i.e. holo-state). Arginine mutations in the dimer interface were generally more deleterious and were treated separately (not shown). The least and most stable server-predicted mutants in the arginine scan were A89R and E78R respectively. The mutant K128A showed the greatest increase in stability from the alanine scan. A charged and a polar mutant that were chemically more similar to Lysine, K128R and K128N, were then considered.

5.3.2. Zebrafish ethics statement

Fish care and experimental protocols were approved under the protocol AUP00000077 by the Animal Care and Use Committee: Biosciences at the University of Alberta under the auspices of the Canadian Council on Animal Care.

5.3.3. A89R and K128N mutagenesis and mRNA synthesis

Plasmids containing the coding sequence for human SOD1 (wildtype, A4V, and G127X variants) (cloned into pCS2+ via Gateway cloning) were gifted from Neil Cashman, and had been created as previously described. The *pCS2+.SOD1^{WT}* plasmid was utilized in mutagenesis reactions to create the novel A89R and K128N mutations. Production of mCherry and Tol2 transposase mRNA was also performed using pCS2+ plasmids containing these coding sequences.

Mutagenesis was performed using the Agilent QuikChange Lightning Site-Directed Mutagenesis kit (Agilent Technologies, Cat. No. 210518) according to package instructions, with primers designed in the online Agilent primer design program (http://www.genomics.agilent.com/primerDesignProgram.jsp) (Table 1). Mutagenized plasmid was then transformed into One Shot Top10 chemically competent cells (Invitrogen, Cat. No. C4040-03). Colonies were sequenced to confirm mutagenesis and stored as glycerol stocks. SOD1 variants, mCherry, and transposase mRNA for injection

were synthesized by linearizing pCS2+ plasmids with FastDigest NotI restriction enzyme (Thermo Fisher Scientific, Cat. No. FD0593), and performing transcription reactions with the mMESSAGE mMACHINE SP6 transcription kit (Ambion, Cat. No. AM1340). After transcription, mRNA products were verified via gel electrophoresis with a RiboRuler High Range ladder, prepared according to package instructions (Thermo Scientific, Cat No. SM1821), then aliquoted and stored at -80°C until use.

Table 5.1. Primers for site-directed mutagenesis (SDM) of the pCS2+. SOD1^{WT} plasmid to generate pCS2+. SOD1^{A89R} and pCS2+.SOD1^{K128N}.

Mutation	Forward SDM primer	Reverse SDM primer
A89R	5'-tgttggagacttgggcaatgtgact**cg**tgacaaagatggt-3'	5'-accatctttgtca**cg**agtcacattgcccaagtctccaaca-3'
K128N	5′-aagcagatgacttgggcaa**c**ggtggaaatgaagaaag -3′	5′-ctttcttcatttccacc**g**ttgcccaagtcatctgctt -3′

Primers were used with Agilent Lightning II SDM kit according to manual instructions. Mutagenic bases that introduce missense mutations are in bold and underlined.

5.3.4. Animal care and embryo injections

Zebrafish were raised and maintained under standard procedures (Westerfield, 2000b). Embryos were collected and kept in E3 embryo media at 28°C with PTU added at 6-8hpf to prevent pigmentation. The *Tg(mnx1:GFP)* transgenic line (ZFIN ID: ZDB-ALT-051025-4) (Flanagan-Steet et al., 2005) (DuVal et al., 2014a) was utilized for visualization of the primary motor axons via GFP fluorescence. Adult transgenic fish were crossed to wildtype AB fish to maintain consistency of GFP expression among embryos. Embryos were injected at the 1-2 cell stage with a total of 1900pg of mRNA in the combinations listed in Table 2, and screened at 24hpf for mCherry fluorescence and GFP expression in the spinal cord. SOD1 mRNA dosages were determined empirically (with guidance from previous studies (Lemmens et al., 2007)) to establish an axonopathy

phenotype detectable above control levels. Transposase mRNA was utilized as a “top-up” to ensure consistent 1900pg total dose among all groups.

Table 5.2. mRNA types and dosages of SOD1 injection groups.

Treatment Group	SOD1 Variant mRNA & Dose	mCherry mRNA	Tol2 mRNA	Total mRNA	n=
mRNA Control	*None*	100pg	1800pg	1900pg	68
K128N 900	K128N 900pg	100pg	900pg	1900pg	66
WT 900	WT 900pg	100pg	900pg	1900pg	44
G127X 900	G127X 900pg	100pg	900pg	1900pg	38
A4V 900	A4V 900pg	100pg	900pg	1900pg	55
A89R 900	A89R 900pg	100pg	900pg	1900pg	49
A4V 1800	A4V 1800pg	100pg	0pg	1900pg	84
A4V 900 + WT 900	A4V 900pg WT 900pg	100pg	0pg	1900pg	63
A4V 900 + K128N 900	A4V 900pg K128N 900pg	100pg	0pg	1900pg	101

mRNA encoding SOD1 contained no more than one mutation at a time. Co-injection groups comprised two sets of SOD1 mRNA, each encoding a separate variant as indicated. Dose indicates amount of mRNA delivered per embryo; sample size (n=) is number of embryos assessed.

5.3.5. Axonopathy assay, imaging, and statistical analysis

At 33-37hpf, embryos were fixed in 4% paraformaldehyde/5% sucrose/0.1M PO_4 for 40 minutes. Fixative was replaced with PBSTw and embryos stored at 4°C until primary motor axons could be assessed (assessments were completed within 24 hours of fixation). The primary motor axons were scored as normal or abnormal as previously done (Lemmens et al., 2007). Briefly, primary motor axons with branching occurring dorsal of or level with the ventral edge of the notochord were scored as abnormal (Fig. 1A, B).

Motor axons exiting both sides of the spinal cord were assessed. The total number of abnormal axons was recorded for each individual embryo and these values were averaged for each injection group. For statistical analysis, Kruskall-Wallis ANOVA with post-hoc Mann-Whitney pairwise comparisons were performed in PastProject for Mac, version 3.09 (Øyvind Hammer, University of Oslo, http://folk.uio.no/ohammer/past/). Motor neuron imaging for Fig. 1 was performed on a Zeiss Axio Observer.Z1 microscope with Zen software (2010, Carl Zeiss Imaging). Z-stacks of motor neurons were flattened and adjusted for rotation, brightness, and contrast in Imaris x64 (version 7.4.0, Bitplane, Badnerstrasse).

5.4. Results

5.4.1. Arginine and alanine scans of the SOD1 peptide reveal de novo destabilizing and stabilizing mutants

Because arginine is statistically overrepresented in observed fALS mutants (approx. 12%, versus a 5.5% incidence of arginine among human proteins according to the UniProt database [https://web.expasy.org/protscale/pscale/A.A.Swiss-Prot.html]), we performed a computational arginine mutation scan of all 153 amino acids in SOD1 (wherein each residue is singularly replaced with arginine), and obtained estimates of the resulting free energy change for monomers and dimers using the Eris server (Yin et al., 2007). This scan yielded the mutant A89R (data not shown), which is not in the dimer interface and does not coordinate metals, but induces non-local destabilization of the dimer interface and protein surface. Thus amino acid A89 is predicted to be a key source of protein instability if changed.

We also sought to predict beneficial mutants with protective properties beyond wildtype SOD1. Because alanine has a small side chain that is chemically inert and offers little interaction with other residues, an alanine substitution can reveal the role of a wildtype amino acid in protein stability (whether stabilizing or destabilizing) (Morrison and Weiss, 2001; Weiss et al., 2000). Thus this scan was performed to detect amino acid positions with residues or side chains that, in terms of overall monomer stability, could be

“improved” when eliminated. From this scan on wildtype SOD1, the mutant K128A showed the greatest increase in stability (not shown). This stabilization could indicate that the wildtype residue, Lysine, may in fact contribute to destabilization. A charged and a polar mutant that are chemically more similar to the original Lysine, K128R and K128N, were then considered, and K128N showed the greatest increase in stability (not shown).

5.4.2. Effects of Novel SOD1 Variants on Inclusion Formation

Our novel variants are predicted to affect SOD1 monomer and dimer stability, with A89R being extremely destabilizing, and K128N being stabilizing. Destabilization of the SOD1 protein increases rates of misfolding and aggregation (Bosco et al., 2010; Bruijn et al., 2004; Grad et al., 2011; Grad et al., 2013; Gruzman et al., 2007; Silverman et al., 2016), hence we employed a SOD1 reporter assay, similar to other fluorescent assays (Ayers et al., 2014; Ayers et al., 2017) and developed by the Cashman lab (not published), to measure the aggregation propensity of these variants. Using U2OS cells transfected with a pCMV.SOD1-GFP vector that acts as a fluorescent reporter of inclusion formation, we measured the effects of these variants on SOD1 aggregation. In two replicates, expression of wildtype SOD1 caused inclusions in relatively few cells (median of 2.4% of total), whereas familial ALS variants L144F, L38V, G93D, G93A, I113T, V148G, G37R, and A4V caused more inclusions (medians between 4.6% and 10.2% of total cells). The predicted destabilizing novel variant A89R also generated inclusions, at higher rates than most variants and similar to A4V, but K128N did not, showing a median of 2.4% of cells with inclusions, highly similar to WT and to two other clinical variants (Appendix 4, Fig. A4.1). These results are preliminary and require more replicates for statistical analysis, but are nonetheless promising.

5.4.3. Motor neuron phenotypes by novel SOD1 mutants reflect predicted severities

The novel mutants identified through arginine and alanine scans, A89R and K128N, are predicted to be destabilizing (A89R) and stabilizing (K128N) compared to wildtype

SOD1. We sought to test these predictions in a living system, by comparing motor neuron phenotype severities caused by expression of human $SOD1^{WT}$ and mutant variants in zebrafish embryonic motor neurons, an *in vivo* model of SOD1 pathology. We hypothesized that destabilizing SOD1 variants, including the novel A89R mutant, would have greater propensity to cause toxicity in motor neurons. Thus we predicted that the severity of motor neuron pathology would increase with expression of destabilizing SOD1 mutants, but not with the novel stabilizing mutant K128N, when compared to $SOD1^{WT}$.

Zebrafish embryos are an established and effective whole organism model of motor neuron pathology in which overexpression of human SOD1 mutants via mRNA injection causes primary motor neuron developmental defects (Lemmens et al., 2007) (Bandmann and Burton, 2010) (Ramesh et al., 2010) (Da Costa et al., 2014) (Fig. 5.1A, B). We compared five human SOD1 variants: wildtype SOD1 or $SOD1^{WT}$; fALS-associated $SOD1^{G127X}$ and $SOD1^{A4V}$; and novel variants A89R ($SOD1^{A89R}$) and K128N ($SOD1^{K128N}$). Other fALS-associated mutations, including G93A and G37R, have been previously modeled in zebrafish (Lemmens et al., 2007) (also Chapters 6, 7). We established mRNA injection dosages and an axonopathy assay along the lines of previous studies (Lemmens et al., 2007). Expression of 900pg of human $SOD1^{WT}$ caused motor axonopathy in zebrafish embryos that was a small but statistically significant increase over control injections delivering inert mRNA. Because the arginine and alanine scans compare the effects of mutations to $SOD1^{WT}$, it is pertinent to evaluate axonopathy of SOD1 variants in relation to axonopathy caused by $SOD1^{WT}$, in addition to the mRNA injection control.

We found significant severity of axonopathy upon expression of fALS SOD1 mutant A4V, a particularly aggressive mutation in terms of disease progression (average patient survival time following disease onset approx. 1.2 years) (Wang et al., 2008b) and axonopathy with expression of fALS mutant $SOD1^{G127X}$, though lower than that of $SOD1^{A4V}$ (average survival time estimated less than 3 years (Andersen et al., 1997; Hansen et al., 1998)). Our results show that the deleterious $SOD1^{A4V}$ and novel $SOD1^{A89R}$ mutant variants cause significantly more axonopathy than mRNA control injection, novel $SOD1^{K128N}$, and $SOD1^{WT}$. In fact, expression of $SOD1^{A89R}$ caused 30% more axonopathy compared to the next most toxic mutant tested (A4V), producing significantly more

axonopathy than any other variant. Regarding the $SOD1^{K128N}$ variant, which is predicted to be more stable than $SOD1^{WT}$, expression in zebrafish embryos produced less axonopathy compared to $SOD1^{WT}$, such that it was not significantly different from the control injection. In other words, $SOD1^{K128N}$ appeared inert. $SOD1^{G127X}$ had an intermediate effect amongst variants tested, causing motoneuron axonopathy similar to $SOD1^{WT}$ and to $SOD1^{A4V}$, but not as severe as $SOD1^{A89R}$ (Fig. 5.1C).

Is the $SOD1^{K128N}$ mutant protein merely benign, or could it be actively protective? To discern whether it is an inert variant that merely does not participate in misfolding and toxicity, or one that can reduce the toxicity of other SOD1 peptides, we performed co-expression of $SOD1^{K128N}$ with $SOD1^{A4V}$, comparing this outcome to co-expression of $SOD1^{WT}$ with $SOD1^{A4V}$, in zebrafish. If $SOD1^{K128N}$ reduces the toxicity of other, more deleterious SOD1 variants, we predicted that axonopathy would decrease upon co-expression of a toxic variant with $SOD1^{K128N}$. As seen in previous work (Lemmens et al., 2007) , co-expression of $SOD1^{A4V}$ and $SOD1^{WT}$ caused more severe axonopathy than $SOD1^{A4V}$ alone, even at a matching dose of total SOD1 mRNA, though these differences were not statistically significant. But zebrafish with $SOD1^{A4V}$ and $SOD1^{K128N}$ co-expression showed little axonopathy (Fig. 5.1D), suggesting that the $SOD1^{K128N}$ variant proteins may have ameliorated the effects of $SOD1^{A4V}$ proteins, and reduced toxicity *in vivo*. In terms of predicting the effects of mutations on SOD1 pathology, to our knowledge this would be the first mutant to confer active protection.

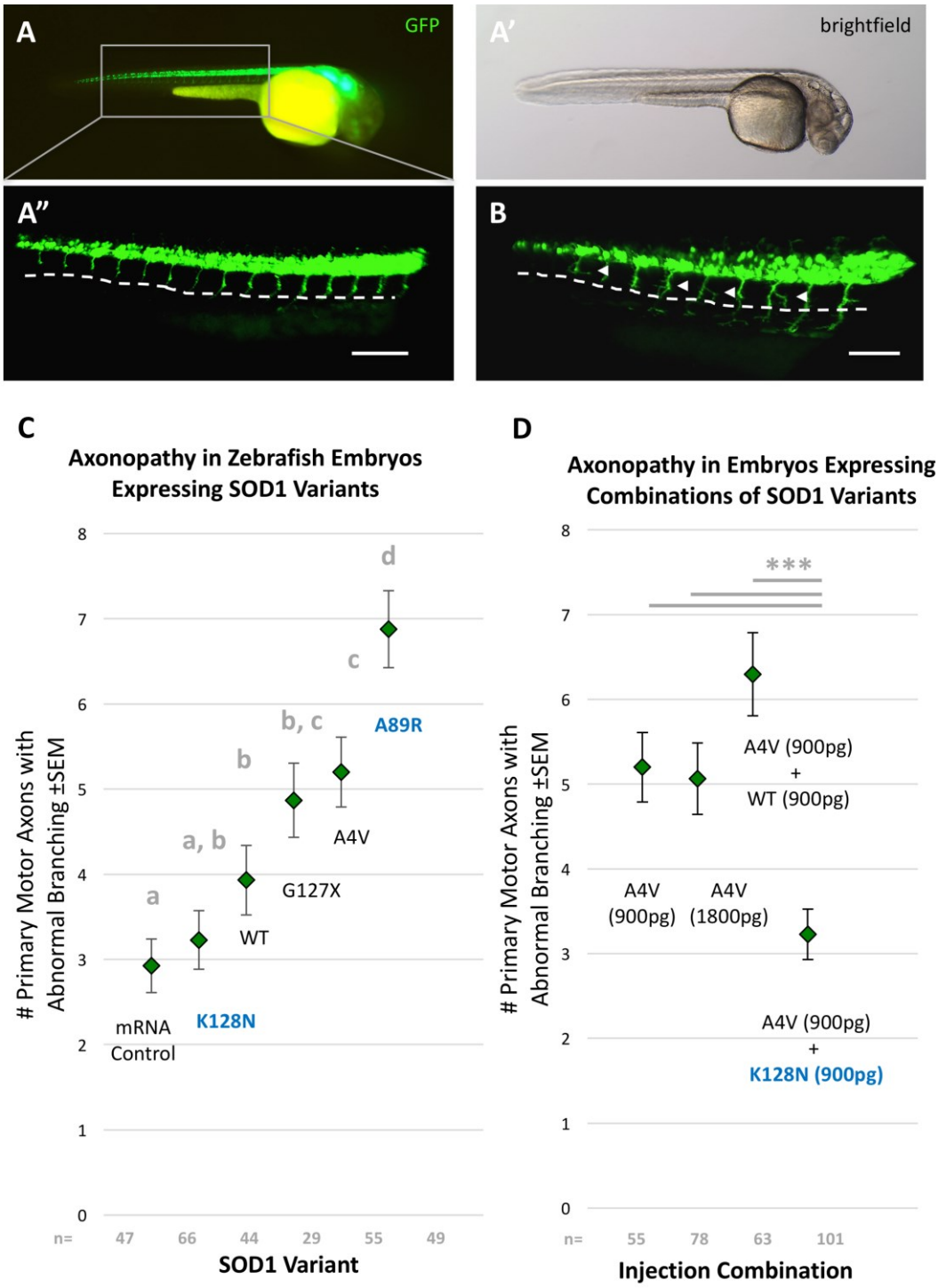

Figure 5.1. SOD1 mutant variants in a zebrafish model of ALS confer motoneuron phenotypic severities that correspond to clinical severity and predicted monomer stability.

A. 35hpf *Tg(mnx1:GFP)* embryo (A, A′) with little axonopathy in the primary motor neurons (inset, A″) as measured by incidents of axon branching at or above the ventral edge of the notochord (dashed line). **B.** 35hpf *Tg(mnx1:GFP)* embryo with significant axon branching (arrowheads) above the ventral edge of the notochord. Scale bars in A″ and B 100μm. **C.** Expression of SOD1 with mutations A4V, G127X, or the novel A89R in zebrafish embryos causes severe primary motor neuron axonopathy, whereas expression of $SOD1^{WT}$ causes mild axonopathy, and expression of novel variant $SOD1^{K128N}$ causes none. Axonopathy was measured via the number of primary motor axons with abnormal branching in embryos Injected with SOD1 variants (900pg SOD1 per embryo). $SOD1^{WT}$ caused mild but significant axonopathy compared to mRNA injection controls. Variants $SOD1^{G127X}$ and $SOD1^{A4V}$ cause significantly more severe axonopathy, with $SOD1^{A4V}$ causing significantly more severe axonopathy than $SOD1^{WT}$. The novel variant $SOD1^{A89R}$, predicted to strongly destabilize the SOD1 monomer and therefore be extremely deleterious, proved the most severe when injected. Injection of the novel $SOD1^{K128N}$ variant, predicted to be stabilizing, caused axonopathy similar to mRNA controls and $SOD1^{WT}$ injected embryos (Kruskall-Wallis ANOVA, $p < 0.05$; data points sharing the same grey letters are not significantly different). **D.** Co-injection of 900pg $SOD1^{A4V}$ + 900pg $SOD1^{WT}$ showed an increase in axonopathy over both 900pg $SOD1^{A4V}$ and 1800pg $SOD1^{A4V}$ doses, though these were not significantly different. Co-injection of $SOD1^{A4V}$ and the predicted beneficial $SOD1^{K128N}$ mutant showed significantly less axonopathy (Kruskall-Wallis ANOVA, *** $p < 0.001$),

suggesting that the SOD1^{K128N} variant may be able to rescue toxicity caused by SOD1^{A4V}. Number of embryos assessed (n=) shown below data points.

5.5. Discussion

ALS is suspected to be a prion-like disease where SOD1 aggregates are found in cases of fALS with SOD1 mutation (Jonsson et al., 2004; Kerman et al., 2010; Shibata et al., 1996; Watanabe et al., 2001). Aggregates have been documented in some sporadic cases as well, though the variety of conformation-dependent SOD1 antibodies used makes estimates of frequency difficult (Da Cruz et al., 2017; Forsberg et al., 2010; Matsumoto et al., 1996; Shibata et al., 1994). In cell culture mutant SOD1 and misfolded wildtype SOD1 undergoes self-propagated misfolding (Grad et al., 2013; Munch et al., 2011; Pokrishevsky et al., 2015; Pokrishevsky et al., 2016; Silverman et al., 2016), and SOD1 self-propagated misfolding is beginning to be assayed in animal and organotypic slice culture models (Ayers et al., 2016a; Ayers et al., 2014). There is some preliminary evidence that mutation in SOD1 might be critical for self-propagated misfolding: SOD1-linked fALS spinal homogenates induced aggregation of a G85R-SOD1:YFP reporter where non-SOD1-linked, sALS homogenates did not (Ayers et al., 2016a). The answers to how SOD1 misfolds have been evasive, especially considering the SOD1 dimer's high stability (Lepock et al., 1990; Malinowski and Fridovich, 1979) and the lack of pattern in mutation distribution along the SOD1 sequence. Despite the very stable dimer structure, there likely exists weak points where mutation increases risk of monomerization and/or loss of native structure, thereby increasing the risk of misfolding and acquired toxicity. We sought to identify possible weak points, and also potential stabilizing points, by scanning the SOD1 peptide and testing novel candidate mutants for increased and decreased misfolding and toxicity *in vitro* and *in vivo*.

The novel mutations, A89R and K128N, showed striking effects on aggregation of GFP-tagged SOD1^{G85R}, in zebrafish motor neuron morphology, and in dimer model stabilities. SOD1^{A89R} causes aggregation similar to known disease variants and extremely high axonopathy, and is predicted to be very unstable in an arginine scan, thus this amino

acid position may either have a significant role in maintaining protein stability, or may be a potential point of weakness with high risk of destabilization and/or misfolding. There are two known publications listing two ALS cases where this residue is changed. In these cases, a single missense mutation changed A89 to T (threonine) (Andersen et al., 2003) or V (valine) (Jacobsson et al., 2001), but the age of onset and progression were not reported. $SOD1^{K128N}$ is a novel beneficial mutant that is not merely non-participatory in SOD1 toxicity- it can rescue the motor neuron phenotype when expressed in conjunction with a toxic variant.

SOD1 aggregation *in vitro* (such as with the GFP-tagged SOD1 vector used here) and zebrafish motor neuron morphology and function (Chapter 6) can be developed as potentially impactful high-throughput assays for testing *in silico* models of SOD1 stability. Such methods to predict and test potentially unstable regions in the contexts of monomer unfolding and dimer stability, as identified in A89 by arginine scanning, could assist in prioritizing target regions for stabilization, e.g. through rational design of pharmaceuticals to stabilize these key regions (as explored in Chapter 6). In contrast to almost all other SOD1 mutants, the novel K128N variant is a stabilizing agent that does *not* confer toxicity and may even prevent toxic effects from other SOD1 variants, which is unique among known SOD1 mutations. This is in contradistinction to the W32S mutation, another beneficial mutation that does not appear to alter the toxic effects of other SOD1 variants, specifically $SOD1^{WT}$ (Chapter 6, Fig. 6.2C). To clarify the differences between beneficial mutants K128N and W32S, however, a more accurate comparison would require co-injection of $SOD1^{W32S}$ mRNA with $SOD1^{A4V}$ mRNA (versus $SOD1^{K128N}$ + $SOD1^{A4V}$) and/or other toxic variants.

Interestingly, a variant in human prion protein (PrP), G127V, confers resistance to multiple strains of misfolded prion, another rarity in proteinopathies (Asante et al., 2015). In this study only one combination of SOD1 variants (K128N and A4V) was tested, thus additional combinations with other deleterious variants will inform whether and how K128N exerts this protection. Some hypotheses for K128N's protective effect include dimerization of $SOD1^{K128N}$ with other variants (or generally conferring dimer stability), enhancing metal binding (demetallation is thought to be a mechanism whereby SOD1 misfolds (Ip et al., 2011; Sirangelo and Iannuzzi, 2017)), or stabilization of the native

monomer (either during protein translation and folding, where mutant SOD1 proteins can misfold (Ayers et al., 2017) or afterward) to discourage misfolding. As amino acid 128 is located in the electrostatic loop, and not at the dimer interface or metal binding sites, the first two hypotheses are less likely. Further *in silico* biophysical modeling of SOD1 variants as homodimer and heterodimer structures may offer clues, as heterodimers of SOD1 variants have been seen in cell culture models (Grad et al., 2011; Kim et al., 2014). Alternatively, SOD1 proteins containing a K128N mutation may be simply non-participatory in misfolding or toxic gain-of-function, and this quality may, with sufficient amounts of $SOD1^{K128N}$ protein, reduce other SOD1 proteins' toxicity, or slow the spread of misfolding or toxicity. Such an outlier offers new opportunities to isolate the conditions and/or protein interactions required for SOD1 to misfold, acquire toxicity, and/or spread, since discrepancies in dimer stabilities, metal binding properties, and tendencies to aggregate among disease-associated mutations have yielded few unifying mechanisms for misfolding and propagation (Antonyuk et al., 2005; Deng et al., 1993; Epple and Neues, 2010; Hough et al., 2004; Mulligan and Chakrabartty, 2013; Rodriguez et al., 2005; Vassall et al., 2011).

In this Chapter we investigated if the predicted stabilities of novel SOD1 mutants, identified using *in silico* amino acid scanning, can suggest good candidate mutants that would strongly influence SOD1 structure and activity. To this end, we used aggregation assays in cell culture and the zebrafish, an *in vivo* ALS model that is amenable to high-throughput assays (Lieschke and Currie, 2007; Zon and Peterson, 2005). Methods to predict highly stable or unstable regions, in the contexts of maintaining native monomer structure and dimer stability, have the potential to guide rational therapeutic strategies. The exploration of mutants by rationally-guided design can also aid the discovery of "super-proteins" with reduced propensity for misfolding and aggregation as well as enhanced functional and thermodynamic properties.

Chapter 6. Tryptophan 32 mediates SOD1 toxicity in an *in vivo* motor neuron model of ALS and is a promising target for small molecule therapeutics

This chapter comprises the manuscript of the same title: Tryptophan 32 mediates SOD1 toxicity in a *in vivo* motor neuron model of ALS and is a promising target for small molecule therapeutics, by Michèle G. DuVal, Vijaya K. Hinge, Natalie Snyder, Richard Kanyo, Jenna Bratvold, Edward Pokrishevsky, Neil R. Cashman, Nikolay Blinov, Andriy Kovalenko, and W. Ted Allison (in review at Neurobiology of Disease, March 2018).

MGD conceived of, performed, statistically analyzed, interpreted and presented all experiments involving zebrafish or drug applications, prioritized drugs to be tested, and was the principal author responsible for drafting the manuscript. VKH conceived of, designed, performed, analyzed and interpreted computational experiments, and wrote the associated portions of the manuscript. NB conceived of, designed, analyzed and interpreted computational experiments, and wrote the associated portions of the manuscript. NS performed TEER experiments. RK performed and analyzed Western blot experiments. JB performed and interpreted aspects of axonopathy experiments and drug application. EP and NRC conceived of residue W32 being a potential therapeutic target and suggested experiments. AK wrote portions of the manuscript associated with computational experiments. WTA conceived of the experiments, interpreted data and participated in writing the manuscript. AK, NB, and WTA supervised, coordinated and funded the work.

6.1. Summary

SOD1 misfolding and spread is proposed as a pathological basis of amyotrophic lateral sclerosis (ALS), but the nature of this misfolding has been difficult to elucidate. Uniquely in SOD1 proteins from humans and other primates, and rarely in other species, a tryptophan residue at position 32 (W32) is predicted to be solvent exposed and to participate in SOD1 misfolding. We hypothesized that W32 is influential in SOD1 acquiring toxicity, as it is known to be important in template-directed misfolding. We tested if W32 contributes to SOD1 cytotoxicity and if it is an appropriate drug target to ameliorate

ALS-like motor neuron deficits in a zebrafish model of motor neuron axon morphology and function (swimming). Embryos injected with human SOD1 variant with W32 substituted for a serine ($SOD1^{W32S}$) had reduced motor neuron axonopathy and motor deficits compared to those injected with wildtype or disease-associated SOD1. A library of FDA-approved small molecules was ranked with virtual screening based on predicted binding to W32, and subsequently filtered for analogues using a pharmacophore model based on molecular features of the uracil moiety of a small molecule previously predicted to interact with W32 (5'-fluorouridine or 5'-FUrd). Along with testing 5'-FUrd and uridine, a lead candidate from this list was selected based on its lower toxicity and improved blood brain barrier penetrance; telbivudine significantly rescued SOD1 toxicity in a dose-dependent manner. The mechanisms whereby the small molecules ameliorated motor neuron phenotypes were specifically mediated through human SOD1 and its residue W32, because these therapeutics had no measurable impact on the effects of tryptophan-deficient human $SOD1^{W32S}$. By substituting W32 for a more evolutionarily conserved residue (serine), we confirmed the significant influence of W32 on human SOD1 toxicity to motor neuron morphology and function; further, we performed pharmaceutical targeting of the W32 residue for rescuing SOD1 toxicity. This unique residue offers future novel insights into SOD1 stability and misfolding, and therefore poses an attractive target for drug therapy.

6.2. Introduction

Amyotrophic lateral sclerosis (ALS) is a devastating neuromuscular degenerative disease with an approximate 2/100,000 incidence, in which the motor neurons controlling musculature gradually degenerate, leading to loss of muscle control including swallowing and respiration. [Cu-Zn] superoxide dismutase 1 (*SOD1*) was the first gene implicated in ALS and, although numerous other ALS associated genes have since been identified (including *TDP43*, *FUS*, *C9ORF72*), mutations in SOD1 remain prominent in familial cases (fALS, approx. 12%) and are found in a small number of sALS cases (approx. 1%) (Brown, 1993; Corcia et al., 2017). The human SOD1 protein, when mutated, has an increased propensity to misfold, and evidence of aggregates of misfolded SOD1 has been

documented in cell culture, murine models, and tissues from patients with fALS (Bidhendi et al., 2016; Chia et al., 2010; Furukawa et al., 2013; Grad et al., 2015; Münch and Bertolotti, 2011; Sasaki et al., 2005; Sundaramoorthy et al., 2013a; Wang et al., 2002; Yamagishi et al., 2007). SOD1 misfolding is likely impactful even in some sporadic ALS and non-SOD1 fALS, because misfolded SOD1 is observed in tissues from these patients (Bosco et al., 2011; Brotherton et al., 2012; Forsberg et al., 2010). The possibility of misfolded SOD1 inducing other SOD1 proteins to misfold in a prion-like manner is intriguing. However the nature of the prion-like SOD1 misfolding itself remains puzzling; unlike other protein misfolding paradigms, the characterization of physiologically relevant amyloid, fibrillization, or critical induction domains in the SOD1 protein has been limited (Banci et al., 2008; DiDonato et al., 2003; Khan et al., 2017; Malinowski and Fridovich, 1979; Stathopulos et al., 2003), partly since mutations in SOD1 do not cluster at any part of the sequence. However a particular residue may hold considerable sway in the misfolding of human SOD1 protein: residue 32, a tryptophan, which we will refer to as W32.

The W32 residue may be a prominent instigator in SOD1 misfolding. The induction or conversion of human wildtype SOD1 ($SOD1^{WT}$) protein to a misfolded state by mutant SOD1 protein has been demonstrated in ALS model mice and in cell culture. $SOD1^{G93A}$ induces $SOD1^{WT}$ to misfold and aggregate, leading to aggregates containing both proteins and accelerated disease progression in mice (Ayers et al., 2016b; Bruijn et al., 1998; Deng et al., 2006; Wang et al., 2009b). This interaction is further elaborated with evidence of $SOD1^{G127X}$ converting $SOD1^{WT}$ to the misfolded state in various cell lines; this interaction is suspected to be mediated by W32 (Grad et al., 2011). The influence of W32 on SOD1 conformation conversion appears significant, as mutation of this residue in $SOD1^{G93A}$ (in cultured motor neurons) (Taylor et al., 2007), $SOD1^{G127X}$, or $SOD1^{G85R}$ (in HEK-293 cells) (Grad et al., 2011) causes a dramatic reduction in their ability to misfold and convert $SOD1^{WT}$, thus reducing inclusions and toxicity. The tryptophan at this residue is not well conserved, being serine in mice, and serine or threonine in many other non-primate vertebrates and invertebrates (Fig. 6.1A). Strikingly, W32 is the only tryptophan in human SOD1 (Grad et al., 2011), and this observation is amplified by noting tryptophan

is not observed in any location of SOD1 amongst a diverse selection of other organisms (Dasmeh and Kepp, 2017).

As seen in many missense mutations, single residues can have considerable influence on the SOD1 monomer's overall stability and propensity to become misfolded; however it is striking to consider the possibility that W32 is especially influential upon SOD1 monomer's capacity to change the conformation of *other* monomers (Grad et al., 2011; Taylor et al., 2007). The ability of one protein to interact with and alter the conformation of another (e.g. misfolded SOD1 inducing the misfolding of a natively folded SOD1, a process that may be referred to as conversion or template-directed misfolding) is the central criterion for the self-propagation and subsequent aggregation of prion-like proteins. Also unique to the W32 residue is the discovery that mutating this tryptophan to a serine (W32S) as completed by Grad et al. (2011) (Grad et al., 2011) above and in our work below, leads to a reduction in overall misfolding and aggregation, making W32S the first SOD1 mutation with potentially beneficial effects. Tryptophan, despite being a hydrophobic residue, is solvent exposed on the third beta-strand of the SOD1 protein. Serine and threonine on the other hand are hydrophilic, which may offer more stability to the surrounding peptide. This may explain why residue 32 in SOD1 homologues of non-primate vertebrates is conserved for serine or threonine (Fig. 6.1A). Other residues evolutionarily unique to primates have been more closely studied, primarily for their contributions to SOD1 stability (especially at the dimer interface) leaving the question of W32 unaddressed (Dasmeh and Kepp, 2017).

We sought to validate the influence of this tryptophan residue in a disparate ALS animal model, the zebrafish, and to provide the first *in vivo* test of candidate small molecules that are predicted to act through interaction with W32 and thereby limit SOD1 misfolding and acquired toxicity. Substitution of tryptophan for serine prevented SOD1 toxicity, thereby rescuing axonopathy and motor deficits; applying candidate drugs predicted to bind W32 likewise rescued these phenotypes in $SOD1^{WT}$-injected embryos. The W32 residue is thus influential in SOD1 toxicity *in vivo*, making it an attractive target for further development of therapeutic interventions.

6.3. Methods

6.3.1. Animal Ethics Statement

Husbandry and breeding of zebrafish for this study was approved under the protocol AUP00000077 by the Animal Care and Use Committee: BioSciences at the University of Alberta, under the auspices of the Canadian Council on Animal Care. Adult zebrafish were maintained according to standard procedures (Westerfield, 2000b) in brackish water (1250±50 μS) at 28.5°C, and fed twice daily with either brine shrimp or juvenile trout chow.

6.3.2. Zebrafish mRNA Injections of SOD1 and Drug Treatments

Human $SOD1^{WT}$ and $SOD1^{G127X}$ were cloned into the pCS2+ vector via Gateway recombination for use in mRNA synthesis. The $SOD1^{W32S}$ vector was created via site-directed mutagenesis of the pCS2+.$SOD1^{WT}$ plasmid, with the following primers: 5'-ttaatgcttcccgacaccttcactggtccattactt-3' (forward) and 5'-aagtaatggaccagtgaaggtgtcgggaagcattaa-3' (reverse). Vectors were linearized with FastDigest NotI (Thermo Fisher, FD0593) and mRNA transcribed using the Ambion mMESSAGE SP6 transcription kit (Thermo Fisher, AM1340). mCherry mRNA and Tol2 mRNA (encoding a protein product that is innocuous to embryonic development) were produced similarly, for sorting injected embryos and for equilibrating total mRNA dosage between injection groups, respectively.

Embryos were collected from *mnx1:GFP* x AB crosses (ZFIN ID: ZDB-ALT-051025-4) (to acquire motor neurons with GFP) and injected with mRNA into the yolk at the 1-2 cell stage. Each embryo was injected with SOD1 mRNA at the doses indicated in the results, 100pg mCherry mRNA, and a top-up of Tol2 mRNA (an innocuous product to normal zebrafish development), bringing the total mRNA dosage to 1900pg. Thus the total mRNA dosage was normalized across all injection groups, including injecting combinations of SOD1 variants. Control mRNA groups were injected with 1800pg Tol2 mRNA plus 100pg mCherry mRNA. Following injection, embryos were maintained in E3 embryo media (Westerfield, 2000b) at 28°C with addition of PTU (Phenylthiourea, used

to inhibit pigmentation) at approximately 10 hours post-fertilization (hpf); at 24hpf they were sorted for mCherry fluorescence (indicating quality mRNA injection).

For 5'-fluorouridine (5'-FUrd), uridine, and telbivudine treatments, the drugs were mixed at the concentrations indicated, with 0.2% DMSO in E3 embryo media. Embryos were injected where indicated as described above, and at 12hpf dead embryos were removed and media replaced with drug-treated media. Vehicle control groups received 0.2% DMSO in embryo media. Embryos were maintained in drug media until fixation or use in Western blots or TEER assay.

6.3.3. Axonopathy Assay

Embryos positive for GFP in the motor neurons were fixed at 34-36hpf in 4% paraformaldehyde for 40 minutes, then transferred to PBSTw (phosphate buffered saline pH7.4 with 0.1% Tween20) until assessment. Axons of the primary motor neurons were scored for abnormal branching as per previous methods (Kabashi et al., 2010; Lemmens et al., 2007; Ramesh et al., 2010; Sakowski et al., 2012). In normal axon development, primary motor axons exit the spinal cord, extending past the notochord ventrally without branching, to innervate the trunk muscles. Axon branching at or before the notochord ventral boundary was scored as abnormal (Fig. 6.1B); the total number of abnormal branches was recorded for each embryo. Researchers were blinded to injection groups during axonopathy assessment.

6.3.4. TEER Assay

The Touch-Evoked Escape Response (TEER) assay (Armstrong and Drapeau, 2013; Kabashi et al., 2011; Kabashi et al., 2010) was deployed to assess motor outputs of embryos that had been injected with mRNA as indicated and raised to 48-50hpf. Embryos screened positive for mCherry fluorescence and without gross body defects were selected for TEER. Each embryo was placed individually in the centre of a 15cm diameter Petri dish, and touched on the tail with fishing line. The subsequent escape swims were recorded using a Basler aCA1300-60gm GigE camera (Basler AG, An der

Srtusbek, Germany) (recording from directly above the dish) and analyzed in Ethovision XT (Noldus Information Technology Inc., Leesburg, USA). Videos were checked for successful tracking prior to analysis; those where the tracking function failed to detect or follow the embryo, or where the embryo failed to respond, were not analyzed. Video recordings were analyzed from the start of movement to the end, measuring for total swimming distance (Fig. 6.1C). Experimenters were blinded to treatment groups during the TEER assay and during video analysis.

6.3.5. Western Blot and Protein Quantification

Embryos injected with $SOD1^{WT}$ and $SOD1^{W32S}$ mRNA at the dosages indicated were screened for mCherry fluorescence. At 30hpf embryos were sorted into biological replicates (five embryos per replicate), de-yolked with de-yolking buffer (Westerfield, 2000b), washed with cold Ringer's solution, and homogenized by using a pestle and brief sonication in cell lysis buffer containing 20mM HEPES, 0.2mM EDTA, 10mM NaCl, 1.5mM $MgCl_2$, 20% glycerol, 0.1% Triton-X, and 0.5% Protease Inhibitor Cocktail Set III (Millipore, CA80053-852). Protein concentration was determined with Qubit® fluorometer (Invitrogen, Carlsbad, CA, USA) prior to SDS-PAGE. SDS-PAGE was set up as previously described (Kanyo et al., 2011) using a Mini-PROTEAN Tetra Cell (Biorad Labroratories, Inc., Herculas, CA, USA). Samples (20µg of total protein/well) were loaded on a 12% gel and run in electrophoresis buffer (25mM Tris, 190mM glycine, 3.5mM SDS). After electrophoresis, gels were equilibrated in Towbin's buffer (25mM Tris, 190mM glycine, 20% methanol) for 15 minutes and protein samples were transferred onto PVDF membrane at 100V for 1 hour.

Membranes were blocked in 5% dried skim milk dissolved in TBST (50 mM Tris, 150 mM NaCl, and 0.05% Tween 20, pH 7.5) for 1 hour. SOD1 was detected with rabbit anti-SOD1 antibody (Enzo Life Sciences, ADI-SOD-100) at 1:10000 dilution. Actin was targeted with a rabbit anti-actin antibody (Sigma, A2066) at 1:1500. All antibodies (primary and secondary) were diluted in 5% skim milk/TBST. Membranes were incubated with primary antibodies overnight at 4°C with gentle agitation. Immunoblots were washed in TBST (4x 15-minutes) and probed with horse-radish peroxidase-conjugated anti-rabbit

secondary antibody (1:1000 dilution; Jackson Immuno, 111-035-003) for 1 hour at room temperature. Following washing in TBST as described above, SOD1 or actin was visualized using Pierce® ECL Western Blotting Substrate (Thermofisher, 32106). Band intensity was measured via densitometry with ImageJ64 for Windows (Wayne Rasband, National Institutes of Health, USA; http://imagej.nih.gov/ij) and SOD1 was quantified by normalizing human SOD1 band intensities to actin band intensities.

6.3.6. Statistical Analysis

Statistical analysis of axonopathy and TEER data was performed using Kruskall-Wallis ANOVA with post-hoc Mann Whitney pairwise comparisons in Stata/SE 14.1 for Mac (2015, StataCorp). Analysis of Western blot band intensity values was performed using one-tailed ANOVA with Dunnet's multiple comparisons in Prism 7 (GraphPad Software).

6.3.7. High throughput Virtual and Pharmacophore Screening studies

The database preparation of FDA (United States Food and Drug Administration) approved compounds, receptor structure preparation, high throughput virtual and pharmacophore screening studies were performed with Molecular Operating Environment (MOE) integrated drug discovery package from Chemical Computing Group (CCG) Inc, (Montreal, Canada) (2018) .

For preparation of the compound database, a library of 1861 FDA approved compounds was downloaded from Drugbank (version 5.0.1) (Wishart et al., 2006) in SDF chemical-data file format (www.drugbank.ca). The SDF format compounds were subjected for database preparation in MOE compatible format then used for the HTVS and pharmacophore screening studies. The preparation included importing SDF format compounds to MOE, removal of counterions and solvent molecules, protonation of compounds at pH=7.0, and energy minimization. The detailed methodology of the protocols used for database preparation can be found in MOE documentation (2018).

For receptor structure preparation, atomic coordinates of the receptor (monomeric apo-SOD1 structure) were taken from the X-ray structure of the human SOD1 enzyme with 5'-FUrd ligand bound to its W32 binding site (PDB code 4A7S) (Wright et al., 2013). The hetero atoms were removed, and only the coordinates of the first SOD1 monomer were used to build the structural model of the receptor. The *Protonate3D* module of MOE was used to assign protonation states of polar amino acids at pH=7.0. Hydrogen atom coordinates missed in the experimental structure were added with the *Protein Structure Preparation* module of the MOE package, and then partial charges were assigned to the receptor atomic sites. Once prepared as described, the above structure was optimized to relax strained geometry and possible steric clashes by using energy minimization with a gradient tolerance of 0.1 Kcal/mol/Å. For minimization, the Generalized Born Volume Integral (GB/VI) formalism and the Amberff10 force field were chosen from the Amber10:EHT option available with MOE.

High throughput virtual and pharmacophore screening was done with the *Dock module* in the MOE package for the HTVS studies, to screen the FDA approved compounds at W32 binding site. Residues from the W32 binding site of SOD1, in particular, Asn19, Phe20, Glu21, Gln22, Lys30, Val31, Trp32, Gly33, Ser34, Asp96, Val97, Ser98, Ile99 and Glu100 were selected as binding site residues for HTVS studies. All other residues within 5 Å distance were also included in the docking site definition for the *triangle matcher ligand placement* method. These are residues Ala1, Thr2, Lys3, Ala4, Val5, Cys6, Val7, Leu8, Lys9, Gln15, Gly16, Ile17, Ile18, Lys23, Glu24, Gly27, Pro28, Val29, Ile35, Lys36, Gly37, Gly93, Val94, Ala95, Asp101, Ser102, Val103, Ile104, Ser105, Leu106 and Ser107. The Amber10:EHT force field option available with MOE allowed us to assign the Amberff10 force field (Case DA 2008) and EHT (extended Hückel theory) (Gerber and Muller, 1995) based parameters for the receptor and compounds, respectively. The atomic partial charges for the receptor assigned from Amberff10 force field (Case DA 2008) and for the ligand AM1-BCC (Jakalian et al., 2000; Jakalian et al., 2002) method charges were assigned. 30 binding poses were generated for each compound from the database by using the *triangle matcher placement* method. These poses were scored with the London ΔG scoring function, and the top 5 poses were refined using *Rigid Receptor* method and finally rescored using GBVI/WSA ΔG scoring function.

The pharmacophore model was built based on the molecular features of the uracil moiety of 5'-FUrd (Fig. 6.3C) (Wright et al., 2013). The model consists of hydrogen bond acceptor atoms from 4, 2 dioxy groups on uracil and aromatic features of pyrimidine ring. The built pharmacophore model was used to identify the uracil-like molecular features in FDA approved compounds obtained from HTVS docking studies. The detailed explanation of methodology and modeling tools used for screening can be found in the MOE package documentation (2018).

6.4. Results

6.4.1. Altering the W32 residue reduces SOD1 toxicity as measured by motor neuron axonopathy and function

The significance of the W32 residue to SOD1 toxicity in the central nervous system was tested in an *in vivo* ALS model of motor neuron morphology and function: zebrafish (DuVal et al., 2014a; Kabashi et al., 2010; Lemmens et al., 2007; Ramesh et al., 2010; Sakowski et al., 2012). Human SOD1 variants were delivered to zebrafish embryos as mRNA shortly after fertilization as per established methods (Lemmens et al., 2007). Injected embryos were then assessed for motor neuron axonopathy and swim performance, with comparisons to control injected groups.

Overexpression of human $SOD1^{WT}$ or fALS disease-associated SOD1 mutants has previously been shown to cause an increased frequency in primary motor neuron axonopathy (defined previously and here as primary axon branching occurring above the ventral boundary of the notochord- see Methods and Fig. 6.1B) compared to that of un-injected or control mRNA injected embryos. The magnitude of this phenotype correlates well with disease severity; we confirmed these past results and extend this trend by injection of $SOD1^{G127X}$, which is an aggressive clinical variant with fairly rapid progression (Andersen et al., 1997; Hansen et al., 1998; Jonsson et al., 2004; Kabashi et al., 2010; Lemmens et al., 2007; Ramesh et al., 2010). $SOD1^{G127X}$ induced 20% more axonopathy than $SOD1^{WT}$ and both these values were significantly increased from controls (34% increase in $SOD1^{WT}$ and 62% in $SOD1^{G127X}$ compared to mRNA controls) (Fig. 6.1D;

p<0.05), thus further confirming in our hands that penetrance of the axonopathy phenotype is a good predictor of disease severity for fALS SOD1 variants. We also assessed the impact of these variants on motor neuron function in zebrafish larvae using the Touch-Evoked Escape Response (TEER) (Armstrong and Drapeau, 2013; Kabashi et al., 2011; Kabashi et al., 2010), where a larva performs a burst of swimming upon being touched on the tail (Fig. 6.1C). Injecting $SOD1^{G127X}$ reduced swim performance 20% more than $SOD1^{WT}$, and both these groups had significantly decreased swim performance from control mRNA injected larvae (distances compared to mRNA controls were 38% and 50% lower in $SOD1^{WT}$ and $SOD1^{G127X}$ groups, respectively) (Fig. 6.1E; p<0.001).

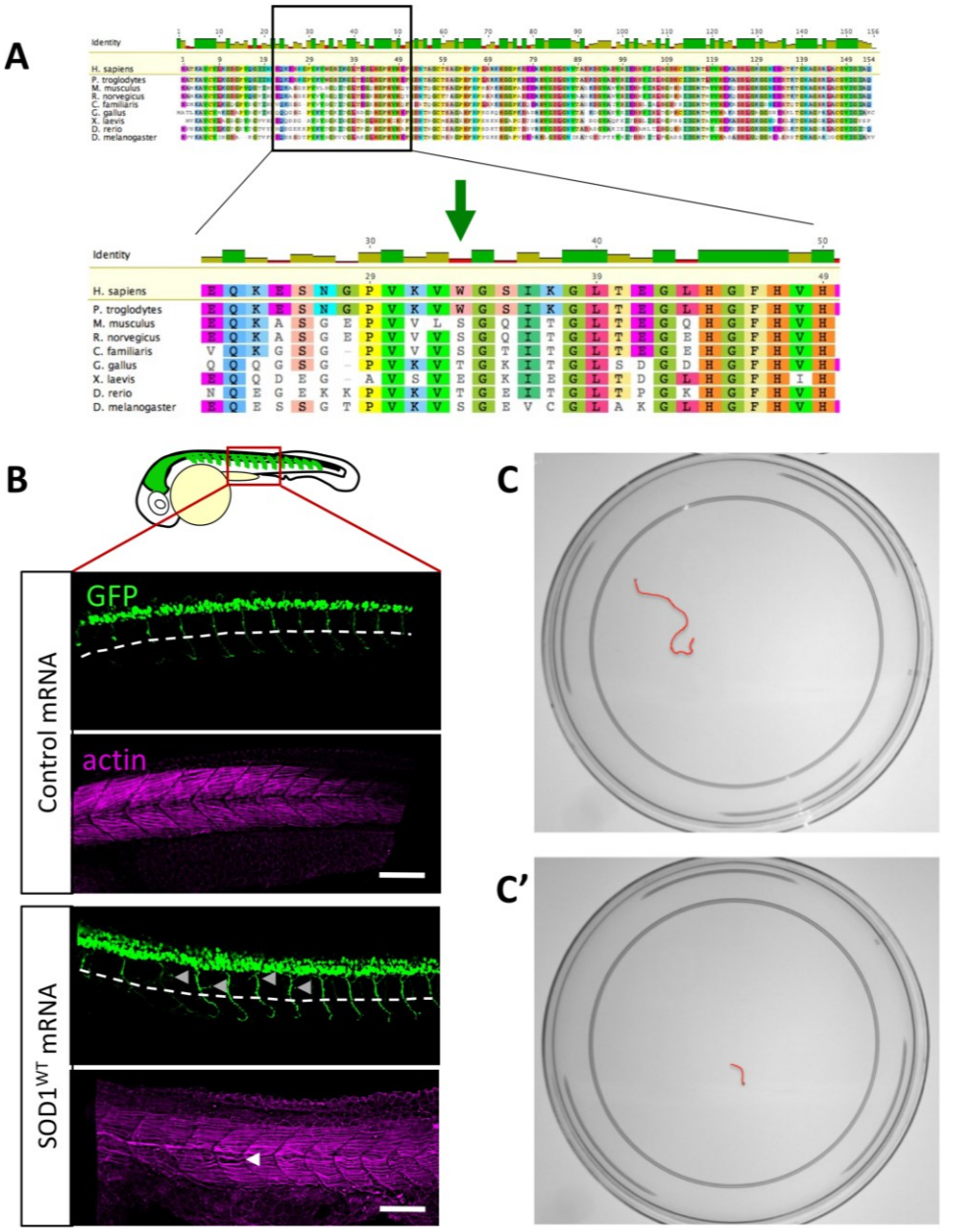
A
Identity
H. sapiens
P. troglodytes
M. musculus
R. norvegicus
C. familiaris
G. gallus
X. laevis
D. rerio
D. melanogaster
B
GFP
actin
Control mRNA
SOD1WT mRNA
C
C'
D
Residue W32 is required for SOD1-induced axonopathy in zebrafish motor neurons
Primary Motor Axons with Abnormal Branching ±SEM
Uninjected
mRNA Control
SOD1W32S
SOD1WT
SOD1G127X
E
Residue W32 is required for SOD1-based reduction in TEER performance
Swim Distance (cm) ± SEM
mRNA Control
SOD1W32S
SOD1WT
SOD1G127X

Figure 6.1. SOD1^{W32S} is less toxic than SOD1^{WT} or a disease-associated mutant *in vivo*.

A. SOD1 peptide sequence alignment showing that tryptophan at residue 32 in human SOD1 (green arrow) is not conserved at homologous residues in non-primates. **B.** Cartoon of a *mnx1:GFP* embryo (approx. 34 hours post-fertilization) with GFP in the motor neurons (hindbrain, spinal cord) and motor neuron axons (exiting the spinal cord). Reconstructions of confocal images of embryo trunks (location depicted by inset) illustrate axons in a control mRNA injected embryo and abnormal axons (SOD1^{WT} mRNA injected embryo). Individual primary axons exit the spinal cord and pass by the notochord (ventral notochord boundary indicated by white dashed line) to innervate the trunk muscles (phalloidin stain for muscle actin). In embryos injected with human SOD1^{WT} and deleterious SOD1 mutants, abnormal primary axons have proximal branching (arrowheads) located above the ventral boundary of the notocord, a metric of axonopathy. Mild disruption of muscle fibres may be visible near abnormal axons (arrowhead). Scale bars 200µm. **C.** Video stills of the Touch Evoked Escape Response (TEER) assay displaying recorded distance of a well-performing zebrafish larva, at 5.61cm (C), and a poorly performing larva, at 1.43cm (C′). **D.** Substituting residue W32 in human SOD1 (SOD1^{W32S}) significantly reduces axonopathy compared to human SOD1^{WT} (SOD1^{WT}) and disease mutant human SOD1^{G127X} (SOD1^{G127X}). SOD1^{WT} and SOD1^{G127X} cause more axonopathy compared to mRNA control injections ($p<0.05$). **E.** Zebrafish embryos injected with SOD1^{WT} or SOD1^{G127X} mRNA swim a shorter total

distance in the TEER assay compared to control mRNA injected fish ($p<0.001$), but not embryos injected with $SOD1^{W32S}$ ($p= 0.89$) (Kruskall-Wallis ANOVA with Mann-Whitney pairwise comparisons). Data values that share matching grey letters are not significantly different. Embryo sample sizes noted below data points.

To assess if residue W32 has an impact on motor neuron deficits induced by human SOD1 overexpression, we engineered $SOD1^{W32S}$ mRNA and delivered it to zebrafish embryos. $SOD1^{W32S}$ injected embryos did not show any increase in axonopathy, in fact producing about half as many motor neuron defects on average compared to $SOD1^{WT}$ (Fig. 6.1D; $p<0.001$). Also, in contrast to $SOD1^{WT}$, $SOD1^{W32S}$ injected larvae did not show impaired motor function, swimming a comparable distance to control larvae in response to a touch on the tail ($p= 0.89$) (Fig. 6.1D). These results support the hypothesis that residue W32 is important for induction of SOD1 cytotoxicity.

An alternative explanation for the significantly lower incidence of axonopathy in embryos injected with $SOD1^{W32S}$ might reside in the kinetics of the transcript or protein abundance: e.g. it is possible that injection of $SOD1^{W32S}$ led to lower levels of protein compared to $SOD1^{WT}$, despite great care to deliver equal doses via mRNA injection. To address this, we measured protein levels in triplicate samples of five 30hpf embryos injected with various mRNA doses of $SOD1^{WT}$ and $SOD1^{W32S}$. Human SOD1 protein (approx. 21 kDa) and the zebrafish endogenous Sod1 protein (approx. 17 kDa) were readily discriminated on Western blots (Fig. 6.2A, larger band absent in protein from uninjected larvae). Western blot analysis in fact reported lower $SOD1^{W32S}$ protein abundance compared to $SOD1^{WT}$ when equal amounts of SOD1 mRNA are injected. To ensure that the less severe phenotypes we observed in $SOD1^{W32S}$ compared to that of $SOD1^{WT}$ were not due to differences in SOD1 protein abundance, we adjusted the doses of mRNA delivered such that the fish produce similar SOD1 protein abundance for each variant. Injection of 1800pg of $SOD1^{W32S}$ mRNA resulted in an amount of protein similar to injection of 450pg of $SOD1^{WT}$ mRNA (Fig. 6.2A). We assessed axonopathy at these doses and found that, while axonopathy increased between 900pg and 1800pg mRNA

doses of $SOD1^{W32S}$, it remained lower than axonopathy in 450pg $SOD1^{WT}$ injected embryos and not significantly different from controls (control average and SEM indicated on graphs with green dotted line and green box respectively) (Fig. 6.2B; p= 0.07). Thus SOD1 harboring the W32S mutation does not induce significant axonopathy above control levels, even when presented as a large mRNA dose or a protein level equivalent to $SOD1^{WT}$. Further, W32 is apparently required for human SOD1 to induce motor neuron defects in this animal model, because when $SOD1^{W32S}$ protein was present in equal abundance to $SOD1^{WT}$ it continued to result in less axonopathy (Fig 6.2B).

Alteration of the W32 residue may render the SOD1 monomer more stable and less vulnerable to templating of protein misfolding and aggregation, or may act in *trans* to confer additional stability onto other monomers. For example, if $SOD1^{W32S}$ were to heterodimerize with a wildtype W32-containing counterpart, or a SOD1 dimer containing $SOD1^{W32S}$ were to interact with another SOD1 dimer, the interaction may reduce the probability of misfolding in the wildtype, W32-containing counterparts (Banerjee et al., 2016; Shi et al., 2016b). To discern whether the W32S substitution confers a protective effect on neighbouring SOD1 proteins (i.e. if $SOD1^{W32S}$ can rescue $SOD1^{WT}$ and its toxicity), we co-injected $SOD1^{WT}$ with $SOD1^{W32S}$ at two different dosage ratios (900pg each or 450pg + 1350pg, respectively). If $SOD1^{W32S}$ can reduce aggregation propensity in neighbouring monomers or dimers, we would predict it could rescue the $SOD1^{WT}$-induced axonopathy. We found a not statistically significant rescue effect at both doses (Fig. 6.2C), which does not support the notion that a W32S substitution in SOD1 was able to prevent or reduce the cytotoxicity of other SOD1 monomers or proteins, or at least not to a significant degree. Thus the $SOD1^{W32S}$ protein has a lower propensity to become toxic, but within our model it does not substantially alter the neurotoxic properties of nearby wildtype (W32-containing) SOD1 proteins.

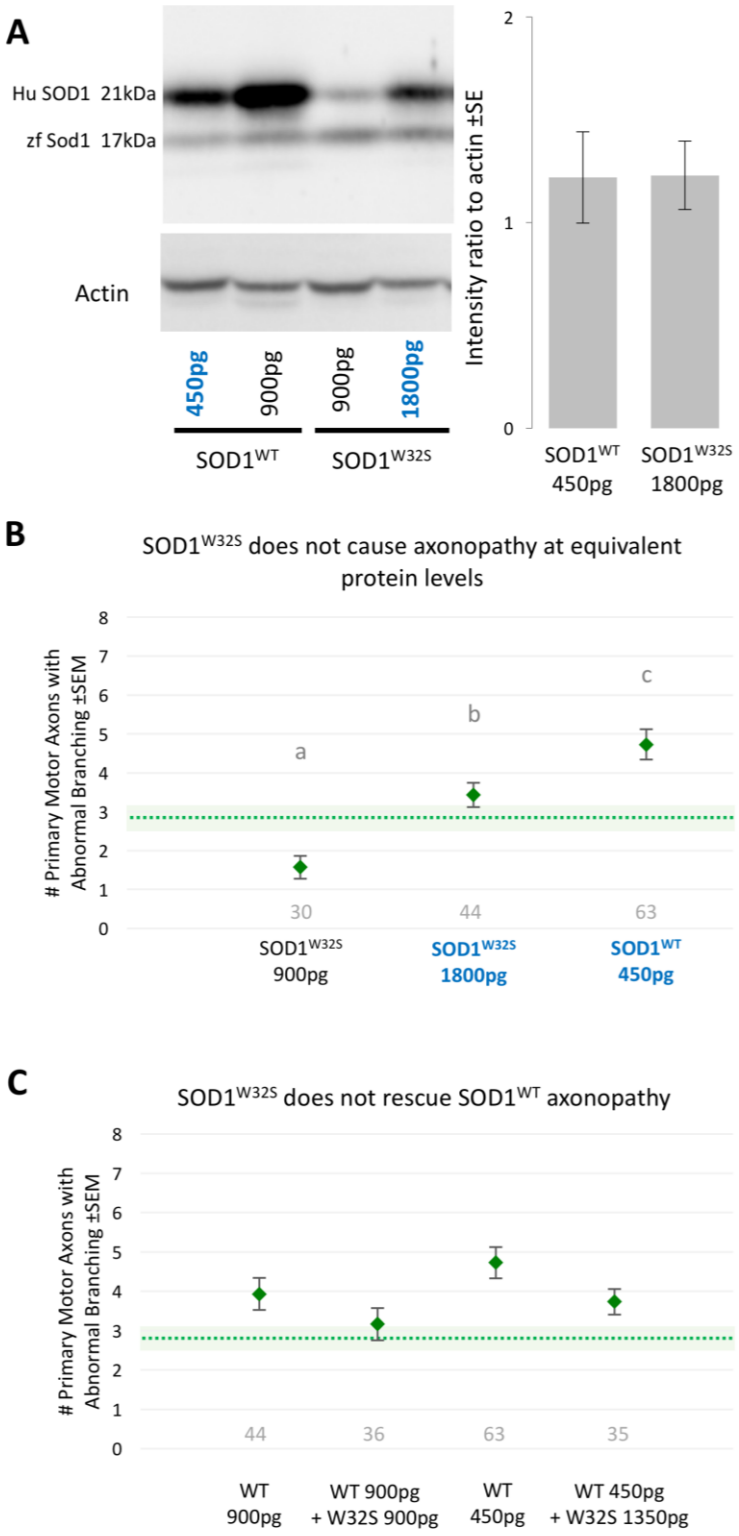

Figure 6.2. At equivalent protein levels, SOD1^{W32S} does not cause a severe axonopathy phenotype compared to SOD1^{WT}.

A. $SOD1^{W32S}$ and $SOD1^{WT}$ mRNA were injected at varying doses to determine equivalent protein levels as measured on Western blot (450pg of WT and 1800pg of W32S; equivalent protein groups highlighted in blue font; quantification shown for n=3 biological replicates containing 10 embryos each). The immunodetection reveals both exogenous human SOD1 (Hu SOD1, band absent in uninjected larvae) and endogenous zebrafish Sod1 (zf Sod1). **B.** At 1800pg, $SOD1^{W32S}$ produces an increase in axonopathy over that of the 900pg dose ($p < 0.001$), but this axonopathy was statistically insignificant compared to control mRNA axonopathy levels (green dotted line with SEM in green shading) ($p=0.07$). $SOD1^{WT}$ at 450pg produces significantly more axonopathy ($p<0.001$). **C.** $SOD1^{W32S}$ was co-injected with $SOD1^{WT}$ to determine if W32S can rescue toxicity caused by $SOD1^{WT}$; while a mild rescue was seen at two dose combinations tested, this was not statistically significant (mRNA control average shown as green dotted line with SEM in green shading). (Kruskall-Wallis ANOVA with Mann-Whitney pairwise comparisons). Data values that share matching grey letters are not significantly different. Embryo sample sizes noted below data points.

6.4.2. The W32 residue is a promising drug target to mitigate SOD1-induced motor neuron deficits

The presence of W32 may universally influence the human SOD1 protein's propensity to become unstable and misfolded, as seen by its effects in both wild type SOD1 and in various mutants (Grad et al., 2011; Taylor et al., 2007), thus W32 would be a desirable target to generally abate SOD1 misfolding and toxicity. 5'-fluorouridine (5'-

FUrd) has been predicted to bind to the W32 residue (Wright et al., 2013) (Fig. 6.3A, B), and so we sought to test this small molecule in our zebrafish model. In addition to testing 5'-FUrd, we performed high throughput virtual screening (HTVS) using a pharmacophore model to identify new compounds which could bind at the W32 binding site of SOD1 and potentially inhibit SOD1 toxicity. The W32 residue is located on the surface of the β-sheet, is highly solvent exposed, and does not have a conventional binding pocket, therefore this site poses difficulties for designing new compounds. This can be overcome by filtering screened compounds through the pharmacophore model, using a template of a compound already confirmed to bind this site on SOD1. Initially, HTVS studies were performed with a library of FDA approved compounds at W32 site of SOD1. The X-ray crystallography study of Wright et. al (Wright et al., 2013) demonstrated that 5'-FUrd binds at the W32 residue of SOD1, and not at the SOD1 dimeric interface as proposed by previous reports (Nowak et al., 2010; Ray et al., 2005) (Fig. 6.3A, B). The molecular interaction features of the uracil moiety of 5'-FUrd at the W32 site were utilized to build the pharmacophore model (Fig. 6.3C). The library of FDA approved compounds from HTVS studies was further filtered through the pharmacophore model and 17 compounds were identified. Among these 17 compounds, ten compounds were selected based on their binding energy, π-π interactions ability with the indole side chain of W32 residue, and similarity to 5'-FUrd (Appendix 5, Table A5.1). Based on analysis of molecular descriptors of top ranked compounds, we selected telbivudine (Fig. 6.4, Ligand L5 in Table A5.1), the blood brain barrier-permeable thymidine analogue used to treat Hepatitis B. Telbivudine impairs viral DNA replication through phosphorylation into telbivudine triphosphate and being incorporated into viral DNA, which terminates elongation. It does not inhibit human polymerases, and it is not incorporated into human DNA. Telbivudine has a good drug safety profile, though with the caveats of myopathy and peripheral neuropathy rarely documented in some patients, and axonopathy (causation inconclusive) at high doses in animal toxicity studies; the mechanisms behind these side effects have not been elucidated (Bridges et al., 2008; Fung et al., 2011; Zhang et al., 2008). Neither uridine nor telbivudine have been tested for rescuing the effects of SOD1 toxicity in an animal model.

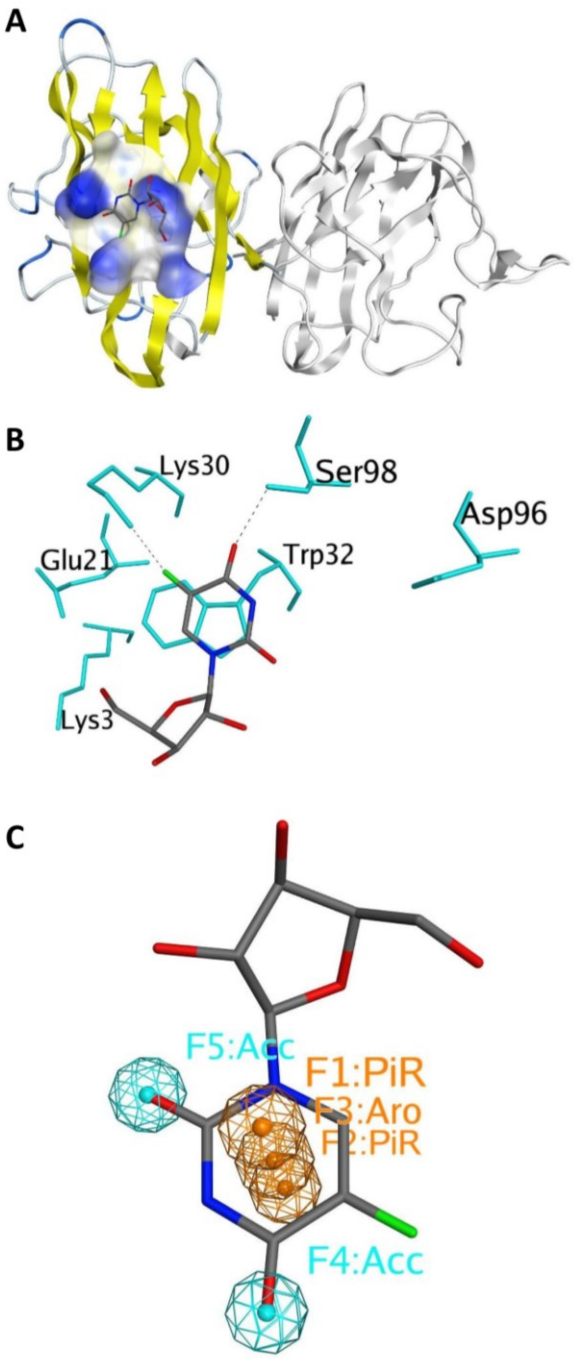

Figure 6.3. Experimental binding mode of 5-fluorouridine (5′-FUrd) at SOD1, and molecular features of 5′-FUrd-based pharmacophore model.

A. SOD1 dimer complexed with 5-FUrd from the X-ray structure of human I113T SOD1 mutant co-crystalized with 5′-FUrd (PDB accession code: 4A7S). SOD1 is shown in

cartoon representation with the first monomer from the 4A7S structure colored according to secondary structure. Solvent exposed surface of residues in the W32 biding site is shown with colors corresponding to the degree of solvent exposure (with blue color indicating a higher exposure). **B.** Experimental conformation of 5′-FUrd in the W32 binding site of the first monomer from the 4A7S structure. The ligand is colored according to its atom types and residues from the binding site are shown in blue. **C.** Pharmacophore model built based on the molecular features of the 5-fluorouracil moiety of 5′-FUrd. These features include hydrogen bond acceptor atoms (from 4, 2 dioxy groups of uracil shown in cyan) and aromatic pyrimidine ring (highlighted in orange).

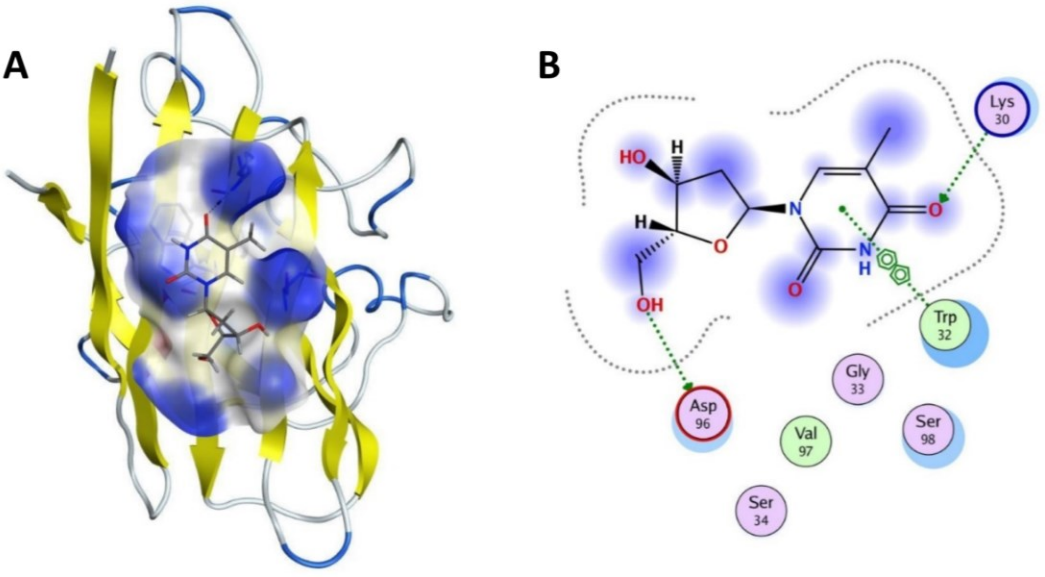

Figure 6.4: Probable binding mode of telbivudine at the W32 binding site of SOD1 predicted with combined high throughput virtual screening (HTVS)/pharmacophore screening.

A. SOD1 monomer complexed with telbivudine. **B.** 2-D interaction map of telbivudine and the receptor.

We proceeded to test 5'-FUrd, uridine, and telbivudine as therapeutics against $SOD1^{WT}$-induced motor neuron toxicity. 5'-FUrd showed partial rescue of axonopathy at a 1.5μM dose (Fig. 6.5A), however higher doses caused adverse effects in uninjected embryos (Fig. 6.5). In contrast, application of uridine or telbivudine showed no adverse effects on survival nor increase in axonopathy compared to vehicle controls (Fig. 6.5). Uridine had a more dramatic rescue than 5'-FUrd, producing significant measurable benefits starting at a 0.5μM dose, in both axonopathy (45% reduction) and TEER performance (24% longer average distance) in $SOD1^{WT}$ injected embryos (Fig. 6.6A, B). Uridine treated embryos showed no significant difference from mRNA controls, and a significant reduction from $SOD1^{WT}$ injected embryos treated with DMSO alone ($p< 0.01$) (Fig. 6.6A, B). However application of higher doses of uridine (5μM) decreased TEER performance, so uridine may also have an upper limit of efficacy, at least as measured by the TEER assay. Telbivudine similarly rescued axonopathy in $SOD1^{WT}$ injected embryos at and above established therapeutic doses (Zhou et al., 2006) (41%, 60%, 55%, 57%, and 82% reduction at 1μg/mL [4.1μM], 5μg/mL [25.6μM], and 10μg/mL [41.3μM] doses respectively) ($p< 0.01$) (Fig. 6.6C).

To ascertain whether the rescue effects of these drugs act via SOD1 and by binding at residue W32 as predicted, or if they mediate some other more general protective mechanism, we applied effective doses of each drug (1.5μM 5'-FUrd, 1.0μM uridine, and 25.6μM telbivudine) to embryos injected with a high dose (1800pg) of $SOD1^{W32S}$. We predicted that if 5'-FUrd, uridine, or telbivudine contribute significantly to a neuroprotective mechanism that is independent of the human SOD1 W32 residue, then their protective effects would be additive with the protective effects of the W32S substitution. We observed that applying neither 5'-FUrd, uridine, nor telbivudine had any apparent impact on embryos injected with 1800pg of $SOD1^{W32S}$ - the resulting axonopathy was unchanged (Fig. 6.6D). The W32 residue is thus required for these uracil-like nucleoside compounds to exhibit their treatment effects on human SOD1. These

compounds and the W32S mutation therefore likely have a shared mechanism to protect neurons, such as stabilizing the SOD1 structure via W32 or disrupting aberrant intermolecular interactions that require this solvent-exposed tryptophan residue.

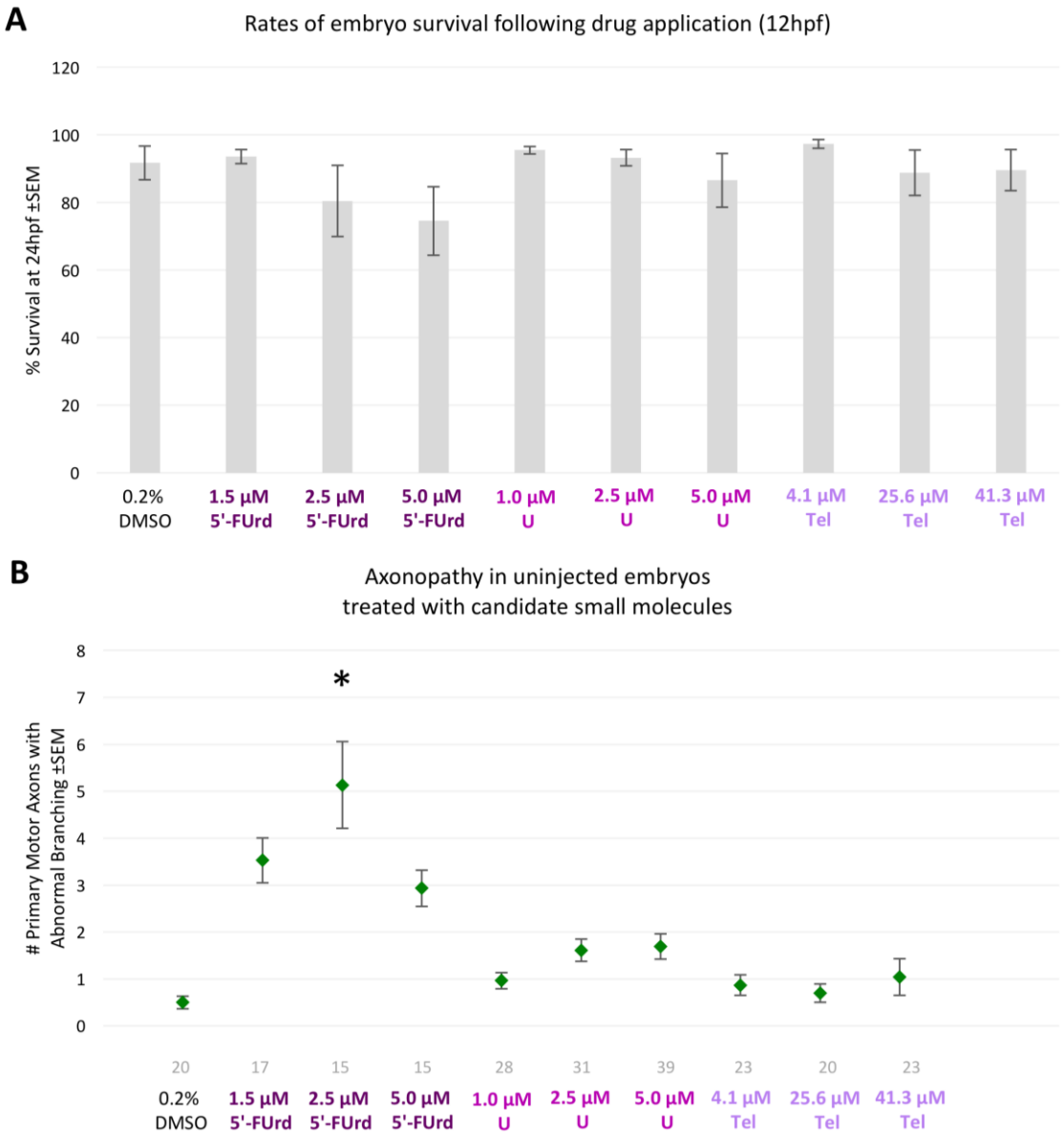

Figure 6.5. Testing for adverse effects of 5'-FUrd, uridine, and telbivudine in zebrafish embryos.

Zebrafish survival [A] and axonopathy [B] following drug exposure indicate that uridine (U) and telbivudine (Tel) are well tolerated, and 5'-fluorouridine (5'-FUrd) is tolerated

within a specific range. Compared to 0.2% DMSO vehicle control-treated embryos, 5′-FUrd exposure does not affect survival or number of abnormal axons below 2.5μM, however at 2.5μM and above survival and axonopathy are affected (* $p<0.05$). Uridine and telbivudine do not show overt effects at the doses tested. Three or more replicates were performed for survival. Embryo sample sizes noted below data points.

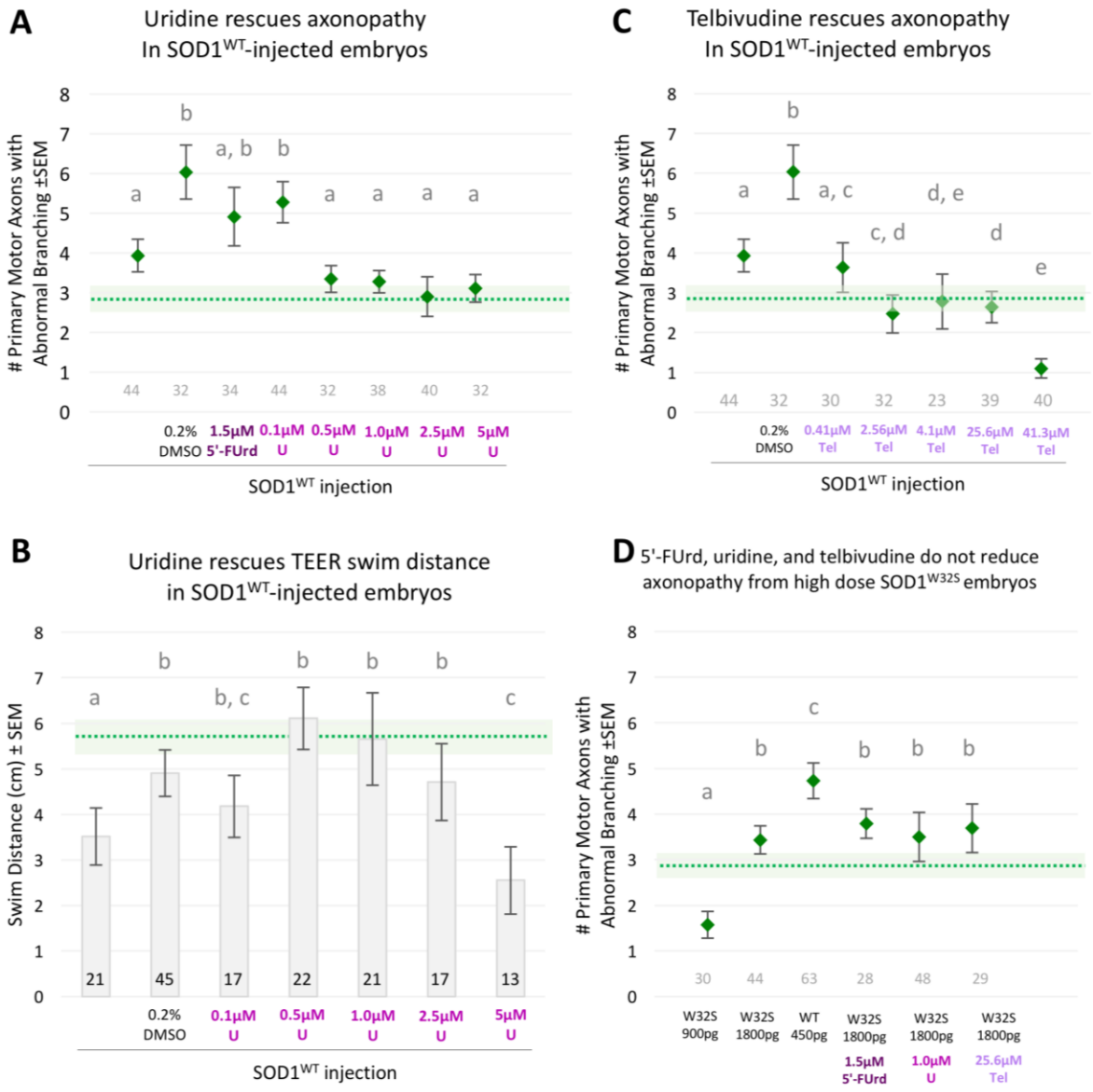

Figure 6.6. Uridine and telbivudine decrease SOD1 toxicity and likely act through the W32 residue.

A. 5′-fluorouridine (5′-FUrd) (dark purple) partially rescues axonopathy. Uridine (U, bright purple/magenta on x-axis) reduces axonopathy in embryos injected with $SOD1^{WT}$ to control mRNA levels (green dotted line with SEM in green shading), starting at a 0.5μM dose. **B.** Uridine (U) also rescues TEER performance in $SOD1^{WT}$-injected embryos back to control mRNA distances (green dotted line with SEM in green shading), in a dose-responsive manner, with greatest rescue at 0.5μM dose. The TEER group with the highest U dose, 5μM, performed less well, suggesting an upper limit for uridine exposure. **C.** Telbivudine (Tel, light purple) similarly reduces axonopathy from $SOD1^{WT}$ at the following doses: 4.1μM (1μg/mL), 25.6μM (5μg/mL), 41.3μM (10μg/mL). Data for $SOD1^{WT}$ and $SOD1^{WT}$ + 0.2% DMSO is re-plotted from [A]. **D**. To determine whether the candidate small molecules exert their rescue effects via the tryptophan residue W32 on SOD1, 5′-FUrd, uridine, or telbivudine at effective doses was applied to $SOD1^{W32S}$ (1800pg)-injected embryos to test whether they would rescue the mild axonopathy. None of the drugs caused a change in axonopathy, suggesting that these small molecules and W32S act in similar mechanisms to confer protection to motor neurons. (Kruskall-Wallis ANOVA with Mann-Whitney pairwise comparisons, $p<0.05$; data from Fig. 2B included here for ease of comparison). Data values that share matching grey letters are not significantly different. All drug solutions included 0.2% DMSO. Embryo sample sizes noted below data points.

6.5. Discussion

The conversion of SOD1 from a natively folded to a misfolded conformation is central to the initiation of ALS pathology in *SOD1* mutation-associated (fALS) disease, and likely in non-*SOD1* associated fALS and sporadic disease as well. What domain, residue, or interaction is minimally sufficient (and therefore therapeutically targetable) for SOD1 conversion has remained ambiguous. Here we deployed an *in vivo* model to assess the impacts of a proposed mediator of SOD1 toxicity. We demonstrated that the impacts of human SOD1 on motor neuron deficits and motor outputs require the sole tryptophan in the human SOD1 protein, W32, and these deficits can be specifically ameliorated by drugs targeting this residue.

The SOD1 W32 residue is an intriguing target due to its solvent exposure despite having a hydrophobic side chain. Because selection has maintained this seemingly odd configuration, at least within primates, it would seem that W32 is mediating some important aspect of SOD1 biology. Previous mapping to determine which domains drive SOD1 conversion suggested residues 24-36; within this region W32 and its adjacent residues are predicted to form a structure unique to human SOD1, correlating perfectly with a contrast to mouse SOD1, that is not readily converted to a misfolded state (Grad et al., 2011). The presence of this tryptophan may simply increase the probability of conversion (suspected to occur via oxidation of W32 (Coelho et al., 2014; Taylor et al., 2007)), or it may exert conversion effects on neighbouring SOD1 proteins (Grad et al., 2011). For example, the lack of a tryptophan in murine SOD1, and lack of murine SOD1 participation in conversion and aggregation, would support the former hypothesis. In experiments done by Grad et al. (Grad et al., 2011), transfection of mouse N2a cells with human $SOD1^{G127X}$ failed to generate detectable misfolded protein. In other words, $SOD1^{G127X}$ had failed to convert mouse SOD1 protein. The presence of a W32 may thus contribute to a SOD1 protein's propensity to be "convertible". However double mutant experiments suggest the latter- that human $SOD1^{G127X}$ and $SOD1^{G85R}$ require a tryptophan at residue 32 to convert $SOD1^{WT}$. HEK-293 cells transfected with $SOD1^{W32S}$, $SOD1^{G127X/W32S}$, or $SOD1^{G85R/W32S}$ had produced less signal for misfolded protein compared to their W32-containing counterparts (Grad et al., 2011). Thus to date there is

evidence of both roles: tryptophan may increase the probability of conversion within a monomer, and/or it may participate in the conversion of another SOD1 monomer.

ALS is a multigenic disease, featuring genetic mutations in critical cell processes such as mitochondrial homeostasis, RNA metabolism, and neuromuscular junction support and function (Corcia et al., 2017). Whether misfolded SOD1 has a central role in all these varieties of ALS pathophysiology remains inconclusive, but protein misfolding, mislocalization, and disruption to proteostasis is a prominent theme among mutations in *SOD1*, *TDP43*, and *FUS* (Ayers et al., 2016b; Blokhuis et al., 2013; Cashman et al., 2012; Farg et al., 2012; Farrawell et al., 2015b; Fushimi et al., 2011; Huang et al., 2011; King et al., 2013; Kwiatkowski et al., 2009; Magrane et al., 2014; Newell et al., 2015; Nordlund et al., 2009; Parakh and Atkin, 2016; Pokrishevsky et al., 2012a; Rabdano et al., 2017; Shiihashi et al., 2016; Takanashi and Yamaguchi, 2014; Wang et al., 2013). Protein misfolding is therefore requisite for initiating downstream pathology. Not only can protein misfolding disrupt proteostasis and confer a toxic gain of function, loss-of-function phenotypes are often observed (Allison et al., 2017). Numerous mutations (185 and counting) have been found in the *SOD1* gene in patients, but evidence exists that mutation is not required for SOD1 to misfold (Bosco et al., 2011; Brotherton et al., 2012; Forsberg et al., 2010; Grad et al., 2011; Graffmo et al., 2013; Pokrishevsky et al., 2012a). There are biochemical qualities or interactions of SOD1 that enable dimer and/or monomer destabilization and possibly template-directed misfolding, despite the considerable stability of the SOD1 dimer (Malinowski and Fridovich, 1979). The W32 residue unique to primates may be one such factor that exerts destabilizing effects on SOD1. W32 is located in the fairly well conserved (among primates; see Fig. 6.1A) sequence for β strand 3; selection pressure on this domain within primates may have lead to retention of the W32 residue despite its suspected destabilizing properties (Dasmeh and Kepp, 2017). There are no known human mutations altering the W32 residue specifically, so this tryptophan can be considered nearly universally present in familial and sporadic ALS cases. If tryptophan is indeed a potent modulator of SOD1 misfolding, it could be an attractive treatment target for all ALS patients.

As found in our experiments, adding candidate small compounds to SOD1^{W32S}-injected embryos (Fig. 6.3D) and our survival data (Fig. 6.5), uridine and telbivudine

tested herein do not increase general (neuromuscular) health, but rescue motor neurons by specifically blocking wild-type SOD1 from exerting toxicity. Telbivudine in particular has many optimal qualities of a candidate therapeutic. As an FDA approved drug currently in use, with a documented and favourable safety profile, it is an example of the promise in evaluating existing drugs for novel applications. We found that the phenotypes measured, axonopathy and TEER, were rescued by different interventions that disrupt a single mediator, W32, which is possibly critical to inter-molecular conversion (Grad et al., 2011). Therefore these phenotypes respond with high specificity to both the effects of human SOD1 expression and interventions that change SOD1 protein behaviour, including toxicity, an addition to W32's previously shown role in SOD1 misfolding (Grad et al., 2011). These multiple interventions also further implicate the W32 residue as a significant mediator of prion-like spread of ALS (Grad et al., 2011; Taylor et al., 2007).

Seeking to understand how mutations affect SOD1 stability, and selecting compounds to stabilize it, are far from new (Alemasov et al., 2017; Anzai et al., 2017; Broom et al., 2015; Das and Plotkin, 2013; Kumar et al., 2017; McAlary et al., 2016; Sekhar et al., 2016; Wright et al., 2013), and most efforts have focused on stabilizing the SOD1 dimer, particularly at the dimer interface. Stabilizing dimers would reduce the frequency of monomerization, which can be considered a rate-limiting step in the spread of SOD1 misfolding (Broom et al., 2015; McAlary et al., 2016; Petrov et al., 2016b; Proctor et al., 2016). But combining dimer-stabilizing compounds with complementary ones that can stabilize the protein at other regions may greatly increase therapeutic efficacy while also reducing the required dose of either compound, which is attractive for drugs that may have undesirable side effects at higher doses. The location of W32 results in a flat and unconventional ligand target; however pharmacophore modeling to predict compound-target interactions has provided exciting results in our animal model that await validation in mammalian ALS models.

6.5.1. Conclusions

The tryptophan at residue 32 of human SOD1 is unique evolutionarily (i.e. limited to primates), and unique within the SOD1 amino acid sequence. Strikingly, modifying W32

in cell culture and in our animal model herein dramatically reduces SOD1 aggregation and toxicity. Further investigation into how this tryptophan contributes to SOD1 structure and stability compared to more conserved residues would reveal new insights into SOD1 folding, unfolding, and misfolding. The W32 is a promising drug target for preventing SOD1 misfolding and toxicity, thereby reducing its contribution to debilitating motor neuron degeneration.

Chapter 7. TDP43 induction of SOD1 toxic gain-of-function requires tryptophans

This Chapter comprises work in collaboration with Neil R. Cashman. The questions, hypotheses, and experiments in this chapter were conceived and designed by Edward Pokrishevsky, Neil R. Cashman, Michèle G. DuVal, and W. Ted Allison. Zebrafish experiments were performed and analyzed by MGD with assistance from Jenna Bratvold, and interpreted by MGD, EP, NRC, and WTA. Vectors for experiments were supplied by EP and NRC and cloning for mRNA production was performed by Gavin Neil. Writing for this chapter was done by MGD with editing and feedback by WTA.

7.1. Summary

SOD1 and *TDP43* are two of the most prominent genes associated with familial amyotrophic lateral sclerosis (fALS), and inclusions of SOD1 or TDP43 protein have been confirmed in some sporadic ALS cases as well. Whether and how SOD1 and TDP43 may interact to effect motor neuron degeneration is just beginning to be clarified, with *in vitro* modelling suggesting that TDP43 is capable of inducing SOD1 to misfold and aggregate. Taking this question to a whole organism model, we found that expression of TDP43 amplifies a SOD1 motor neuron toxicity phenotype in zebrafish. Fascinatingly, the aetiology of this interaction may be reduced to a few key amino acids: tryptophans in both SOD1 and TDP43 are critical mediators, such that substitution of these tryptophans abolishes the resultant phenotype. This SOD1 toxicity can also be abrogated with 5'-fluorouridine, a compound predicted to interact with the SOD1 tryptophan, W32, even in the presence of TDP43. Identifying interactions and other links between known factors in ALS may help unify multiple known pathological processes, and could inform on critical nodes between these processes as therapeutic targets.

7.2. Introduction

Familial amyotrophic lateral sclerosis (fALS) is a genetically complex disease with links to variants in multiple genes, including those that comprise, or facilitate the formation of, inclusions: *SOD1*, *FUS*, *ATXN2*, and *TDP43* (Corcia et al., 2017). Mutations in TAR DNA-Binding Protein 43 (*TDP43*) (Cairns et al., 2007; Davidson et al., 2007; Huey et al., 2012; Neumann et al., 2006b) and other genes (e.g. *C9ORF72*, *SQSMT1*, *CHCHD10*, and *FUS* (Corcia et al., 2017; Couratier et al., 2017; Neumann, 2013; Neumann et al., 2009)) are linked to both ALS and frontotemporal dementia (FTD). Shared gene links, combined with a 5-15% incidence of FTD among ALS patients and strong co-heritability (Beeldman et al., 2016; Lattante et al., 2015), support the idea that ALS and FTD sit along a disease spectrum with shared features, including TDP43 inclusions (Hasegawa et al., 2008). In addition to a prominence of *TDP43* mutations in fALS (approx. 4%) (Corcia et al., 2017), ubiquitinated wildtype TDP43 has been found in tissues of sporadic and non-*SOD1*/*FUS* ALS (Shintaku et al., 2017; Tan et al., 2007), implicating TDP43 as a significant mediator in progression of motor neuron pathology.

While there is no evidence of TDP43 inclusions in transgenic mutant SOD1 mouse models (Robertson et al., 2007) (and to date we are unaware of any mutant SOD1 and TDP43 co-expression experiments in whole animal models), prior investigations had found that TDP43 influences SOD1 misfolding *in vitro* (Higashi et al., 2010). Expression of cytosolic TDP43, with a disrupted NLS domain ($TDP43^{\Delta NLS}$) to mimic pathological mislocalization (Igaz et al., 2011b; Neumann et al., 2006b; Winton et al., 2008), can induce human wildtype [Cu, Zn] superoxide dismutase 1 (huSOD1 or SOD1) to misfold in transfected cell lines and in primary motor neuron cultures of transgenic $huSOD1^{WT}$ mice. This misfolded SOD1 (detected using antibodies against disease-specific epitopes) can then be transmitted to neighbouring cells (Pokrishevsky et al., 2016). How TDP43 induces SOD1 to misfold is yet to be determined. This same group and others identified a tryptophan at amino acid position 32 in SOD1 as critical in the SOD1 misfolding induction process (Grad et al., 2011; Taylor et al., 2007). We have previously determined the impact of this tryptophan, called W32, and found that it is required for the ability of human SOD1 to acquire toxic properties in a zebrafish model of motor neuron toxicity (Chapter 6). Thus the relevance of W32 in SOD1 has guided our follow-up investigation

into the TDP43 induction of SOD1 toxicity. In collaboration with the Cashman research group, we hypothesized that tryptophans in TDP43 are necessary for its induction of SOD1 to misfold and aggregate (unpublished), and to become toxic (this Chapter).

The amino acid tryptophan has a large hydrophobic residue (Chothia, 1976), and because of this unique quality, it tends to be utilized in residue clusters that exclude surrounding solvents (such as water), or to connect distant peptides in tertiary and/or quaternary protein structures. Because of their hydrophobic nature, tryptophans have a tendency to interact with each other (Samanta et al., 2000). For example, tryptophans are powerful mediators of myoglobin peptide aggregation (Cecchini et al., 2012); and aromatic groups, like that of tryptophans, are known to interact in the formation of amyloid fibrils (Azriel and Gazit, 2001; Cohen et al., 2006; Gazit, 2002). Despite these characteristics, the single tryptophan W32 of SOD1 is located in the third β strand, is not near the SOD1 dimer interface, and is solvent-exposed. Thus W32 of SOD1 is available for interaction with tryptophans of other SOD1 monomers or of other proteins. Wildtype TDP43 contains 6 tryptophans. Notably, none of the tryptophans in SOD1 or TDP43 are changed or affected by known ALS-associated mutations (Lagier-Tourenne and Cleveland, 2009). We hypothesize that interactions between TDP43 and SOD1 are mediated through their respective tryptophans, resulting in SOD1 misfolding (Pokrishevsky et al., 2016) and unpublished data) and SOD1 toxicity. To test this hypothesis, axonopathy caused by co-expression of human $SOD1^{WT}$ and $TDP43^{\Delta NLS}$ was compared to expression of combinations with respective tryptophans changed to serines. Zebrafish motor neuron axonopathy was additively rescued with increasing substitution of serines, and in TDP43, we found that 2 of the 6 tryptophans may account for most of the induction effect on SOD1.

The significant role of W32 on SOD1 acquiring toxicity makes it an attractive target for small molecule therapeutics. At least one small molecule is predicted to bind SOD1 at or near W32: 5'-fluorouridine (5'-FUrd) (Wright et al., 2013). We previously tested whether this small molecule can rescue axonopathy caused by expression of $SOD1^{WT}$ alone; in this Chapter we tested the rescue effects of 5'-FUrd in [$SOD1^{WT}$; $TDP43^{WT}$]- and in [$SOD1^{WT}$; $TDP43^{\Delta NLS}$]-injected embryos. Within a limited dosage range, 5'-FUrd can rescue axonopathy caused by SOD1 (Chapter 6) and by SOD1-TDP43 toxicity.

7.3. Methods

7.3.1. Animal Ethics Statement

Use of zebrafish for this study was approved by the Animal Care and Use Committee: BioSciences at the University of Alberta under protocol AUP00000077, under the auspices of the Canadian Council on Animal Care. Adult zebrafish were maintained and bred according to standard procedures, including housing in brackish water (1250±50 µS) at 28.5°C, with twice daily feeding of either brine shrimp or juvenile trout chow.

7.3.2. Expression of human SOD1 and TDP43 in zebrafish

Vectors containing human SOD1 and N-terminal HA-tagged TDP43, including versions with variations indicated, were gifted from Neil Cashman. Inserts were cloned using Gateway recombination into the pCS2+ expression vector for mRNA synthesis. mRNA production was done using FastDigest NotI restriction enzyme (Thermo Fisher, FD0593) and the Ambion mMESSAGE SP6 transcription kit (Thermo Fisher, AM1340). mRNA was co-injected with mCherry mRNA into 1-2-cell stage embryos from *Tg(mnx1:GFP)* transgenics (ZFIN ID: ZDB-ALT-051025-4) crossed to wild type AB fish; embryos were screened at 24 hours post-fertilization (hpf) for mCherry fluorescence indicating successful injection.

Effective dosage of *SOD1* and *TDP43* mRNA were determined empirically, with previous publications as guides, for a measurable phenotype above background (control mRNA) levels, but below maximum levels of axonopathy. To enable comparison between injection groups, total mRNA dose was made constant by top-up with innocuous Tol2 transposase mRNA, for a total 1900pg mRNA per embryo.

7.3.3. Assessment of axonopathy

Embryos were raised to 36hpf, fixed in 4% formaldehyde for 40 minutes, and assessed for axonopathy via GFP expression in the primary motor neurons. Dysmorphic embryos were not assessed. The axonopathy phenotype is an established assay for abnormal development of the primary motor neurons caused by overexpression of wildtype and mutant SOD1. Briefly, primary motor axons with branching dorsal of the ventral notochord boundary are scored as abnormal; total counts of abnormal axons were recorded per embryo (Fig. 7.1A).

7.3.4. Drug rescue using 5'-fluorouridine

The effective dosage of 5-fluorouridine (5'-FUrd) was determined by establishing a dose-response curve for survival and axonopathy. Embryo media was replaced with media containing either drug or vehicle control when embryos reached 12hpf or approximately 3-somite stage. For 5'-FUrd rescue, treatment media contained 5'-FUrd, 5μM uridine, and 0.2% DMSO, whereas vehicle control media contained 5μM uridine and 0.2% DMSO. Embryos were kept in drug media until fixation in 4% formaldehyde at 36hpf.

7.3.5. Immunohistochemistry

For visualization of muscle fibers, whole embryos were fixed at 36hpf as described above, permeabilized with acetone for 3.5 minutes, and incubated in Alexafluor-555 phalloidin for 1 hour. Embryos were subsequently mounted on slides using 1.5% low-melting point agarose and imaged on a Zeiss LSM 700 confocal laser microscope with Zen 2010 software (Carl Zeiss Imaging).

For immunohistochemistry on embryos injected with SOD1 and HA-TDP43 mRNA products, embryos were fixed at 30hpf and cryopreserved as previously described (DuVal et al., 2014a) using step-wise sucrose/0.1M PO_4 washes and freezing in sucrose/0.1M PO_4 mixed with Clear Frozen Section Compound (VWR, 95057-838) overnight at -80°C. 10μm cryosections were mounted on Superfrost Plus microscope slides (Fisher Scientific, 12-550-15), allowed to air-dry, and frozen at -80°C overnight. Slides were then thawed,

blocked in 10% normal goat serum/PBSTw, and incubated in primary antibodies overnight: 1:500 rabbit αSOD1-100 (Enzo Life Sciences, ADI-SOD-100) and 1:100 mouse αHA (Abcam, ab130275). After washes with PBSTw, slides were incubated in Alexafluor 488 anti-rabbit and Alexafluor 647 anti-mouse antibodies overnight. Following final washes, slides were imaged on a Zeiss LSM 700 scanning confocal microscope with Zen 2010 software (Carl Zeiss Imaging).

7.4. Results

7.4.1. SOD1 and TDP43 cause motor axon pathology via tryptophan residues

Primary motor axons were assessed for abnormal morphology in embryos injected with *SOD1* and/or *TDP43* mRNA; in normal development, primary axons extend from the spinal cord, past the notochord to innervate the trunk muscles. These axons rarely show branching above the ventral notochord boundary at 34-36hpf, and abnormal axon development includes branching above this boundary (Fig. 7.1A, A'). Abnormal branching may disrupt muscle fiber patterning as well (Fig. 7.1A'). Expression of *SOD1* and *TDP43* mRNA in injected embryos was confirmed using immunohistochemistry against SOD1 and the HA tag in TDP43 constructs (Fig. 7.1B). Overexpression of human wildtype SOD1 caused elevated axonopathy in zebrafish embryos, and expression of human wildtype TDP43 increased axonopathy to a similar degree (Fig. 7.1C), as was previously found (Kabashi et al., 2010).

Axonopathy increased further with co-expression of $SOD1^{WT}$ and $TDP43^{WT}$ (Fig. 7.1C), which supports our hypothesis that TDP43 can induce (or increase) SOD1 toxicity. We also co-expressed SOD1 with the $TDP43^{\Delta NLS}$ variant, which has a disrupted nuclear localization sequence. This modified TDP43 variant was observed to be mislocalized to the cytosol in HEK293 cells (unpublished), and based on previous models we expected that this mislocalization (Barmada et al., 2010; Igaz et al., 2011a; Ritson et al., 2010) would increase opportunities for TDP43 to enhance SOD1 toxicity. However the resultant axonopathy was not as dramatic compared to expression of [$SOD1^{WT}$ and $TDP43^{WT}$]. Next, to test their requirement in SOD1-TDP43 interaction, we substituted tryptophans for

serines in SOD1 and TDP43. Substitution of the W32 residue in SOD1 (W32S) effectively rescued SOD1-TDP43^{WT} induced axonopathy (Fig. 7.1C). Complete tryptophan substitution in the TDP43$^{\Delta NLS}$ variant (TDP43$^{\Delta NLS\ Trpless}$- all tryptophans switched to serines) lead to mild reductions in axonopathy (Fig. 7.1C). Alongside aggregation assays in cell culture (unpublished), we used our *in vivo* motor neuron axonopathy assay to test which pairs among the 6 tryptophans in TDP43 are most requisite for enhancing toxicity. mRNA of either TDP43$^{W68S/W113S}$ or TDP43$^{W68S/W172S}$ was co-injected with SOD1^{WT}, as these combinations of tryptophan substitutions had shown the most impact in cell culture. Mutation of W68 and W113 showed a mild but significant reduction in axonopathy compared to SOD1^{WT} + TDP43^{WT} expression, but mutation of W68 and W172 showed greater ablation of synergy (Fig. 7.1C). Thus TDP43 can enhance SOD1 pathology in zebrafish motor neurons, and W32 in SOD1 and two tryptophans in TDP43 appear to play pivotal roles in enhancing toxicity.

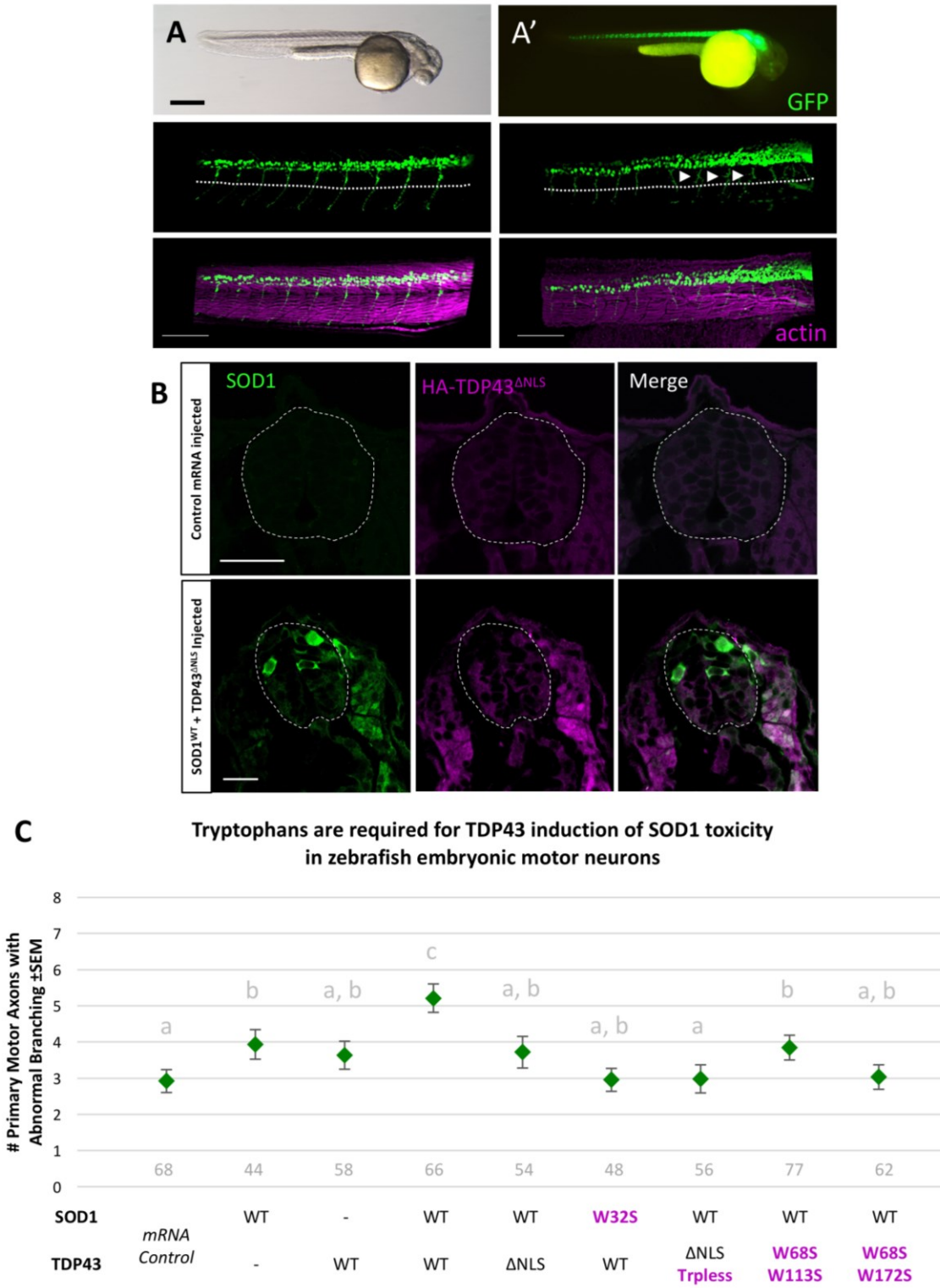

Figure 7.1. SOD1 and TDP43 synergy in axon toxicity is mediated through tryptophans.

A. A *Tg(mnx1:GFP)* embryo (36 hours post-fertilization) with GFP in the motor neurons. Abnormal primary axons (arrowheads) have proximal branches located above the ventral boundary of the notocord (dashed line), a metric of axonopathy. Muscle actin stained in magenta, showing disrupted fiber patterns where significant axonopathy occurs. Scale bars 0.5mm (A, A′), and 200μm (fluorescent images). **B.** Sections of 30hpf zebrafish spinal cords and adjacent muscle immunolabeled for $SOD1^{WT}$ and HA-$TDP43^{\Delta NLS}$. Spinal cords outlined with white dashed lines. Scale bars 20μm. **C.** Tryptophans W32 in SOD1 and W68, W113, and W172 in TDP43 are the primary relevant residues for induction of SOD1 misfolding and toxicity. Individually, injection of SOD1 or TDP43 mRNA causes axonopathy above control mRNA levels, but combined injection causes significantly more axonopathy above individual levels. Substitution of tryptophan W32 for serine in SOD1 (W32S) or of all 6 tryptophans in TDP43 ("ΔNLS-Trpless") is sufficient to rescue axonopathy in co-expression experiments. Changing tryptophans 68 and 113 (W68S/W113S) lead to mild rescue compared to [$SOD1^{WT}$ + $TDP43^{WT}$] injections, but not compared to [$SOD1^{WT}$ + $TDP43^{\Delta NLS}$] injections. However changing tryptophans 68 and 172 (W68S/W172S) reduced axonopathy more, showing similar rescue efficacy in co-expression as $TDP43^{\Delta NLS\text{-}Trpless}$, suggesting that W68 and W172 in TDP43 are critical for inducing SOD1 toxicity. Data points with shared grey letters are not significantly different (significance $p<0.05$, Kruskall-Wallis ANOVA with Mann-Whitney pairwise comparisons). Embryo sample sizes noted below data points.

7.4.2. 5'-fluorouridine rescues SOD1-TDP43 motor axon pathology

5'-fluorouridine (5'-FUrd) was able to reduce SOD1^{G93A}-AcGFP misfolding in cells transfected with SOD1 and TDP43 (unpublished), so we tested its capacity to rescue SOD1-TDP43-induced axonopathy in zebrafish. A low dose of 1.5µM 5'-FUrd rescued the axonopathy phenotype significantly in [SOD1^{WT}; TDP43^{WT}]- injected embryos and in [SOD1^{WT}; TDP43$^{\Delta NLS}$]- embryos (Fig. 7.2). However the dose profile of 5'-FUrd is a reminder to pursue candidate compounds with caution: while doses of up to 5µM 5'-FUrd did not significantly affect embryos survival over the first 24 hours of life (drug applied at 12hpf), primary motor axon defects (abnormal branching) may accumulate at higher doses in un-injected embryos (Appendix 6, Fig. A6.1).

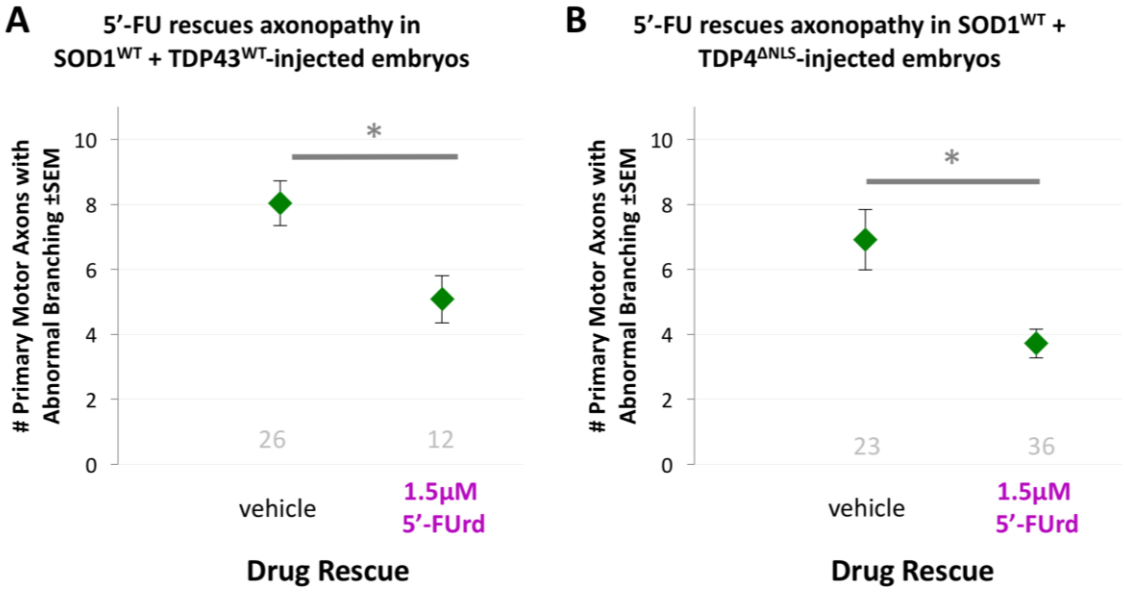

Figure 7.2. Zebrafish embryonic motor neuron axonopathy caused by SOD1-TDP-43 can be rescued with 5-fluorouridine.

A. Axonopathy in SOD1-TDP43 injected embryos can be partially but significantly rescued with a low dose of 5'-fluorouridine (5'-FUrd). **B.** A significant reduction is also observed with 5'-FUrd in SOD1 + TDP43^{dNLS}-injected embryos. * $p<0.05$ (Mann-Whitney pairwise comparisons); embryo sample sizes noted below each graph.

7.5. Discussion

In current research, SOD1 and TDP43 are heavily interrogated for their roles in ALS pathology, both in mutant and in wildtype forms. The majority of ALS cases does not have a genetic or heritable component, and there are few mechanistic links between ALS genes, which limits the scope of our understanding. Some of the few examples include: Ataxin 2 (ATXN2), which interacts with TDP43 in normal function and, upon accumulation of over 32 CAG repeats, induces TDP43 mislocalization and aggregation (Lagier-Tourenne and Cleveland, 2010); association between C9ORF72 hexanucleotide repeat expansions and TDP43 aggregation and mislocalization leading to neuron death, with suspicion that C9ORF72 with expanded repeats triggers TDP43 (Chew et al., 2015; Todd and Petrucelli, 2016); and genetic interactions and shared RNA processing complexes between TDP43 and FUS/TLS, though this last example has not yielded clear pathological interactions (Baloh, 2012a; Farrawell et al., 2015a; Kabashi et al., 2011; Lanson et al., 2011; Ling et al., 2010a; Wang et al., 2011). SOD1 and TDP43 are two prominent genetic lesions in fALS, with common features such as protein aggregation (Bidhendi et al., 2016; Farrawell et al., 2015a; Grad et al., 2015; Nonaka et al., 2013) and mitochondrial disruptions (Cozzolino et al., 2009; De Vos et al., 2007; Pickles et al., 2016; Wang et al., 2016; Wong et al., 1995). ALS-associated TDP43 mutations lead to cytosolic mislocalization (Armstrong and Cairns, 2011; Barmada et al., 2010; Pokrishevsky et al., 2012a; Woerner et al., 2016), increasing the probability of interaction between the two proteins. To date, however, investigations have yielded little genetic interaction between SOD1 and TDP43, such as failure of SOD1 mRNA to rescue TDP43 knockdown- or mutant-induced axonopathy in zebrafish (Farrawell et al., 2015b; Furukawa et al., 2011; Kabashi et al., 2011; Kabashi et al., 2010; Laird et al., 2010; Wang et al., 2016). From these studies we understand that SOD1 cannot replace TDP43 function or otherwise restore regulatory pathways that TDP43 participates in. It is also known that TDP43 protein, especially in mutant form, aggregates and can cause pathology without the presence of SOD1 mutations.

Our findings are in concordance with previous literature, however with the novel addition of a synergy between SOD1 and TDP43, and a molecular pathway that contributes to intermolecular induction of SOD1 misfolding: tryptophan residues. In this work, we present a link between the two proteins that elaborates the network of ALS pathology: SOD1 and TDP43 participate in a complex interaction wherein misfolding of either SOD1 or TDP43 can cause cell toxicity, but SOD1 misfolding and toxicity can be amplified upon interaction with TDP43. The implications of this interaction comprise several exciting avenues for further investigation, including the roles of tryptophan residues in promoting aggregation of SOD1, TDP43, and in intermolecular interactions between the two, as well as a novel link between pathologies in fALS with SOD1 mutations and ALS where no *SOD1* mutations are found. For example, while some studies have found sporadic ALS (sALS) patient samples that yield SOD1 aggregates (Gruzman et al., 2007), whether misfolded SOD1 is a hallmark of all ALS is yet to be settled (Brotherton et al., 2012). Nonetheless, evidence exists for SOD1 misfolding without mutation, and in such a scenario, the de-stabilization and misfolding of SOD1, a protein renowned for its stability (Lepock et al., 1990; Malinowski and Fridovich, 1979; Stathopulos et al., 2003; Weser et al., 1989), would demand catalysis by one or more external factors. Cytosolic translocation of TDP43 (Moisse et al., 2009; Wang et al., 2008a; Wang et al., 2016; Zhang et al., 2007) is suspected to provoke a toxic gain of function- herein we propose that this gain of function includes inducing SOD1 to acquire toxic capability. Like prion disease and other prion-like neurodegenerative diseases, misfolding of SOD1 is proposed to be induced through several mechanisms (Mulligan and Chakrabartty, 2013), including mutation (Alemasov et al., 2017; Broom et al., 2015; Shi et al., 2016a), templated misfolding (Ayers et al., 2016b; Chia et al., 2010; Munch et al., 2011; Silverman et al., 2016), demetallation (Ip et al., 2011; Sirangelo and Iannuzzi, 2017), oxidative damage (Mulligan et al., 2012; Taylor et al., 2007), and influence from other proteins such as TDP43 and FUS (Pokrishevsky et al., 2016; Pokrishevsky et al., 2012a). The relevance of the identified set of tryptophan residues to the development of SOD1 and TDP43 toxicity at the whole organism level is an especially compelling avenue for further exploration, including targeted pharmacological intervention to reduce SOD1 aggregation as demonstrated with a candidate small molecule, 5’-FUrd.

We selected 5'-fluorouridine (5'-FUrd), a candidate drug predicted to interact with the W32-containing pocket of SOD1 protein (Wright et al., 2013), to further test the interaction between SOD1 and TDP43 by attempting to block it. 5'-FUrd successfully reduced SOD1 aggregation in cell culture (unpublished) and motor neuron toxicity in a vertebrate model, making it an attractive candidate for further testing as a powerful therapeutic for ALS with SOD1 mutation and possibly non-SOD1 ALS. Drug therapy may be preferable over other approaches like silencing expression of SOD1 and TDP43, as knock out and knock down models also show neuron dysfunction (Fischer et al., 2012; Ivannikov and Van Remmen, 2015; Kabashi et al., 2010; Muller et al., 2006; Shi et al., 2014). We established an *in vivo* assay to test for candidate drugs that decrease SOD1 aggregation and toxicity. This model is cost effective and amenable to high-throughput screening for ALS therapeutics. However the efficacy of 5'-FUrd to rescue axonopathy in zebrafish motor neurons is limited to a low dose, with higher doses showing lack of rescue, and even some additional effects, on axonopathy rates in both injected and un-injected embryos (Appendix 6, Fig. A6.1). These findings also highlight the importance of monitoring for independent effects, including pharmacological effects, of candidate therapeutic compounds on both healthy and disease models, and the phenotypes measured therein.

There are few mechanistic links that unify the motor neuron degeneration seen in fALS and sALS, and so a possible link between two of the most prominent genetic factors, SOD1 and TDP43, is a new and encouraging avenue. Knowing how such factors interact and intersect may provide new revelations in ALS motor neuron pathology such as RNA processing, inclusion formation, and axon transport. Therapeutic strategies can then be focused on critical nodes that may be revealed by these interactions, such as W32, a seemingly "vulnerable spot" on SOD1.

Chapter 8. Conclusions & Future Directions

This chapter includes content (with some modifications) from the following publication:

Allison WT, DuVal MG, Nguyen-Phuoc K, Leighton PLA (2017) Reduced Abundance and Subverted Functions of Proteins in Prion-Like Diseases: Gained Functions Fascinate but Lost Functions Affect Aetiology. Int J Mol Sci. 2017 18(10) pii:E2223. doi: 10.3390.ijms18102223 (Allison et al., 2017). Manuscript writing was performed primarily by WTA with contributions from MGD, KNP, and PLAL.

8.1. Summary of findings and remaining gaps in the photoreceptor development network

In this thesis the effects and interplay of three factors, *gdf6a*, *tbx2b*, and *thrβ*, on cone subtype development were explored. In Chapter 2, *gdf6a* was identified as a novel regulator of blue cone abundance, and also of red cone abundance in Chapter 3. The role of *tbx2b* in promoting UV cones was found to be influenced by *gdf6a*, such that photoreceptor precursors become more vulnerable to reduced *tbx2b* levels when *gdf6a* is lost. In Chapter 3, the cone development network is further elaborated with *thrβ* and its intersections with *gdf6a* and *tbx2b*. To study *thrβ*, we employed both morpholino knock-down and dominant negative models. *Thrβ* was determined to have a dynamic role in zebrafish cone development, promoting red cones during early retinal development, inhibiting UV cones throughout, and limiting blue cones late in retinal development. *Thrβ* and *tbx2b* were discovered to act in a shared pathway in UV cone fate, where the suppressing actions of *thrβ* are downstream of the positive actions of *tbx2b*, enabling knockdown of *thrβ* to partially rescue UV cones in *tbx2b* mutants. The relationships between *gdf6a* and *thrβ*, however, were not as obvious from combined disruption experiments. Despite their matching positive influences on red cones and opposite influences on blue cones, combined *gdf6a*/*thrβ* disruption caused a reduction or total loss of both cone subtypes, leaving UV cone abundances intact. An additional unanticipated

lamination phenotype in *gdf6a*$^{s327/s327}$; *thrβ* morphant retinas revealed another potential intersection in retinal development.

8.1.1. Cone subtype precursor populations

As the list of cone differentiation factors grows, there is mounting evidence that the four cone subtypes in zebrafish are derived from separate precursor populations. Some factors like *tbx2b* function in the production of only one cone subtype, whereas others act on multiple subtypes. However the cone subtypes no longer share matching lists of regulatory factors (or matching responses to the same factors). These differences point to unique precursor populations and may suggest shared progenitors between types, akin to the shared precursor between red cones and some horizontal cells (Suzuki et al., 2013a). Bipolar cells, horizontal cells, and amacrine cells share lineages with photoreceptors in mice and zebrafish, with *Prdm1* inhibiting bipolar cell fate in favour of photoreceptors (mice) (Brzezinski et al., 2010; Brzezinski et al., 2013; Katoh et al., 2010) and *ptf1a* directing *atoh7*+ progenitors away from photoreceptor toward horizontal or amacrine cell fate (zebrafish) (Jusuf et al., 2011; Poggi et al., 2005). The diversity of horizontal and amacrine cell subtypes, of which our understanding is limited but growing in terms of subtype development (Boije et al., 2016; Kay et al., 2011; Wassle et al., 2009), leaves open the possibility of other shared lineages between photoreceptor subtypes and subtypes of these interneurons in addition to that between red cones and some horizontal cells. If this hypothesis were true, the *gdf6a* and *tbx2b* zebrafish mutants may have additional phenotypes among horizontal or amacrine cell subtypes in addition to reduced cone subtypes. *Gdf6a* and/or *tbx2b* may be acting at the base of these lineages, where they may promote both cone photoreceptor subtype and horizontal/amacrine cell fate (in which case the mutants could have a paucity of both). Alternatively, *gdf6a* and/or *tbx2b* could be “fate-switching” factors that promote the cone photoreceptor subtype instead of the horizontal/amacrine cell fate (in which case the mutants could have an excess of horizontal or amacrine cell types). As discussed below, the *gdf6a* mutant retinas have a host of phenotypes that complicate this picture, and this hypothesized role in the

photoreceptor lineage would have to be reconciled with *gdf6a*'s other observed roles in proliferation, progenitor survival, and differentiation.

8.1.2. Green-sensitive cones and rods

For technical reasons, green cones were the only cone subtype not studied in the *gdf6a* and *tbx2b* mutants, nor in *thrβ* disruption models. Only one gene required for green cone development has been identified: *six7* is required for green cone survival in the zebrafish retina (Ogawa et al., 2015). Whether and how this transcription factor intersects with the other factors (*gdf6a*, *tbx2b*, *thrβ*) is yet to be determined. Compound mutants of *gdf6a*, *tbx2b*, and *six7* could be created (as each gene is located on a separate chromosome) to test for genetic interactions, and a transgenic reporter of one of the four green opsins, *Tg(-2.1opn1mw1:eGFP)*^{pt112}, could be used to detect and measure green cones (Zou et al., 2012; Zou et al., 2010). Unfortunately this transgenic line is not available in Canada and currently zebrafish cannot be imported due to import restrictions, which is crippling the Canadian zebrafish research community (Hanwell et al., 2016). The *Rh2* (often also called *MWS*) cone opsin, the typical gnathostome middle wave-sensitive opsin, has been lost in mammals (Collin et al., 2009; Collin et al., 2003; Collin and Trezise, 2004). This opsin is most homologous to the gnathostome rod opsin *Rh1*, and phylogenetic analysis suggests that *Rh1* emerged from a duplication of the *Rh2* gene (Collin et al., 2003). Nonetheless no evidence to date suggests that a shared opsin evolutionary lineage translates into a shared developmental precursor between green cones and rods (Raymond et al., 1993b; Sotolongo-Lopez et al., 2016). Zebrafish green cones occur in double cone formations with red cones (Nawrocki et al., 1985; Robinson et al., 1995), so their development may be more akin to red cones, however to the author's knowledge there is very limited published work to assert this beyond close timing of their appearance in the retina in chick (Bruhn and Cepko, 1996) and zebrafish (Larison and Bremiller, 1990; Stenkamp et al., 1997).

The position of rods in the photoreceptor developmental lineage was initially proposed to be near the base, with mouse *Nrl* distinguishing rods from a cone "default" fate. Over the course of the thesis program investigations into zebrafish rod development

we performed by a colleague, A. Phil Oel. He found that expression of *nrl* in post-mitotic UV cones is sufficient to induce rod characteristics, which reveals a surprising degree of plasticity in at least one photoreceptor type. This capacity of *nrl* may be greater than the capacity of *thrβ*, which cannot change cone identity beyond early stages of photoreceptor development ((Suzuki et al., 2013a) and Chapter 3). CRISPR/Cas9-based knock-out of the zebrafish endogenous *nrl* gene revealed that zebrafish *nrl* has similar functions to mammalian *Nrl* (Mears et al., 2001; Mitton et al., 2000a): it is required for rod development in larvae. The lack of rods in larval *nrl* mutants was accompanied by an equivalent increase of UV cone abundance (but not blue or red cones), matching the increased S-cone abundance in mouse *Nrl* knockouts. At the time of writing, this work was in preparation for submission.

Are S-cones and UV cones a "default state"? The studies of *Nrl* in mice (Mears et al., 2001; Ng et al., 2011) and the work in zebrafish *nrl* by A. Phil Oel above could be interpreted this way. This is the assumed identity when *Nrl* and *nrl* are lacking, and it is plastic, changing its characters with ectopic *nrl* or *thrβ* expression (though green cones also appear to respond to ectopic *thrβ* by expressing red opsin (Suzuki et al., 2013a)). In terms of embryonic photoreceptor development, timing of identity assumption is important to consider as well- UV cone opsin mRNA is among the last to appear (Stenkamp et al., 1997) and so we speculate that UV cone precursors may remain uncommitted or otherwise plastic the longest, allowing for "co-opting" by ectopic factors.

8.1.3. Dorsoventral Patterning and Differentiation

In *Drosophila*, mice, zebrafish, and chick, dorsoventral patterning is a prominent feature in retinal development. Several of the major factors in cone subtype differentiation and opsin expression are subject to dorsoventral gradients of expression and/or availability in the retina, for example: *Wingless* (*Drosophila*) (Legent and Treisman, 2008; Tomlinson, 2003), *gdf6a* and other BMPs and their downstream targets (zebrafish and mice) (Gosse and Baier, 2009; Koshiba-Takeuchi et al., 2000; Murali et al., 2005); retinoic acid and its receptors (zebrafish (Hyatt et al., 1996; Mitchell et al., 2015a; Perz-Edwards et al., 2001; Prabhudesai et al., 2005; Stevens et al., 2011), mouse (McCaffery et al.,

1999; McCaffrery et al., 1993), and chick (Mey et al., 1997; Nicotra et al., 1994; Stenkamp et al., 1993)); and thyroid signalling genes and receptors (zebrafish (Bagci et al., 2015; Guo et al., 2014; Suzuki et al., 2013a; Thisse et al., 2003), mouse (Corbo et al., 2007; Ng et al., 2010; Roberts et al., 2006), and chick (Trimarchi et al., 2008)) (Viets et al., 2016). These patterns create appropriate conditions at relevant developmental stages for proliferation, cell cycle exit, and differentiation. Based on opsin expression, zebrafish photoreceptors are first detected in the ventral retina, then appear in a spatial sequence at the nasal, dorsal, and finally temporal retina (Easter and Malicki, 2002; Raymond and Barthel, 2004; Raymond et al., 1995b). Rods are also first detected in the ventral retina, thus the conditions at the ventral retina are critical during early stages of photoreceptor differentiation. However in later stages such conditions may be detrimental for some cone subtypes, (e.g retinoic acid signaling (Stevens et al., 2011)). In *gdf6a* mutants the ventral retina is expanded (French et al., 2009; Gosse and Baier, 2009) and blue and red cones are reduced, and excess RA exposure in wildtype embryos favours rods and reduces red cones (Stevens et al., 2011), thus it's plausible that expanded expression of RA genes contributes to the reduction of cones in *gdf6a* mutants. Interestingly, the UV cones are spared in *gdf6a* mutants. Based on these and other observations discussed in Chapter 3, UV cones are not affected like other subtypes, and their progenitors may therefore be unique.

Evidence of negative regulation of UV cone abundance and opsin expression in rainbow trout (Allison et al., 2006a; Hawryshyn, 2003; Raine et al., 2010; Veldhoen et al., 2006), the observed excess S-cone and UV cone phenotypes in both mouse *Thrβ* knockouts (Ng et al., 2001a; Ng et al., 2011; Pessoa et al., 2008) and zebrafish *thrβ* disruption models, along with preliminary evidence for excess *thrβ* expression in *tbx2b* mutants (which have few UV cones) (Appendix 2, Fig. A2.6), strongly indicate that Thrβ actively limits abundance of UV cones and their orthologues. Availability of active thyroid hormone appears to be spatially regulated. For example, in the early chick retina (before the appearance of photoreceptor precursors), *Dio2* expression (activating thyroid hormone or TH) is highest in the ventral retina and lowest in the center, and *Dio3* expression (inactivating TH) is highest across the midline (Trimarchi et al., 2008). To our knowledge, such a detailed examination of the spatial expression of deiodinases or

thyroid hormone receptors in the zebrafish retina has not been published to date, but this knowledge may provide insight into UV cone differentiation and the novel UV phenotype discussed next.

The partial rescue of UV cones in *tbx2b*$^{fby/fby}$; *thrβ* morphant zebrafish mirrors the pattern of rod appearance: UV cones were most concentrated at the retina midline, suggestive of additional necessary conditions in that area for UV cones to differentiate and/or survive. The opposite pattern is typical of larval zebrafish rods, in which rods appear in a dense patch in the ventral retina, with a second patch in the far dorsal retina, and the lowest density at the midline. The underlying mechanism for the UV cone phenotype at midline may therefore be also linked to a mechanism that also regulates the embryonic distribution of rods. Whether the conditions at midline that are favourable to UV cones occur independently of *thrβ* knockdown, or as a result thereof, is unclear. A similar midline localization of UV cones has been observed in *tbx2b*$^{lor/lor}$ mutants, which have a less severe phenotype and may retain some *tbx2b* expression (Raymond et al., 2014).

One hypothetical mechanism is that UV cones are influenced by a well-known mediator of rod development: retinoic acid (RA) signaling (Prabhudesai et al., 2005; Stevens et al., 2011). For example, early experiments of excess retinoic acid exposure measured reduced cone and increased rod abundances (Hyatt et al., 1996; Prabhudesai et al., 2005); this may be mediated through *RARαb* which is expressed in the ventral retina and is positively associated with rod fate (Stevens et al., 2011). Towards the retina midline, expression of *RAR□b* may reach low enough levels to allow production of some UV cones (though this would not explain the lack of UV cones in the dorsal retina). Or retinoid X receptors, which also respond to RA signaling, may bind different gene targets as homodimers compared to as heterodimers with Thrβ. Upon *thrβ* knock down, a decrease in heterodimers may disinhibit UV cone identity. But there are some points to counter RA involvement in UV cone specification: follow-up work on the effects of RA signaling on photoreceptors shows positive regulation of rod fate, largely at the expense of red cones, and not as much UV or blue cones (Hyatt et al., 1996; Mitchell et al., 2015a; Stevens et al., 2011). In *gdf6a* mutants the ventral retina and thus expression of RA receptors are expanded, yet UV cone abundance remains stable unless an additional

insult (i.e. reduction in *tbx2b*) is present. Cell non-autonomous mechanisms may not be involved at all; when *tbx2b*$^{lor/lor}$ donor cells were transplanted into a wildtype retina, the donor cells rarely assumed a UV cone fate, suggesting that external factors are unlikely to rescue the phenotype (Alvarez-Delfin et al., 2009). Alternative (but non-exclusive) hypotheses include partial compensation or functional redundancy by similar genes, such as *tbx2a* (Thisse et al., 2004), *tbx5a*, or *tbx5b* (Albalat et al., 2010), or that an optimal balance of multiple factors exists only at the midline. For example, *thrβ* knockdown may lead to disinhibition of key genes, or levels of BMP signaling factors or their downstream genes may be sufficient at the midline to stochastically overcome *tbx2b* loss of function and promote UV cone identity. Interestingly, the spacing between UV cones in *tbx2b*$^{fby/fby}$; *thrβ* morphants, or between rods in wildtypes, appear otherwise random. Thus a stochastic influence, such as a mix of signaling factors, may be at play for both.

To rule out one or more of these regulatory mechanisms, the patterns of deiodinases, BMP receptors and retinoic acid signaling receptors, as well as candidate redundant genes for *tbx2b*, could be examined in wildtype, *tbx2b*$^{fby/fby}$, and *tbx2b*$^{fby/fby}$; *thrβ* morphant retinas to determine if 1) any change in deiodinase, BMP signaling or retinoic acid signaling may contribute to the *lots-of-rods* phenotype, and 2) if knockdown of *thrβ* alters expression of any of these genes in the mutants, specifically at the midline. Changes to expression of any of these genes would propose novel and exciting possible gene targets for *thrβ*. If RA signaling is changed in *tbx2b*$^{fby/fby}$ mutants, knockdown of RA receptors or pharmacological inhibition of retinoic acid may partially rescue the phenotype as well (it would then be curious to consider if blocking the effects of RA signaling in *gdf6a* mutants would rescue blue and red cone abundances). However work performed by colleagues suggests this prediction is too simple, as reduction in RA synthesis genes actually resulted in reduced UV and blue cone abundances, suggesting that a minimum level of RA and/or appropriate timing of RA signaling is needed for photoreceptors (Cheng, 2016). The tight regulation of RA levels that is apparently required for correct photoreceptor type abundances may further point to an element of stochasticity, at least in UV cone generation.

8.1.4. Early actions of gdf6a signaling may have downstream effects including cone subtype abundances

The zebrafish *gdf6a* mutants are complex, with multiple retinal phenotypes including microphthalmia, coloboma, reduced proliferation, increased apoptosis, and accelerated differentiation (Asai-Coakwell et al., 2013; French et al., 2009; French et al., 2013; Valdivia et al., 2016). RNA microarray data from *gdf6a* mutants showed downregulation of genes involved in proliferation (*mcm3*, *mycn*, *myca*, *pcna*, *uhrf1*, *cad*), retinal ganglion cell (*atoh7*), horizontal and amacrine cell (*foxn4*), photoreceptor (*rx1*, *fpgs*), and cone (*ndrg1b*, *tbx2b*) development. Genes for retinoic acid synthesis (*crabp1b*, *aldh1a3*) and a regulator of cell cycle progression (*cdc16*) were upregulated (French et al., 2013). It is not yet clear how these events contribute to disruption in blue and red cone subtype abundances, and why UV cone abundances appear unaffected. As dorsoventral retina patterning is disrupted in *gdf6a* mutants, indicated by an enhanced area of ventral retina identity, the themes in the above section are relevant to discussion of *gdf6a*'s role in photoreceptor development. Hypotheses for how reduced proliferation, increased apoptosis, or accelerated differentiation may affect resulting cone abundances are discussed below. A summary figure of the general hypothesized effects of each is shown in Fig. 8.1.

Proliferation, in terms of number of mitotic cells and expression of proliferation genes, is reduced in *gdf6a* mutants (Valdivia et al., 2016). This phenotype appears to contribute significantly to the microphthalmic phenotype, as one attempt at rescue with an apoptosis inhibitor did not alter *gdf6a* mutants' eye size (French et al., 2013). Does this reduction in the rate of proliferation affect the outcomes of all retinal types equally? Only a small number of retinal neuron types have been examined, but skewed populations of *atoh7*-expressing cells and the cone subtypes examined here suggest the outcomes may be indeed disproportionate (Fig. 8.1A). Skewed populations may also be explained by the wave of increased apoptosis at 2dpf (den Hollander et al., 2010; French et al., 2013; Gosse and Baier, 2009), as we do not currently know whether this wave consists of specific retinal progenitor types (Fig. 8.1B). Determining whether proliferation, apoptosis, or a combination of the two are the causes of disturbed photoreceptor

abundances could be done with lineage tracing. By tracing retinal progenitors at different stages, the rates of proliferation and death among different progenitor populations can be tracked. For example, precursors of interest can be tracked using either fluorescent protein reporter lines or, where reporters are not available or expression of precursor genes is very transient, a Cre-lox lineage tracing system like that developed by Solek et al. (Solek et al., 2017), where restricted expression of Cre induces removal of floxed GFP to allow mCherry expression in cells of interest. Lineage tracing promoters that could be utilized in preliminary experiments include (but are not limited to) *pax6a* or *rx1* for tracing all retinal progenitors (Lakowski et al., 2007; Shen and Raymond, 2004b), *atoh7* for retinal ganglion cell precursors (GFP reporter line available) (Poggi et al., 2005; Willardsen et al., 2009), *vsx2* for bipolar cells and Müller glia (Vitorino et al., 2009) (reporter lines available) (Almeida et al., 2014; Batista et al., 2008; Engerer et al., 2017; Jusuf et al., 2011; Vitorino et al., 2009), *ptf1a* (horizontal cells and amacrine cells (reporter line available) (Boije et al., 2015; Jusuf et al., 2012; Weber et al., 2014), and *crx* for photoreceptors (Liu et al., 2001; Shen and Raymond, 2004b). This system, combined with markers to assess proliferation and apoptosis such as PCNA and caspase-3, would inform whether reduced proliferation and/or increased apoptosis is biased toward certain stages or precursor populations.

Accelerated differentiation early in retinal development may also skew final proportions of the 7 major retinal cell types. Because the retinal cell types follow a birth order (with overlap), accelerated differentiation without compensation to the progenitor pool would lead to a greater proportion of early-born types (Fig. 8.1C), which are typically the retinal ganglion cells, horizontal cells, and cone photoreceptors (Bassett and Wallace, 2012). Initial observations of a potential skew towards early-born cells have been published (Valdivia et al., 2016), but further evidence is required, such as early cell cycle exit or early appearance of key differentiation markers (with or without accompanying changes in proliferation or apoptosis). Markers for a diversity of lineages and cell types would be needed to ascertain if certain populations differentiate early upon *gdf6a* loss, such as the preliminary list above.

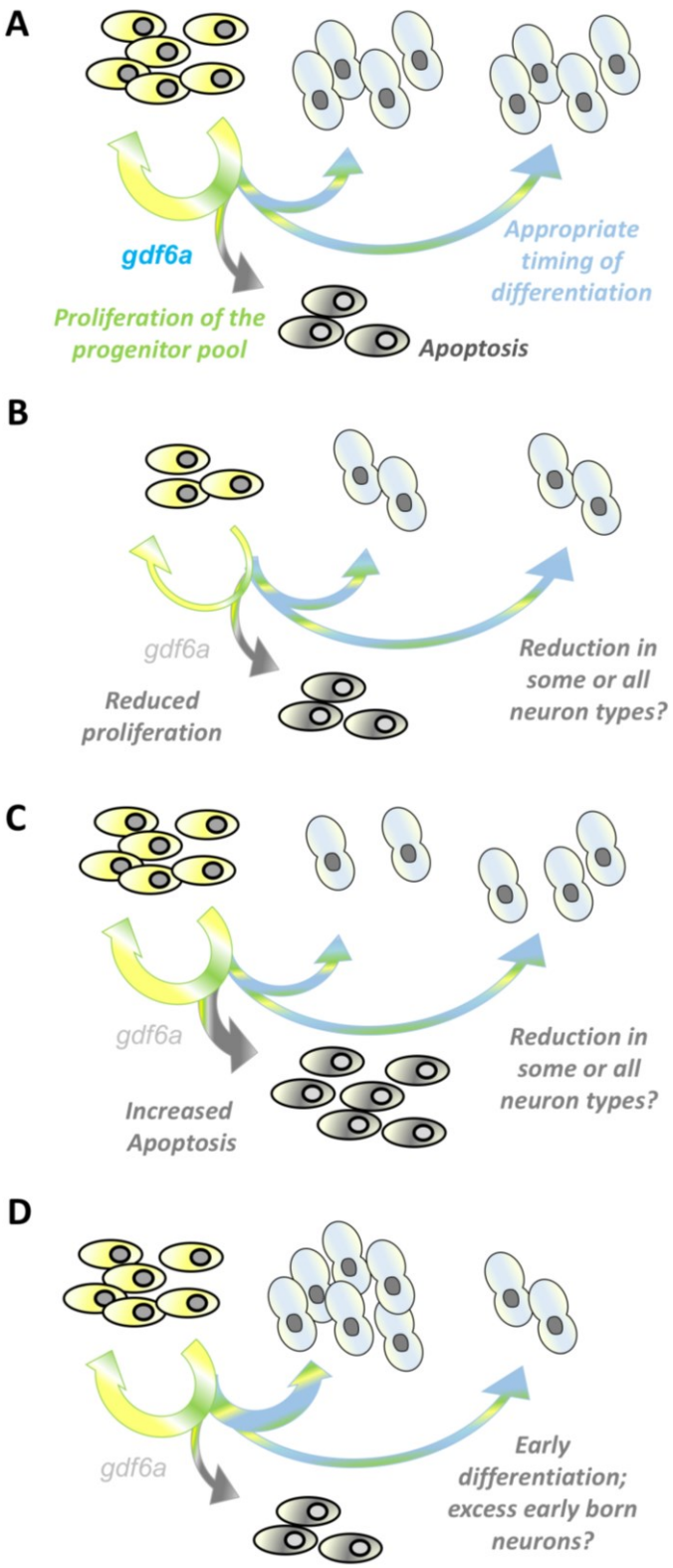

Figure 8.1. Proposed roles of *gdf6a* in maintenance of the retinal stem cell pool and differentiation.

A. The retinal progenitor pool (yellow cells) proliferates during retinal development. Differentiating cells (blue cells) exit the pool at different stages of development; for simplicity these differentiating cells are grouped into early (left) and late (right) differentiating populations, which will give rise to early and late born neurons respectively. Some apoptosis occurs as part of normal development (grey cells). Gdf6a signaling is thought to regulate proliferation and timing of differentiation, as loss of function results in reduced proliferation, increased apoptosis, and possibly accelerated differentiation. **B.** Possible consequences of a *gdf6a* loss-induced decrease in proliferation (thinned arrow) include fewer cells of all neural types, or a reduction in only some types. **C.** Likewise, increased apoptosis (thickened arrow) may affect some or all neural types. **D.** Early differentiation may result in excess early born neural types and fewer late born types, especially if proliferation of the progenitor pool does not compensate.

8.1.5. Conclusions

Humans depend on their vision for daily function, and fear losing this sense the most (Scott et al., 2016). At this time, vision loss due to retinal degeneration is irreversible, but emerging technologies have the potential to replace lost retinal cells via regeneration or implantation of stem cell-cultivated neurons. As photoreceptors (and cone photoreceptors in particular) are critical for light detection in humans, the success of these approaches is measured by the quantity and quality of photoreceptors generated, and subsequently the rate of survival, function, and connectivity of said photoreceptors in the recipient eye. Procuring a large number and diversity of photoreceptor types is not possible without a concerted expansion of our knowledge of cone development (Brzezinski and Reh, 2015;

Gamm et al., 2015). The first goals in this thesis have this purpose in mind: to identify factors that ensure cone subtype diversity, and to understand how they fit and interact in the regulatory network of cone differentiation. The cell extrinsic (e.g. *gdf6a* and BMP signaling) and cell intrinsic (e.g. transcription factors such as *tbx2b* and *thrβ*) factors can be used for screening and manipulating progenitor cells to maximize photoreceptor production, a strategy that can be applied to endogenous stem cell activation or the cultivation of exogenous stem cells.

The retina is an extension of the CNS and retinal degenerations share many of the same pathologies that are discussed below. For example, inflammation, oxidative stress, disrupted proteostasis, and build-up of misfolded proteins are common features in models of age-related macular degeneration (Ferrington et al., 2016; Gupta et al., 2016; Hernandez-Zimbron et al., 2018; Hyttinen et al., 2017; Kauppinen et al., 2016; Lenox et al., 2015; Salminen et al., 2010). While age-related macular degeneration is multigenic, there are also many monogenic retinal degenerations that can be explained by loss of function and/or gain of function (Tzekov et al., 2011). The context of the underlying degenerative disease will be important when replacing lost retinal neurons, especially where the underlying cause cannot be treated. Newly-implanted or regenerated photoreceptors may be become victims of ongoing disease processes, such as inflammation or toxic byproducts of apoptosis. Future work modeling implantation or regeneration in models of retinal degeneration could include co-treatments to minimize these possible insults, such as applying gene therapy (where suitable), immunomodulators, and/or pro-neural factors, in comparison to implantation or regeneration into degeneration models without these.

8.2. Summary of findings and finding new links in a complex neurodegeneration

In this thesis, the studies related to ALS motor neuron degeneration investigated a novel contributor to genetic susceptibility to motor neuron dysfunction, disease severity, and progression in aging, variability of toxicity and protein behaviour (Chapters 5, 6) and

interactions between known agents of pathology (Chapter 7). A novel modifier locus of neuromuscular junction health, *gdf6a*, was identified with the zebrafish null mutant *gdf6a*$^{s327/s327}$. Combining this mutation with a transgenic zebrafish model of SOD1-associated ALS, we found that *gdf6a* loss enhances motor neuron degeneration phenotypes with aging, including swim endurance, neuromuscular junction maintenance, and number of surviving motor neurons (Chapter 4). Subsequent work focused on the puzzling case of SOD1 mutations and their effects on SOD1 toxicity *in vivo*. Novel mutations identified by *in silico* modeling were tested *in vitro* and *in vivo*, and the intriguing results present new residues of interest towards understanding SOD1 protein stability. One such amino acid position is a promising therapeutic drug target (Chapters 5, 6). Finally, a possible interaction (initially described in cell culture) between SOD1 and TDP43 was tested in zebrafish. The co-expression of SOD1 and TDP43 enhanced the motor axon phenotype, but was rescued by substituting key tryptophans in both SOD1 and TDP43, thus the mechanism behind this enhanced toxicity may involve these tryptophans (Chapter 7).

8.2.1. The neurodegeneration spectrum

Despite the struggle to identify a unifying genetic, environmental, or other cause of ALS pathology, there are recurring themes in ALS and FTD (and other neurodegenerative diseases) (Block and Hong, 2005; Bossy-Wetzel et al., 2004; Haass and Selkoe, 2007; Halliwell, 2006; Hetz and Mollereau, 2014; Lagier-Tourenne et al., 2010; Lau and Tymianski, 2010; Lin and Beal, 2006; Radi et al., 2014; Ransohoff, 2016; Rubinsztein, 2006; Schreij et al., 2016) that insinuate a continuum of neuron pathology that manifests in numerous ways. Common pathologic mechanisms in seemingly disparate neurodegenerations (such as Alzheimer's, Parkinson's, Huntington's, ALS, FTD and others) suggest that, while the initial causes may be diverse and variable, many of them converge toward common neurologic dysfunctions shared across diseases. In other words, distinct neurodegenerative disease categories like Alzheimer's, Parkinson's, ALS, FTD, tauopathies, and others may not be so distinct. This has already been proposed for ALS and FTD, as they share many genetic links and are increasingly thought

as being on a spectrum. Common functions that are disrupted include DNA methylation, RNA processing, mitochondrial function, vesicle trafficking, immune response, and proteostasis. These cellular processes have incredible complexity in function and regulation, with a vast network of RNAs and proteins participating in the development, maintenance, and function of each. Thus disruption in any of a large number of genes may cause disruption or toxicity of varying severity and progression. As these processes are highly active in neurons, neurons are especially vulnerable to disturbances and are often the first to manifest disease.

8.2.2. Finding mechanistic links between genes in fALS

Extreme genetic heterogeneity, including a growing list of modifier loci, means ALS and other neurodegenerations don't arise from singular causes, but rather an accumulation of risk factors and susceptibilities (Renton et al., 2014). In this section, susceptibility will be discussed in terms of motor neurons' unique vulnerability to the gene mutations associated with ALS, despite many of these genes being expressed in multiple tissues and cell types. However susceptibility in terms of the specific genetic makeup and life history of each patient also contributes to the wide variation in disease onset, severity, and progression, but for the sake of length this will not be explored here. Nonetheless both of these aspects, in addition to many other issues, make modeling ALS and devising efficacious therapies extremely challenging. The considerations explored below may help to frame future questions and approaches to understanding ALS and other neurodegenerations.

Motor neuron diseases include ALS, primary lateral sclerosis, progressive muscular atrophy, hereditary spastic paraplegia, frontotemporal lobar degeneration, progressive bulbar palsy, and pseudobulbar palsy (Love et al., 2008). Because the motor neurons are most strongly (and sometimes the only system) affected, the causes of motor neuron disease likely underscore inherent vulnerabilities that are particularly heightened in the motor neurons compared to other neurons or cell types. Many of the genes affected in motor neuron disease are ubiquitously expressed, such as *SOD1*, *SMN1*, *TDP43*, *FUS*, *OPTN*, and *UBQLN2*, are strongly suspected to be ubiquitous (*C9ORF72*, *TBK1*), or are

highly expressed throughout the CNS (*ATXN2*) (2015). The functions of these proteins are also not unique to motor neurons: defects in RNA transcription and splicing, protein processing and degradation (e.g. proteasomal degradation of proteins including misfolded protein, autophagy), trafficking (e.g. endosomal trafficking, axonal transport), free radical clearance, cytoskeletal integrity, glial function, and neuromuscular junction maintenance and function (e.g. glutamate regulation) are all proposed mechanisms for motor neuron death (reviewed by Boillee et al. (Boillee et al., 2006) and Rothstein (Rothstein, 2009)). Motor neurons have high metabolic demands, producing and transporting cellular contents along some of the longest axons in the body, and depending upon a tremendous amount of mitochondrial, transcriptional, translational, and proteasomal activity. Hence the critical threshold of insults that will instigate dysfunction in motor neurons is probably much lower than for other cell types. It is therefore understood that multiple systems go awry, and increasing genetic evidence shows that accumulation of susceptibilities is more reflective of disease. Careful design of experiments to reflect these realities may give more fruitful results. For example, combining disease models may reveal novel genetic or other interactions that disrupt one or more cellular processes, which may not otherwise be obvious in each model alone.

The approximately 20 genes with mutations that are most common in fALS are the most promising starting points to search for intersections and other mechanistic links that could unify multiple proposed disease mechanisms. Therefore further work modeling multiple risk factors simultaneously is needed, along the lines of the genetic interactions found between *TDP43* and *FUS* (Baloh, 2012b; Farrawell et al., 2015b; Kabashi et al., 2011; Lanson et al., 2011; Ling et al., 2010b; Wang et al., 2011), *TDP43* and *ATXN2* (Lagier-Tourenne and Cleveland, 2010), our work examining *gdf6a* loss of function and *SOD1* mutant expression (Chapter 4), and SOD1 and TDP43 co-expression experiments (Chapter 7). Ideally, any mechanistic links revealed will point to cellular dysfunctions that are the most common and/or most destructive to motor neurons. In addition to targeting the instigating genetic defects (where known), prioritizing the most common and destructive downstream effects for intervention (Golde et al., 2013) could greatly enhance motor neuron survival and offer treatment options for patients without identified mutations.

Retinal degeneration and other neurodegenerations are linked, and presence of one can often be indicative of another. For example, detection of amyloid-β plaques in aging retinas is increasingly common (Alexandrov et al., 2011; Koronyo-Hamaoui et al., 2011; Tsai et al., 2014). Possible increased incidence of retinal thinning in ALS patients (Mukherjee et al., 2017), Huntington's patients (Kersten et al., 2015), Parkinson's patients (Satue et al., 2018; Satue et al., 2017), and extensive documentation of retinal changes in Alzheimer's (reviewed by Kusne et al. (Kusne et al., 2017)) suggest retinal involvement in numerous diseases. The retinal neurons are sensitive to oxidative stress and protein misfolding (Tzekov et al., 2011) just as is the rest of the CNS, but many, more subtle, disease modifiers in neurodegenerations may have additional roles in retinal development, survival, and function. In this thesis, the roles of *gdf6a* in photoreceptor development and neuromuscular junction maintenance present a novel link between retinal degeneration and motor neuron degeneration. Other links that have been found include retinal degeneration in spinocerebellar ataxia 7 (OMIM# 607640), caused by mutation in *ATXN7*, which was demonstrated to interact with and disrupt *Crx* in a mouse model (Chen et al., 2004; La Spada et al., 2001), and *OPTN* as a risk variant for glaucoma (Rezaie et al., 2002; Weishaupt et al., 2013) and as a rare cause of ALS (Del Bo et al., 2011; Iida et al., 2012; Li et al., 2015; Maruyama et al., 2010; van Blitterswijk et al., 2012). The multiple roles of developmental genes will become increasingly linked to age-related diseases such as neurodegeneration, and in the future retinal degenerations and other neurodegenerations will increasingly share disease loci.

8.2.3. Contribution of SOD1 loss of function to disease

Despite the lack of overt, ALS-like motor neuron phenotype in the *Sod1* knockout mouse (Reaume et al., 1996a), the role of SOD1 loss of function in ALS is an emerging topic of exploration in the literature. It is now understood that *Sod1* null mice are subject to increased oxidative stress and are more susceptible to neuron loss following axonal and ischemic brain injuries (Kondo et al., 1997; Reaume et al., 1996a), changes in neuromuscular junction structure and function (Ivannikov and Van Remmen, 2015), muscle oxidative stress and associated atrophy, and progressive distal motor neuron

degeneration associated with high oxidative stress (Fischer et al., 2012; Ivannikov and Van Remmen, 2015; Muller et al., 2006; Shi et al., 2014). Many but not all ALS patients show diminished SOD1 activity or increased oxidative stress, thus loss of function cannot fully account for disease. The considerably less intense phenotype of the *Sod1* knockout mouse compared to mutant SOD1 transgenic models shows that loss of function is not sufficient to kill motor neurons, but nonetheless it may be a significant contributor, as reduction or loss of SOD1 function could further weaken a neuron's ability to cope with stresses associated with misfolded protein accumulation (Petrov et al., 2016a; van Blitterswijk et al., 2011). Therapeutic approaches that risk reducing normally-folded SOD1 may thus have unwanted consequences.

Many changes found in neurons with misfolded SOD1 overlap with changes in SOD1 knockout neurons, including increased oxidative stress, risk of excitotoxicity, neuromuscular junction changes, denervation and muscle atrophy. A significant part of this overlap can be explained by the reduced oxidative activity of all misfolded SOD1 proteins measured to date (Boillee et al., 2006; Saccon et al., 2013; Turner and Talbot, 2008). While it is not clear if the abundance of normally-folded SOD1 decreases with disease course (as found with PrP^{C} in prion diseases (Llorens et al., 2016; Mays et al., 2014; Mays et al., 2015)), certainly the propagated misfolding of SOD1 to conformers with reduced function could explain a loss-of-function component in ALS pathology. Other processes in ALS including endoplasmic reticulum stress, mitochondrial dysfunction, oxidative damage, and apoptosis could conceivably result from either misfolded protein toxicity or SOD1 loss of function: the difficulty lies in determining the relative contribution of each toward pathologies. What is yet to be concluded is whether wildtype SOD1 is more likely to reduce aggregation and spread (Witan et al., 2009), or to become victim to conversion.

In light of the findings in SOD1 loss of function, some caveats should be considered when studying the role of SOD1 in ALS pathology. For example, regarding loss of function, SOD1 abundance or function may not be reduced in all cell types or in all cell compartments. It is also possible that only some cell types are susceptible to SOD1 loss-of-function-induced stress, i.e., disparate tissues and some classes of neurons. The

diversity of SOD1 mutations that occur in ALS may result in different misfolding kinetics and degrees of loss-of-function or toxic gain-of-function in each instance.

8.2.4. Screening and improving therapeutics against protein misfolding

The list of proteins that misfold and aggregate in neurodegeneration continues to grow. Aggregates of misfolded and ubiquitinated proteins may not be toxic to neurons, but rather the monomers and small oligomers of misfolded protein could be (Klein et al., 2001; Lambert et al., 1998; Lue et al., 1999; McLean et al., 1999; Walsh et al., 2002). These are attractive targets to stop toxicity at the source, and therapeutic approaches considered include gene editing (e.g. CRISPR/Cas9) or antisense oligonucleotide therapy (Touznik et al., 2017; van Roon-Mom et al., 2018) to correct or reduce expression of mutant proteins, antibodies against disease-specific epitopes (Urushitani, 2011), and drugs to stabilize proteins against misfolding (Wright et al., 2013). As discussed earlier, reducing overall protein expression may not be ideal if the subsequent reduction in function also proves detrimental, and delivery of oligonucleotides to neurons where they're needed currently faces numerous hurdles such as the need to screen for potential off-target effects (Fu et al., 2013) or limited capacity of viral vectors for delivery (Choi et al., 2016) (reviewed in (Kruminis-Kaszkiel et al., 2018)). Antibodies against disease-specific epitopes are attractive because they can be designed against epitopes common across many conformers and mutations, and natively folded protein would, in theory, be unaffected. But this approach cannot be effective until a misfolded protein load is present, and may increase inflammation, which contributes to neuron death. Stabilizing drugs, if designed or selected and tested carefully, can act before proteins misfold, would be effective on all natively-folded proteins, and would not decrease protein function. However drugs often have side effects, can interact with other medications (especially pertinent considering both neurodegeneration and pharmaceutical usage increase with age), and must be selected for blood-brain-barrier permeability.

Due to the high variability in mutations (and probably conformations) of misfolded SOD1 protein, a combination of approaches would be most effective. To effectively reduce the burden of misfolded SOD1 (or other protein), a combination of therapies to

target misfolded protein for degradation and to enhance proper protein folding or stabilization would likely be more effective than one alone. Validation of such strategies will require whole organism models of SOD1 (or other protein) misfolding, where rates of misfolding can be measured and ideally tracked over time to monitor progression. A mouse model expressing G85R-SOD1:YFP allows for detection of inclusions, misfolded protein, and even seeding (Ayers et al., 2016a; Ayers et al., 2014; Ayers et al., 2016b). But because the neural tissues are not visible (i.e. mice are not transparent), mice still must be sacrificed at defined time points for analysis. Zebrafish can serve as a complementary model with an additional advantage: thanks to a combination of mutations, including CRISPR/Cas9-induced, completely transparent fish lacking pigmentation in the skin and retinal pigment epithelium (Antinucci and Hindges, 2016) are available (in Canada too!). Generating transparent fish that transgenically express a SOD1 reporter, like G85R-SOD1:YFP in mice (Ayers et al., 2014) or the *in vitro* systems (Ayers et al., 2017), including that in Appendix 4, would enable longitudinal monitoring of SOD1 misfolding and inclusion formation in live fish. Importantly, the intact CNS of a mouse, fish, or other vertebrate model would provide the contexts needed for screening therapeutics: measurable outcomes of toxicity, a vascular system and blood-brain barrier, immune cells like glia and astrocytes, and fully differentiated and functional motor neurons innervating muscles.

SOD1 does not act alone in causing neuromuscular degeneration; as discussed above, likely an accumulation of genetic defects, misfolded proteins, inflammation, and/or other factors must occur. Importantly, these downstream processes are already causing motor neuron death by the time of diagnosis, so in all cases a therapeutic strategy based solely on prevention is not ideal. Hence therapies targeting the shared downstream pathologic consequences would be applicable to more cases (including sporadic cases of ALS) and can ameliorate ongoing disease in conjunction with a preventative therapy, such as protein stabilizing drugs. Some approaches to reducing pathologies include bolstering the proteostasis network (e.g. enhancing autophagy (Barmada et al., 2014; Crippa et al., 2010; Wang et al., 2012) or stimulating the heat shock response (Kieran et al., 2004)), ameliorating ER stress (e.g. repressing translation (Das et al., 2015; Vieira et al., 2015)), reducing apoptosis (Matus et al., 2013), and supplying neurotrophic factors

(Lewis and Suzuki, 2014). These are but a few areas that have been suggested for development of new therapies, and the many mechanistic and pathological overlaps between motor neuron disease and other neurodegenerations might result in future therapies against multiple degenerations.

8.2.5. Conclusions

The roles of prominent misfolded proteins, SOD1 and TDP43, in addition to the more subtle modifying gene, *gdf6a*, to motor neuron health were interrogated in this thesis. Motor neurons are subject to numerous genetic, physiological, and cellular forces that determine their health and function through development and across an organism's lifespan. The challenges that motor neurons face are not entirely unique but are nonetheless complex, with multiple misfolded proteins and a mix of gain and loss of function mechanisms that, especially for SOD1, are not fully understood. For ALS we currently face a hazy constellation of genetic features and disease mechanisms whose potential connections may be revealed through purposeful experiments. Why motor neurons are primarily affected in cases like ALS remains to be answered, but the numerous overlaps in pathological mechanism between ALS and other neurodegenerations (and along those lines, retinal degeneration and neurodegenerations) may translate into powerful therapies that combine strategies to target unique features such as mutations and their products and strategies to mitigate downstream dysfunctions.

Bibliography

2015. Interactive human protein atlas launches. Cancer Discov. 5**,** 339.

Abel, E. D., et al., 1999a. Divergent roles for thyroid hormone receptor beta isoforms in the endocrine axis and auditory system. Journal of Clinical Investigation. 104**,** 291-300.

Abel, E. D., et al., 1999b. Novel insight from transgenic mice into thyroid hormone resistance and the regulation of thyrotropin. Journal of Clinical Investigation. 103**,** 271-279.

Abel, O., et al., 2012. ALSoD: A user-friendly online bioinformatics tool for amyotrophic lateral sclerosis genetics. Hum Mutat. 33**,** 1345-51.

Aberle, H., et al., 2002. wishful thinking encodes a BMP type II receptor that regulates synaptic growth in Drosophila. Neuron. 33**,** 545-58.

Abrahams, A., et al., 2010. The T-box transcription factor Tbx2: its role in development and possible implication in cancer. IUBMB Life. 62**,** 92-102.

Acampora, D., et al., 1998. Murine Otx1 and Drosophila otd genes share conserved genetic functions required in invertebrate and vertebrate brain development. Development. 125**,** 1691-1702.

Acampora, D., et al., 2001. Otx genes in brain morphogenesis. Progress in Neurobiology. 64**,** 69-95.

Agbaga, M.-P., 2016. Different Mutations in ELOVL4 Affect Very Long Chain Fatty Acid Biosynthesis to Cause Variable Neurological Disorders in Humans. 854**,** 129-135.

Agbaga, M. P., et al., 2008. Role of Stargardt-3 macular dystrophy protein (ELOVL4) in the biosynthesis of very long chain fatty acids. Proc Natl Acad Sci U S A. 105**,** 12843-8.

Agulnik, S. I., et al., 1996. Evolution of mouse T-box genes by tandem duplication and cluster dispersion. Genetics. 144**,** 249-254.

Aguzzi, A., Calella, A. M., 2009. Prions: protein aggregation and infectious diseases. Physiol Rev. 89**,** 1105-52.

Akamatsu, M., et al., 2013. A unique mouse model for investigating the properties of amyotrophic lateral sclerosis-associated protein TDP-43, by in utero electroporation. Neurosci Res. 77**,** 234-41.

Albalat, R., et al., 2010. Identification and characterisation of the developmental expression pattern of tbx5b, a novel tbx5 gene in zebrafish. Gene Expr Patterns. 10**,** 24-30.

Aleman, M., et al., 2011. Evaluation of epidemiological, clinical, and pathological features of neuroaxonal dystrophy in Quarter Horses. J Am Vet Med Assoc. 239**,** 823-33.

Alemasov, N. A., et al., 2017. Dynamic properties of SOD1 mutants can predict survival time of patients carrying familial amyotrophic lateral sclerosis. Journal of Biomolecular Structure & Dynamics. 35**,** 645-656.

Alexandrov, P. N., et al., 2011. Retinal amyloid peptides and complement factor H in transgenic models of Alzheimer's disease. Neuroreport. 22**,** 623-7.

Allison, W. T., Rainbow trout as a model of retinal photoreceptor death and regeneration. Vol. Ph. D. University of Victoria, Victoria, BC, Canada, 2004, pp. 205.

Allison, W. T., et al., 2010a. Ontogeny of cone photoreceptor mosaics in zebrafish. J Comp Neurol. 518**,** 4182-95.

Allison, W. T., et al., 2010b. Ontogeny of Cone Photoreceptor Mosaics in Zebrafish. Journal of Comparative Neurology. 518**,** 4182-4195.

Allison, W. T., et al., 2003. Ontogeny of ultraviolet-sensitive cones in the retina of rainbow trout (Oncorhynchus mykiss). Journal of Comparative Neurology. 461**,** 294-306.

Allison, W. T., et al., 2006a. Degeneration and regeneration of ultraviolet cone photoreceptors during development in rainbow trout. Journal of Comparative Neurology. 499**,** 702-715.
Allison, W. T., et al., 2017. Reduced Abundance and Subverted Functions of Proteins in Prion-Like Diseases: Gained Functions Fascinate but Lost Functions Affect Aetiology. International Journal of Molecular Sciences. 18.
Allison, W. T., et al., 2004. Visual pigment composition in zebrafish: Evidence for a rhodopsin-porphyropsin interchange system. Visual Neuroscience. 21**,** 945-952.
Allison, W. T., et al., 2006b. Proteomic analysis of opsins and thyroid hormone-induced retinal development using isotope-coded affinity tags (ICAT) and mass spectrometry. Molecular Vision. 12**,** 655-672.
Almeida, A. D., et al., 2014. Spectrum of Fates: a new approach to the study of the developing zebrafish retina. Development. 141**,** 1971-80.
Alvarez-Delfin, K., et al., 2009. Tbx2b is required for ultraviolet photoreceptor cell specification during zebrafish retinal development. Proc Natl Acad Sci U S A. 106**,** 2023-8.
Andersen, P. M., et al., 1997. Phenotypic heterogeneity in motor neuron disease patients with CuZn-superoxide dismutase mutations in Scandinavia. Brain. 120**,** 1723-1737.
Andersen, P. M., et al., 2003. Sixteen novel mutations in the Cu/Zn superoxide dismutase gene in amyotrophic lateral sclerosis: a decade of discoveries, defects and disputes. Amyotroph Lateral Scler Other Motor Neuron Disord. 4**,** 62-73.
Andre, E., et al., 1998. A novel isoform of the orphan nuclear receptor ROR beta is specifically expressed in pineal gland and retina. Gene. 216**,** 277-283.
Antinucci, P., Hindges, R., 2016. A crystal-clear zebrafish for in vivo imaging. Sci Rep. 6**,** 29490.
Antonyuk, S., et al., 2005. Structural consequences of the familial amyotrophic lateral sclerosis SOD1 mutant His46Arg. Protein Science. 14**,** 1201-1213.
Anzai, I., et al., 2017. A misfolded dimer of Cu/Zn-superoxide dismutase leading to pathological oligomerization in amyotrophic lateral sclerosis. Protein Science. 26**,** 484-496.
Applebury, M. L., et al., 2000. The murine cone photoreceptor: A single cone type expresses both S and M opsins with retinal spatial patterning. Neuron. 27**,** 513-523.
Arai, T., et al., 2006. TDP-43 is a component of ubiquitin-positive tau-negative inclusions in frontotemporal lobar degeneration and amyotrophic lateral sclerosis. Biochem Biophys Res Commun. 351**,** 602-11.
Aranda, A., Pascual, A., 2001. Nuclear hormone receptors and gene expression. Physiol Rev. 81**,** 1269-304.
Armstrong, G. A., Drapeau, P., 2013. Loss and gain of FUS function impair neuromuscular synaptic transmission in a genetic model of ALS. Hum Mol Genet. 22**,** 4282-92.
Armstrong, R. A., Cairns, N. J., 2011. Spatial patterns of TDP-43 neuronal cytoplasmic inclusions (NCI) in fifteen cases of frontotemporal lobar degeneration with TDP-43 proteinopathy (FTLD-TDP). Neurological Sciences. 32**,** 653-659.
Arnold, E. S., et al., 2013. ALS-linked TDP-43 mutations produce aberrant RNA splicing and adult-onset motor neuron disease without aggregation or loss of nuclear TDP-43. Proceedings of the National Academy of Sciences of the United States of America. 110**,** E736-E745.
Asai-Coakwell, M., et al., 2007a. GDF6, a novel locus for a spectrum of ocular developmental anomalies. American Journal of Human Genetics. 80**,** 306-315.
Asai-Coakwell, M., et al., 2007b. GDF6, a novel locus for a spectrum of ocular developmental anomalies. Am J Hum Genet. 80**,** 306-15.

Asai-Coakwell, M., et al., 2009. Incomplete penetrance and phenotypic variability characterize Gdf6-attributable oculo-skeletal phenotypes. Hum Mol Genet. 18**,** 1110-21.
Asai-Coakwell, M., et al., 2013. Contribution of growth differentiation factor 6-dependent cell survival to early-onset retinal dystrophies. Hum Mol Genet. 22**,** 1432-42.
Asante, E. A., et al., 2015. A naturally occurring variant of the human prion protein completely prevents prion disease. Nature. 522**,** 478-81.
Asaoka, Y., et al., 2014. The Hippo pathway controls a switch between retinal progenitor cell proliferation and photoreceptor cell differentiation in zebrafish. PLoS One. 9**,** e97365.
Ash, P. E., et al., 2010a. Neurotoxic effects of TDP-43 overexpression in C. elegans. Hum Mol Genet. 19**,** 3206-18.
Ash, P. E. A., et al., 2010b. Neurotoxic effects of TDP-43 overexpression in C-elegans. Human Molecular Genetics. 19**,** 3206-3218.
Augsburger, A., et al., 1999. BMPs as mediators of roof plate repulsion of commissural neurons. Neuron. 24**,** 127-41.
Awano, T., et al., 2009. Genome-wide association analysis reveals a SOD1 mutation in canine degenerative myelopathy that resembles amyotrophic lateral sclerosis. Proceedings of the National Academy of Sciences of the United States of America. 106**,** 2794-2799.
Ayers, J. I., et al., 2016a. Distinct conformers of transmissible misfolded SOD1 distinguish human SOD1-FALS from other forms of familial and sporadic ALS. Acta Neuropathol. 132**,** 827-840.
Ayers, J. I., et al., 2014. Experimental transmissibility of mutant SOD1 motor neuron disease. Acta Neuropathol. 128**,** 791-803.
Ayers, J. I., et al., 2016b. Prion-like propagation of mutant SOD1 misfolding and motor neuron disease spread along neuroanatomical pathways. Acta Neuropathologica. 131**,** 103-114.
Ayers, J. I., et al., 2017. Relationship between mutant Cu/Zn superoxide dismutase 1 maturation and inclusion formation in cell models. J Neurochem. 140**,** 140-150.
Azriel, R., Gazit, E., 2001. Analysis of the structural and functional elements of the minimal active fragment of islet amyloid polypeptide (IAPP) - An experimental support for the key role of the phenylalanine residue in amyloid formation. Journal of Biological Chemistry. 276**,** 34156-34161.
Bagci, E., et al., 2015. Deiodinase knockdown during early zebrafish development affects growth, development, energy metabolism, motility and phototransduction. PLoS One. 10**,** e0123285.
Bahadorani, S., et al., 2013. Expression of zinc-deficient human superoxide dismutase in Drosophila neurons produces a locomotor defect linked to mitochondrial dysfunction. Neurobiology of Aging. 34**,** 2322-2330.
Baines, R. A., 2004. Synaptic strengthening mediated by bone morphogenetic protein-dependent retrograde signaling in the Drosophila CNS. J Neurosci. 24**,** 6904-11.
Baker, H. F., et al., 1994. Induction of beta (A4)-amyloid in primates by injection of Alzheimer's disease brain homogenate. Comparison with transmission of spongiform encephalopathy. Mol Neurobiol. 8**,** 25-39.
Baloh, R. H., 2012a. How do the RNA-binding proteins TDP-43 and FUS relate to amyotrophic lateral sclerosis and frontotemporal degeneration, and to each other? Current Opinion in Neurology. 25**,** 701-707.

Baloh, R. H., 2012b. How do the RNA-binding proteins TDP-43 and FUS relate to amyotrophic lateral sclerosis and frontotemporal degeneration, and to each other? Curr Opin Neurol. 25**,** 701-7.
Banci, L., et al., 2008. SOD1 and Amyotrophic Lateral Sclerosis: Mutations and Oligomerization. Plos One. 3.
Bandmann, O., Burton, E. A., 2010. Genetic zebrafish models of neurodegenerative diseases. Neurobiol Dis. 40**,** 58-65.
Banerjee, V., et al., 2016. Superoxide Dismutase 1 (SOD1)-Derived Peptide Inhibits Amyloid Aggregation of Familial Amyotrophic Lateral Sclerosis SOD1 Mutants. ACS Chem Neurosci. 7**,** 1595-1606.
Banyai, L., et al., 2010. Agrin binds BMP2, BMP4 and TGFbeta1. Plos One. 5**,** e10758.
Barmada, S. J., et al., 2014. Autophagy induction enhances TDP43 turnover and survival in neuronal ALS models. Nat Chem Biol. 10**,** 677-85.
Barmada, S. J., et al., 2010. Cytoplasmic mislocalization of TDP-43 is toxic to neurons and enhanced by a mutation associated with familial amyotrophic lateral sclerosis. J Neurosci. 30**,** 639-49.
Barros, A. C., et al., 1998. Absence of thyroid hormone receptor beta-retinoid X receptor interactions in auditory function and in the pituitary-thyroid axis. Neuroreport. 9**,** 2933-7.
Bartram, U., et al., 2001. Double-outlet right ventricle and overriding tricuspid valve reflect disturbances of looping, myocardialization, endocardial cushion differentiation, and apoptosis in TGF-beta(2)-knockout mice. Circulation. 103**,** 2745-52.
Bassett, E. A., Wallace, V. A., 2012. Cell fate determination in the vertebrate retina. Trends Neurosci. 35**,** 565-73.
Batista, M. F., et al., 2008. Zebrafish V2 cells develop into excitatory CiD and Notch signalling dependent inhibitory VeLD interneurons. Dev Biol. 322**,** 263-75.
Baumann, L., et al., 2016. Thyroid disruption in zebrafish (Danio rerio) larvae: Different molecular response patterns lead to impaired eye development and visual functions. Aquat Toxicol. 172**,** 44-55.
Bayat, V., et al., 2011. The BMP signaling pathway at the Drosophila neuromuscular junction and its links to neurodegenerative diseases. Curr Opin Neurobiol. 21**,** 182-8.
Becker, C. G., Becker, T., 2008. Adult zebrafish as a model for successful central nervous system regeneration. Restorative Neurology and Neuroscience. 26**,** 71-80.
Becker, T., et al., 1998. Readiness of zebrafish brain neurons to regenerate a spinal axon correlates with differential expression of specific cell recognition molecules. Journal of Neuroscience. 18**,** 5789-5803.
Becker, T., et al., 1997. Axonal regrowth after spinal cord transection in adult zebrafish. Journal of Comparative Neurology. 377**,** 577-595.
Beeldman, E., et al., 2016. The cognitive profile of ALS: a systematic review and meta-analysis update. Journal of Neurology Neurosurgery and Psychiatry. 87**,** 611-619.
Behesti, H., et al., 2006. The level of BMP4 signaling is critical for the regulation of distinct T-box gene expression domains and growth along the dorso-ventral axis of the optic cup. BMC Dev Biol. 6**,** 62.
Behesti, H., et al., 2009. Loss of Tbx2 delays optic vesicle invagination leading to small optic cups. Dev Biol. 333**,** 360-72.
Bendotti, C., Carri, M. T., 2004. Lessons from models of SOD1-linked familial ALS. Trends Mol Med. 10**,** 393-400.

Benedetti, L., et al., 2016. INaP selective inhibition reverts precocious inter- and motorneurons hyperexcitability in the Sod1-G93R zebrafish ALS model. Sci Rep. 6, 24515.
Bennett, L. D., et al., 2014. Effect of reduced retinal VLC-PUFA on rod and cone photoreceptors. Invest Ophthalmol Vis Sci. 55, 3150-7.
Bernardos, R. L., et al., 2007. Late-stage neuronal progenitors in the retina are radial Muller glia that function as retinal stem cells. J Neurosci. 27, 7028-40.
Bernstein, P. S., et al., 2001. Diverse macular dystrophy phenotype caused by a novel complex mutation in the ELOVL4 gene. Invest Ophthalmol Vis Sci. 42, 3331-6.
Bertrand, S., et al., 2007. Unexpected novel relational links uncovered by extensive developmental profiling of nuclear receptor expression. PLoS Genet. 3, e188.
Bibliowicz, J., et al., 2011. Toward a better understanding of human eye disease insights from the zebrafish, Danio rerio. Prog Mol Biol Transl Sci. 100, 287-330.
Bidhendi, E. E., et al., 2016. Two superoxide dismutase prion strains transmit amyotrophic lateral sclerosis-like disease. J Clin Invest. 126, 2249-53.
Bilican, B., Goding, C. R., 2006. Cell cycle regulation of the T-box transcription factor tbx2. Exp Cell Res. 312, 2358-66.
Billings, N. A., et al., 2010. Analysis of thyroid response element activity during retinal development. PLoS One. 5, e13739.
Billon, N., et al., 2002. Normal timing of oligodendrocyte development depends on thyroid hormone receptor alpha 1 (TRalpha1). EMBO J. 21, 6452-60.
Bilotta, J., Saszik, S., 2001. The zebrafish as a model visual system. International Journal of Developmental Neuroscience. 19, 621-629.
Blechinger, S. R., et al., 2002. The heat-inducible zebrafish hsp70 gene is expressed during normal lens development under non-stress conditions. Mech Dev. 112, 213-5.
Block, M. L., Hong, J. S., 2005. Microglia and inflammation-mediated neurodegeneration: multiple triggers with a common mechanism. Prog Neurobiol. 76, 77-98.
Blokhuis, A. M., et al., 2013. Protein aggregation in amyotrophic lateral sclerosis. Acta Neuropathologica. 125, 777-794.
Bocharova, O. V., et al., 2005. In vitro conversion of full-length mammalian prion protein produces amyloid form with physical properties of PrP(Sc). J Mol Biol. 346, 645-59.
Bohnsack, B. L., Kahana, A., 2013. Thyroid hormone and retinoic acid interact to regulate zebrafish craniofacial neural crest development. Dev Biol. 373, 300-9.
Boije, H., et al., 2015. The Independent Probabilistic Firing of Transcription Factors: A Paradigm for Clonal Variability in the Zebrafish Retina. Dev Cell. 34, 532-43.
Boije, H., et al., 2016. Horizontal Cells, the Odd Ones Out in the Retina, Give Insights into Development and Disease. Front Neuroanat. 10, 77.
Boillee, S., et al., 2006. ALS: a disease of motor neurons and their nonneuronal neighbors. Neuron. 52, 39-59.
Bollag, R. J., et al., 1994. An ancient family of embryonically expressed mouse genes sharing a conserved protein motif with the T locus. Nat Genet. 7, 383-9.
Bosco, D. A., et al., 2011. Proteostasis and Movement Disorders: Parkinson's Disease and Amyotrophic Lateral Sclerosis. Cold Spring Harbor Perspectives in Biology. 3.
Bosco, D. A., et al., 2010. Wild-type and mutant SOD1 share an aberrant conformation and a common pathogenic pathway in ALS. Nat Neurosci. 13, 1396-403.
Bossy-Wetzel, E., et al., 2004. Molecular pathways to neurodegeneration. Nat Med. 10 Suppl, S2-9.

Bovolenta, P., et al., 1997. Implication of OTX2 in pigment epithelium determination and neural retina differentiation. Journal of Neuroscience. 17**,** 4243-4252.
Brett, J. R., 1964. The respiratory metabolism and swimming performance of young sockeye salmon. Journal of the Fisheries Research Board of Canada. 21**,** 1183-1226.
Bridges, E. G., et al., 2008. Nonclinical safety profile of telbivudine, a novel potent antiviral agent for treatment of hepatitis B. Antimicrobial Agents and Chemotherapy. 52**,** 2521-2528.
Brignull, H. R., et al., 2007. The stress of misfolded proteins: C-elegans models for neurodegenerative disease and aging. Molecular Aspects of the Stress Response: Chaperones, Membranes and Networks. 594**,** 167-189.
Brockerhoff, S. E., Fadool, J. M., 2011. Genetics of photoreceptor degeneration and regeneration in zebrafish. Cell Mol Life Sci. 68**,** 651-9.
Brockerhoff, S. E., et al., 1997. A new form of inherited red-blindness identified in zebrafish. J Neurosci. 17**,** 4236-42.
Broom, H. R., et al., 2015. Destabilization of the dimer interface is a common consequence of diverse ALS-associated mutations in metal free SOD1. Protein Science. 24**,** 2081-2089.
Brotherton, T. E., et al., 2012. Localization of a toxic form of superoxide dismutase 1 protein to pathologically affected tissues in familial ALS. Proceedings of the National Academy of Sciences of the United States of America. 109**,** 5505-5510.
Browman, H. I., Hawryshyn, C. W., 1994. RETINOIC ACID MODULATES RETINAL DEVELOPMENT IN THE JUVENILES OP A TELEOST FISH. Journal of Experimental Biology. 193**,** 191-207.
Brown, A., et al., 1998. The Human PAX6 Mutation Database. Nucleic Acids Res. 26**,** 259-64.
Brown, D. I., Griendling, K. K., 2009. Nox proteins in signal transduction. Free Radic Biol Med. 47**,** 1239-53.
Brown, R. H., 1993. Mutations in Cu/Zn Superoxide-Dismutase (Sod1) Are Associated with Familial Amyotrophic-Lateral-Sclerosis (Als). Free Radical Biology and Medicine. 15**,** 471-471.
Bruhn, S. L., Cepko, C. L., 1996. Development of the pattern of photoreceptors in the chick retina. J Neurosci. 16**,** 1430-9.
Bruijn, L. I., et al., 1997. ALS-linked SOD1 mutant G85R mediates damage to astrocytes and promotes rapidly progressive disease with SOD1-containing inclusions. Neuron. 18**,** 327-338.
Bruijn, L. I., et al., 1998. Aggregation and motor neuron toxicity of an ALS-linked SOD1 mutant independent from wild-type SOD1. Science. 281**,** 1851-1854.
Bruijn, L. I., et al., 2004. Unraveling the mechanisms involved in motor neuron degeneration in ALS. Annual Review of Neuroscience. 27**,** 723-749.
Bruneau, S., Rosa, F. M., 1997. Dynamo, a new zebrafish DVR member of the TGF-beta superfamily is expressed in the posterior neural tube and is up-regulated by Sonic hedgehog. Mech Dev. 61**,** 199-212.
Brzezinski, J. A., Reh, T. A., 2015. Photoreceptor cell fate specification in vertebrates. Development. 142**,** 3263-73.
Brzezinski, J. A. t., et al., 2010. Blimp1 controls photoreceptor versus bipolar cell fate choice during retinal development. Development. 137**,** 619-29.
Brzezinski, J. A. t., et al., 2013. Blimp1 (Prdm1) prevents re-specification of photoreceptors into retinal bipolar cells by restricting competence. Dev Biol. 384**,** 194-204.

Burmeister, M., et al., 1996. Ocular retardation mouse caused by Chx10 homeobox null allele: impaired retinal progenitor proliferation and bipolar cell differentiation. Nat Genet. 12**,** 376-84.

Butler, S. J., Dodd, J., 2003. A role for BMP heterodimers in roof plate-mediated repulsion of commissural axons. Neuron. 38**,** 389-401.

Cairns, N. J., et al., 2007. TDP-43 in familial and sporadic frontotemporal lobar degeneration with ubiquitin inclusions. American Journal of Pathology. 171**,** 227-240.

Cardoso, L. F., et al., 2014. Resistance to thyroid hormone due to mutations in the THRB gene impairs bone mass and affects calcium and phosphorus homeostasis. Bone. 67**,** 222-7.

Carl, M., et al., 2002. Six3 inactivation reveals its essential role for the formation and patterning of the vertebrate eye. Development. 129**,** 4057-63.

Case DA , D. T., CheathamTE 3rd, Simmerling CL, Wang J, Duke RE, Luo R, Crowley MRCW, Walker RC, Zhang W, Merz KM, Wang B, Hayik S, Roitberg A, Seabra G, Kolossváry I, Wong KF, Paesani F, Vanicek J, Wu X, Brozell SR, Steinbrecher T, Gohlke H, Yang L, Tan C, Mongan J, Hornak V, Cui G, Mathews DH, Seetin MG, Sagui C, Babin V, Kollman PA, 2008. Amber 10. University of California.

Cashman, N., et al., 2012. Propagated misfolding of SOD1 in ALS. Prion. 6**,** 12-12.

Cashman, N. R., et al., 2007. Active and passive immunization of superoxide dismutase-1 disease-specific epitopes in a mouse model of amyotrophic lateral sclerosis. Annals of Neurology. 62**,** 542-543.

Caughey, B., et al., 2009. Getting a grip on prions: oligomers, amyloids, and pathological membrane interactions. Annu Rev Biochem. 78**,** 177-204.

Cecchini, P., et al., 2012. The role of tryptophan in protein fibrillogenesis: relevance of Trp7 and Trp14 to the amyloidogenic properties of myoglobin. Protein Eng Des Sel. 25**,** 199-203.

Chang, C., Hemmati-Brivanlou, A., 1999. Xenopus GDF6, a new antagonist of noggin and a partner of BMPs. Development. 126**,** 3347-57.

Chapman, D. L., et al., 1996. Expression of the T-box family genes, Tbx1-Tbx5, during early mouse development. Dev Dyn. 206**,** 379-90.

Chatonnet, F., et al., 2013. Genome-wide analysis of thyroid hormone receptors shared and specific functions in neural cells. Proc Natl Acad Sci U S A. 110**,** E766-75.

Chen, H., et al., 2014. Modeling ALS with iPSCs Reveals that Mutant SOD1 Misregulates Neurofilament Balance in Motor Neurons. Cell Stem Cell. 14**,** 796-809.

Chen, S., et al., 2004. Interference of Crx-dependent transcription by ataxin-7 involves interaction between the glutamine regions and requires the ataxin-7 carboxy-terminal region for nuclear localization. Hum Mol Genet. 13**,** 53-67.

Chen, S. M., et al., 1997. Crx, a novel Otx-like paired-homeodomain protein, binds to and transactivates photoreceptor cell-specific genes. Neuron. 19**,** 1017-1030.

Cheng, C. S. T., Characterization of Retinoic Acid Synthesis and Signalling in Vertebrate Eye Development. Department of Biological Sciences, Vol. Doctor of Philosophy. University of Alberta, 2016.

Cheng, S. Y., et al., 2010. Molecular aspects of thyroid hormone actions. Endocr Rev. 31**,** 139-70.

Chew, J., et al., 2015. Neurodegeneration. C9ORF72 repeat expansions in mice cause TDP-43 pathology, neuronal loss, and behavioral deficits. Science. 348**,** 1151-4.

Chi, N. C., et al., 2008. Foxn4 directly regulates tbx2b expression and atrioventricular canal formation. Genes Dev. 22**,** 734-9.

Chia, R., et al., 2010. Superoxide Dismutase 1 and tgSOD1(G93A) Mouse Spinal Cord Seed Fibrils, Suggesting a Propagative Cell Death Mechanism in Amyotrophic Lateral Sclerosis. Plos One. 5.
Cho, G. S., et al., 2011. Role of Tbx2 in defining the territory of the pronephric nephron. Development. 138, 465-474.
Choi, J. G., et al., 2016. Lentivirus pre-packed with Cas9 protein for safer gene editing. Gene Ther. 23, 627-33.
Choi, T. Y., et al., 2017. Bone morphogenetic protein signaling governs biliary-driven liver regeneration in zebrafish through tbx2b and id2a. Hepatology. 66, 1616-1630.
Chothia, C., 1976. The nature of the accessible and buried surfaces in proteins. J Mol Biol. 105, 1-12.
Chou, H. J., et al., 2013. BMP4 is a peripherally-derived factor for motor neurons and attenuates glutamate-induced excitotoxicity in vitro. Plos One. 8, e58441.
Chow, R. L., et al., 1999. Pax6 induces ectopic eyes in a vertebrate. Development. 126, 4213-22.
Chow, R. L., Lang, R. A., 2001. Early eye development in vertebrates. Annu Rev Cell Dev Biol. 17, 255-96.
Clanton, J. A., et al., 2013. Fgf signaling governs cell fate in the zebrafish pineal complex. Development. 140, 323-32.
Clavaguera, F., et al., 2009. Transmission and spreading of tauopathy in transgenic mouse brain. Nat Cell Biol. 11, 909-13.
Cleveland, D. W., 1999. From Charcot to SOD1: Mechanisms of selective motor neuron death in ALS. Neuron. 24, 515-520.
Coelho, F. R., et al., 2014. Oxidation of the Tryptophan 32 Residue of Human Superoxide Dismutase 1 Caused by Its Bicarbonate-dependent Peroxidase Activity Triggers the Non-amyloid Aggregation of the Enzyme. Journal of Biological Chemistry. 289, 30690-30701.
Cohen, F. E., Prusiner, S. B., 1998. Pathologic conformations of prion proteins. Annu Rev Biochem. 67, 793-819.
Cohen, T., et al., 2006. Inhibition of amyloid fibril formation and cytotoxicity by hydroxyindole derivatives. Biochemistry. 45, 4727-4735.
Collin, S. P., et al., 2009. The evolution of early vertebrate photoreceptors. Philos Trans R Soc Lond B Biol Sci. 364, 2925-40.
Collin, S. P., et al., 2003. Ancient colour vision: multiple opsin genes in the ancestral vertebrates. Curr Biol. 13, R864-5.
Collin, S. P., Trezise, A. E., 2004. The origins of colour vision in vertebrates. Clin Exp Optom. 87, 217-23.
Collinge, J., 2001. Prion diseases of humans and animals: their causes and molecular basis. Annu Rev Neurosci. 24, 519-50.
Coolen, M., et al., 2005. Phylogenomic analysis and expression patterns of large Maf genes in Xenopus tropicalis provide new insights into the functional evolution of the gene family in osteichthyans. Development Genes and Evolution. 215, 327-339.
Corbo, J. C., et al., 2010. CRX ChIP-seq reveals the cis-regulatory architecture of mouse photoreceptors. Genome Res. 20, 1512-25.
Corbo, J. C., et al., 2007. A typology of photoreceptor gene expression patterns in the mouse. Proc Natl Acad Sci U S A. 104, 12069-74.
Corcia, P., et al., 2017. Genetics of amyotrophic lateral sclerosis. Rev Neurol (Paris). 173, 254-262.

Cossette, S. M. M., Drysdale, T. A., 2004. Early expression of thyroid hormone receptor beta and retinoid X receptor gamma in the Xenopus embryo. Differentiation. 72, 239-249.
Couratier, P., et al., 2017. ALS and frontotemporal dementia belong to a common disease spectrum. Revue Neurologique. 173, 273-279.
Cozzolino, M., et al., 2009. Oligomerization of Mutant SOD1 in Mitochondria of Motoneuronal Cells Drives Mitochondrial Damage and Cell Toxicity. Antioxidants & Redox Signaling. 11, 1547-U3.
Crippa, V., et al., 2010. The small heat shock protein B8 (HspB8) promotes autophagic removal of misfolded proteins involved in amyotrophic lateral sclerosis (ALS). Hum Mol Genet. 19, 3440-56.
Crosier, P. S., et al., 2002. Pathways in blood and vessel development revealed through zebrafish genetics. Int J Dev Biol. 46, 493-502.
Da Costa, M. M., et al., 2014. A new zebrafish model produced by TILLING of SOD1-related amyotrophic lateral sclerosis replicates key features of the disease and represents a tool for in vivo therapeutic screening. Dis Model Mech. 7, 73-81.
Da Cruz, S., et al., 2017. Misfolded SOD1 is not a primary component of sporadic ALS. Acta Neuropathol. 134, 97-111.
Daniele, L. L., et al., 2005. Cone-like morphological, molecular, and electrophysiological features of the photoreceptors of the Nrl knockout mouse. Investigative Ophthalmology & Visual Science. 46, 2156-2167.
Dann, S. G., et al., 2004. Salmonid opsin sequences undergo positive selection and indicate an alternate evolutionary relationship in Oncorhynchus. Journal of Molecular Evolution. 58, 400-412.
Darras, V. M., et al., 2011. Thyroid hormone receptors in two model species for vertebrate embryonic development: chicken and zebrafish. J Thyroid Res. 2011, 402320.
Das, A., Plotkin, S. S., 2013. SOD1 exhibits allosteric frustration to facilitate metal binding affinity. Proc Natl Acad Sci U S A. 110, 3871-6.
Das, I., et al., 2015. Preventing proteostasis diseases by selective inhibition of a phosphatase regulatory subunit. Science. 348, 239-42.
Dasmeh, P., Kepp, K. P., 2017. Superoxide dismutase 1 is positively selected to minimize protein aggregation in great apes. Cellular and Molecular Life Sciences. 74, 3023-3037.
Davey, J. C., et al., 1994. Cloning of a thyroid hormone-responsive Rana catesbeiana c-erbA-beta gene. Dev Genet. 15, 339-46.
Davidson, M. G., et al., 1998. Retinal degeneration associated with vitamin E deficiency in hunting dogs. J Am Vet Med Assoc. 213, 645-51.
Davidson, Y., et al., 2007. Ubiquitinated pathological lesions in frontotemporal lobar degeneration contain the TAR DNA-binding protein, TDP-43. Acta Neuropathologica. 113, 521-533.
De Jesus-Cortes, H., et al., 2012. Neuroprotective efficacy of aminopropyl carbazoles in a mouse model of Parkinson disease. Proc Natl Acad Sci U S A. 109, 17010-5.
de Melo, J., et al., 2011. The Spalt family transcription factor Sall3 regulates the development of cone photoreceptors and retinal horizontal interneurons. Development. 138, 2325-2336.
De Vos, K. J., et al., 2007. Familial amyotrophic lateral sclerosis-linked SOD1 mutants perturb fast axonal transport to reduce axonal mitochondria content. Human Molecular Genetics. 16, 2720-2728.

Deininger, M., et al., 1995. Detection of two transforming growth factor-beta-related morphogens, bone morphogenetic proteins-4 and -5, in RNA of multiple sclerosis and Creutzfeldt-Jakob disease lesions. Acta Neuropathol. 90**,** 76-9.
DeJesus-Hernandez, M., et al., 2011. Expanded GGGGCC hexanucleotide repeat in noncoding region of C9ORF72 causes chromosome 9p-linked FTD and ALS. Neuron. 72**,** 245-56.
Del Bo, R., et al., 2011. Novel optineurin mutations in patients with familial and sporadic amyotrophic lateral sclerosis. J Neurol Neurosurg Psychiatry. 82**,** 1239-43.
den Hollander, A. I., et al., 2010. Genetic defects of GDF6 in the zebrafish out of sight mutant and in human eye developmental anomalies. BMC Genet. 11**,** 102.
Deng, H., et al., 1993. Amyotrophic lateral sclerosis and structural defects in Cu,Zn superoxide dismutase. Science. 261**,** 1047-1051.
Deng, H. X., et al., 2006. Conversion to the amyotrophic lateral sclerosis phenotype is associated with intermolecular linked insoluble aggregates of SOD1 in mitochondria. Proceedings of the National Academy of Sciences of the United States of America. 103**,** 7142-7147.
Derynck, R., Zhang, Y., 1996. Intracellular signalling: the mad way to do it. Curr Biol. 6**,** 1226-9.
Desplats, P., et al., 2009. Inclusion formation and neuronal cell death through neuron-to-neuron transmission of alpha-synuclein. Proc Natl Acad Sci U S A. 106**,** 13010-5.
Dheen, T., et al., 1999. Zebrafish tbx-c functions during formation of midline structures. Development. 126**,** 2703-13.
DiDonato, M., et al., 2003. ALS mutants of human superoxide dismutase form fibrous aggregates via framework destabilization (vol 332, pg 601, 2003). Journal of Molecular Biology. 334**,** 175-175.
Dion, P. A., et al., 2009. Genetics of motor neuron disorders: new insights into pathogenic mechanisms. Nat Rev Genet. 10**,** 769-82.
Domingos, P. M., et al., 2004. Regulation of R7 and R8 differentiation by the spalt genes. Developmental Biology. 273**,** 121-133.
Dorsky, R. I., et al., 1997. Regulation of neuronal diversity in the Xenopus retina by Delta signalling. Nature. 385**,** 67-70.
Dorval, K. M., et al., 2006. CHX10 targets a subset of photoreceptor genes. J Biol Chem. 281**,** 744-51.
Dowling, J. E., 2012. The retina : an approachable part of the brain. Belknap, Cambridge, Mass. ; London.
Drummond, B. E., et al., 2017. The tbx2a/b transcription factors direct pronephros segmentation and corpuscle of Stannius formation in zebrafish. Dev Biol. 421**,** 52-66.
Du, Y., et al., 2018. A Genome-wide Expression Association Analysis Identifies Genes and Pathways Associated with Amyotrophic Lateral Sclerosis. Cell Mol Neurobiol. 38**,** 635-639.
DuVal, M. G., Allison, W. T., 2017. Impacts of the retinal environment and photoreceptor type on functional regeneration. Neural Regeneration Research. 12**,** 376-379.
Duval, M. G., et al., 2013. Longitudinal fluorescent observation of retinal degeneration and regeneration in zebrafish using fundus lens imaging. Molecular Vision. 19**,** 1082-1095.
DuVal, M. G., et al., 2014a. Growth Differentiation Factor 6 As a Putative Risk Factor in Neuromuscular Degeneration. Plos One. 9.
DuVal MG, G. M., Watson DE, Zerulla TC, Tierney KB, Allison WT, Growth Differentiation Factor 6 as a putative risk factor in neuromuscular degeneration. Accepted pending minor revision Oct. 22, 2013. PLoS ONE, 2013.

DuVal, M. G., et al., 2014b. gdf6a Is Required for Cone Photoreceptor Subtype Differentiation and for the Actions of tbx2b in Determining Rod Versus Cone Photoreceptor Fate. Plos One. 9.
Easter, S. S., Hitchcock, P. F., 2000. Stem Cells and Regeneration in the Retina: What Fish Have Taught Us about Neurogenesis. The Neuroscientist. 6**,** 454-464.
Easter, S. S., Jr., Malicki, J. J., 2002. The zebrafish eye: developmental and genetic analysis. Results Probl Cell Differ. 40**,** 346-70.
Eaton, B. A., Davis, G. W., 2005. LIM Kinase1 controls synaptic stability downstream of the type II BMP receptor. Neuron. 47**,** 695-708.
Elden, A. C., et al., 2010. Ataxin-2 intermediate-length polyglutamine expansions are associated with increased risk for ALS. Nature. 466**,** 1069-75.
Elsaeidi, F., et al., 2018. Notch Suppression Collaborates with Ascl1 and Lin28 to Unleash a Regenerative Response in Fish Retina, But Not in Mice. Journal of Neuroscience. 38**,** 2246-2261.
Emerson, M. M., et al., 2013. Otx2 and onecut1 promote the fates of cone photoreceptors and horizontal cells and repress rod photoreceptors. Dev Cell. 26**,** 59-72.
Engerer, P., et al., 2017. Uncoupling of neurogenesis and differentiation during retinal development. EMBO J. 36**,** 1134-1146.
Enright, J. M., et al., 2015. Transcriptome profiling of developing photoreceptor subtypes reveals candidate genes involved in avian photoreceptor diversification. J Comp Neurol. 523**,** 649-68.
Epple, M., Neues, F., 2010. Synchrotron microcomputer tomography for the non-destructive visualization of the fish skeleton. Journal of Applied Ichthyology. 26**,** 286-288.
Erter, C. E., et al., 2001. Wnt8 is required in lateral mesendodermal precursors for neural posteriorization in vivo. Development. 128**,** 3571-83.
Essner, J. J., et al., 1999. Overexpression of thyroid hormone receptor alpha 1 during zebrafish embryogenesis disrupts hindbrain patterning and implicates retinoic acid receptors in the control of hox gene expression. Differentiation. 65**,** 1-11.
Evers, P., Uylings, H. B., 1994. Effects of microwave pretreatment on immunocytochemical staining of vibratome sections and tissue blocks of human cerebral cortex stored in formaldehyde fixative for long periods. J Neurosci Methods. 55**,** 163-72.
Fadool, J. M., Dowling, J. E., 2008. Zebrafish: A model system for the study of eye genetics. Progress in Retinal and Eye Research. 27**,** 89-110.
Farg, M. A., et al., 2012. Mutant FUS induces endoplasmic reticulum stress in amyotrophic lateral sclerosis and interacts with protein disulfide-isomerase. Neurobiology of Aging. 33**,** 2855-2868.
Farin, H. F., et al., 2013. Tbx2 terminates shh/fgf signaling in the developing mouse limb bud by direct repression of gremlin1. PLoS Genet. 9**,** e1003467.
Farrawell, N. E., et al., 2015a. Distinct partitioning of ALS associated TDP-43, FUS and SOD1 mutants into cellular inclusions. Sci Rep. 5**,** 13416.
Farrawell, N. E., et al., 2015b. Distinct partitioning of ALS associated TDP-43, FUS and SOD1 mutants into cellular inclusions. Scientific Reports. 5.
Farrell, A. P., 2007. Comparisons of swimming performance in rainbow trout using constant acceleration and critical swimming speed tests. Journal of Fish Biology. 72**,** 693-710.
Fassier, C., et al., 2010. Zebrafish atlastin controls motility and spinal motor axon architecture via inhibition of the BMP pathway. Nat Neurosci. 13**,** 1380-7.

Fausett, B. V., Goldman, D., 2006. A role for alpha1 tubulin-expressing Muller glia in regeneration of the injured zebrafish retina. J Neurosci. 26, 6303-13.
Fay, D. S., et al., 1998. In vivo aggregation of beta-amyloid peptide variants. J Neurochem. 71, 1616-25.
Feng, Z., Ko, C. P., 2008. Schwann cells promote synaptogenesis at the neuromuscular junction via transforming growth factor-beta1. J Neurosci. 28, 9599-609.
Ferraiuolo, L., et al., 2011. Molecular pathways of motor neuron injury in amyotrophic lateral sclerosis. Nat Rev Neurol. 7, 616-30.
Ferrington, D. A., et al., 2016. Defects in retinal pigment epithelial cell proteolysis and the pathology associated with age-related macular degeneration. Prog Retin Eye Res. 51, 69-89.
Fetcho, J. R., 2007. The utility of zebrafish for studies of the comparative biology of motor systems. Journal of Experimental Zoology Part B-Molecular and Developmental Evolution. 308b, 550-562.
Fichelson, P., et al., 2012. Orthodenticle and Kruppel homolog 1 regulate Drosophila photoreceptor maturation. Proc Natl Acad Sci U S A. 109, 7893-8.
Filali, M., et al., 2011. Sensorimotor and cognitive functions in a SOD1(G37R) transgenic mouse model of amyotrophic lateral sclerosis. Behavioural Brain Research. 225, 215-221.
Finno, C. J., et al., 2015. Blood and Cerebrospinal Fluid alpha-Tocopherol and Selenium Concentrations in Neonatal Foals with Neuroaxonal Dystrophy. J Vet Intern Med. 29, 1667-75.
Finno, C. J., et al., 2011. Equine degenerative myeloencephalopathy in Lusitano horses. J Vet Intern Med. 25, 1439-46.
Finno, C. J., et al., 2017. Pigment retinopathy in warmblood horses with equine degenerative myeloencephalopathy and equine motor neuron disease. Vet Ophthalmol. 20, 304-309.
Fischer, L. R., et al., 2012. Absence of SOD1 leads to oxidative stress in peripheral nerve and causes a progressive distal motor axonopathy. Exp Neurol. 233, 163-71.
Flamant, F., Samarut, J., 2003. Thyroid hormone receptors: lessons from knockout and knock-in mutant mice. Trends Endocrinol Metab. 14, 85-90.
Flanagan-Steet, H., et al., 2005. Neuromuscular synapses can form in vivo by incorporation of initially aneural postsynaptic specializations. Development. 132, 4471-81.
Fleisch, V. C., et al., 2011. Investigating regeneration and functional integration of CNS neurons: lessons from zebrafish genetics and other fish species. Biochim Biophys Acta. 1812, 364-80.
Floris, G., et al., 2015. Clinical phenotypes and radiological findings in frontotemporal dementia related to TARDBP mutations. J Neurol. 262, 375-84.
Fong, S. H., et al., 2005. Wnt signalling mediated by Tbx2b regulates cell migration during formation of the neural plate. Development. 132, 3587-96.
Forbes-Osborne, M. A., et al., 2013. Insulinoma-associated 1a (Insm1a) is required for photoreceptor differentiation in the zebrafish retina. Dev Biol. 380, 157-71.
Forrest, D., et al., 1990. Contrasting developmental and tissue-specific expression of alpha and beta thyroid hormone receptor genes. EMBO J. 9, 1519-28.
Forrest, D., Swaroop, A., 2012. Minireview: the role of nuclear receptors in photoreceptor differentiation and disease. Mol Endocrinol. 26, 905-15.
Forsberg, K., et al., 2010. Novel antibodies reveal inclusions containing non-native SOD1 in sporadic ALS patients. PLoS One. 5, e11552.

Fossat, N., et al., 2007. A new GFP-tagged line reveals unexpected Otx2 protein localization in retinal photoreceptors. BMC Dev Biol. 7, 122.
Fraichard, A., et al., 1997. The T3R alpha gene encoding a thyroid hormone receptor is essential for post-natal development and thyroid hormone production. EMBO J. 16, 4412-20.
Fraser, B., et al., 2013a. Regeneration of Cone Photoreceptors when Cell Ablation Is Primarily Restricted to a Particular Cone Subtype. Plos One. 8.
Fraser, B., et al., 2013b. Regeneration of cone photoreceptors when cell ablation is primarily restricted to a particular cone subtype. Plos One. 8, e55410.
French, C. R., Patterning the zebrafish visual system requires the actions of Pbx transcription factors, and a downstream growth factor, Gdf6a. Department of Biological Sciences, Vol. Ph. D. . University of Alberta, Edmonton, Alberta, Canada, 2010, pp. 220.
French, C. R., et al., 2007. Pbx homeodomain proteins pattern both the zebrafish retina and tectum. BMC Dev Biol. 7, 85.
French, C. R., et al., 2009. Gdf6a is required for the initiation of dorsal-ventral retinal patterning and lens development. Dev Biol. 333, 37-47.
French, C. R., et al., 2013. Apoptotic and proliferative defects characterize ocular development in a microphthalmic BMP model. Invest Ophthalmol Vis Sci. 54, 4636-47.
Freund, C. L., et al., 1997. Cone-rod dystrophy due to mutations in a novel photoreceptor-specific homeobox gene (CRX) essential for maintenance of the photoreceptor. Cell. 91, 543-553.
Frey, D., et al., 2000. Early and selective loss of neuromuscular synapse subtypes with low sprouting competence in motoneuron diseases. Journal of Neuroscience. 20, 2534-2542.
Frost, B., Diamond, M. I., 2010. Prion-like mechanisms in neurodegenerative diseases. Nat Rev Neurosci. 11, 155-9.
Fu, Y., et al., 2013. High-frequency off-target mutagenesis induced by CRISPR-Cas nucleases in human cells. Nat Biotechnol. 31, 822-6.
Fujieda, H., et al., 2009. Retinoic acid receptor-related orphan receptor alpha regulates a subset of cone genes during mouse retinal development. J Neurochem. 108, 91-101.
Fung, J., et al., 2011. Nucleoside/nucleotide analogues in the treatment of chronic hepatitis B. Journal of Antimicrobial Chemotherapy. 66, 2715-2725.
Furukawa, A., et al., 2002. The mouse Crx 5'-upstream transgene sequence directs cell-specific and developmentally regulated expression in retinal photoreceptor cells. J Neurosci. 22, 1640-7.
Furukawa, T., et al., 1997a. rax, a novel paired-type homeobox gene, shows expression in the anterior neural fold and developing retina. Proc Natl Acad Sci U S A. 94, 3088-93.
Furukawa, T., et al., 1997b. Crx, a novel otx-like homeobox gene, shows photoreceptor-specific expression and regulates photoreceptor differentiation. Cell. 91, 531-541.
Furukawa, T., et al., 1999. Retinopathy and attenuated circadian entrainment in Crx-deficient mice. Nat Genet. 23, 466-70.
Furukawa, Y., et al., 2011. A seeding reaction recapitulates intracellular formation of Sarkosyl-insoluble transactivation response element (TAR) DNA-binding protein-43 inclusions. J Biol Chem. 286, 18664-72.
Furukawa, Y., et al., 2013. Intracellular seeded aggregation of mutant Cu,Zn-superoxide dismutase associated with amyotrophic lateral sclerosis. Febs Letters. 587, 2500-2505.
Fushimi, K., et al., 2011. Expression of human FUS/TLS in yeast leads to protein aggregation and cytotoxicity, recapitulating key features of FUS proteinopathy. Protein & Cell. 2, 141-149.

Gajavelli, S., et al., 2004. BMP signaling initiates a neural crest differentiation program in embryonic rat CNS stem cells. Exp Neurol. 188**,** 205-23.
Galbiati, M., et al., 2012. The anabolic/androgenic steroid nandrolone exacerbates gene expression modifications induced by mutant SOD1 in muscles of mice models of amyotrophic lateral sclerosis. Pharmacol Res. 65**,** 221-30.
Gamborino, M. J., et al., 2001. Role of thyroid hormone in craniofacial and eye development using a rat model. Ophthalmic Res. 33**,** 283-91.
Gamm, D. M., et al., 2015. Report on the National Eye Institute Audacious Goals Initiative: Photoreceptor Regeneration and Integration Workshop. Transl Vis Sci Technol. 4**,** 2.
Gamse, J. T., et al., 2002. Otx5 regulates genes that show circadian expression in the zebrafish pineal complex. Nat Genet. 30**,** 117-21.
Garrity, D. M., et al., 2002. The heartstrings mutation in zebrafish causes heart/fin Tbx5 deficiency syndrome. Development. 129**,** 4635-45.
Gassman, A., et al., 2013. Small molecule suppressors of Drosophila kinesin deficiency rescue motor axon development in a zebrafish model of spinal muscular atrophy. PLoS One. 8**,** e74325.
Gauthier, K., et al., 1999. Different functions for the thyroid hormone receptors TRalpha and TRbeta in the control of thyroid hormone production and post-natal development. EMBO J. 18**,** 623-31.
Gazit, E., 2002. A possible role for pi-stacking in the self-assembly of amyloid fibrils. Faseb Journal. 16**,** 77-83.
Gemberling, M., et al., 2013. The zebrafish as a model for complex tissue regeneration. Trends in Genetics. 29**,** 611-620.
Gerber, P. R., Muller, K., 1995. Mab, a Generally Applicable Molecular-Force Field for Structure Modeling in Medicinal Chemistry. Journal of Computer-Aided Molecular Design. 9**,** 251-268.
Gibson-Brown, J. J., et al., 1996. Evidence of a role for T-box genes in the evolution of limb morphogenesis and the specification of forelimb/hindlimb identity. Mech Dev. 56**,** 93-101.
Gibson-Brown, J. J., et al., 1998a. Involvement of T-box genes Tbx2-Tbx5 in vertebrate limb specification and development. Development. 125**,** 2499-509.
Gibson-Brown, J. J., et al., 1998b. Expression of T-box genes Tbx2-Tbx5 during chick organogenesis. Mech Dev. 74**,** 165-9.
Gilbert, M. J., et al., 2013. Zebrafish (Danio rerio) as a model for the study of aging and exercise: Physical ability and trainability decreases with age. Exp Gerontol.
Gitcho, M. A., et al., 2008. TDP-43 A315T mutation in familial motor neuron disease. Annals of Neurology. 63**,** 535-538.
Glaschke, A., et al., 2010. Developmental Changes of Cone Opsin Expression but Not Retinal Morphology in the Hypothyroid Pax8 Knockout Mouse. Investigative Ophthalmology & Visual Science. 51**,** 1719-1727.
Glaschke, A., et al., 2011. Thyroid hormone controls cone opsin expression in the retina of adult rodents. J Neurosci. 31**,** 4844-51.
Golde, T. E., et al., 2013. Thinking laterally about neurodegenerative proteinopathies. J Clin Invest. 123**,** 1847-55.
Goldshmit, Y., et al., 2012. Fgf-dependent glial cell bridges facilitate spinal cord regeneration in zebrafish. J Neurosci. 32**,** 7477-92.

Gong, Y. H., et al., 2000. Restricted expression of G86R Cu/Zn superoxide dismutase in astrocytes results in astrocytosis but does not cause motoneuron degeneration. Journal of Neuroscience. 20**,** 660-665.
Gonzalez-Cordero, A., et al., 2017. Recapitulation of Human Retinal Development from Human Pluripotent Stem Cells Generates Transplantable Populations of Cone Photoreceptors. Stem Cell Reports. 9**,** 820-837.
Gonzalez-Rodriguez, J., et al., 2010. Mutational screening of CHX10, GDF6, OTX2, RAX and SOX2 genes in 50 unrelated microphthalmia-anophthalmia-coloboma (MAC) spectrum cases. Br J Ophthalmol. 94**,** 1100-4.
Gorsuch, R. A., Hyde, D. R., 2014. Regulation of Müller glial dependent neuronal regeneration in the damaged adult zebrafish retina. Experimental Eye Research. 123**,** 131-140.
Gosse, N. J., Baier, H., 2009. An essential role for Radar (Gdf6a) in inducing dorsal fate in the zebrafish retina. Proc Natl Acad Sci U S A. 106**,** 2236-41.
Goutel, C., et al., 2000. The ventralizing activity of Radar, a maternally expressed bone morphogenetic protein, reveals complex bone morphogenetic protein interactions controlling dorso-ventral patterning in zebrafish. Mech Dev. 99**,** 15-27.
Grad, L. I., et al., 2015. From molecule to molecule and cell to cell: prion-like mechanisms in amyotrophic lateral sclerosis. Neurobiol Dis. 77**,** 257-65.
Grad, L. I., et al., 2011. Intermolecular transmission of superoxide dismutase 1 misfolding in living cells. Proceedings of the National Academy of Sciences of the United States of America. 108**,** 16398-16403.
Grad, L. I., et al., 2013. Intercellular propagated misfolding of wild-type Cu-Zn superoxide dismutase. Prion. 7**,** 76-76.
Graff, J. M., 1997. Embryonic patterning: to BMP or not to BMP, that is the question. Cell. 89**,** 171-4.
Graff, J. M., et al., 1996. Xenopus Mad proteins transduce distinct subsets of signals for the TGF beta superfamily. Cell. 85**,** 479-87.
Graffmo, K. S., et al., 2013. Expression of wild-type human superoxide dismutase-1 in mice causes amyotrophic lateral sclerosis. Hum Mol Genet. 22**,** 51-60.
Griesinger, I. B., et al., 2000. Autosomal dominant macular atrophy at 6q14 excludes CORD7 and MCDR1/PBCRA loci. Invest Ophthalmol Vis Sci. 41**,** 248-55.
Griffith, A. J., et al., 2002. Knock-in mouse model for resistance to thyroid hormone (RTH): an RTH mutation in the thyroid hormone receptor beta gene disrupts cochlear morphogenesis. J Assoc Res Otolaryngol. 3**,** 279-88.
Grindley, J. C., et al., 1995. The role of Pax-6 in eye and nasal development. Development. 121**,** 1433-42.
Gross, J. M., Dowling, J. E., 2005a. Tbx2b is essential for neuronal differentiation along the dorsal/ventral axis of the zebrafish retina. Proceedings of the National Academy of Sciences of the United States of America. 102**,** 4371-4376.
Gross, J. M., Dowling, J. E., 2005b. Tbx2b is essential for neuronal differentiation along the dorsal/ventral axis of the zebrafish retina. Proc Natl Acad Sci U S A. 102**,** 4371-6.
Gruzman, A., et al., 2007. Common molecular signature in SOD1 for both sporadic and familial amyotrophic lateral sclerosis. Proc Natl Acad Sci U S A. 104**,** 12524-9.
Guest, W. C., et al., 2011. Generalization of the prion hypothesis to other neurodegenerative diseases: an imperfect fit. J Toxicol Environ Health A. 74**,** 1433-59.

Guo, C., et al., 2014. Intrinsic expression of a multiexon type 3 deiodinase gene controls zebrafish embryo size. Endocrinology. 155**,** 4069-80.
Gupta, V., et al., 2016. One protein, multiple pathologies: multifaceted involvement of amyloid beta in neurodegenerative disorders of the brain and retina. Cell Mol Life Sci. 73**,** 4279-4297.
Gurney, M. E., et al., 1994. Motor-Neuron Degeneration in Mice That Express a Human Cu,Zn Superoxide-Dismutase Mutation. Science. 264**,** 1772-1775.
Haass, C., Selkoe, D. J., 2007. Soluble protein oligomers in neurodegeneration: lessons from the Alzheimer's amyloid beta-peptide. Nat Rev Mol Cell Biol. 8**,** 101-12.
Habets, P. E. M. H., et al., 2002. Cooperative action of Tbx2 and Nkx2.5 inhibits ANF expression in the atrioventricular canal: implications for cardiac chamber formation. Genes & Development. 16**,** 1234-1246.
Hafler, B. P., et al., 2012. Transcription factor Olig2 defines subpopulations of retinal progenitor cells biased toward specific cell fates. Proc Natl Acad Sci U S A. 109**,** 7882-7.
Hagerman, G. F., et al., 2016. Rapid Recovery of Visual Function Associated with Blue Cone Ablation in Zebrafish. Plos One. 11.
Hall, C. J., et al., 2002. Radar is required for the establishment of vascular integrity in the zebrafish. Dev Biol. 251**,** 105-17.
Halliwell, B., 2006. Oxidative stress and neurodegeneration: where are we now? J Neurochem. 97**,** 1634-58.
Hamaoka, T., et al., 2002. Visualization of rod photoreceptor development using GFP-transgenic zebrafish. Genesis. 34**,** 215-20.
Han, S. S. W., et al., 2011. Constructing and Deconstructing Stem Cell Models of Neurological Disease. Neuron. 70**,** 626-644.
Hanel, M. L., Hensey, C., 2006. Eye and neural defects associated with loss of GDF6. BMC Dev Biol. 6**,** 43.
Hansen, C., et al., 1998. Novel 4-bp insertion in exon 5 of the CuZn superoxide dismutase (SOD1) gene associated with familial amyotrophic lateral sclerosis. Human Mutation. S327-S328.
Hanwell, D., et al., 2016. Restrictions on the Importation of Zebrafish into Canada Associated with Spring Viremia of Carp Virus. Zebrafish. 13 Suppl 1**,** S153-63.
Hao, H., et al., 2012. Transcriptional Regulation of Rod Photoreceptor Homeostasis Revealed by In Vivo NRL Targetome Analysis. Plos Genetics. 8**,** 380-394.
Harraz, M. M., et al., 2008. SOD1 mutations disrupt redox-sensitive Rac regulation of NADPH oxidase in a familial ALS model. J Clin Invest. 118**,** 659-70.
Harrelson, Z., et al., 2004. Tbx2 is essential for patterning the atrioventricular canal and for morphogenesis of the outflow tract during heart development. Development. 131**,** 5041-5052.
Harvey, C. B., Williams, G. R., 2002. Mechanism of thyroid hormone action. Thyroid. 12**,** 441-446.
Hasegawa, M., et al., 2008. Phosphorylated TDP-43 in frontotemporal lobar degeneration and amyotrophic lateral sclerosis. Annals of Neurology. 64**,** 60-70.
Hashimoto, K., et al., 2001. An unliganded thyroid hormone receptor causes severe neurological dysfunction. Proc Natl Acad Sci U S A. 98**,** 3998-4003.
Hashimoto, Y., et al., 2005. Transforming growth factor beta2 is a neuronal death-inducing ligand for amyloid-beta precursor protein. Mol Cell Biol. 25**,** 9304-17.

Havis, E., et al., 2006. Unliganded thyroid hormone receptor is essential for Xenopus laevis eye development. Embo Journal. 25**,** 4943-4951.
Hawryshyn, C. W., 2003. Regeneration of ultraviolet-sensitive cones in the retinal cone mosaic of thyroxin-challenged post-juvenile rainbow trout (Oncorhynchus mykiss). Journal of Experimental Biology. 206**,** 2665-2673.
Hayata, T., et al., 1999. Expression of Xenopus T-box transcription factor, tbx2 in Xenopus embryo. Dev Genes Evol. 209**,** 625-8.
Hayes, K. C., 1974. Pathophysiology of vitamin E deficiency in monkeys. Am J Clin Nutr. 27**,** 1130-40.
Heisenberg, C. P., et al., 2001. A mutation in the Gsk3-binding domain of zebrafish Masterblind/Axin1 leads to a fate transformation of telencephalon and eyes to diencephalon. Genes Dev. 15**,** 1427-34.
Hennig, A. K., et al., 2008. Regulation of photoreceptor gene expression by Crx-associated transcription factor network. Brain Res. 1192**,** 114-33.
Henrique, D., et al., 1997. Maintenance of neuroepithelial progenitor cells by Delta-Notch signalling in the embryonic chick retina. Curr Biol. 7**,** 661-70.
Henriquez, J. P., et al., 2011. The Wnt and BMP families of signaling morphogens at the vertebrate neuromuscular junction. Int J Mol Sci. 12**,** 8924-46.
Hernandez-Zimbron, L. F., et al., 2018. Age-Related Macular Degeneration: New Paradigms for Treatment and Management of AMD. Oxid Med Cell Longev. 2018**,** 8374647.
Herpin, A., et al., 2004. Transforming growth factor-beta-related proteins: an ancestral and widespread superfamily of cytokines in metazoans. Dev Comp Immunol. 28**,** 461-85.
Herrmann, B. G., et al., 1990. Cloning of the T gene required in mesoderm formation in the mouse. Nature. 343**,** 617-22.
Herrmann, B. G., Lehrach, H., 1988. From phenotype to gene: molecular cloning in the Brachyury (T) locus region. Curr Top Microbiol Immunol. 137**,** 77-81.
Hetz, C., Mollereau, B., 2014. Disturbance of endoplasmic reticulum proteostasis in neurodegenerative diseases. Nat Rev Neurosci. 15**,** 233-49.
Hewamadduma, C. A., et al., 2013. Tardbpl splicing rescues motor neuron and axonal development in a mutant tardbp zebrafish. Hum Mol Genet. 22**,** 2376-86.
Higashi, S., et al., 2010. TDP-43 physically interacts with amyotrophic lateral sclerosis-linked mutant CuZn superoxide dismutase. Neurochemistry International. 57**,** 906-913.
Hill, R. E., et al., 1991. Mouse small eye results from mutations in a paired-like homeobox-containing gene. Nature. 354**,** 522-5.
Hirano, A., et al., 1995. Craniofacial deformities associated with juvenile hyperthyroidism. Cleft Palate Craniofac J. 32**,** 328-33.
Hocking, J. C., et al., 2008. TGFbeta ligands promote the initiation of retinal ganglion cell dendrites in vitro and in vivo. Mol Cell Neurosci. 37**,** 247-60.
Hodin, R. A., et al., 1989. Identification of a thyroid hormone receptor that is pituitary-specific. Science. 244**,** 76-9.
Hoodless, P. A., et al., 1996. MADR1, a MAD-related protein that functions in BMP2 signaling pathways. Cell. 85**,** 489-500.
Hoover, F., et al., 1998. Retinoid X receptor gamma gene transcripts are expressed by a subset of early generated retinal cells and eventually restricted to photoreceptors. Journal of Comparative Neurology. 391**,** 204-213.

Hopiavuori, B. R., et al., 2018. Homozygous Expression of Mutant ELOVL4 Leads to Seizures and Death in a Novel Animal Model of Very Long-Chain Fatty Acid Deficiency. Mol Neurobiol. 55**,** 1795-1813.

Houbrechts, A. M., et al., 2016. Deiodinase knockdown affects zebrafish eye development at the level of gene expression, morphology and function. Mol Cell Endocrinol. 424**,** 81-93.

Hough, M. A., et al., 2004. Dimer destabilization in superoxide dismutase may result in disease-causing properties: Structures of motor neuron disease mutants. Proceedings of the National Academy of Sciences. 101**,** 5976-5981.

Howland, D. S., et al., 2002. Focal loss of the glutamate transporter EAAT2 in a transgenic rat model of SOD1 mutant-mediated amyotrophic lateral sclerosis (ALS). Proceedings of the National Academy of Sciences of the United States of America. 99**,** 1604-1609.

Huang, C., et al., 2012. Mutant TDP-43 in motor neurons promotes the onset and progression of ALS in rats. Journal of Clinical Investigation. 122**,** 107-118.

Huang, C., et al., 2011. FUS Transgenic Rats Develop the Phenotypes of Amyotrophic Lateral Sclerosis and Frontotemporal Lobar Degeneration. Plos Genetics. 7.

Huey, E. D., et al., 2012. FUS and TDP43 genetic variability in FTD and CBS. Neurobiology of Aging. 33.

Hurley, F. M., et al., 2004. Neuroprotective effects of delayed administration of growth/differentiation factor-5 in the partial lesion model of Parkinson's disease. Exp Neurol. 185**,** 281-9.

Hyatt, G. A., et al., 1996. Retinoic acid alters photoreceptor development in vivo. Proc Natl Acad Sci U S A. 93**,** 13298-303.

Hyttinen, J. M. T., et al., 2017. DNA damage response and autophagy in the degeneration of retinal pigment epithelial cells-Implications for age-related macular degeneration (AMD). Ageing Res Rev. 36**,** 64-77.

Igaz, L. M., et al., 2011a. Dysregulation of the ALS-associated gene TDP-43 leads to neuronal death and degeneration in mice. J Clin Invest. 121**,** 726-38.

Igaz, L. M., et al., 2011b. Dysregulation of the ALS-associated gene TDP-43 leads to neuronal death and degeneration in mice. Journal of Clinical Investigation. 121**,** 726-738.

Iida, A., et al., 2012. Optineurin mutations in Japanese amyotrophic lateral sclerosis. J Neurol Neurosurg Psychiatry. 83**,** 233-5.

Ino, H., 2003. Antigen retrieval by heating en bloc for pre-fixed frozen material. J Histochem Cytochem. 51**,** 995-1003.

Ip, P., et al., 2011. ALS-causing SOD1 mutations promote production of copper-deficient misfolded species. J Mol Biol. 409**,** 839-52.

Ivannikov, M. V., Van Remmen, H., 2015. Sod1 gene ablation in adult mice leads to physiological changes at the neuromuscular junction similar to changes that occur in old wild-type mice. Free Radic Biol Med. 84**,** 254-262.

Jaarsma, D., et al., 2000. Human Cu/Zn superoxide dismutase (SOD1) overexpression in mice causes mitochondrial vacuolization, axonal degeneration, and premature motoneuron death and accelerates motoneuron disease in mice expressing a familial amyotrophic lateral sclerosis mutant SOD1. Neurobiology of Disease. 7**,** 623-643.

Jaarsma, D., et al., 2008. Neuron-specific expression of mutant superoxide dismutase is sufficient to induce amyotrophic lateral sclerosis in transgenic mice. Journal of Neuroscience. 28**,** 2075-2088.

Jacobs, J. J. L., et al., 2000. Senescence bypass screen identifies TBX2, which represses Cdkn2a (p19(ARF)) and is amplified in a subset of human breast cancers. Nature Genetics. 26**,** 291-299.
Jacobsson, J., et al., 2001. Superoxide dismutase in CSF from amyotrophic lateral sclerosis patients with and without CuZn-superoxide dismutase mutations. Brain. 124**,** 1461-1466.
Jadhav, A. P., et al., 2006. Notch 1 inhibits photoreceptor production in the developing mammalian retina. Development. 133**,** 913-23.
Jakalian, A., et al., 2000. Fast, efficient generation of high-quality atomic Charges. AM1-BCC model: I. Method. Journal of Computational Chemistry. 21**,** 132-146.
Jakalian, A., et al., 2002. Fast, efficient generation of high-quality atomic charges. AM1-BCC model: II. Parameterization and validation. Journal of Computational Chemistry. 23**,** 1623-1641.
James, R. E., Broihier, H. T., 2011. Crimpy inhibits the BMP homolog Gbb in motoneurons to enable proper growth control at the Drosophila neuromuscular junction. Development. 138**,** 3273-86.
Jarrett, J. T., Lansbury, P. T., Jr., 1993. Seeding "one-dimensional crystallization" of amyloid: a pathogenic mechanism in Alzheimer's disease and scrapie? Cell. 73**,** 1055-8.
Jia, L., et al., 2009a. Retinoid-related orphan nuclear receptor RORbeta is an early-acting factor in rod photoreceptor development. Proc Natl Acad Sci U S A. 106**,** 17534-9.
Jia, L., et al., 2009b. Retinoid-related orphan nuclear receptor ROR beta is an early-acting factor in rod photoreceptor development. Proceedings of the National Academy of Sciences of the United States of America. 106**,** 17534-17539.
Johnson, D. A., et al., 2006. Mosaic deletion of Rb arrests rod differentiation and stimulates ectopic synaptogenesis in the mouse retina. Journal of Comparative Neurology. 498**,** 112-128.
Johnston, R. J., Jr., et al., 2011. Interlocked feedforward loops control cell-type-specific Rhodopsin expression in the Drosophila eye. Cell. 145**,** 956-68.
Jones, I., et al., 2002. Molecular cloning and expression of thyroid hormone receptor alpha during salmonid development. Gen Comp Endocrinol. 125**,** 226-35.
Jonsson, P. A., et al., 2004. Minute quantities of misfolded mutant superoxide dismutase-1 cause amyotrophic lateral sclerosis. Brain. 127**,** 73-88.
Jonsson, P. A., et al., 2006a. Disulphide-reduced superoxide dismutase-1 in CNS of transgenic amyotrophic lateral sclerosis models. Brain. 129**,** 451-464.
Jonsson, P. A., et al., 2006b. Motor neuron disease in mice expressing the wild type-like D90A mutant superoxide dismutase-1. Journal of Neuropathology and Experimental Neurology. 65**,** 1126-1136.
Jucker, M., Walker, L. C., 2013. Self-propagation of pathogenic protein aggregates in neurodegenerative diseases. Nature. 501**,** 45-51.
Jusuf, P. R., et al., 2012. Biasing amacrine subtypes in the Atoh7 lineage through expression of Barhl2. J Neurosci. 32**,** 13929-44.
Jusuf, P. R., et al., 2011. Origin and determination of inhibitory cell lineages in the vertebrate retina. J Neurosci. 31**,** 2549-62.
Kabashi, E., et al., 2011. FUS and TARDBP but not SOD1 interact in genetic models of amyotrophic lateral sclerosis. PLoS Genet. 7**,** e1002214.
Kabashi, E., et al., 2010. Gain and loss of function of ALS-related mutations of TARDBP (TDP-43) cause motor deficits in vivo. Hum Mol Genet. 19**,** 671-83.

Kahlem, P., Newfeld, S. J., 2009. Informatics approaches to understanding TGFbeta pathway regulation. Development. 136, 3729-40.
Kaiser, D. M., et al., 2012. Amyloid beta precursor protein and prion protein have a conserved interaction affecting cell adhesion and CNS development. PLoS One. 7, e51305.
Kakizawa, T., et al., 2007. Two differentially active alternative promoters control the expression of the zebrafish orphan nuclear receptor gene Rev-erbalpha. J Mol Endocrinol. 38, 555-68.
Kalueff, A. V., et al., 2013. Towards a comprehensive catalog of zebrafish behavior 1.0 and beyond. Zebrafish. 10, 70-86.
Kane, M. D., et al., 2000. Evidence for seeding of beta -amyloid by intracerebral infusion of Alzheimer brain extracts in beta -amyloid precursor protein-transgenic mice. J Neurosci. 20, 3606-11.
Kaneshige, M., et al., 2000. Mice with a targeted mutation in the thyroid hormone beta receptor gene exhibit impaired growth and resistance to thyroid hormone. Proc Natl Acad Sci U S A. 97, 13209-14.
Kanyo, R., et al., 2011. Adrenergic Regulation of the Distribution of Transducer of Regulated cAMP-Response Element-Binding Protein (TORC2) in Rat Pinealocytes. Endocrinology. 152, 3440-3450.
Kashlan, O. N., et al., 2015. Histological Bulbar Manifestations in the ALS Rat. Neurodegenerative Diseases. 15, 121-126.
Kaslin, J., et al., 2008. Proliferation, neurogenesis and regeneration in the non-mammalian vertebrate brain. Philos Trans R Soc Lond B Biol Sci. 363, 101-22.
Kassen, S. C., et al., 2007. Time course analysis of gene expression during light-induced photoreceptor cell death and regeneration in albino zebrafish. Dev Neurobiol. 67, 1009-31.
Katoh, K., et al., 2010. Blimp1 suppresses Chx10 expression in differentiating retinal photoreceptor precursors to ensure proper photoreceptor development. J Neurosci. 30, 6515-26.
Katsuno, M., et al., 2011. Transforming growth factor-beta signaling in motor neuron diseases. Curr Mol Med. 11, 48-56.
Kaufman, C. K., et al., 2009. Chemical genetic screening in the zebrafish embryo. Nat Protoc. 4, 1422-32.
Kauppinen, A., et al., 2016. Inflammation and its role in age-related macular degeneration. Cell Mol Life Sci. 73, 1765-86.
Kay, J. N., et al., 2011. Neurod6 expression defines new retinal amacrine cell subtypes and regulates their fate. Nat Neurosci. 14, 965-72.
Kelley, M. W., et al., 1995. Ligands of steroid/thyroid receptors induce cone photoreceptors in vertebrate retina. Development. 121, 3777-85.
Kennel, P. F., et al., 1996. Neuromuscular function impairment is not caused by motor neurone loss in FALS mice: An electromyographic study. Neuroreport. 7, 1427-1431.
Kerman, A., et al., 2010. Amyotrophic lateral sclerosis is a non-amyloid disease in which extensive misfolding of SOD1 is unique to the familial form. Acta Neuropathologica. 119, 335-344.
Kersten, H. M., et al., 2015. Optical coherence tomography findings in Huntington's disease: a potential biomarker of disease progression. J Neurol. 262, 2457-65.
Khan, M. A. I., et al., 2017. Cu/Zn Superoxide Dismutase Forms Amyloid Fibrils under Near Physiological Quiescent Conditions: The Roles of Disulfide Bonds and Effects of Denaturant. Acs Chemical Neuroscience. 8, 2019-2026.

Khuansuwan, S., et al., 2016. A transcription factor network controls cell migration and fate decisions in the developing zebrafish pineal complex. Development. 143**,** 2641-50.
Kiecker, C., Niehrs, C., 2001. A morphogen gradient of Wnt/beta-catenin signalling regulates anteroposterior neural patterning in Xenopus. Development. 128**,** 4189-201.
Kieran, D., et al., 2004. Treatment with arimoclomol, a coinducer of heat shock proteins, delays disease progression in ALS mice. Nat Med. 10**,** 402-5.
Kim, H. T., Kim, J. W., 2012. Compartmentalization of vertebrate optic neuroephithelium: external cues and transcription factors. Mol Cells. 33**,** 317-24.
Kim, J., et al., 2014. Dimerization, oligomerization, and aggregation of human amyotrophic lateral sclerosis copper/zinc superoxide dismutase 1 protein mutant forms in live cells. J Biol Chem. 289**,** 15094-103.
Kim, J., et al., 2005. GDF11 controls the timing of progenitor cell competence in developing retina. Science. 308**,** 1927-30.
Kim, J. W., et al., 2016. Recruitment of Rod Photoreceptors from Short-Wavelength-Sensitive Cones during the Evolution of Nocturnal Vision in Mammals. Dev Cell. 37**,** 520-32.
King, A., et al., 2013. Mixed tau, TDP-43 and p62 pathology in FTLD associated with a C9ORF72 repeat expansion and p.Ala239Thr MAPT (tau) variant. Acta Neuropathologica. 125**,** 303-310.
Kiskinis, E., et al., 2014. Pathways Disrupted in Human ALS Motor Neurons Identified through Genetic Correction of Mutant SOD1. Cell Stem Cell. 14**,** 781-795.
Kizil, C., et al., 2012. Adult neurogenesis and brain regeneration in zebrafish. Dev Neurobiol. 72**,** 429-61.
Klein, W. L., et al., 2001. Targeting small Abeta oligomers: the solution to an Alzheimer's disease conundrum? Trends Neurosci. 24**,** 219-24.
Koike, C., et al., 2007. Functional roles of Otx2 transcription factor in postnatal mouse retinal development. Mol Cell Biol. 27**,** 8318-29.
Kondo, T., et al., 1997. Reduction of CuZn-superoxide dismutase activity exacerbates neuronal cell injury and edema formation after transient focal cerebral ischemia. J Neurosci. 17**,** 4180-9.
Koronyo-Hamaoui, M., et al., 2011. Identification of amyloid plaques in retinas from Alzheimer's patients and noninvasive in vivo optical imaging of retinal plaques in a mouse model. Neuroimage. 54 Suppl 1**,** S204-17.
Koshiba-Takeuchi, K., et al., 2000. Tbx5 and the retinotectum projection. Science. 287**,** 134-7.
Krieglstein, K., et al., 2002. TGF-beta and the regulation of neuron survival and death. J Physiol Paris. 96**,** 25-30.
Kroehne, V., et al., 2011. Regeneration of the adult zebrafish brain from neurogenic radial glia-type progenitors. Development. 138**,** 4831-41.
Kruminis-Kaszkiel, E., et al., 2018. CRISPR/Cas9 Technology as an Emerging Tool for Targeting Amyotrophic Lateral Sclerosis (ALS). Int J Mol Sci. 19.
Kumar, V., et al., 2017. Computing disease-linked SOD1 mutations: deciphering protein stability and patient-phenotype relations. Scientific Reports. 7.
Kusne, Y., et al., 2017. Visual system manifestations of Alzheimer's disease. Acta Ophthalmol. 95**,** e668-e676.
Kwan, K. M., et al., 2007. The Tol2kit: A multisite Gateway-based construction kit for Tol2 transposon transgenesis constructs. Developmental Dynamics. 236**,** 3088-3099.

Kwiatkowski, T. J., et al., 2009. Mutations in the FUS/TLS Gene on Chromosome 16 Cause Familial Amyotrophic Lateral Sclerosis. Science. 323, 1205-1208.
La Spada, A. R., et al., 2001. Polyglutamine-expanded ataxin-7 antagonizes CRX function and induces cone-rod dystrophy in a mouse model of SCA7. Neuron. 31, 913-27.
Lagier-Tourenne, C., Cleveland, D. W., 2009. Rethinking ALS: the FUS about TDP-43. Cell. 136, 1001-4.
Lagier-Tourenne, C., Cleveland, D. W., 2010. NEURODEGENERATION An expansion in ALS genetics. Nature. 466, 1052-1053.
Lagier-Tourenne, C., et al., 2010. TDP-43 and FUS/TLS: emerging roles in RNA processing and neurodegeneration. Human Molecular Genetics. 19, R46-R64.
Laird, A. S., et al., 2010. Progranulin is neurotrophic in vivo and protects against a mutant TDP-43 induced axonopathy. PLoS One. 5, e13368.
Lakowski, J., et al., 2010. Cone and rod photoreceptor transplantation in models of the childhood retinopathy Leber congenital amaurosis using flow-sorted Crx-positive donor cells. Hum Mol Genet. 19, 4545-59.
Lakowski, J., et al., 2011. Effective transplantation of photoreceptor precursor cells selected via cell surface antigen expression. Stem Cells. 29, 1391-404.
Lakowski, J., et al., 2007. Mechanisms controlling Pax6 isoform expression in the retina have been conserved between teleosts and mammals. Dev Biol. 307, 498-520.
Lamba, D., et al., 2008a. Neural regeneration and cell replacement: a view from the eye. Cell Stem Cell. 2, 538-49.
Lamba, D., et al., 2008b. Neural regeneration and cell replacement: A view from the eye. Cell Stem Cell. 2, 538-549.
Lambert, M. P., et al., 1998. Diffusible, nonfibrillar ligands derived from Abeta1-42 are potent central nervous system neurotoxins. Proc Natl Acad Sci U S A. 95, 6448-53.
Lanson, N. A., et al., 2011. A Drosophila model of FUS-related neurodegeneration reveals genetic interaction between FUS and TDP-43. Human Molecular Genetics. 20, 2510-2523.
Larison, K. D., Bremiller, R., 1990. Early onset of phenotype and cell patterning in the embryonic zebrafish retina. Development. 109, 567-76.
Lattante, S., et al., 2015. Defining the genetic connection linking amyotrophic lateral sclerosis (ALS) with frontotemporal dementia (FTD). Trends in Genetics. 31, 263-273.
Lau, A., Tymianski, M., 2010. Glutamate receptors, neurotoxicity and neurodegeneration. Pflugers Arch. 460, 525-42.
Legent, K., Treisman, J. E., 2008. Wingless signaling in Drosophila eye development. Methods Mol Biol. 469, 141-61.
Lekven, A. C., et al., 2001. Zebrafish wnt8 encodes two wnt8 proteins on a bicistronic transcript and is required for mesoderm and neurectoderm patterning. Dev Cell. 1, 103-14.
Lemmens, R., et al., 2007. Overexpression of mutant superoxide dismutase 1 causes a motor axonopathy in the zebrafish. Hum Mol Genet. 16, 2359-65.
Lenkowski, J. R., et al., 2013. Retinal regeneration in adult zebrafish requires regulation of TGFbeta signaling. Glia. 61, 1687-97.
Lenox, A. R., et al., 2015. Unfolded protein response is activated in aged retinas. Neurosci Lett. 609, 30-5.
Lepock, J. R., et al., 1990. Contribution of Conformational Stability and Reversibility of Unfolding to the Increased Thermostability of Human and Bovine Superoxide-Dismutase Mutated at Free Cysteines. Journal of Biological Chemistry. 265, 21612-21618.

Lewis, C. M., Suzuki, M., 2014. Therapeutic applications of mesenchymal stem cells for amyotrophic lateral sclerosis. Stem Cell Res Ther. 5**,** 32.
Lewis, K. E., Eisen, J. S., 2003. From cells to circuits: development of the zebrafish spinal cord. Prog Neurobiol. 69**,** 419-49.
Li, C., et al., 2015. Optineurin mutations in patients with sporadic amyotrophic lateral sclerosis in China. Amyotroph Lateral Scler Frontotemporal Degener. 16**,** 485-9.
Li, C., et al., 2011. Astrocytes: implications for neuroinflammatory pathogenesis of Alzheimer's disease. Curr Alzheimer Res. 8**,** 67-80.
Li, J., et al., 2013. Establishing a novel C. elegans model to investigate the role of autophagy in amyotrophic lateral sclerosis. Acta Pharmacologica Sinica. 34**,** 644-650.
Li, Y. X., et al., 2000. Double-stranded RNA injection produces null phenotypes in zebrafish. Dev Biol. 217**,** 394-405.
Liachko, N. F., et al., 2010. Phosphorylation Promotes Neurotoxicity in a Caenorhabditis elegans Model of TDP-43 Proteinopathy. Journal of Neuroscience. 30**,** 16208-16219.
Lieschke, G. J., Currie, P. D., 2007. Animal models of human disease: zebrafish swim into view. Nature Reviews Genetics. 8**,** 353-367.
Lin, M. T., Beal, M. F., 2006. Mitochondrial dysfunction and oxidative stress in neurodegenerative diseases. Nature. 443**,** 787-95.
Ling, S. C., et al., 2010a. ALS-associated mutations in TDP-43 increase its stability and promote TDP-43 complexes with FUS/TLS. Proc Natl Acad Sci U S A. 107**,** 13318-23.
Ling, S. C., et al., 2010b. ALS-associated mutations in TDP-43 increase its stability and promote TDP-43 complexes with FUS/TLS. Proceedings of the National Academy of Sciences of the United States of America. 107**,** 13318-13323.
Lingbeek, M. E., et al., 2002. The T-box repressors TBX2 and TBX3 specifically regulate the tumor suppressor gene p14ARF via a variant T-site in the initiator. J Biol Chem. 277**,** 26120-7.
Liu, H., et al., 2017. Retinoid-Related Orphan Receptor beta and Transcriptional Control of Neuronal Differentiation. Nuclear Receptors in Development and Disease. 125**,** 227-255.
Liu, H., et al., 2008. NeuroD1 regulates expression of thyroid hormone receptor 2 and cone opsins in the developing mouse retina. J Neurosci. 28**,** 749-56.
Liu, H., et al., 2013. An isoform of retinoid-related orphan receptor beta directs differentiation of retinal amacrine and horizontal interneurons. Nat Commun. 4**,** 1813.
Liu, Q., et al., 2007. Differential expression of photoreceptor-specific genes in the retina of a zebrafish cadherin2 mutant glass onion and zebrafish cadherin4 morphants. Exp Eye Res. 84**,** 163-75.
Liu, Y., et al., 2001. Isolation and characterization of a zebrafish homologue of the cone rod homeobox gene. Invest Ophthalmol Vis Sci. 42**,** 481-7.
Liu, Y. W., Chan, W. K., 2002. Thyroid hormones are important for embryonic to larval transitory phase in zebrafish. Differentiation. 70**,** 36-45.
Liu, Y. W., et al., 2000. Temporal expression and T3 induction of thyroid hormone receptors alpha1 and beta1 during early embryonic and larval development in zebrafish, Danio rerio. Mol Cell Endocrinol. 159**,** 187-95.
Livne-Bar, I., et al., 2006. Chx10 is required to block photoreceptor differentiation but is dispensable for progenitor proliferation in the postnatal retina. Proc Natl Acad Sci U S A. 103**,** 4988-93.

Llorens, F., et al., 2016. Identification of new molecular alterations in fatal familial insomnia. Hum Mol Genet. 25, 2417-2436.
Loosli, F., et al., 2003. Loss of eyes in zebrafish caused by mutation of chokh/rx3. EMBO Rep. 4, 894-9.
Loosli, F., et al., 2001. Medaka eyeless is the key factor linking retinal determination and eye growth. Development. 128, 4035-44.
Loosli, F., et al., 1999. Six3 overexpression initiates the formation of ectopic retina. Genes Dev. 13, 649-54.
Love, S., et al., Greenfield's Neuropathology. Set. A Hodder Arnold Publication. Oxford University Press, Incorporated,, New York, 2008, pp. 1 online resource (2400 p.).
Ludtke, T. H. W., et al., 2013. Tbx2 Controls Lung Growth by Direct Repression of the Cell Cycle Inhibitor Genes Cdkn1a and Cdkn1b. Plos Genetics. 9.
Lue, L. F., et al., 1999. Soluble amyloid beta peptide concentration as a predictor of synaptic change in Alzheimer's disease. Am J Pathol. 155, 853-62.
Luk, K. C., et al., 2012. Pathological alpha-synuclein transmission initiates Parkinson-like neurodegeneration in nontransgenic mice. Science. 338, 949-53.
Ma, H., et al., 2014. Suppressing thyroid hormone signaling preserves cone photoreceptors in mouse models of retinal degeneration. Proc Natl Acad Sci U S A. 111, 3602-7.
Ma, L., et al., 2005. Bmp2 is essential for cardiac cushion epithelial-mesenchymal transition and myocardial patterning. Development. 132, 5601-11.
Macias-Silva, M., et al., 1996. MADR2 is a substrate of the TGFbeta receptor and its phosphorylation is required for nuclear accumulation and signaling. Cell. 87, 1215-24.
Mackenzie, I. R., et al., 2007. Pathological TDP-43 distinguishes sporadic amyotrophic lateral sclerosis from amyotrophic lateral sclerosis with SOD1 mutations. Ann Neurol. 61, 427-34.
MacLaren, R. E., et al., 2006. Retinal repair by transplantation of photoreceptor precursors. Nature. 444, 203-7.
Magrane, J., et al., 2014. Abnormal mitochondrial transport and morphology are common pathological denominators in SOD1 and TDP43 ALS mouse models. Human Molecular Genetics. 23, 1413-1424.
Mahlamaki, E. H., et al., 2002. Frequent amplification of 8q24, 11q, 17q, and 20q-specific genes in pancreatic cancer. Genes Chromosomes Cancer. 35, 353-8.
Malinowski, D. P., Fridovich, I., 1979. Subunit Association and Side-Chain Reactivities of Bovine Erythrocyte Superoxide-Dismutase in Denaturing Solvents. Biochemistry. 18, 5055-5060.
Mandal, M. N., et al., 2004. Characterization of mouse orthologue of ELOVL4: genomic organization and spatial and temporal expression. Genomics. 83, 626-35.
Manning, L., et al., 2006. Regional morphogenesis in the hypothalamus: a BMP-Tbx2 pathway coordinates fate and proliferation through Shh downregulation. Dev Cell. 11, 873-85.
Mansergh, F. C., et al., 2010. Loss of photoreceptor potential from retinal progenitor cell cultures, despite improvements in survival. Exp Eye Res. 91, 500-12.
Marc, R. E., et al., 2007. Neural reprogramming in retinal degeneration. Investigative Ophthalmology & Visual Science. 48, 3364-3371.
Marchand, O., et al., 2001. Molecular cloning and characterization of thyroid hormone receptors in teleost fish. J Mol Endocrinol. 26, 51-65.

Marelli, F., et al., 2016. Patterns of thyroid hormone receptor expression in zebrafish and generation of a novel model of resistance to thyroid hormone action. Mol Cell Endocrinol. 424, 102-17.
Marquardt, T., et al., 2001. Pax6 is required for the multipotent state of retinal progenitor cells. Cell. 105, 43-55.
Marques, G., 2005. Morphogens and synaptogenesis in Drosophila. J Neurobiol. 64, 417-34.
Marques, G., et al., 2003. Retrograde Gbb signaling through the Bmp type 2 receptor wishful thinking regulates systemic FMRFa expression in Drosophila. Development. 130, 5457-70.
Marsh-Armstrong, N., et al., 2004. Thyroid hormone controls the development of connections between the spinal cord and limbs during Xenopus laevis metamorphosis. Proc Natl Acad Sci U S A. 101, 165-70.
Marsh-Armstrong, N., et al., 1994. Retinoic acid is necessary for development of the ventral retina in zebrafish. Proc Natl Acad Sci U S A. 91, 7286-90.
Martin, N., et al., 2012a. Physical and functional interaction between PML and TBX2 in the establishment of cellular senescence. Embo Journal. 31, 95-109.
Martin, N., et al., 2012b. Physical and functional interaction between PML and TBX2 in the establishment of cellular senescence. EMBO J. 31, 95-109.
Martinez-De Luna, R. I., et al., 2011. The Retinal Homeobox (Rx) gene is necessary for retinal regeneration. Dev Biol. 353, 10-8.
Maruyama, H., et al., 2010. Mutations of optineurin in amyotrophic lateral sclerosis. Nature. 465, 223-6.
Massague, J., 1996. TGFbeta signaling: receptors, transducers, and Mad proteins. Cell. 85, 947-50.
Mathers, P. H., et al., 1997. The Rx homeobox gene is essential for vertebrate eye development. Nature. 387, 603-7.
Matsukawa, T., et al., 2004. Axonal regeneration of fish optic nerve after injury. Biological & Pharmaceutical Bulletin. 27, 445-451.
Matsumoto, S., et al., 1996. Sporadic amyotrophic lateral sclerosis with dementia and Cu/Zn superoxide dismutase-positive Lewy body-like inclusions. Clin Neuropathol. 15, 41-6.
Matsuo, T., et al., 1993. A mutation in the Pax-6 gene in rat small eye is associated with impaired migration of midbrain crest cells. Nat Genet. 3, 299-304.
Matsushima, D., et al., 2011. Combinatorial regulation of optic cup progenitor cell fate by SOX2 and PAX6. Development. 138, 443-454.
Matus, S., et al., 2013. Functional contribution of the transcription factor ATF4 to the pathogenesis of amyotrophic lateral sclerosis. PLoS One. 8, e66672.
Maugeri, A., et al., 2004. A novel mutation in the ELOVL4 gene causes autosomal dominant Stargardt-like macular dystrophy. Invest Ophthalmol Vis Sci. 45, 4263-7.
Maurer, K. A., et al., 2014. Notch signaling differentially regulates Atoh7 and Neurog2 in the distal mouse retina. Development. 141, 3243-54.
Mays, C. E., et al., 2014. Prion disease tempo determined by host-dependent substrate reduction. J Clin Invest. 124, 847-58.
Mays, C. E., et al., 2015. Prion Infectivity Plateaus and Conversion to Symptomatic Disease Originate from Falling Precursor Levels and Increased Levels of Oligomeric PrPSc Species. J Virol. 89, 12418-26.

McAlary, L., et al., 2016. Susceptibility of Mutant SOD1 to Form a Destabilized Monomer Predicts Cellular Aggregation and Toxicity but Not In vitro Aggregation Propensity. Front Neurosci. 10**,** 499.
McCabe, B. D., et al., 2003. The BMP homolog Gbb provides a retrograde signal that regulates synaptic growth at the Drosophila neuromuscular junction. Neuron. 39**,** 241-54.
McCaffery, P., et al., 1999. Dorsal and ventral retinal territories defined by retinoic acid synthesis, break-down and nuclear receptor expression. Mech Dev. 82**,** 119-30.
McCaffrery, P., et al., 1993. Changing patterns of the retinoic acid system in the developing retina. Dev Biol. 158**,** 390-9.
McClelland, G. B., et al., 2006. Temperature- and exercise-induced gene expression and metabolic enzyme changes in skeletal muscle of adult zebrafish (Danio rerio). J Physiol. 577**,** 739-51.
McDonald, E. C., et al., 2010a. Separable transcriptional regulatory domains within Otd control photoreceptor terminal differentiation events. Dev Biol. 347**,** 122-32.
McDonald, E. C., et al., 2010b. Separable transcriptional regulatory domains within Otd control photoreceptor terminal differentiation events. Developmental Biology. 347**,** 122-132.
McGown, A., et al., 2013. Early interneuron dysfunction in ALS: insights from a mutant sod1 zebrafish model. Ann Neurol. 73**,** 246-58.
McIlvain, V. A., Knox, B. E., 2007. Nr2e3 and Nrl can reprogram retinal precursors to the rod fate in Xenopus retina. Developmental Dynamics. 236**,** 1970-1979.
McLean, C. A., et al., 1999. Soluble pool of Abeta amyloid as a determinant of severity of neurodegeneration in Alzheimer's disease. Ann Neurol. 46**,** 860-6.
McLellan, G. J., et al., 2003. Clinical and pathological observations in English cocker spaniels with primary metabolic vitamin E deficiency and retinal pigment epithelial dystrophy. Vet Rec. 153**,** 287-92.
Mears, A. J., et al., 2001. Nrl is required for rod photoreceptor development. Nat Genet. 29**,** 447-52.
Meeker, N. D., et al., 2007. Method for isolation of PCR-ready genomic DNA from zebrafish tissues. Biotechniques. 43**,** 610-+.
Metz, G. A., et al., 2000. Efficient testing of motor function in spinal cord injured rats. Brain Res. 883**,** 165-77.
Mey, J., et al., 1997. Retinoic acid synthesis in the developing chick retina. J Neurosci. 17**,** 7441-9.
Milam, A. H., et al., 2002. The nuclear receptor NR2E3 plays a role in human retinal photoreceptor differentiation and degeneration. Proc Natl Acad Sci U S A. 99**,** 473-8.
Mishra, M., et al., 2010. Pph13 and orthodenticle define a dual regulatory pathway for photoreceptor cell morphogenesis and function. Development. 137**,** 2895-904.
Mitchell, D. M., et al., 2015a. Retinoic Acid Signaling Regulates Differential Expression of the Tandemly-Duplicated Long Wavelength-Sensitive Cone Opsin Genes in Zebrafish. PLoS Genet. 11**,** e1005483.
Mitchell, J. C., et al., 2015b. Wild type human TDP-43 potentiates ALS-linked mutant TDP-43 driven progressive motor and cortical neuron degeneration with pathological features of ALS. Acta Neuropathologica Communications. 3.
Mitton, K. P., et al., 2000a. The leucine zipper of NRL interacts with the CRX homeodomain. A possible mechanism of transcriptional synergy in rhodopsin regulation. J Biol Chem. 275**,** 29794-9.

Mitton, K. P., et al., 2000b. The leucine zipper of NRL interacts with the CRX homeodomain - A possible mechanism of transcriptional synergy in rhodopsin regulation. Journal of Biological Chemistry. 275**,** 29794-29799.
Miyazono, K., et al., 2005. BMP receptor signaling: transcriptional targets, regulation of signals, and signaling cross-talk. Cytokine Growth Factor Rev. 16**,** 251-63.
Mizeracka, K., et al., 2013. Notch1 is required in newly postmitotic cells to inhibit the rod photoreceptor fate. Development. 140**,** 3188-97.
Moisse, K., et al., 2009. Divergent patterns of cytosolic TDP-43 and neuronal progranulin expression following axotomy: implications for TDP-43 in the physiological response to neuronal injury. Brain Res. 1249**,** 202-11.
Molecular Operating Environment (MOE), 2013.08. Chemical Computing Group ULC, 1010 Sherbrooke St. West, Suite #910, Montreal, QC, Canada, H3A 2R7, 2018.
Mollereau, B., et al., 2001. Two-step process for photoreceptor formation in Drosophila. Nature. 412**,** 911-913.
Moran, C., et al., 2013. An adult female with resistance to thyroid hormone mediated by defective thyroid hormone receptor alpha. J Clin Endocrinol Metab. 98**,** 4254-61.
Morgan, B. R., et al., 2013. Characterization of Intercostal Muscle Pathology in Canine Degenerative Myelopathy: A Disease Model for Amyotrophic Lateral Sclerosis. Journal of Neuroscience Research. 91**,** 1639-1650.
Morris, A. C., et al., 2011. Microarray analysis of XOPS-mCFP zebrafish retina identifies genes associated with rod photoreceptor degeneration and regeneration. Invest Ophthalmol Vis Sci. 52**,** 2255-66.
Morris, A. C., et al., 2008. Genetic dissection reveals two separate pathways for rod and cone regeneration in the teleost retina. Dev Neurobiol. 68**,** 605-19.
Morris, A. C., et al., 2005. Cone survival despite rod degeneration in XOPS-mCFP transgenic zebrafish. Invest Ophthalmol Vis Sci. 46**,** 4762-71.
Morrison, K. L., Weiss, G. A., 2001. Combinatorial alanine-scanning. Current Opinion in Chemical Biology. 5**,** 302-307.
Morrow, E. M., et al., 1999. NeuroD regulates multiple functions in the developing neural retina in rodent. Development. 126**,** 23-36.
Mukherjee, N., et al., 2017. Retinal thinning in amyotrophic lateral sclerosis patients without ophthalmic disease. PLoS One. 12**,** e0185242.
Muller, D. P., 2010. Vitamin E and neurological function. Mol Nutr Food Res. 54**,** 710-8.
Muller, F. L., et al., 2006. Absence of CuZn superoxide dismutase leads to elevated oxidative stress and acceleration of age-dependent skeletal muscle atrophy. Free Radic Biol Med. 40**,** 1993-2004.
Mulligan, V. K., Chakrabartty, A., 2013. Protein misfolding in the late-onset neurodegenerative diseases: Common themes and the unique case of amyotrophic lateral sclerosis. Proteins: Structure, Function, and Bioinformatics. 81**,** 1285-1303.
Mulligan, V. K., et al., 2012. Early Steps in Oxidation-Induced SOD1 Misfolding: Implications for Non-Amyloid Protein Aggregation in Familial ALS. Journal of Molecular Biology. 421**,** 631-652.
Münch, C., Bertolotti, A., 2011. Self-propagation and transmission of misfolded mutant SOD1: Prion or prion-like phenomenon? Cell Cycle. 10**,** 1711-1711.
Munch, C., et al., 2011. Prion-like propagation of mutant superoxide dismutase-1 misfolding in neuronal cells. Proc Natl Acad Sci U S A. 108**,** 3548-53.

Murali, D., et al., 2005. Distinct developmental programs require different levels of Bmp signaling during mouse retinal development. Development. 132, 913-23.
Muranishi, Y., et al., 2011. An Essential Role for RAX Homeoprotein and NOTCH-HES Signaling in Otx2 Expression in Embryonic Retinal Photoreceptor Cell Fate Determination. Journal of Neuroscience. 31, 16792-16807.
Murphey, R. D., Zon, L. I., 2006. Small molecule screening in the zebrafish. Methods. 39, 255-61.
Murray, M. B., et al., 1988. Isolation and characterization of rat cDNA clones for two distinct thyroid hormone receptors. J Biol Chem. 263, 12770-7.
Nagai, M., et al., 2001. Rats expressing human cytosolic copper-zinc superoxide dismutase transgenes with amyotrophic lateral sclerosis: Associated mutations develop motor neuron disease. Journal of Neuroscience. 21, 9246-9254.
Nakamura, M., et al., 2008. Phosphorylated Smad2/3 immunoreactivity in sporadic and familial amyotrophic lateral sclerosis and its mouse model. Acta Neuropathol. 115, 327-34.
Nakamura, M., et al., 2013. Activation of transforming growth factor-beta/Smad signaling reduces aggregate formation of mislocalized TAR DNA-binding protein-43. Neurodegener Dis. 11, 182-93.
Nakamura, M., et al., 2012. Regionally different immunoreactivity for Smurf2 and pSmad2/3 in TDP-43-positive inclusions of amyotrophic lateral sclerosis. Neuropathol Appl Neurobiol.
Nakano, T., et al., 2012. Self-Formation of Optic Cups and Storable Stratified Neural Retina from Human ESCs. Cell Stem Cell. 10, 771-785.
Narayan, D. S., et al., 2016. A review of the mechanisms of cone degeneration in retinitis pigmentosa. Acta Ophthalmologica. 94, 748-754.
Nardone, R., et al., 2016. Canine degenerative myelopathy: a model of human amyotrophic lateral sclerosis. Zoology. 119, 64-73.
Nawrocki, L., et al., 1985. Larval and adult visual pigments of the zebrafish, Brachydanio rerio. Vision Res. 25, 1569-76.
Nelson, B. R., et al., 2006. Notch activity is downregulated just prior to retinal ganglion cell differentiation. Dev Neurosci. 28, 128-41.
Nelson, B. R., et al., 2007. Transient inactivation of Notch signaling synchronizes differentiation of neural progenitor cells. Dev Biol. 304, 479-98.
Nelson, S. M., et al., 2008. The Developmental Sequence of Gene Expression Within the Rod Photoreceptor Lineage in Embryonic Zebrafish. Developmental Dynamics. 237, 2903-2917.
Nelson, S. M., et al., 2009. Retinal homeobox 1 is required for retinal neurogenesis and photoreceptor differentiation in embryonic zebrafish. Dev Biol. 328, 24-39.
Neumann, M., 2013. Frontotemporal lobar degeneration and amyotrophic lateral sclerosis: Molecular similarities and differences. Revue Neurologique. 169, 793-798.
Neumann, M., et al., 2009. A new subtype of frontotemporal lobar degeneration with FUS pathology. Brain. 132, 2922-2931.
Neumann, M., et al., 2006a. Ubiquitinated TDP-43 in frontotemporal lobar degeneration and amyotrophic lateral sclerosis. Science. 314, 130-3.
Neumann, M., et al., 2006b. Ubiquitinated TDP-43 in frontotemporal lobar degeneration and amyotrophic lateral sclerosis. Science. 314, 130-133.
Newell, K., et al., 2015. Behavioral Variant-Frontotemporal Dementia And Parkinson Disease Associated With Tau, Alpha-Synuclein, And TDP43 Neuropathology. Journal of Neuropathology and Experimental Neurology. 74, 599-599.

Ng, L., et al., 2015. Age-Related Hearing Loss and Degeneration of Cochlear Hair Cells in Mice Lacking Thyroid Hormone Receptor beta1. Endocrinology. 156, 3853-65.
Ng, L., et al., 2001a. A thyroid hormone receptor that is required for the development of green cone photoreceptors. Nature Genetics. 27, 94-98.
Ng, L., et al., 2011. Two transcription factors can direct three photoreceptor outcomes from rod precursor cells in mouse retinal development. J Neurosci. 31, 11118-25.
Ng, L., et al., 2010. Type 3 deiodinase, a thyroid-hormone-inactivating enzyme, controls survival and maturation of cone photoreceptors. J Neurosci. 30, 3347-57.
Ng, L., et al., 2001b. Suppression of the deafness and thyroid dysfunction in Thrb-null mice by an independent mutation in the Thra thyroid hormone receptor alpha gene. Human Molecular Genetics. 10, 2701-2708.
Nguyen, M., Arnheiter, H., 2000. Signaling and transcriptional regulation in early mammalian eye development: a link between FGF and MITF. Development. 127, 3581-91.
Nguyen-Chi, M. E., et al., 2012. Morphogenesis and cell fate determination within the adaxial cell equivalence group of the zebrafish myotome. PLoS Genet. 8, e1003014.
Nicotra, C. M., et al., 1994. Retinoid dynamics in chicken eye during pre- and postnatal development. Mol Cell Biochem. 132, 45-55.
Nikonov, S. S., et al., 2005. Photoreceptors of Nrl(-/-) mice coexpress functional S- and M-cone opsins having distinct inactivation mechanisms. Journal of General Physiology. 125, 287-304.
Nishida, A., et al., 2003. Otx2 homeobox gene controls retinal photoreceptor cell fate and pineal gland development. Nat Neurosci. 6, 1255-63.
Nishimura, A. L., et al., 2004. A mutation in the vesicle-trafficking protein VAPB causes late-onset spinal muscular atrophy and amyotrophic lateral sclerosis. Am J Hum Genet. 75, 822-31.
Noel, N. C. L., Allison, W. T., 2018. Connectivity of cone photoreceptor telodendria in the zebrafish retina. Journal of Comparative Neurology. 526, 609-625.
Nonaka, T., et al., 2013. Prion-like Properties of Pathological TDP-43 Aggregates from Diseased Brains. Cell Reports. 4, 124-134.
Nordlund, A., et al., 2009. Functional features cause misfolding of the ALS-provoking enzyme SOD1. Proceedings of the National Academy of Sciences of the United States of America. 106, 9667-9672.
Nowak, R. J., et al., 2010. Improving Binding Specificity of Pharmacological Chaperones That Target Mutant Superoxide Dismutase-1 Linked to Familial Amyotrophic Lateral Sclerosis Using Computational Methods. Journal of Medicinal Chemistry. 53, 2709-2718.
O'Shea, P. J., et al., 2005. Contrasting skeletal phenotypes in mice with an identical mutation targeted to thyroid hormone receptor alpha1 or beta. Mol Endocrinol. 19, 3045-59.
O'Shea, P. J., et al., 2003. A thyrotoxic skeletal phenotype of advanced bone formation in mice with resistance to thyroid hormone. Mol Endocrinol. 17, 1410-24.
Ochocinska, M. J., Hitchcock, P. F., 2007. Dynamic expression of the basic helix-loop-helix transcription factor neuroD in the rod and cone photoreceptor lineages in the retina of the embryonic and larval zebrafish. J Comp Neurol. 501, 1-12.
Ochocinska, M. J., Hitchcock, P. F., 2009. NeuroD regulates proliferation of photoreceptor progenitors in the retina of the zebrafish. Mech Dev. 126, 128-41.

Oeda, T., et al., 2001. Oxidative stress causes abnormal accumulation of familial amyotrophic lateral sclerosis-related mutant SOD1 in transgenic Caenorhabditis elegans. Human Molecular Genetics. 10, 2013-2023.
Ogawa, M., et al., 2014. Neuronal Loss and Decreased GLT-1 Expression Observed in the Spinal Cord of Pembroke Welsh Corgi Dogs With Canine Degenerative Myelopathy. Veterinary Pathology. 51, 591-602.
Ogawa, Y., et al., 2015. Homeobox transcription factor Six7 governs expression of green opsin genes in zebrafish. Proc Biol Sci. 282, 20150659.
Oh, E. C. T., et al., 2007. Transformation of cone precursors to functional rod photoreceptors by bZIP transcription factor NRL. Proceedings of the National Academy of Sciences of the United States of America. 104, 1679-1684.
Okada, I., et al., 2011. SMOC1 is essential for ocular and limb development in humans and mice. Am J Hum Genet. 88, 30-41.
Okamoto, K., et al., 2015. An autopsy case of familial amyotrophic lateral sclerosis with a TARDBP Q343R mutation. Neuropathology. 35, 462-8.
Onishi, A., et al., 2010. Pias3-dependent SUMOylation controls mammalian cone photoreceptor differentiation. Nat Neurosci. 13, 1059-65.
Onishi, A., et al., 2009. Pias3-dependent SUMOylation directs rod photoreceptor development. Neuron. 61, 234-46.
Oofusa, K., et al., 2001. Expression of thyroid hormone receptor beta A gene assayed by transgenic Xenopus laevis carrying its promoter sequences. Molecular and Cellular Endocrinology. 181, 97-110.
Ortiga-Carvalho, T. M., et al., 2014. Thyroid hormone receptors and resistance to thyroid hormone disorders. Nat Rev Endocrinol. 10, 582-91.
Ortin-Martinez, A., et al., 2014. Number and Distribution of Mouse Retinal Cone Photoreceptors: Differences between an Albino (Swiss) and a Pigmented (C57/BL6) Strain. Plos One. 9.
Ortin-Martinez, A., et al., 2016. A Reinterpretation of Cell Transplantation: GFP Transfer from Donor to Host Photoreceptors. Stem Cells.
Packham, E. A., Brook, J. D., 2003. T-box genes in human disorders. Hum Mol Genet. 12 Spec No 1, R37-44.
Pan, Y., et al., 2010. Regulation of photoreceptor gene expression by the retinal homeobox (Rx) gene product. Dev Biol. 339, 494-506.
Pant, S. D., et al., 2013. Molecular Mechanisms Regulating Ocular Apoptosis in Zebrafish gdf6a Mutants. Investigative Ophthalmology & Visual Science. 54, 5871-5879.
Parakh, S., Atkin, J. D., 2016. Protein folding alterations in amyotrophic lateral sclerosis. Brain Research. 1648, 633-649.
Paxton, C., et al., 2002. Murine Tbx2 contains domains that activate and repress gene transcription. Gene. 283, 117-24.
Pazos-Moura, C., et al., 2000. Cardiac dysfunction caused by myocardium-specific expression of a mutant thyroid hormone receptor. Circ Res. 86, 700-6.
Pearson, R. A., et al., 2016. Donor and host photoreceptors engage in material transfer following transplantation of post-mitotic photoreceptor precursors. Nature Communications. 7, 13029.
Pennesi, M. E., et al., 2003. BETA2/NeuroD1 null mice: a new model for transcription factor-dependent photoreceptor degeneration. J Neurosci. 23, 453-61.

Perides, G., et al., 1995. Neuroprotective effect of human osteogenic protein-1 in a rat model of cerebral hypoxia/ischemia. Neurosci Lett. 187**,** 21-4.
Perz-Edwards, A., et al., 2001. Retinoic acid-mediated gene expression in transgenic reporter zebrafish. Dev Biol. 229**,** 89-101.
Pessoa, C. N., et al., 2008. Thyroid hormone action is required for normal cone opsin expression during mouse retinal development. Invest Ophthalmol Vis Sci. 49**,** 2039-45.
Petkova, A. T., et al., 2005. Self-propagating, molecular-level polymorphism in Alzheimer's beta-amyloid fibrils. Science. 307**,** 262-5.
Petrov, D., et al., 2016a. Effect of Oxidative Damage on the Stability and Dimerization of Superoxide Dismutase 1. Biophys J. 110**,** 1499-509.
Petrov, D., et al., 2016b. Effect of Oxidative Damage on the Stability and Dimerization of Superoxide Dismutase 1. Biophysical Journal. 110**,** 1499-1509.
Pflugfelder, G. O., et al., 1992. The lethal(1)optomotor-blind gene of Drosophila melanogaster is a major organizer of optic lobe development: isolation and characterization of the gene. Proc Natl Acad Sci U S A. 89**,** 1199-203.
Picher-Martel, V., et al., 2016. From animal models to human disease: a genetic approach for personalized medicine in ALS. Acta Neuropathol Commun. 4**,** 70.
Pickles, S., et al., 2016. ALS-linked misfolded SOD1 species have divergent impacts on mitochondria. Acta Neuropathol Commun. 4**,** 43.
Pittack, C., et al., 1997. Fibroblast growth factors are necessary for neural retina but not pigmented epithelium differentiation in chick embryos. Development. 124**,** 805-16.
Plaut, I., 2000. Effects of fin size on swimming performance, swimming behaviour and routine activity of zebrafish Danio rerio. J Exp Biol. 203**,** 813-20.
Poggi, L., et al., 2005. Influences on neural lineage and mode of division in the zebrafish retina in vivo. J Cell Biol. 171**,** 991-9.
Pokrishevsky, E., et al., 2015. Misfolded wild-type SOD1 induced by pathological FUS or TDP-43 transmits intercellularly and is propagation-competent. Prion. 9**,** S7-S8.
Pokrishevsky, E., et al., 2016. TDP-43 or FUS-induced misfolded human wild-type SOD1 can propagate intercellularly in a prionlike fashion. Scientific Reports. 6.
Pokrishevsky, E., et al., 2012a. Aberrant Localization of FUS and TDP43 Is Associated with Misfolding of SOD1 in Amyotrophic Lateral Sclerosis. Plos One. 7.
Pokrishevsky, E., et al., 2012b. Aberrant localization of FUS and TDP43 is associated with misfolding of SOD1 in amyotrophic lateral sclerosis. Plos One. 7**,** e35050.
Porter, F. D., et al., 1997. Lhx2, a LIM homeobox gene, is required for eye, forebrain, and definitive erythrocyte development. Development. 124**,** 2935-44.
Power, D. M., et al., 2001. Thyroid hormones in growth and development of fish. Comp Biochem Physiol C Toxicol Pharmacol. 130**,** 447-59.
Powers, S., et al., 2017. Embryonic Exposure to the Environmental Neurotoxin BMAA Negatively Impacts Early Neuronal Development and Progression of Neurodegeneration in the Sod1-G93R Zebrafish Model of Amyotrophic Lateral Sclerosis. Toxicological Sciences. 157**,** 129-140.
Prabhudesai, S. N., et al., 2005. Targeted effects of retinoic acid signaling upon photoreceptor development in zebrafish. Dev Biol. 287**,** 157-67.
Pramatarova, A., et al., 2001. Neuron-specific expression of mutant superoxide dismutase 1 in transgenic mice does not lead to motor impairment. Journal of Neuroscience. 21**,** 3369-3374.

Prince, S., et al., 2004. Tbx2 directly represses the expression of the p21(WAF1) cyclin-dependent kinase inhibitor. Cancer Res. 64, 1669-74.
Proctor, E. A., et al., 2016. Nonnative SOD1 trimer is toxic to motor neurons in a model of amyotrophic lateral sclerosis. Proceedings of the National Academy of Sciences of the United States of America. 113, 614-619.
Provost, E., et al., 2007. Viral 2A peptides allow expression of multiple proteins from a single ORF in transgenic zebrafish embryos. Genesis. 45, 625-9.
Prudencio, M., et al., 2010. An examination of wild-type SOD1 in modulating the toxicity and aggregation of ALS-associated mutant SOD1. Human Molecular Genetics. 19, 4774-4789.
Prusiner, S. B., 1982. Novel proteinaceous infectious particles cause scrapie. Science. 216, 136-44.
Prusiner, S. B., 1998. Prions. Proc Natl Acad Sci U S A. 95, 13363-83.
Quarta, E., et al., 2015. Increased anxiety-like behavior and selective learning impairments are concomitant to loss of hippocampal interneurons in the presymptomatic SOD1(G93A) ALS mouse model. Journal of Comparative Neurology. 523, 1622-1638.
Quignodon, L., et al., 2007. A point mutation in the activation function 2 domain of thyroid hormone receptor alpha1 expressed after CRE-mediated recombination partially recapitulates hypothyroidism. Mol Endocrinol. 21, 2350-60.
Rabdano, S. O., et al., 2017. Onset of disorder and protein aggregation due to oxidation-induced intermolecular disulfide bonds: case study of RRM2 domain from TDP-43. Scientific Reports. 7.
Radi, E., et al., 2014. Apoptosis and oxidative stress in neurodegenerative diseases. J Alzheimers Dis. 42 Suppl 3, S125-52.
Raine, J. C., et al., 2010. Systemic thyroid hormone is necessary and sufficient to induce ultraviolet-sensitive cone loss in the juvenile rainbow trout retina. J Exp Biol. 213, 493-501.
Ramachandran, R., et al., 2012. Insm1a-mediated gene repression is essential for the formation and differentiation of Muller glia-derived progenitors in the injured retina. Nat Cell Biol. 14, 1013-23.
Ramesh, T., et al., 2010. A genetic model of amyotrophic lateral sclerosis in zebrafish displays phenotypic hallmarks of motoneuron disease. Dis Model Mech. 3, 652-62.
Ransohoff, R. M., 2016. How neuroinflammation contributes to neurodegeneration. Science. 353, 777-83.
Ratnaparkhi, A., et al., 2008. A Drosophila model of ALS: human ALS-associated mutation in VAP33A suggests a dominant negative mechanism. Plos One. 3, e2334.
Ravits, J. M., La Spada, A. R., 2009. ALS motor phenotype heterogeneity, focality, and spread Deconstructing motor neuron degeneration. Neurology. 73, 805-811.
Ray, S. S., et al., 2005. Small-molecule-mediated stabilization of familial amyotrophic lateral sclerosis-linked superoxide dismutase mutants against unfolding and aggregation. Proceedings of the National Academy of Sciences of the United States of America. 102, 3639-3644.
Raymond, P. A., Barthel, L. K., 2004. A moving wave patterns the cone photoreceptor mosaic array in the zebrafish retina. Int J Dev Biol. 48, 935-45.
Raymond, P. A., et al., 1995a. Developmental Patterning of Rod and Cone Photoreceptors in Embryonic Zebrafish. Journal of Comparative Neurology. 359, 537-550.

Raymond, P. A., et al., 1995b. Developmental patterning of rod and cone photoreceptors in embryonic zebrafish. J Comp Neurol. 359**,** 537-50.
Raymond, P. A., et al., 1993a. EXPRESSION OF ROD AND CONE VISUAL PIGMENTS IN GOLDFISH AND ZEBRAFISH - A RHODOPSIN-LIKE GENE IS EXPRESSED IN CONES. Neuron. 10**,** 1161-1174.
Raymond, P. A., et al., 1993b. Expression of rod and cone visual pigments in goldfish and zebrafish: a rhodopsin-like gene is expressed in cones. Neuron. 10**,** 1161-74.
Raymond, P. A., et al., 2014. Patterning the cone mosaic array in zebrafish retina requires specification of ultraviolet-sensitive cones. PLoS One. 9**,** e85325.
Reaume, A. G., et al., 1996a. Motor neurons in Cu/Zn superoxide dismutase-deficient mice develop normally but exhibit enhanced cell death after axonal injury. Nat Genet. 13**,** 43-7.
Reaume, A. G., et al., 1996b. Motor neurons in Cu/Zn superoxide dismutase-deficient mice develop normally but exhibit enhanced cell death after axonal injury. Nature Genetics. 13**,** 43-47.
Redmond, K. L., et al., 2010. T-box 2 represses NDRG1 through an EGR1-dependent mechanism to drive the proliferation of breast cancer cells. Oncogene. 29**,** 3252-3262.
Reed, N. P., Mortlock, D. P., 2010. Identification of a distant cis-regulatory element controlling pharyngeal arch-specific expression of zebrafish gdf6a/radar. Dev Dyn. 239**,** 1047-60.
Refetoff, S., et al., 2014. Classification and proposed nomenclature for inherited defects of thyroid hormone action, cell transport, and metabolism. Thyroid. 24**,** 407-9.
Refetoff, S., Dumitrescu, A. M., 2007. Syndromes of reduced sensitivity to thyroid hormone: genetic defects in hormone receptors, cell transporters and deiodination. Best Pract Res Clin Endocrinol Metab. 21**,** 277-305.
Reichert, S., et al., 2013. A BMP regulatory network controls ectodermal cell fate decisions at the neural plate border. Development. 140**,** 4435-44.
Reimer, M. M., et al., 2013. Dopamine from the brain promotes spinal motor neuron generation during development and adult regeneration. Dev Cell. 25**,** 478-91.
Renton, A. E., et al., 2014. State of play in amyotrophic lateral sclerosis genetics. Nat Neurosci. 17**,** 17-23.
Renton, A. E., et al., 2011. A hexanucleotide repeat expansion in C9ORF72 is the cause of chromosome 9p21-linked ALS-FTD. Neuron. 72**,** 257-68.
Rezaie, T., et al., 2002. Adult-onset primary open-angle glaucoma caused by mutations in optineurin. Science. 295**,** 1077-9.
Rhee, S. G., 2006. Cell signaling. H2O2, a necessary evil for cell signaling. Science. 312**,** 1882-3.
Ribeiro, I., et al., 2007. Tbx2 and Tbx3 regulate the dynamics of cell proliferation during heart remodeling. PLoS One. 2**,** e398.
Richter, C. P., et al., 2011. Complete activation of thyroid hormone receptor beta by T3 is essential for normal cochlear function and morphology in mice. Cell Physiol Biochem. 28**,** 997-1008.
Riesenberg, A. N., et al., 2009. Pax6 regulation of Math5 during mouse retinal neurogenesis. Genesis. 47**,** 175-87.
Rihel, J., Schier, A. F., 2012. Behavioral screening for neuroactive drugs in zebrafish. Dev Neurobiol. 72**,** 373-85.
Riis, R. C., et al., 1999. Ocular manifestations of equine motor neuron disease. Equine Vet J. 31**,** 99-110.
Riis, R. C., et al., 1981. Vitamin E deficiency retinopathy in dogs. Am J Vet Res. 42**,** 74-86.

Rissi, M., et al., 1995. Zebrafish Radar: a new member of the TGF-beta superfamily defines dorsal regions of the neural plate and the embryonic retina. Mech Dev. 49**,** 223-34.
Ritson, G. P., et al., 2010. TDP-43 mediates degeneration in a novel Drosophila model of disease caused by mutations in VCP/p97. J Neurosci. 30**,** 7729-39.
Robberecht, W., Philips, T., 2013. The changing scene of amyotrophic lateral sclerosis. Nature Reviews Neuroscience. 14**,** 248-264.
Roberts, M. R., et al., 2005. Retinoid X receptor (gamma) is necessary to establish the S-opsin gradient in cone photoreceptors of the developing mouse retina. Invest Ophthalmol Vis Sci. 46**,** 2897-904.
Roberts, M. R., et al., 2006. Making the gradient: thyroid hormone regulates cone opsin expression in the developing mouse retina. Proc Natl Acad Sci U S A. 103**,** 6218-23.
Robertson, J., et al., 2007. Lack of TDP-43 abnormalities in mutant SOD1 transgenic mice shows disparity with ALS. Neuroscience Letters. 420**,** 128-132.
Robinson, J., et al., 1995. Temporal and spatial patterns of opsin gene expression in zebrafish (Danio rerio). Vis Neurosci. 12**,** 895-906.
Rodriguez, J. A., et al., 2005. Destabilization of apoprotein is insufficient to explain Cu,Zn-superoxide dismutase-linked ALS pathogenesis. Proceedings of the National Academy of Sciences. 102**,** 10516-10521.
Rodriguez, M., et al., 2008. Tbx3 represses E-cadherin expression and enhances melanoma invasiveness. Cancer Research. 68**,** 7872-7881.
Rosen, D. R., et al., 1993. Mutations in Cu/Zn superoxide dismutase gene are associated with familial amyotrophic lateral sclerosis. Nature. 362**,** 59-62.
Rothstein, J. D., 2009. Current hypotheses for the underlying biology of amyotrophic lateral sclerosis. Ann Neurol. 65 Suppl 1**,** S3-9.
Rovsing, L., et al., 2011. Crx broadly modulates the pineal transcriptome. Journal of Neurochemistry. 119**,** 262-274.
Rowland, L. P., Shneider, N. A., 2001. Medical progress: Amyotrophic lateral sclerosis. New England Journal of Medicine. 344**,** 1688-1700.
Rubinsztein, D. C., 2006. The roles of intracellular protein-degradation pathways in neurodegeneration. Nature. 443**,** 780-6.
Ruschke, K., et al., 2012. BMPs are mediators in tissue crosstalk of the regenerating musculoskeletal system. Cell Tissue Res. 347**,** 521-44.
Ruvinsky, I., Silver, L. M., 1997. Newly identified paralogous groups on mouse chromosomes 5 and 11 reveal the age of a T-box cluster duplication. Genomics. 40**,** 262-266.
Saccon, R. A., et al., 2013. Is SOD1 loss of function involved in amyotrophic lateral sclerosis? Brain. 136**,** 2342-58.
Sakowski, S. A., et al., 2012. Neuromuscular effects of G93A-SOD1 expression in zebrafish. Molecular Neurodegeneration. 7.
Salbreux, G., et al., 2012. Coupling mechanical deformations and planar cell polarity to create regular patterns in the zebrafish retina. PLoS Comput Biol. 8**,** e1002618.
Salminen, A., et al., 2010. Endoplasmic reticulum stress in age-related macular degeneration: trigger for neovascularization. Mol Med. 16**,** 535-42.
Samanta, U., et al., 2000. Environment of tryptophan side chains in proteins. Proteins-Structure Function and Genetics. 38**,** 288-300.
Sanchez-Camacho, C., Bovolenta, P., 2009. Emerging mechanisms in morphogen-mediated axon guidance. Bioessays. 31**,** 1013-25.

Santos, G. M., et al., 2006. Negative regulation of superoxide dismutase-1 promoter by thyroid hormone. Mol Pharmacol. 70**,** 793-800.
Santos-Ferreira, T., et al., 2016. Retinal transplantation of photoreceptors results in donor–host cytoplasmic exchange. Nature Communications. 7**,** 13028.
Sapkota, D., et al., 2014. Onecut1 and Onecut2 redundantly regulate early retinal cell fates during development. Proceedings of the National Academy of Sciences of the United States of America. 111**,** E4086-E4095.
Sasagawa, S., et al., 2002. Axes establishment during eye morphogenesis in Xenopus by coordinate and antagonistic actions of BMP4, Shh, and RA. Genesis. 33**,** 86-96.
Sasaki, S., et al., 1999. Ligand-induced recruitment of a histone deacetylase in the negative-feedback regulation of the thyrotropin beta gene. EMBO J. 18**,** 5389-98.
Sasaki, S., et al., 2005. Ultrastructural study of aggregates in the spinal cord of transgenic mice with a G93A mutant SOD1 gene. Acta Neuropathologica. 109**,** 247-255.
Sato, S., et al., 2007. Dkk3-Cre BAC transgenic mouse line: a tool for highly efficient gene deletion in retinal progenitor cells. Genesis. 45**,** 502-7.
Satoh, S., et al., 2009. The spatial patterning of mouse cone opsin expression is regulated by bone morphogenetic protein signaling through downstream effector COUP-TF nuclear receptors. J Neurosci. 29**,** 12401-11.
Satue, M., et al., 2018. Retinal and Choroidal Changes in Patients with Parkinson's Disease Detected by Swept-Source Optical Coherence Tomography. Curr Eye Res. 43**,** 109-115.
Satue, M., et al., 2017. Evaluation of Progressive Visual Dysfunction and Retinal Degeneration in Patients With Parkinson's Disease. Invest Ophthalmol Vis Sci. 58**,** 1151-1157.
Scheer, N., et al., 2001. An instructive function for Notch in promoting gliogenesis in the zebrafish retina. Development. 128**,** 1099-107.
Schindelin, J., et al., 2012. Fiji: an open-source platform for biological-image analysis. Nat Methods. 9**,** 676-82.
Schmid, B., et al., 2013. Loss of ALS-associated TDP-43 in zebrafish causes muscle degeneration, vascular dysfunction, and reduced motor neuron axon outgrowth. Proc Natl Acad Sci U S A. 110**,** 4986-91.
Schmidt, R., et al., 2014. Stab wound injury of the zebrafish adult telencephalon: a method to investigate vertebrate brain neurogenesis and regeneration. J Vis Exp. e51753.
Schmidt-Ott, U., et al., 1994. Number, identity, and sequence of the Drosophila head segments as revealed by neural elements and their deletion patterns in mutants. Proc Natl Acad Sci U S A. 91**,** 8363-7.
Schmidt-Ott, U., et al., 1995. Analysis of neural elements in head-mutant Drosophila embryos suggests segmental origin of the optic lobes. Roux Arch Dev Biol. 205**,** 31-44.
Schreiber, A. M., et al., 2009. Cell-cell interactions during remodeling of the intestine at metamorphosis in Xenopus laevis. Dev Biol. 331**,** 89-98.
Schreij, A. M., et al., 2016. Endocytic membrane trafficking and neurodegenerative disease. Cell Mol Life Sci. 73**,** 1529-45.
Schwarz, M., et al., 2000. Spatial specification of mammalian eye territories by reciprocal transcriptional repression of Pax2 and Pax6. Development. 127**,** 4325-34.
Scott, A. W., et al., 2016. Public Attitudes About Eye and Vision Health. JAMA Ophthalmology. 134**,** 1111.
Sedletcaia, A., Evans, T., 2011a. Heart Chamber Size in Zebrafish Is Regulated Redundantly by Duplicated tbx2 Genes. Developmental Dynamics. 240**,** 1548-1557.

Sedletcaia, A., Evans, T., 2011b. Heart chamber size in zebrafish is regulated redundantly by duplicated tbx2 genes. Dev Dyn. 240**,** 1548-57.
Sekhar, A., et al., 2016. Probing the free energy landscapes of ALS disease mutants of SOD1 by NMR spectroscopy. Proceedings of the National Academy of Sciences of the United States of America. 113**,** E6939-E6945.
Seko, Y., et al., 2012. Derivation of human differential photoreceptor-like cells from the iris by defined combinations of CRX, RX and NEUROD. PLoS One. 7**,** e35611.
Senut, M. C., et al., 2004. An element in the alpha1-tubulin promoter is necessary for retinal expression during optic nerve regeneration but not after eye injury in the adult zebrafish. J Neurosci. 24**,** 7663-73.
Settle, S. H., Jr., et al., 2003. Multiple joint and skeletal patterning defects caused by single and double mutations in the mouse Gdf6 and Gdf5 genes. Dev Biol. 254**,** 116-30.
Shan, X. Y., et al., 2009. Mislocalization of TDP-43 in the G93A mutant SOD1 transgenic mouse model of ALS. Neuroscience Letters. 458**,** 70-74.
Sharon, D., et al., 2003. Shared mutations in NR2E3 in enhanced S-cone syndrome, Goldmann-Favre syndrome, and many cases of clumped pigmentary retinal degeneration. Archives of Ophthalmology. 121**,** 1316-1323.
Shefner, J. M., et al., 1999. Mice lacking cytosolic copper/zinc superoxide dismutase display a distinctive motor axonopathy. Neurology. 53**,** 1239-1246.
Shen, Y. C., Raymond, P. A., 2004a. Zebrafish cone-rod (crx) homeobox gene promotes retinogenesis. Dev Biol. 269**,** 237-51.
Shen, Y. C., Raymond, P. A., 2004b. Zebrafish cone-rod (crx) homeobox gene promotes retinogenesis. Developmental Biology. 269**,** 237-251.
Shi, Y., et al., 2016a. Gibbs Energy of Superoxide Dismutase Heterodimerization Accounts for Variable Survival in Amyotrophic Lateral Sclerosis. J Am Chem Soc. 138**,** 5351-62.
Shi, Y., et al., 2014. The lack of CuZnSOD leads to impaired neurotransmitter release, neuromuscular junction destabilization and reduced muscle strength in mice. PLoS One. 9**,** e100834.
Shi, Y. H., et al., 2016b. Gibbs Energy of Superoxide Dismutase Heterodimerization Accounts for Variable Survival in Amyotrophic Lateral Sclerosis. Journal of the American Chemical Society. 138**,** 5351-5362.
Shibata, N., et al., 1996. Immunohistochemical study on superoxide dismutases in spinal cords from autopsied patients with amyotrophic lateral sclerosis. Dev Neurosci. 18**,** 492-8.
Shibata, N., et al., 1994. Cu/Zn superoxide dismutase-like immunoreactivity in Lewy body-like inclusions of sporadic amyotrophic lateral sclerosis. Neurosci Lett. 179**,** 149-52.
Shibusawa, N., et al., 2003. Thyroid hormone receptor DNA binding is required for both positive and negative gene regulation. J Biol Chem. 278**,** 732-8.
Shiihashi, G., et al., 2016. Mislocated FUS is sufficient for gain-of-toxic-function amyotrophic lateral sclerosis phenotypes in mice. Brain. 139**,** 2380-2394.
Shintaku, M., et al., 2017. Novel intracytoplasmic inclusions immunoreactive for phosphorylated-TDP43 and cystatin C in anterior horn cells in a case of sporadic amyotrophic lateral sclerosis. Neuropathology. 37**,** 526-534.
Showell, C., et al., 2006. Developmental expression patterns of Tbx1, Tbx2, Tbx5, and Tbx20 in Xenopus tropicalis. Developmental Dynamics. 235**,** 1623-1630.
Showers, M. O., et al., 1991. Isolation and characterization of a cDNA encoding a chicken beta thyroid hormone receptor. DNA Cell Biol. 10**,** 211-21.

Sidi, S., et al., 2003. Maternal induction of ventral fate by zebrafish radar. Proc Natl Acad Sci U S A. 100, 3315-20.
Silverman, J. M., et al., 2016. Disease Mechanisms in ALS: Misfolded SOD1 Transferred Through Exosome-Dependent and Exosome-Independent Pathways. Cell Mol Neurobiol. 36, 377-81.
Simeone, A., et al., 1992. Nested Expression Domains of 4 Homeobox Genes in Developing Rostral Brain. Nature. 358, 687-690.
Simeone, A., et al., 1993. A Vertebrate Gene-Related to Orthodenticle Contains a Homeodomain of the Bicoid Class and Demarcates Anterior Neuroectoderm in the Gastrulating Mouse Embryo. Embo Journal. 12, 2735-2747.
Sinclair, C. S., et al., 2002. TBX2 is preferentially amplified in BRCA1- and BRCA2-related breast tumors. Cancer Res. 62, 3587-91.
Sinclair, C. S., et al., 2003. The 17q23 amplicon and breast cancer. Breast Cancer Res Treat. 78, 313-22.
Singh, M. S., et al., 2016. Transplanted photoreceptor precursors transfer proteins to host photoreceptors by a mechanism of cytoplasmic fusion. Nat Commun. 7, 13537.
Singh, R., et al., 2012. Tbx2 and Tbx3 induce atrioventricular myocardial development and endocardial cushion formation. Cellular and Molecular Life Sciences. 69, 1377-1389.
Sinha, S., et al., 2000. Differential DNA binding and transcription modulation by three T-box proteins, T, TBX1 and TBX2. Gene. 258, 15-29.
Sirangelo, I., Iannuzzi, C., 2017. The Role of Metal Binding in the Amyotrophic Lateral Sclerosis-Related Aggregation of Copper-Zinc Superoxide Dismutase. Molecules. 22.
Sjoberg, M., et al., 1992. Thyroid-Hormone Receptors in Chick Retinal Development - Differential Expression of Messenger-Rnas for Alpha and N-Terminal Variant Beta-Receptors. Development. 114, 39-47.
Snelson, C. D., et al., 2008a. Formation of the asymmetric pineal complex in zebrafish requires two independently acting transcription factors. Dev Dyn. 237, 3538-44.
Snelson, C. D., et al., 2008b. Tbx2b is required for the development of the parapineal organ. Development. 135, 1693-702.
Solek, C. M., et al., 2017. Lineage tracing of dlx1a/2a and dlx5a/6a expressing cells in the developing zebrafish brain. Dev Biol. 427, 131-147.
Soto, C., et al., 2006. Amyloids, prions and the inherent infectious nature of misfolded protein aggregates. Trends in Biochemical Sciences. 31, 150-155.
Sotolongo-Lopez, M., et al., 2015. TALEN-mediated mutagenesis establishes a role for six7 in photoreceptor patterning in zebrafish. Investigative Ophthalmology & Visual Science. 56.
Sotolongo-Lopez, M., et al., 2016. Genetic Dissection of Dual Roles for the Transcription Factor six7 in Photoreceptor Development and Patterning in Zebrafish. Plos Genetics. 12.
Spence, J. R., et al., 2007. Retina regeneration in the chick embryo is not induced by spontaneous Mitf downregulation but requires FGF/FGFR/MEK/Erk dependent upregulation of Pax6. Mol Vis. 13, 57-65.
Sperber, G. H., 1992. Current concepts in embryonic craniofacial development. Crit Rev Oral Biol Med. 4, 67-72.
Srinivas, M., et al., 2006a. Activation of the blue opsin gene in cone photoreceptor development by retinoid-related orphan receptor beta. Mol Endocrinol. 20, 1728-41.
Srinivas, M., et al., 2006b. Activation of the blue opsin gene in cone photoreceptor development by retinoid-related orphan receptor beta. Molecular Endocrinology. 20, 1728-1741.

Stathopulos, P. B., et al., 2003. Cu/Zn superoxide dismutase mutants associated with amyotrophic lateral sclerosis show enhanced formation of aggregates in vitro. Proceedings of the National Academy of Sciences of the United States of America. 100, 7021-7026.
Stenkamp, D. L., et al., 1997. Spatiotemporal coordination of rod and cone photoreceptor differentiation in goldfish retina. Journal of Comparative Neurology. 382, 272-284.
Stenkamp, D. L., et al., 1993. Retinoid effects in purified cultures of chick embryo retina neurons and photoreceptors. Invest Ophthalmol Vis Sci. 34, 2425-36.
Stenkamp, D. L., et al., 1996. Temporal expression of rod and cone opsins in embryonic goldfish retina predicts the spatial organization of the cone mosaic. Investigative Ophthalmology & Visual Science. 37, 363-376.
Stevens, C. B., et al., 2011. Plasticity of photoreceptor-generating retinal progenitors revealed by prolonged retinoic acid exposure. BMC Dev Biol. 11, 51.
Storm, E. E., et al., 1994. Limb alterations in brachypodism mice due to mutations in a new member of the TGF beta-superfamily. Nature. 368, 639-43.
Strelau, J., et al., 2009. Progressive postnatal motoneuron loss in mice lacking GDF-15. J Neurosci. 29, 13640-8.
Strettoi, E., et al., 2002. Morphological and functional abnormalities in the inner retina of the rd/rd mouse. Journal of Neuroscience. 22, 5492-5504.
Sun, C., et al., 2018. Transcripts within rod photoreceptors of the Zebrafish retina. Bmc Genomics. 19.
Sundaramoorthy, V., et al., 2013a. Extracellular wildtype and mutant SOD1 induces ER-Golgi pathology characteristic of amyotrophic lateral sclerosis in neuronal cells. Cellular and Molecular Life Sciences. 70, 4181-4195.
Sundaramoorthy, V., et al., 2013b. Extracellular wildtype and mutant SOD1 induces ER-Golgi pathology characteristic of amyotrophic lateral sclerosis in neuronal cells. Cell Mol Life Sci. 70, 4181-95.
Suzuki, S. C., et al., 2013a. Cone photoreceptor types in zebrafish are generated by symmetric terminal divisions of dedicated precursors. Proc Natl Acad Sci U S A. 110, 15109-14.
Suzuki, S. C., et al., 2013b. Cone photoreceptor types in zebrafish are generated by symmetric terminal divisions of dedicated precursors. Proceedings of the National Academy of Sciences of the United States of America. 110, 15109-15114.
Suzuki, T., et al., 2004. Tbx Genes Specify Posterior Digit Identity through Shh and BMP Signaling. Dev Cell. 6, 43-53.
Swaroop, A., et al., 2010. Transcriptional regulation of photoreceptor development and homeostasis in the mammalian retina. Nat Rev Neurosci. 11, 563-76.
Swarup, V., et al., 2011. Pathological hallmarks of amyotrophic lateral sclerosis/frontotemporal lobar degeneration in transgenic mice produced with TDP-43 genomic fragments. Brain. 134, 2610-2626.
Tahayato, A., et al., 2003. Otd/Crx, a dual regulator for the specification of ommatidia subtypes in the Drosophila retina. Dev Cell. 5, 391-402.
Takabatake, Y., et al., 2002. Conserved expression control and shared activity between cognate T-box genes Tbx2 and Tbx3 in connection with Sonic hedgehog signaling during Xenopus eye development. Dev Growth Differ. 44, 257-71.
Takabatake, Y., et al., 2000. Conserved and divergent expression of T-box genes Tbx2-Tbx5 in Xenopus. Mech Dev. 91, 433-7.

Takahashi, K., et al., 2007. Induction of pluripotent stem cells from adult human fibroblasts by defined factors. Cell. 131**,** 861-872.
Takahashi, K., Yamanaka, S., 2006. Induction of pluripotent stem cells from mouse embryonic and adult fibroblast cultures by defined factors. Cell. 126**,** 663-676.
Takanashi, K., Yamaguchi, A., 2014. Aggregation of ALS-linked FUS mutant sequesters RNA binding proteins and impairs RNA granules formation. Biochemical and Biophysical Research Communications. 452**,** 600-607.
Takayama, S., et al., 2008. An F-domain introduced by alternative splicing regulates activity of the zebrafish thyroid hormone receptor alpha. Gen Comp Endocrinol. 155**,** 176-89.
Takechi, M., et al., 2003. Fluorescence visualization of ultraviolet-sensitive cone photoreceptor development in living zebrafish. FEBS Letters. 553**,** 90-94.
Takechi, M., Kawamura, S., 2005. Temporal and spatial changes in the expression pattern of multiple red and green subtype opsin genes during zebrafish development. J Exp Biol. 208**,** 1337-45.
Takechi, M., et al., 2008. Identification of cis-acting elements repressing blue opsin expression in zebrafish UV cones and pineal cells. J Biol Chem. 283**,** 31625-32.
Tan, C. F., et al., 2007. TDP-43 immunoreactivity in neuronal inclusions in familial amyotrophic lateral sclerosis with or without SOD1 gene mutation. Acta Neuropathologica. 113**,** 535-542.
Taskesen, E., et al., 2017. Susceptible genes and disease mechanisms identified in frontotemporal dementia and frontotemporal dementia with Amyotrophic Lateral Sclerosis by DNA-methylation and GWAS. Sci Rep. 7**,** 8899.
Tassabehji, M., et al., 2008. Mutations in GDF6 are associated with vertebral segmentation defects in Klippel-Feil syndrome. Hum Mutat. 29**,** 1017-27.
Taylor, D. M., et al., 2007. Tryptophan 32 potentiates aggregation and cytotoxicity of a copper/zinc superoxide dismutase mutant associated with familial amyotrophic lateral sclerosis. Journal of Biological Chemistry. 282**,** 16329-16335.
Taylor, M. R., et al., 2005. The zebrafish pob gene encodes a novel protein required for survival of red cone photoreceptor cells. Genetics. 170**,** 263-73.
Taylor, S. M., et al., 2015. The bHLH Transcription Factor NeuroD Governs Photoreceptor Genesis and Regeneration Through Delta-Notch Signaling. Investigative Ophthalmology & Visual Science. 56**,** 7496-7515.
Taylor, W. R., van Dyke, G. C., 1985. Revised procedures for staining and clearing small fishes and other vertebrates for bone and cartilage study. Cybium. 9**,** 107 - 119.
Terada, K., et al., 2006. Nucleosome regulator Xhmgb3 is required for cell proliferation of the eye and brain as a downstream target of Xenopus rax/Rx1. Dev Biol. 291**,** 398-412.
Tesla, R., et al., 2012. Neuroprotective efficacy of aminopropyl carbazoles in a mouse model of amyotrophic lateral sclerosis. Proc Natl Acad Sci U S A. 109**,** 17016-21.
Thi Thu, H. N., et al., 2013. Tbx2a is required for specification of endodermal pouches during development of the pharyngeal arches. PLoS One. 8**,** e77171.
Thisse, B., et al., 2004. Spatial and temporal expression of the zebrafish genome by large-scale in situ hybridization screening. Methods Cell Biol. 77**,** 505-19.
Thisse, C., et al., 2003. Spatial and temporal expression patterns of selenoprotein genes during embryogenesis in zebrafish. Gene Expr Patterns. 3**,** 525-32.
Thisse, C., Thisse, B., 2008. High-resolution in situ hybridization to whole-mount zebrafish embryos. Nat Protoc. 3**,** 59-69.

Thummel, R., et al., 2010. Pax6a and Pax6b are required at different points in neuronal progenitor cell proliferation during zebrafish photoreceptor regeneration. Exp Eye Res. 90, 572-82.
Tierney, K. B., 2011a. Behavioural assessments of neurotoxic effects and neurodegeneration in zebrafish. Biochim Biophys Acta. 1812, 381-9.
Tierney, K. B., 2011b. Swimming performance assessment in fishes. J Vis Exp.
Tinnikov, A., et al., 2002. Retardation of post-natal development caused by a negatively acting thyroid hormone receptor alpha1. EMBO J. 21, 5079-87.
Todd, T. W., Petrucelli, L., 2016. Insights into the pathogenic mechanisms of Chromosome 9 open reading frame 72 (C9orf72) repeat expansions. Journal of Neurochemistry. 138, 145-162.
Tohya, S., et al., 1999. Formation of cone mosaic of zebrafish retina. Journal of Theoretical Biology. 200, 231-244.
Tomlinson, A., 2003. Patterning the peripheral retina of the fly: decoding a gradient. Dev Cell. 5, 799-809.
Touznik, A., et al., 2017. LNA/DNA mixmer-based antisense oligonucleotides correct alternative splicing of the SMN2 gene and restore SMN protein expression in type 1 SMA fibroblasts. Sci Rep. 7, 3672.
Trimarchi, J. M., et al., 2008. Thyroid hormone components are expressed in three sequential waves during development of the chick retina. BMC Dev Biol. 8, 101.
Tsai, K. J., et al., 2010. Elevated expression of TDP-43 in the forebrain of mice is sufficient to cause neurological and pathological phenotypes mimicking FTLD-U. J Exp Med. 207, 1661-73.
Tsai, Y., et al., 2014. Ocular changes in TgF344-AD rat model of Alzheimer's disease. Invest Ophthalmol Vis Sci. 55, 523-34.
Turner, B. J., Talbot, K., 2008. Transgenics, toxicity and therapeutics in rodent models of mutant SOD1-mediated familial ALS. Prog Neurobiol. 85, 94-134.
Tycko, R., Wickner, R. B., 2013. Molecular Structures of Amyloid and Prion Fibrils: Consensus versus Controversy. Accounts of Chemical Research. 46, 1487-1496.
Tzekov, R., et al., 2011. Protein misfolding and retinal degeneration. Cold Spring Harb Perspect Biol. 3, a007492.
Ulisse, S., et al., 1996. Dominant-negative mutant thyroid hormone receptors prevent transcription from Xenopus thyroid hormone receptor beta gene promoter in response to thyroid hormone in Xenopus tadpoles in vivo. Proceedings of the National Academy of Sciences. 93, 1205-1209.
Uribe, R. A., et al., 2012. Id2a functions to limit Notch pathway activity and thereby influence the transition from proliferation to differentiation of retinoblasts during zebrafish retinogenesis. Dev Biol. 371, 280-92.
Urushitani, M., 2011. [Antibody therapy targeting ALS-linked misfolded protein]. Rinsho Shinkeigaku. 51, 1162-4.
Vaccaro, A., et al., 2012. Methylene blue protects against TDP-43 and FUS neuronal toxicity in C. elegans and D. rerio. Plos One. 7, e42117.
Valdivia, L. E., et al., 2016. Antagonism between Gdf6a and retinoic acid pathways controls timing of retinal neurogenesis and growth of the eye in zebrafish. Development. 143, 1087-98.
van Blitterswijk, M., et al., 2011. Anti-superoxide dismutase antibodies are associated with survival in patients with sporadic amyotrophic lateral sclerosis. Amyotroph Lateral Scler. 12, 430-8.

van Blitterswijk, M., et al., 2012. Novel optineurin mutations in sporadic amyotrophic lateral sclerosis patients. Neurobiol Aging. 33**,** 1016 e1-7.
Van Deerlin, V. M., et al., 2008. TARDBP mutations in amyotrophic lateral sclerosis with TDP-43 neuropathology: a genetic and histopathological analysis. Lancet Neurol. 7**,** 409-16.
Van Hoecke, A., et al., 2012. EPHA4 is a disease modifier of amyotrophic lateral sclerosis in animal models and in humans. Nat Med. 18**,** 1418-22.
van Mullem, A., et al., 2012. Clinical phenotype and mutant TRalpha1. N Engl J Med. 366**,** 1451-3.
van Roon-Mom, W. M. C., et al., 2018. Dose-Dependent Lowering of Mutant Huntingtin Using Antisense Oligonucleotides in Huntington Disease Patients. Nucleic Acid Ther. 28**,** 59-62.
Vance, C., et al., 2009. Mutations in FUS, an RNA Processing Protein, Cause Familial Amyotrophic Lateral Sclerosis Type 6. Science. 323**,** 1208-1211.
Vance, K. W., et al., 2005a. Tbx2 is overexpressed and plays an important role in maintaining proliferation and suppression of senescence in melanomas. Cancer Research. 65**,** 2260-2268.
Vance, K. W., et al., 2005b. Tbx2 is overexpressed and plays an important role in maintaining proliferation and suppression of senescence in melanomas. Cancer Res. 65**,** 2260-8.
Vandendries, E. R., et al., 1996. orthodenticle is required for photoreceptor cell development in the Drosophila eye. Dev Biol. 173**,** 243-55.
Varga, A. C., Wrana, J. L., 2005. The disparate role of BMP in stem cell biology. Oncogene. 24**,** 5713-21.
Vassall, K. A., et al., 2011. Decreased stability and increased formation of soluble aggregates by immature superoxide dismutase do not account for disease severity in ALS. Proceedings of the National Academy of Sciences. 108**,** 2210-2215.
Vawter, M. P., et al., 1996. TGFbeta1 and TGFbeta2 concentrations are elevated in Parkinson's disease in ventricular cerebrospinal fluid. Exp Neurol. 142**,** 313-22.
Veien, E. S., et al., 2008. Canonical Wnt signaling is required for the maintenance of dorsal retinal identity. Development. 135**,** 4101-11.
Veldhoen, K., et al., 2006. Spatio-temporal characterization of retinal opsin gene expression during thyroid hormone-induced and natural development of rainbow trout. Visual Neuroscience. 23**,** 169-179.
Verhoeven, M. C., et al., 2011. Wnt signaling regulates atrioventricular canal formation upstream of BMP and Tbx2. Birth Defects Res A Clin Mol Teratol. 91**,** 435-40.
Vieira, F. G., et al., 2015. Guanabenz Treatment Accelerates Disease in a Mutant SOD1 Mouse Model of ALS. PLoS One. 10**,** e0135570.
Viets, K., et al., 2016. Mechanisms of Photoreceptor Patterning in Vertebrates and Invertebrates. Trends Genet. 32**,** 638-59.
Vihtelic, T. S., et al., 1999. Cloning and characterization of six zebrafish photoreceptor opsin cDNAs and immunolocalization of their corresponding proteins. Visual Neuroscience. 16**,** 571-585.
Vihtelic, T. S., Hyde, D. R., 2000. Light-induced rod and cone cell death and regeneration the adult albino zebrafish (Danio rerio) retina. Journal of Neurobiology. 44**,** 289-307.
Vitorino, M., et al., 2009. Vsx2 in the zebrafish retina: restricted lineages through derepression. Neural Dev. 4**,** 14.
Voronina, V. A., et al., 2004. Mutations in the human RAX homeobox gene in a patient with anophthalmia and sclerocornea. Hum Mol Genet. 13**,** 315-22.

Waldron, P. V., et al., 2018. Transplanted Donor- or Stem Cell-Derived Cone Photoreceptors Can Both Integrate and Undergo Material Transfer in an Environment-Dependent Manner. Stem Cell Reports. 10, 406-421.
Walker, L. C., et al., 2016. The Prion-Like Properties of Amyloid-beta Assemblies: Implications for Alzheimer's Disease. Cold Spring Harb Perspect Med. 6.
Wall, D. S., et al., 2009. Progenitor cell proliferation in the retina is dependent on Notch-independent Sonic hedgehog/Hes1 activity. J Cell Biol. 184, 101-12.
Walsh, D. M., et al., 2002. Naturally secreted oligomers of amyloid beta protein potently inhibit hippocampal long-term potentiation in vivo. Nature. 416, 535-9.
Wan, J., Goldman, D., 2017. Opposing Actions of Fgf8a on Notch Signaling Distinguish Two Muller Glial Cell Populations that Contribute to Retina Growth and Regeneration. Cell Reports. 19, 849-862.
Wang, I. F., et al., 2012. Autophagy activators rescue and alleviate pathogenesis of a mouse model with proteinopathies of the TAR DNA-binding protein 43. Proc Natl Acad Sci U S A. 109, 15024-9.
Wang, I. F., et al., 2013. Autophagy activation ameliorates neuronal pathogenesis of FTLD-U mice: a new light for treatment of TARDBP/TDP-43 proteinopathies. Autophagy. 9, 239-40.
Wang, I. F., et al., 2008a. TDP-43, the signature protein of FTLD-U, is a neuronal activity-responsive factor. J Neurochem. 105, 797-806.
Wang, J., et al., 2009a. An ALS-Linked Mutant SOD1 Produces a Locomotor Defect Associated with Aggregation and Synaptic Dysfunction When Expressed in Neurons of Caenorhabditis elegans. Plos Genetics. 5.
Wang, J., et al., 2002. Fibrillar inclusions and motor neuron degeneration in transgenic mice expressing superoxide dismutase 1 with a disrupted copper-binding site. Neurobiology of Disease. 10, 128-138.
Wang, J. W., et al., 2011. The ALS-associated proteins FUS and TDP-43 function together to affect Drosophila locomotion and life span. J Clin Invest. 121, 4118-26.
Wang, L. J., et al., 2009b. Wild-type SOD1 overexpression accelerates disease onset of a G85R SOD1 mouse. Human Molecular Genetics. 18, 1642-1651.
Wang, Q., et al., 2008b. Protein aggregation and protein instability govern familial amyotrophic lateral sclerosis patient survival. PLoS Biol. 6, e170.
Wang, S., et al., 2014. A gene regulatory network controls the binary fate decision of rod and bipolar cells in the vertebrate retina. Dev Cell. 30, 513-27.
Wang, S. W., et al., 2001. Requirement for math5 in the development of retinal ganglion cells. Genes Dev. 15, 24-9.
Wang, W., et al., 2016. The inhibition of TDP-43 mitochondrial localization blocks its neuronal toxicity. Nat Med. 22, 869-78.
Wassle, H., et al., 2009. Glycinergic transmission in the Mammalian retina. Front Mol Neurosci. 2, 6.
Watabe, T., Miyazono, K., 2009. Roles of TGF-beta family signaling in stem cell renewal and differentiation. Cell Res. 19, 103-15.
Watanabe, M., et al., 2001. Histological evidence of protein aggregation in mutant SOD1 transgenic mice and in amyotrophic lateral sclerosis neural tissues. Neurobiol Dis. 8, 933-41.

Watson, M. R., et al., 2008. A Drosophila model for amyotrophic lateral sclerosis reveals motor neuron damage by human SOD1. Journal of Biological Chemistry. 283**,** 24972-24981.
Weber, I. P., et al., 2014. Mitotic position and morphology of committed precursor cells in the zebrafish retina adapt to architectural changes upon tissue maturation. Cell Rep. 7**,** 386-97.
Wegorzewska, I., et al., 2009. TDP-43 mutant transgenic mice develop features of ALS and frontotemporal lobar degeneration. Proc Natl Acad Sci U S A. 106**,** 18809-14.
Weinberger, C., et al., 1986. The c-erb-A gene encodes a thyroid hormone receptor. Nature. 324**,** 641-6.
Weishaupt, J. H., et al., 2013. A novel optineurin truncating mutation and three glaucoma-associated missense variants in patients with familial amyotrophic lateral sclerosis in Germany. Neurobiol Aging. 34**,** 1516 e9-15.
Weiss, G. A., et al., 2000. Rapid mapping of protein functional epitopes by combinatorial alanine scanning. Proceedings of the National Academy of Sciences of the United States of America. 97**,** 8950-8954.
Weser, U., et al., 1989. Mummified Enzymes. Nature. 341**,** 696-696.
Westerfield, M., 2000a. The zebrafish book. A guide for the laboratory use of zebrafish (Danio rerio). University of Oregon Press, Eugene, OR.
Westerfield, M., 2000b. The zebrafish book. A guide for the laboratory use of zebrafish (Danio rerio). University of Oregon Press, Eugene, OR 97403.
Willardsen, M. I., et al., 2009. Temporal regulation of Ath5 gene expression during eye development. Dev Biol. 326**,** 471-81.
Williams, G. R., 2000. Cloning and characterization of two novel thyroid hormone receptor beta isoforms. Mol Cell Biol. 20**,** 8329-42.
Wils, H., et al., 2010. TDP-43 transgenic mice develop spastic paralysis and neuronal inclusions characteristic of ALS and frontotemporal lobar degeneration. Proc Natl Acad Sci U S A. 107**,** 3858-63.
Wilson, S. G., et al., 2016. Tracking the fate of her4 expressing cells in the regenerating retina using her4:Kaede zebrafish. Experimental Eye Research. 145**,** 75-87.
Wine-Lee, L., et al., 2004. Signaling through BMP type 1 receptors is required for development of interneuron cell types in the dorsal spinal cord. Development. 131**,** 5393-403.
Wininger, F. A., et al., 2011. Degenerative Myelopathy in a Bernese Mountain Dog with a Novel SOD1 Missense Mutation. Journal of Veterinary Internal Medicine. 25**,** 1166-1170.
Winton, M. J., et al., 2008. Disturbance of nuclear and cytoplasmic TAR DNA-binding protein (TDP-43) induces disease-like redistribution, sequestration, and aggregate formation. Journal of Biological Chemistry. 283**,** 13302-13309.
Wishart, D. S., et al., 2006. DrugBank: a comprehensive resource for in silico drug discovery and exploration. Nucleic Acids Research. 34**,** D668-D672.
Wishart, T. M., et al., 2014. Dysregulation of ubiquitin homeostasis and beta-catenin signaling promote spinal muscular atrophy. J Clin Invest. 124**,** 1821-34.
Witan, H., et al., 2009. Wild-type Cu/Zn superoxide dismutase (SOD1) does not facilitate, but impedes the formation of protein aggregates of amyotrophic lateral sclerosis causing mutant SOD1. Neurobiology of Disease. 36**,** 331-342.
Woerner, A. C., et al., 2016. Cytoplasmic protein aggregates interfere with nucleocytoplasmic transport of protein and RNA. Science. 351**,** 173-6.
Wolman, M., Granato, M., 2012. Behavioral genetics in larval zebrafish: learning from the young. Dev Neurobiol. 72**,** 366-72.

Wong, P. C., et al., 1995. An Adverse Property of a Familial Als-Linked Sod1 Mutation Causes Motor-Neuron Disease Characterized by Vacuolar Degeneration of Mitochondria. Neuron. 14**,** 1105-1116.
Wood, W. M., et al., 1994. Structural and functional characterization of the genomic locus encoding the murine beta 2 thyroid hormone receptor. Mol Endocrinol. 8**,** 1605-17.
Wood, W. M., et al., 1991. Isolation and characterization of mouse complementary DNAs encoding alpha and beta thyroid hormone receptors from thyrotrope cells: the mouse pituitary-specific beta 2 isoform differs at the amino terminus from the corresponding species from rat pituitary tumor cells. Mol Endocrinol. 5**,** 1049-61.
Wright, G. S. A., et al., 2013. Ligand binding and aggregation of pathogenic SOD1. Nature Communications. 4.
Wyss-Coray, T., et al., 2000. Alzheimer's disease-like cerebrovascular pathology in transforming growth factor-beta 1 transgenic mice and functional metabolic correlates. Ann N Y Acad Sci. 903**,** 317-23.
Xiao, L., et al., 2013. BMP signaling specifies the development of a large and fast CNS synapse. Nat Neurosci. 16**,** 856-64.
Xu, Y. F., et al., 2010. Wild-type human TDP-43 expression causes TDP-43 phosphorylation, mitochondrial aggregation, motor deficits, and early mortality in transgenic mice. J Neurosci. 30**,** 10851-9.
Yamada, M., et al., 2000. Expression of chick Tbx-2, Tbx-3, and Tbx-5 genes during early heart development: evidence for BMP2 induction of Tbx2. Dev Biol. 228**,** 95-105.
Yamagishi, S., et al., 2007. An In Vitro Model for Lewy Body-Like Hyaline Inclusion/Astrocytic Hyaline Inclusion: Induction by ER Stress with an ALS-Linked SOD1 Mutation. Plos One. 2.
Yamanaka, K., et al., 2008. Astrocytes as determinants of disease progression in inherited amyotrophic lateral sclerosis. Nature Neuroscience. 11**,** 251-253.
Yamano, K., Miwa, S., 1998. Differential gene expression of thyroid hormone receptor alpha and beta in fish development. Gen Comp Endocrinol. 109**,** 75-85.
Yang, H. Q., et al., 2014. Species-dependent neuropathology in transgenic SOD1 pigs. Cell Research. 24**,** 464-481.
Yang, L., et al., 2006. Isl1Cre reveals a common Bmp pathway in heart and limb development. Development. 133**,** 1575-85.
Yang, Y. M., et al., 2013. A Small Molecule Screen in Stem-Cell-Derived Motor Neurons Identifies a Kinase Inhibitor as a Candidate Therapeutic for ALS. Cell Stem Cell. 12**,** 713-726.
Yaoita, Y., et al., 1990. Xenopus laevis alpha and beta thyroid hormone receptors. Proc Natl Acad Sci U S A. 87**,** 8684.
Yaron, O., et al., 2006. Notch1 functions to suppress cone-photoreceptor fate specification in the developing mouse retina. Development. 133**,** 1367-78.
Ye, M., et al., 2010. Mutation of the bone morphogenetic protein GDF3 causes ocular and skeletal anomalies. Hum Mol Genet. 19**,** 287-98.
Yen, P. M., Chin, W. W., 1994. New advances in understanding the molecular mechanisms of thyroid hormone action. Trends Endocrinol Metab. 5**,** 65-72.
Yin, S. Y., et al., 2007. Eris: an automated estimator of protein stability. Nature Methods. 4**,** 466-467.

Yokota, T., et al., 2001. Delayed-onset ataxia in mice lacking alpha -tocopherol transfer protein: model for neuronal degeneration caused by chronic oxidative stress. Proc Natl Acad Sci U S A. 98**,** 15185-90.
Yokota, T., et al., 1996. Retinitis pigmentosa and ataxia caused by a mutation in the gene for the alpha-tocopherol-transfer protein. N Engl J Med. 335**,** 1770-1.
Yokota, T., et al., 1997. Friedreich-like ataxia with retinitis pigmentosa caused by the His101Gln mutation of the alpha-tocopherol transfer protein gene. Ann Neurol. 41**,** 826-32.
Yoshida, S., et al., 2004a. Expression profiling of the developing and mature Nrl-/- mouse retina: identification of retinal disease candidates and transcriptional regulatory targets of Nrl. Hum Mol Genet. 13**,** 1487-503.
Yoshida, S., et al., 2004b. Expression profiling of the developing and mature Nrl(-/-) mouse retina: identification of retinal disease candidates and transcriptional regulatory targets of Nrl. Human Molecular Genetics. 13**,** 1487-1503.
Yoshimatsu, T., et al., 2014. Transmission from the dominant input shapes the stereotypic ratio of photoreceptor inputs onto horizontal cells. Nat Commun. 5**,** 3699.
Zhang, K., et al., 2001. A 5-bp deletion in ELOVL4 is associated with two related forms of autosomal dominant macular dystrophy. Nat Genet. 27**,** 89-93.
Zhang, L., et al., 2012. High temperature requirement factor A1 (HTRA1) gene regulates angiogenesis through transforming growth factor-beta family member growth differentiation factor 6. J Biol Chem. 287**,** 1520-6.
Zhang, X. S., et al., 2008. Clinical features of adverse reactions associated with telbivudine. World Journal of Gastroenterology. 14**,** 3549-3553.
Zhang, Y. J., et al., 2007. Progranulin mediates caspase-dependent cleavage of TAR DNA binding protein-43. J Neurosci. 27**,** 10530-4.
Zhou, S., et al., 2015. Differentiation of human embryonic stem cells into cone photoreceptors through simultaneous inhibition of BMP, TGFbeta and Wnt signaling. Development. 142**,** 3294-306.
Zhou, X. J., et al., 2006. Pharmacokinetics of telbivudine in healthy subjects and absence of drug interaction with lamivudine or adefovir dipivoxil. Antimicrobial Agents and Chemotherapy. 50**,** 2309-2315.
Zirzow, S., et al., 2009. Expression and requirement of T-box transcription factors Tbx2 and Tbx3 during secondary palate development in the mouse. Dev Biol. 336**,** 145-55.
Zon, L. I., Peterson, R. T., 2005. In vivo drug discovery in the zebrafish. Nature Reviews Drug Discovery. 4**,** 35-44.
Zou, J., et al., 2012. Crb Apical Polarity Proteins Maintain Zebrafish Retinal Cone Mosaics via Intercellular Binding of Their Extracellular Domains. Developmental Cell. 22**,** 1261-1274.
Zou, J., et al., 2010. Restricted Localization of Ponli, a Novel Zebrafish MAGUK-Family Protein, to the Inner Segment Interface Areas between Green, Red, and Blue Cones. Investigative Ophthalmology & Visual Science. 51**,** 1738-1746.
Zuber, M. E., et al., 2003. Specification of the vertebrate eye by a network of eye field transcription factors. Development. 130**,** 5155-67.

Appendix 1. Chapter 2 Supplemental Information

This appendix contains supplemental figures as referenced in Chapter 2.

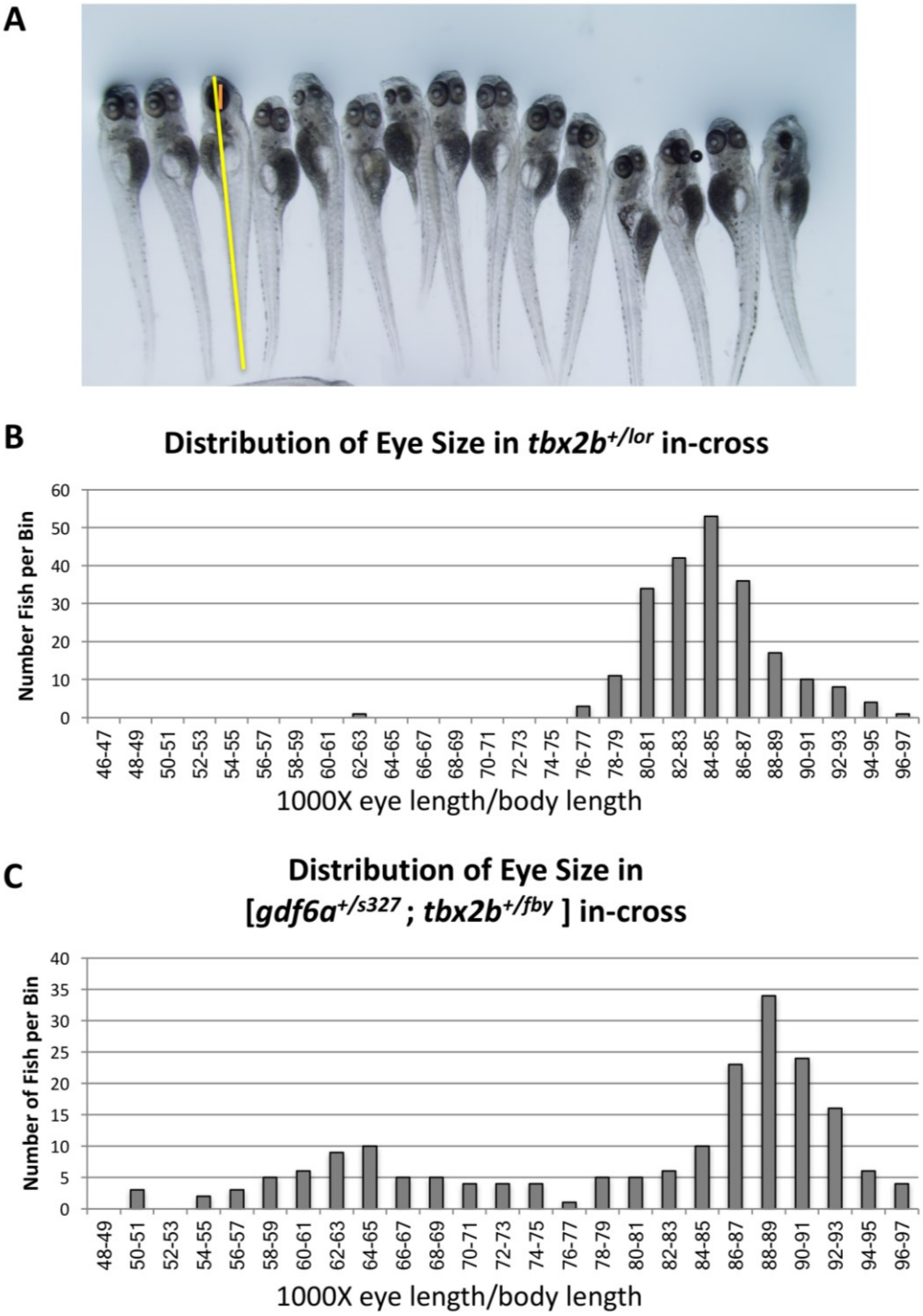

Figure A1.1. Eye size in various compound mutants shows no obvious change in severity of the microphthalmia phenotype (compare to Figure 2.1C).

A. Eye diameter along the anterior-posterior axis (orange line) was measured at 6dpf and normalized to body length (not including tail fin) (yellow line). Both normophthalmic and microphthalmic larvae are shown. **B**. Ratios of eye length to body length among the progeny of an in-cross of *tbx2b*$^{+/lor}$ fish show no obvious difference from wild type fish, (n=220). **C**. The same ratios among the progeny of an in-cross of [*gdf6a*$^{+/s327}$;*tbx2b*$^{+/fby}$] fish show the expected Mendelian abundance of ~25% microphthlamic fish (see also Fig 3B). The normophthalmic fish have eye sizes distributed in a normal fashion (Shapiro-Wilk Normality test, p>0.05). Among the microphthalmic progeny, there is also a normal distribution of eye size (Shapiro-Wilk test, p>0.05) (n=194).

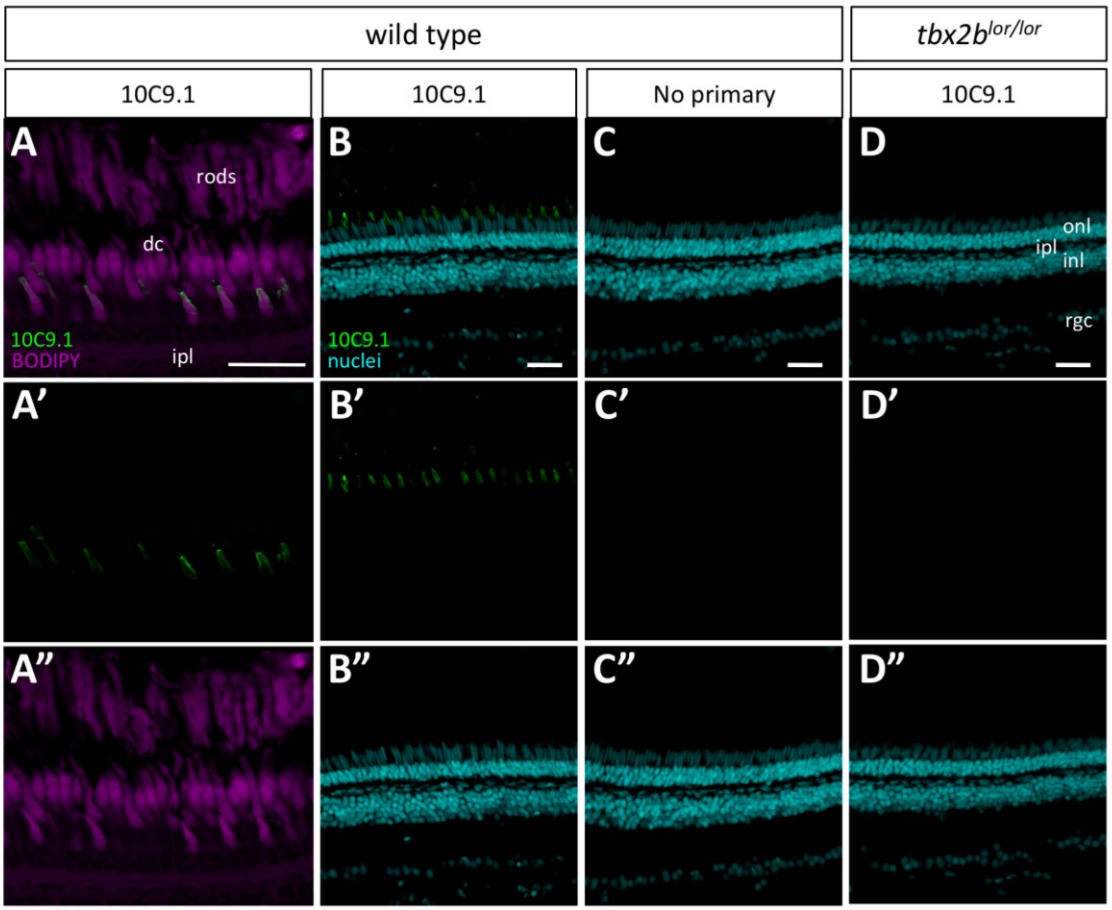

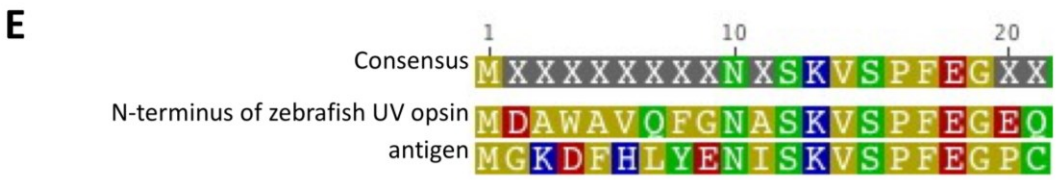

Figure A1.2. Antibody 10C9.1 specifically labels the outer segments of a class of short single cones in the adult zebrafish retina, as seen in Figure 5. **A.** Localization of 10C9.1 labelling to single cone outer segments as clarified by Bodipy counterstain of lipid-rich photoreceptor cell bodies and outer segments. **B-D.** 10C9.1 specificity is supported by localized labeling in the adult retina (B), a lack of labeling when adjacent retinal cryosections are treated identically except for omission of primary antibody (C), and by a dramatic decrease in number of cells labeled when 10C9.1 is applied to retinas from adult zebrafish mutants (*tbx2b*$^{lor/lor}$) that have a paucity of UV cones (D). Other negative controls included applying other rat IgGs as primary antibody, and these produced equivalent results to panel C. Retinas in panels B and D were treated identically including equivalent application of 10C9.1 antibody, and simultaneous processing of tissue by inclusion in the same tissue block prior to cryosectioning. The specificity of 10C9.1 is supported by the paucity of labeling in *tbx2b*$^{lor/lor}$ retinas (D), which are known to have few UV cones. Scale bars 30μm. “rods” indicates rod outer segments; dc, double cones; ipl; inner plexiform layer; onl, outer nuclear layer; inl, inner nuclear layer; rgc, retinal ganglion cell layer. **E.** An alignment of the antigen used to raise 10C9.1 in rats, which represents the 20 N-terminal amino acids from rainbow trout UV opsin plus a C-terminal cysteine to enable linkage of the peptide to the carrier protein keyhole limpet hemocyanin.

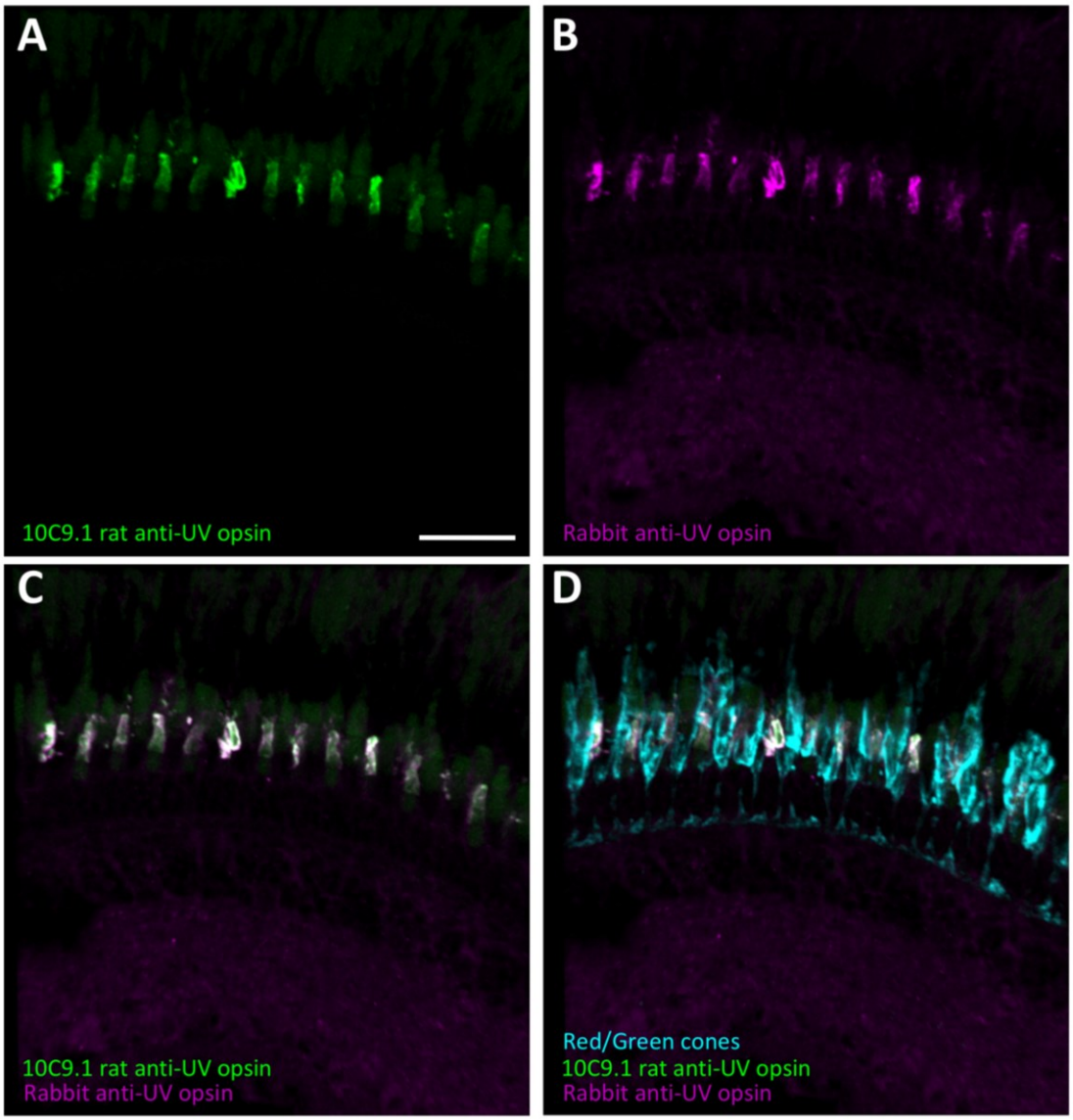

Figure A1.3. 10C9.1 colocalizes with existing rabbit anti-UV antibody (provided by David Hyde, University of Notre Dame). Scale bar 30μm. Both the 10C9.1 rat anti-UV and Hyde rabbit anti-UV are somewhat over-exposed to demonstrate background/autofluorescent labeling.

Appendix 2. Chapter 3 Supplemental Information

This appendix contains supplemental figures for Chapter 3 and preliminary qPCR data relevant to Chapters 3 and 8.

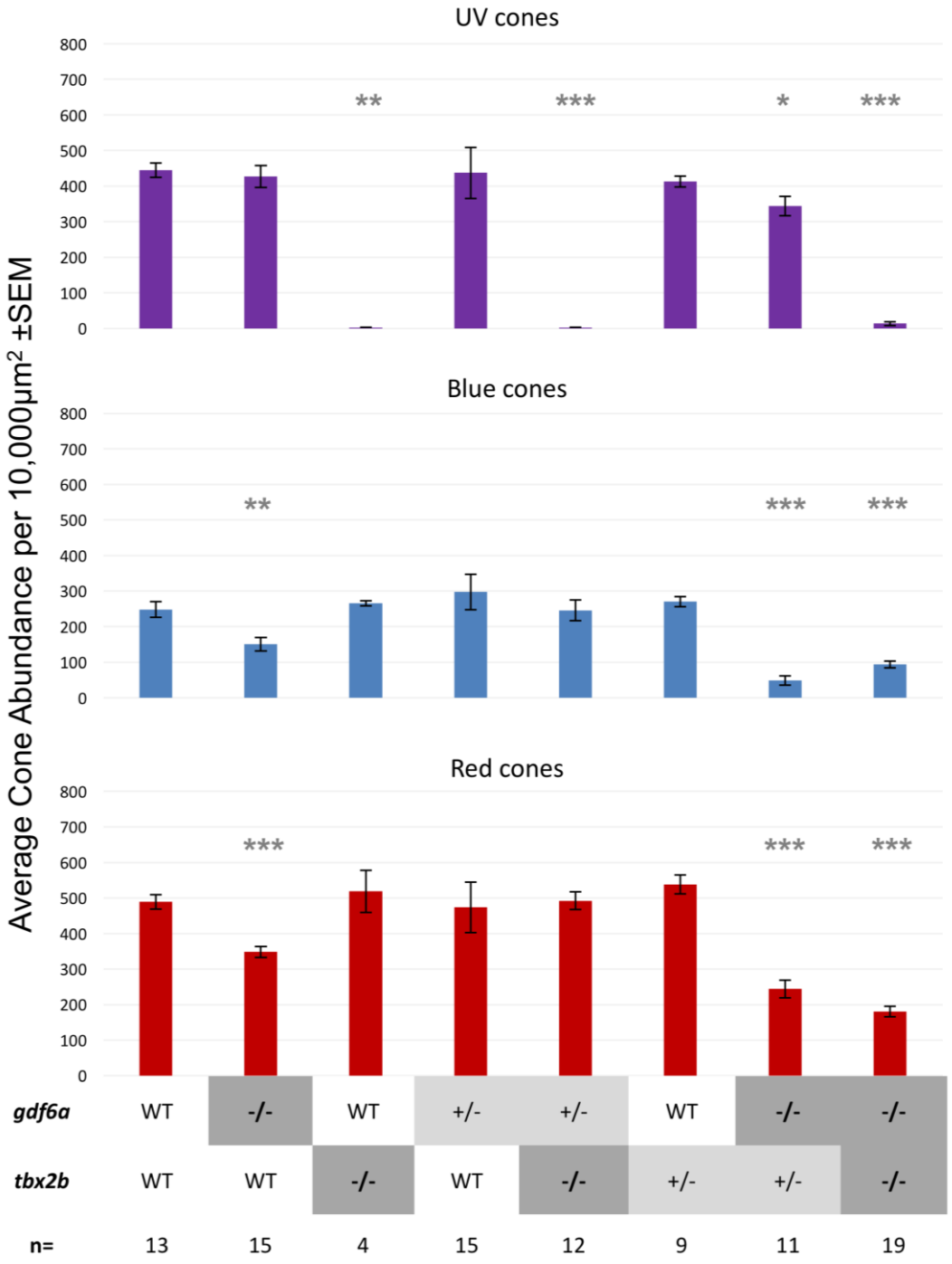

Figure A2.1. Average cone abundances in embryos of *gdf6a*$^{+/s327}$; *tbx2b*$^{+/fby}$ mutant incrosses.

Representation of Figure 1 data as average abundances of UV, blue, and red cones per 10,000μm^2. Cones were quantified in 4dpf compound mutants; statistical comparisons were performed against wildtype sibling values (Kruskall Wallis ANOVA, *p< 0.05, ** p>0.01, ***p>0.001).

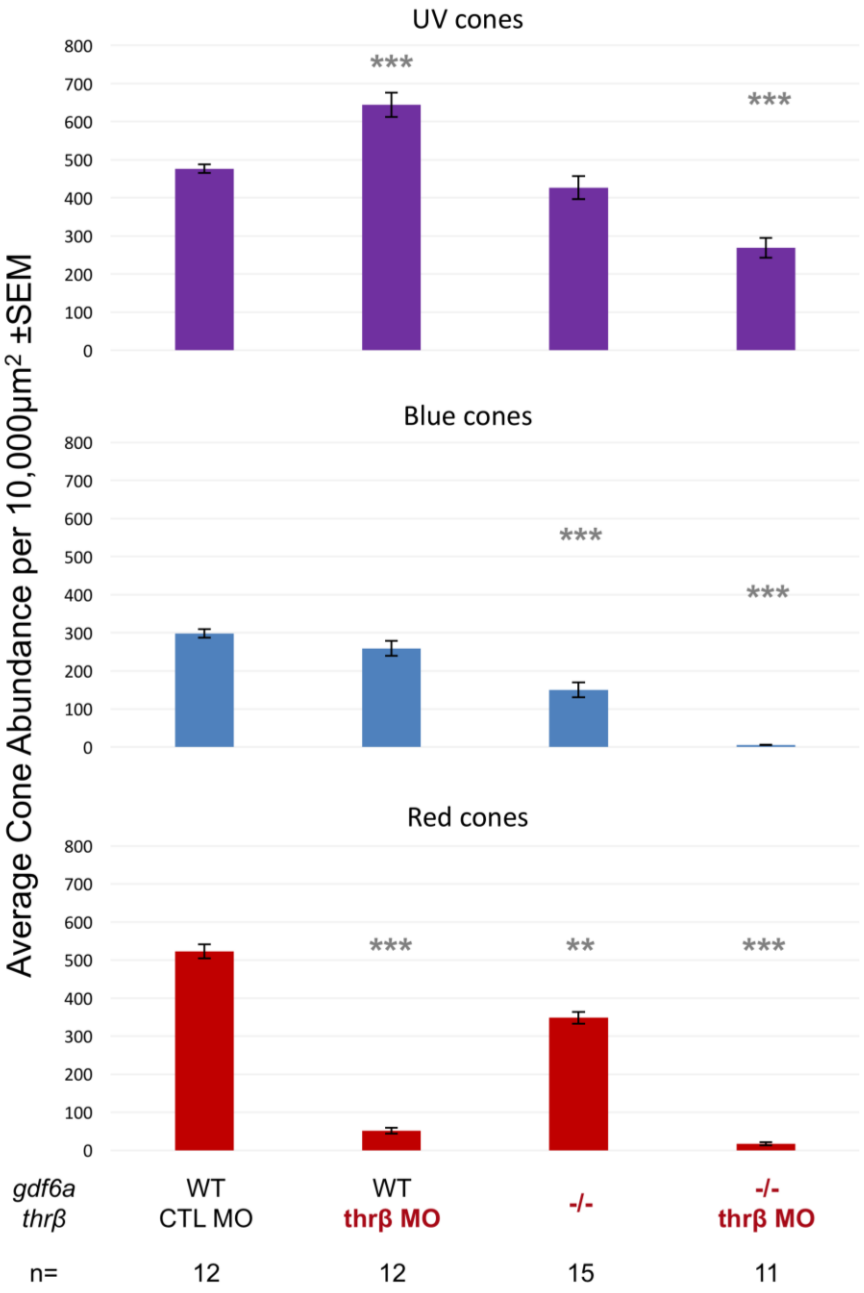

Figure A2.2. Average cone abundances in MO-injected *gdf6a* mutants.

Representation of Figure 2 data as average abundances of UV, blue, and red cones per 10,000µm^2. Cones were quantified in 4dpf embryos; statistical comparisons were performed against control (CTL) MO-injected wildtype sibling values (Kruskall Wallis ANOVA, *p< 0.05, ** p>0.01, ***p>0.001).

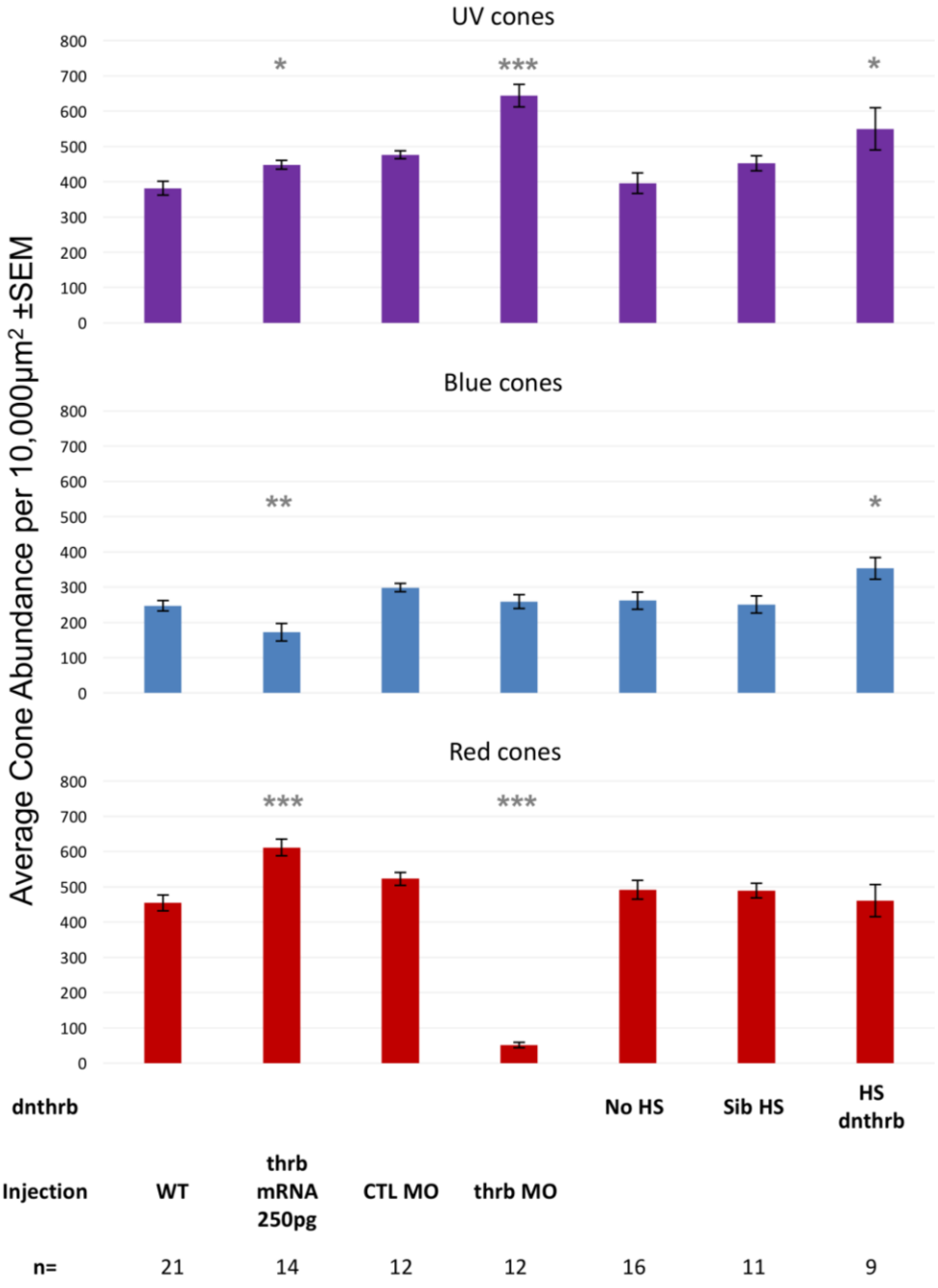

Figure A2.3. Average cone abundances in MO-injected embryos and *dnthrβ* embryos.

Representation of Figure 3 data and supplemental data shown as average abundances of UV, blue, and red cones per 10,000µm^2. Cones were quantified in 4dpf embryos

with control (CTL) or *thrβ* MO injection, and in *dnthrβ* embryos (with and without heat shock [HS] shown) and siblings; statistical comparisons were performed against CTL MO or sibling values (Kruskall Wallis ANOVA, *p< 0.05, ** p>0.01, ***p>0.001).

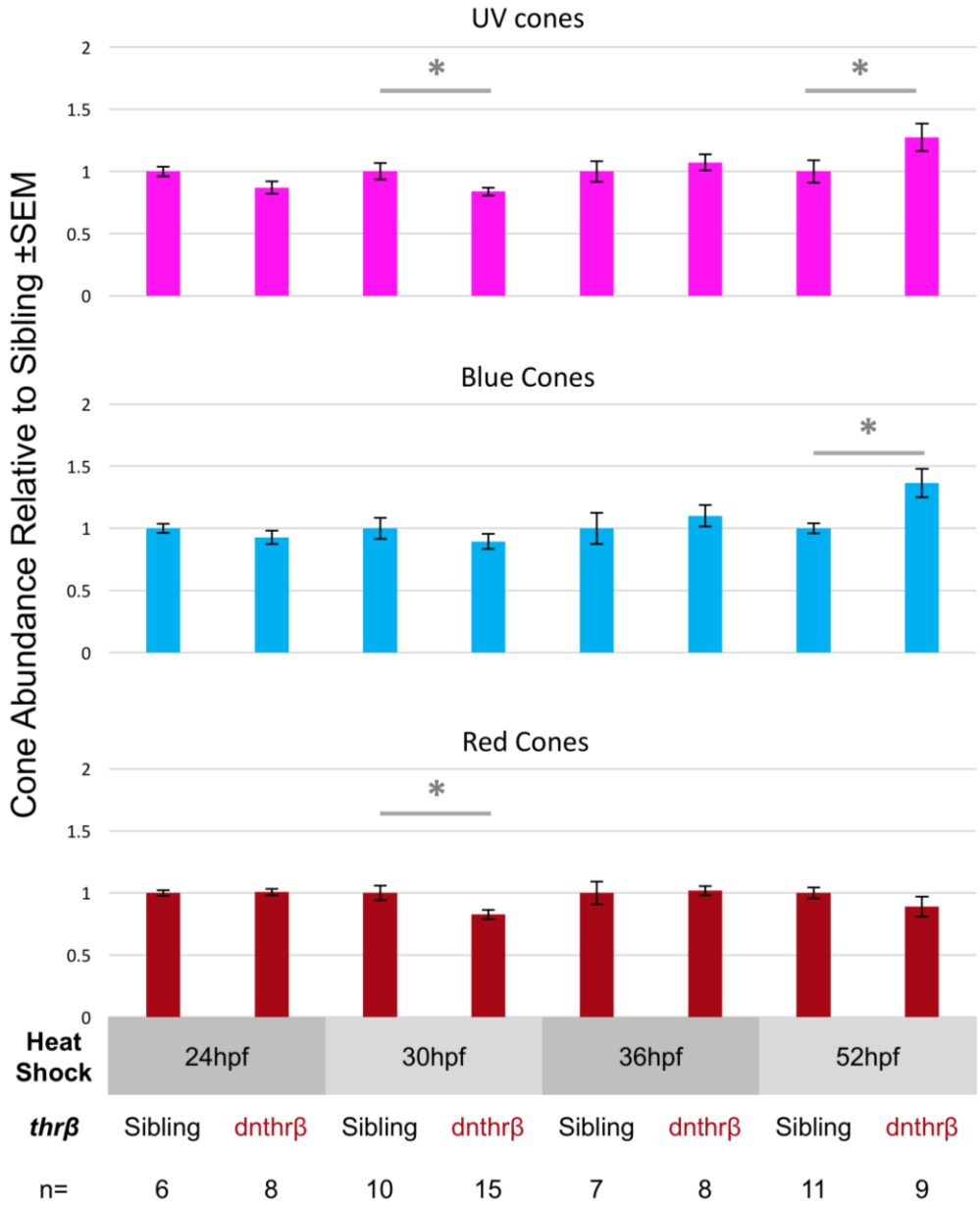

Supplemental Figure 4. Normalized UV, blue, and red cone abundances following induction of *dnthrβ* at 24, 30, 36, and 52 hours post-fertilization.

Transgenic embryos (*dnthrβ*) and nontransgenic siblings (Sibling) were heat shocked at the ages indicated, and cone subtype abundances were measured at 4dpf. Values for transgenics are normalized to nontransgenic siblings that were heat shocked at the same age (Kruskall-Wallis pairwise comparisons with exact permutation, *$p<0.05$)

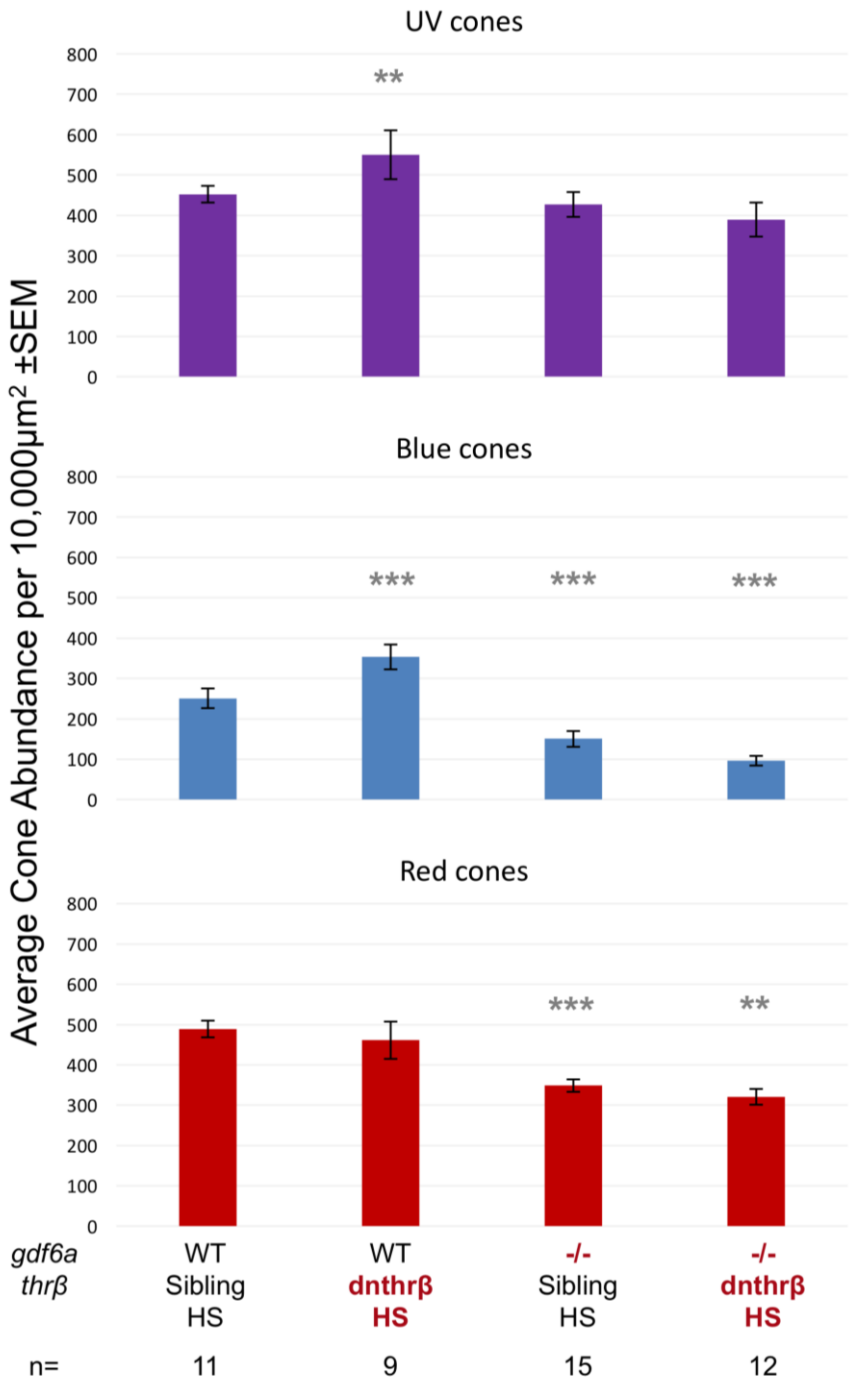

Figure A.2.5. Average cone abundances in *gdf6a* ; *dnthrβ* mutants.

Representation of Figure 4 data as average abundances of UV, blue, and red cones per 10,000µm^2. Cones were quantified in 4dpf embryos that were either wildtype or *gdf6a*$^{s327/s327}$ and either transgenic or non-transgenic (Sibling) for *dnthrβ*; all embryos

were heat shocked at 52hof. Statistical comparisons were performed against wildtype sibling values (Kruskall Wallis ANOVA, *p< 0.05, ** p>0.01, ***p>0.001).

Using quantitative RT-PCR (qPCR), we measured relative transcript abundances for *gdf6a*, *tbx2b*, and *thrβ* in the following groups: wildtype, *gdf6a*$^{s327/s327}$, *tbx2b*$^{lor/lor}$, heat shocked *dnthrβ* transgenic, and heat shocked non-transgenic siblings. Transcript levels were normalized to average wildtype values. Groups were run in triplicate, with RNA from 10 whole embryos per replicate. Primer design and validation, RNA extraction, cDNA synthesis, qPCR reactions and analysis were performed by Gavin Neil.

2.1. Methods for qPCR

Embryos from incrosses of wildtype, *gdf6a*$^{+/s327}$, *tbx2b*$^{lor/lor}$, and *dnthrβ* transgenic fish were collected and screened for appropriate phenotype where necessary: embryos of *gdf6a*$^{+/s327}$ fish were selected for microphthalmia at 48hpf, and embryos from *dnthrβ* transgenics were heat shocked at 46hpf and sorted for GFP expression prior to fixation. Whole embryos were fixed in RNAlater (Qiagen 76104) at 52hpf.

RNA extraction was performed with an RNeasy mini kit (Qiagen 74106) plus DNase 1 enzyme (Qiagen 79254). RNA was aliquoted and stored at -80°C until use. cDNA was synthesized with Quantabio qscript supermix (Quantabio 95048-100) and final product was diluted 1:10 for use in qPCR. For quantitative PCR (qPCR), a master mix was made with 5μL SYBR green and 2.5μL each of forward and reverse primers (final primer concentrations 3.2μM). Primers used are listed in Table A2.1; primer validation was performed with a cDNA dilution series, using the same reaction parameters as indicated below. *Beta-actin* served as an endogenous control. Reactions each consisted of 7.5μL master mix and 2.5μL of cDNA (or water as no template control) for a final volume of 10μL. Three biological replicates of 10 embryos were run in triplicate reactions for all groups.

Quantitative PCR was run in a 7500 Fast Real-Time PCR system at the following parameters:

Hold: 95°C x 2 minutes

Cycling (40 cycles): 95°C x 15s ; 60°C x 1 minute

Melt curve stage (2 cycles): 95°C x 15s; 60°C x 1 minute

Expression values of *gdf6a*$^{+/s327}$, *tbx2b*$^{lor/lor}$, and *dnthrβ* samples were calculated as percentage of wildtype values (Figure A2.1).

Table A2.1. Primers used for qPCR.

Target	Forward primer	Reverse primer
Beta actin	5' – GGG ACA GGT CAT CAC CAT TG – 3'	5' GAT GTC GAC GTC ACA CTT CA – 3'
gdf6a	5' CTT CCG CAA CTG TCC AAG TAC TCT - 3'	5' TTG CGA GTC TTT TTT TTT CCT TGT - 3'
tbx2b	5' CAG CAC GGC GTC CTC TCT - 3'	5' GTG AGC AGG TTT GTG CTT TGA G - 3'
thrβ	5' - TGA CAG ACC TGC GCA TGA TT - 3'	5' GGA AAG AGC TCT GTG GGA CAT T - 3'

2.2. Transcripts of *gdf6a*, *tbx2b*, and *thrβ* in *gdf6a*$^{s327/s327}$, *tbx2b*$^{lor/lor}$, and *dnthrβ* zebrafish

While neither of the mutants or the *dnthrβ* groups' expression values reached statistical significance compared to wildtype values (Mann-Whitney U test, significance at $p<0.05$), there are promising trends that are described below. Because samples consisted of whole embryos, changes in transcript levels in the eyes may have been obscured by expression in the rest of the body.

Expression levels of the *gdf6a* transcript were unchanged except in *gdf6a* mutants, which had a high expression (166%) compared to wildtypes. The *gdf6a s327* mutation is a point mutation resulting in a premature stop codon, thus enhanced transcript levels may be a results of feedback mechanisms.

Tbx2b expression also showed no significant change. *Tbx2b* mutants had lower (but nonsignificant) expression of *tbx2b* compared to wildtypes, at 46% of wildtype levels. The *lor* mutation is suspected to be in an upstream regulatory sequence, as these mutants had shown reduced mRNA expression through RT-PCR at 20 and 28hpf by others (Alvarez-Delfin et al., 2009), with no mutation in the coding region. Thus the *lor* mutation appears to partially reduce *tbx2b* expression.

Expression of *thrβ* showed surprising though statistically non-significant results: *dnthrβ* transgenics did not have different levels than wildtype, but non-transgenic siblings did, showing almost twice as much transcript (193%). *Tbx2b* mutants had even higher levels at 231% of wildtype, and *gdf6a* mutants were also slightly increased (141%). Though these values did not reach significance, it may be possible that tbx2b and gdf6a contribute to regulation of *thrβ* expression via suppressive mechanisms or pathways, and when *gdf6a* or *tbx2b* are reduced, *thrβ* expression is dysregulated. Both *gdf6a* and *tbx2b* mutants have reduced cone phenotypes (Chapter 3), which may be (in part) due to *thrβ* overexpression. This potentiality is also discussed in Chapter 8.

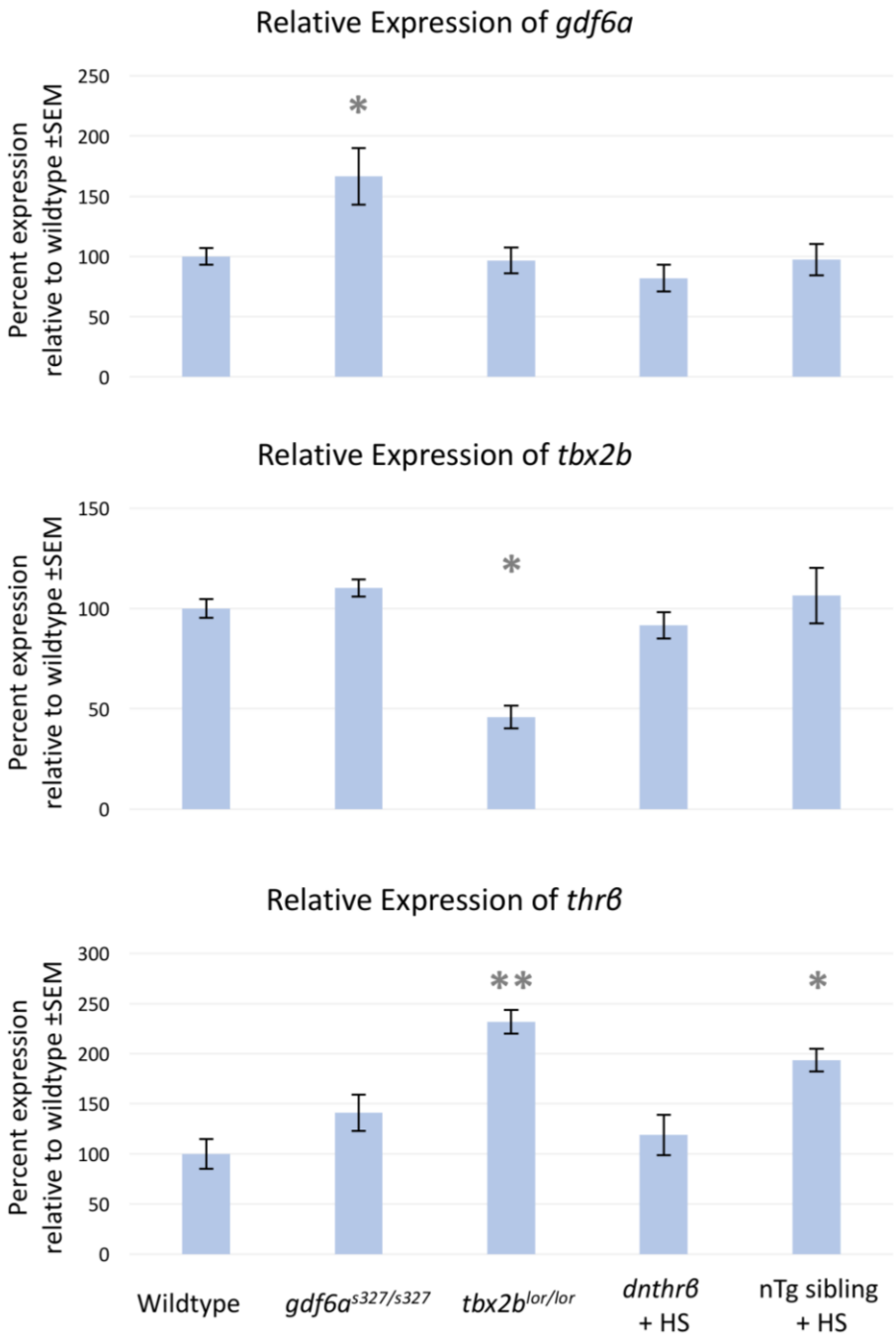

Figure A2.6. Relative expression of *gdf6a*, *tbx2b*, and *thrβ* in wildtype, *gdf6a*$^{s327/s327}$, *tbx2b*$^{lor/lor}$, and *dnthrβ* transgenic and nontransgenic sibling embryos (2dpf).

Dnthrβ transgenic and nontransgenic (nTg) siblings were heat shocked (+HS) 4 hours prior to preservation in RNAlater.

Appendix 3. Chapter 4 Supplemental Information

This appendix contains supplemental figures for Chapter 4.

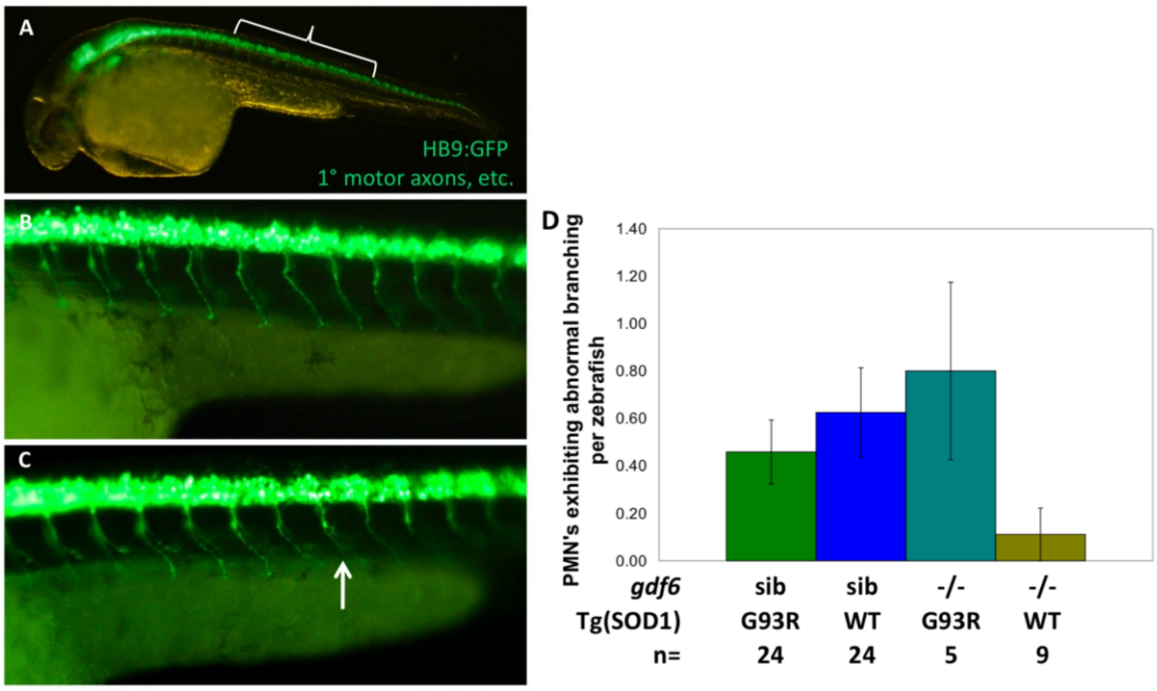

Figure A3.1. In larval zebrafish, mutations in *gdf6a* do not appreciably sensitize Sod1^{G93R} zebrafish to develop ALS-like symptoms.

Four genotypes combining *gdf6a*$^{-/-}$ alleles and Sod1^{G93R} alleles were examined in Tg(HB9:eGFP) zebrafish expressing GFP in the axons of primary motor neurons (PMN), or via immunohistochemistry. **A.** Bracket indicates position of axons quantified, magnified in B, C. **B.** Normal primary motor axons. **C.** An example of an abnormal primary motor neuron axon (arrow). **D.** Quantification of primary motor axons in 30 hours post-fertilization embryos show no difference based on *gdf6a* genotype; Thus effects are not developmental, and accord with a late-onset phenotype. Results indicated no significant effect of *gdf6a* on the presence of axonopathies ($p \geq 0.315$,

n≥5 larvae per genotype), although the highest rate of PMN axon abnormalities were observed in *gdf6a*$^{-/-}$; Sod1$^{+/G93R}$ larvae.

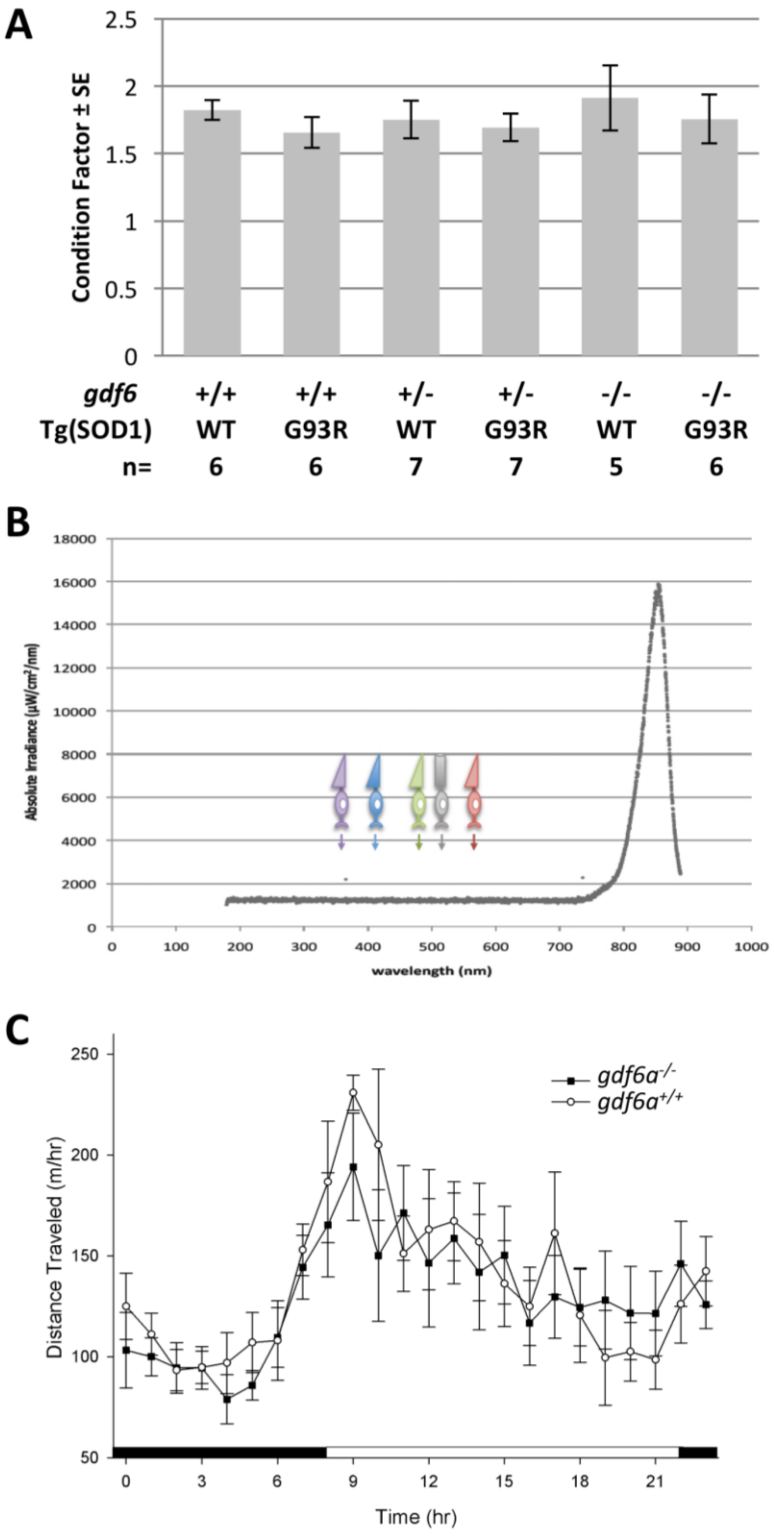

Figure A3.2. Eliminating alternate hypotheses that might account for differences in swimming behaviour between *gdf6a*$^{-/-}$ zebrafish and their siblings.

Our overall conclusion is that *gdf6a* mutants have deficits in endurance due to a progressive loss of spinal motor neurons and disrupted neuromuscular junctions. Alternative explanations for these fish having reduced endurance are eliminated here. **A.** Body morphology was not significantly different based on genotype. Condition factor was determined using the standard formula from mass (g) and body length (BL, in mm), calculated as 100000Xmass/BL3. Condition factor did not vary based on genotype. Sample sizes (number of fish) indicated at the bottom of graph. **B.** Acute deficits in vision cannot account for differences between microphthalmic *gdf6a*$^{-/-}$ fish and their wildtype siblings. Infrared lighting conditions during behavioural tracking of zebrafish excludes a role for visual dysfunction in the assays of fish activity, power or endurance. Grey trace indicates photons available to fish during recording sessions. Arrows annotate the maximal wavelength of sensitivity of photoreceptors in zebrafish [73]: rod photoreceptors (grey) and cone photoreceptors (coloured to indicate spectral sensitivity, magenta for ultraviolet-sensitive cone, and blue-, green- and red-sensitive cones are indicated by the cognate colour) are documented. In sum, the infrared conditions used prevented vision from impacting behaviour of wild type or mutant fish the during tracking of fish movement in the open field test, endurance tests or sprint tests. **C.***Gdf6a*$^{-/-}$ zebrafish in open field test shows no significant difference in average movement compared to wild type siblings. Fish movement tracked over 24 hours, bar below abscissa indicates lights on and off. Mutant fish had near-normal activity levels throughout the circadian cycle. A

lower average movement in mutants is noted immediately after the lights turn on (0800–0900 h, compared to siblings), though this difference is not expected to occur in normal husbandry conditions: The data herein tracked groups of mutant fish, or groups of sibling fish, maintained in separate tanks (because automated video tracking of individuals in mixed populations was unreliable), whereas in normal husbandry conditions the microphthalmic *gdf6a*$^{-/-}$ mutants were housed in the same tanks as their siblings. This is impactful, because breeding is cued by lights turning on, and microphthalmic fish had increased movement during breeding (and bred successfully) only if housed with normal fish. If all fish in a tank are microphthalmic *gdf6a*$^{-/-}$, they fail to exhibit breeding behaviour and thus have less vigorous movement. Because our *gdf6a*$^{-/-}$ fish were raised in mixed populations with normophthalmic siblings, they likely had near-normal movement activity when the lights were automatically turned on each morning. This data is summarized in Figure 4.4C, concluding no significant difference in total movement between genotypes.

Appendix 4. Chapter 5 Supplemental Information

This appendix contains supplemental figures for Chapter 5.

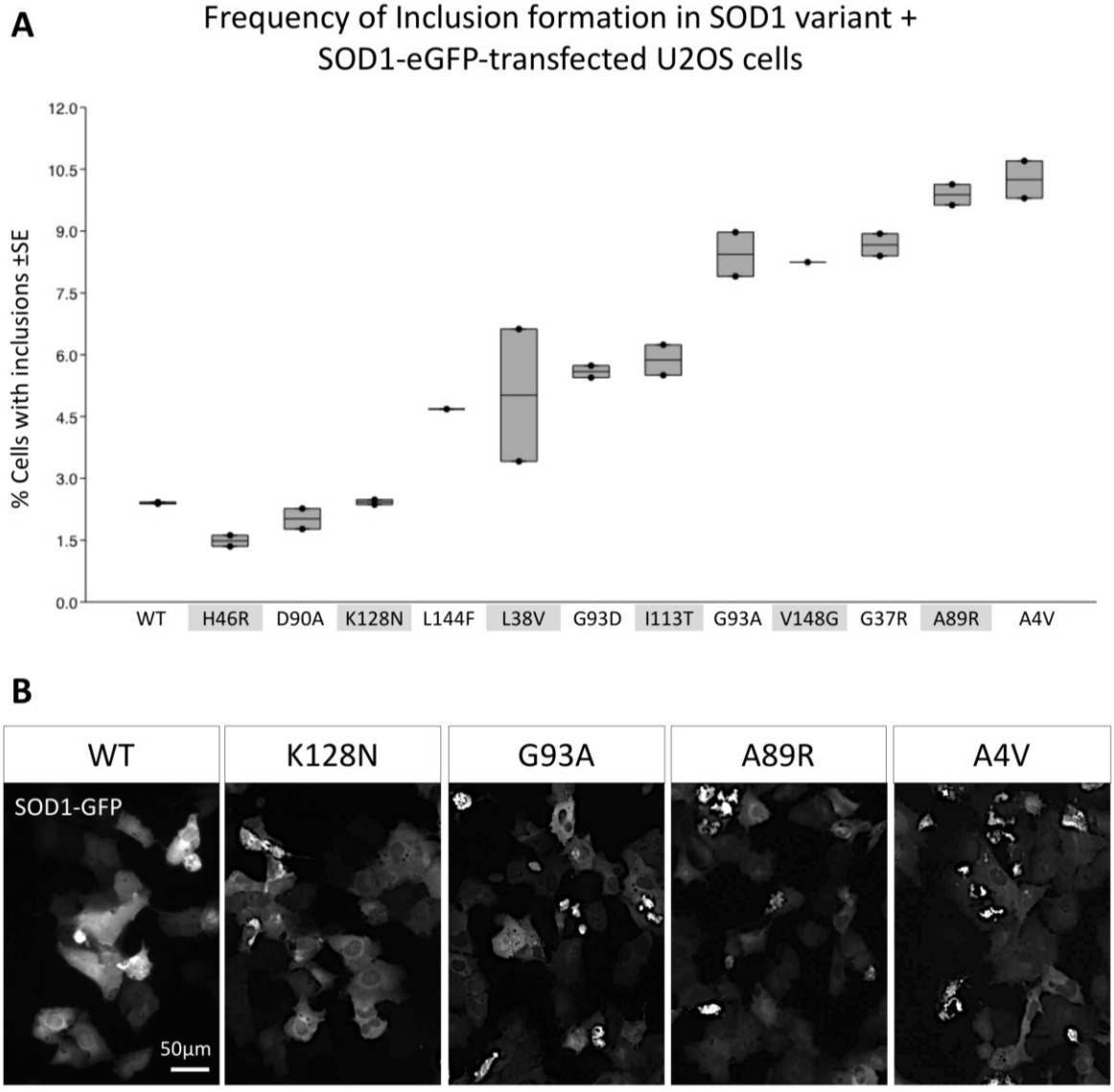

Figure A4.1. Frequency of inclusion formation by novel SOD1 variants compared to wildtype and clinical mutant variants.

A. U2OS cells were transfected with a pCMV.SOD1-GFP reporter vector and a vector with the SOD1 variant indicated, and imaged for GFP fluorescence following incubation for 24 hours. The number of cells with one or more inclusions is reported as a percentage of total cells. One or two replicates per variant shown; boxplot shows

median and standard error, with individual data points (black dots) shown. Transfection with $SOD1^{WT}$ caused inclusions in a small percentage of cells, whereas clinical mutations L144F, L38V, G93D, I113T, G93A, V148G, G37R, and A4V caused inclusions in a greater percentage of cells. Novel variant A89R caused inclusions at a relatively high rate similar to A4V, but novel variant K128N caused inclusions at a rate similar to WT. Results are preliminary and require replication for statistical analysis. **B.** Selection of representative images of cells transfected with SOD1-eGFP and variants indicated.

Appendix 5. Chapter 6 Supplemental Information

This appendix contains supplemental information for Chapter 6.

Table A5.1. Top-ranked compounds binding at the W32 site of SOD1 identified in high throughput virtual screening (HTVS) and pharmacophore screening of a library of FDA approved compounds

Supplemental Table 1. Top-ranked compounds binding at the W32 site of SOD1 identified in high throughput virtual screening (HTVS) and pharmacophore screening of a library of FDA approved compounds. [1]

Rank	Ligand name	ΔG (Kcal/mol)	TPSA (Å^2)	Acc	Don	Log S	Log P	Lipinski Violation count	Oprea violation count	Rotable bonds	BBBP	Toxic?
1	L-1	-10.3	110.6	7	2	-0.93	-1.03	0	0	1	yes	unknown
2	L-2	-8.9	99.0	7	3	-1.36	-1.15	0	0	3	yes	yes
3	L-3	-7.8	87.0	6	4	-2.01	-0.11	0	0	2	unknown	unknown
4	L-4	-7.6	104.8	8	2	-8.02	4.63	0	2	6	unknown	yes
5	**L-5 Telbivudine**	**-7.6**	**99.0**	**7**	**3**	**-0.29**	**-0.17**	**0**	**0**	**2**	**yes**	**no**
6	L-6	-7.5	152.7	12	3	-3.73	0.81	2	3	11	unknown	mild
7	L-7	-7.4	78.0	6	2	-1.42	-0.23	0	0	2	yes	unknown
8	L-8	-6.7	58.6	5	1	-1.27	-0.01	0	0	1	unknown	yes
9	L-9	-6.7	99.0	7	3	-0.66	-1.60	0	0	2	yes	yes
10	L-10	-6.6	78.8	6	2	-0.79	-1.01	0	0	2	yes	yes
	5'-FUrd	**-5.3**	**119.3**	**8**	**4**	**-0.26**	**-2.61**	**0**	**0**	**2**	**yes**	**possible**
	Uridine	**-4.6**	**119.3**	**8**	**4**	**0.13**	**-2.84**	**0**	**0**	**2**	**yes**	**no**

The HTVS and pharmacophore screening studies were performed with the MOE integrated drug discovery software package (*Molecular Operating Environment (MOE)*, 2013.08; Chemical Computing Group Inc., 1010 Sherbooke St. West, Suite #910, Montreal, QC, Canada, H3A 2R7, 2016). The chemical descriptors for the ligand molecules were calculated with MOE package, and blood brain barrier permeability (BBBP) and toxicity information of ligands were taken from Drugbank database (https://www.drugbank.ca). ΔG- London binding free energy (Kcal/mol); TPSA-the polar surface area of a compound; *Acc* and *Don*- numbers of hydrogen bond acceptor (O and N atoms) and donor atoms (OH and NH atoms), respectively; Log S- logarithm of aqueous solubility of a compound; Log P- logarithm of the octanol/water partition

coefficient of a compound. Uridine and 5′-fluorouridine (5′-FUrd) are presented for comparison.

Appendix 6. Chapter 7 Supplemental Information

This appendix contains supplemental figures for Chapter 7.

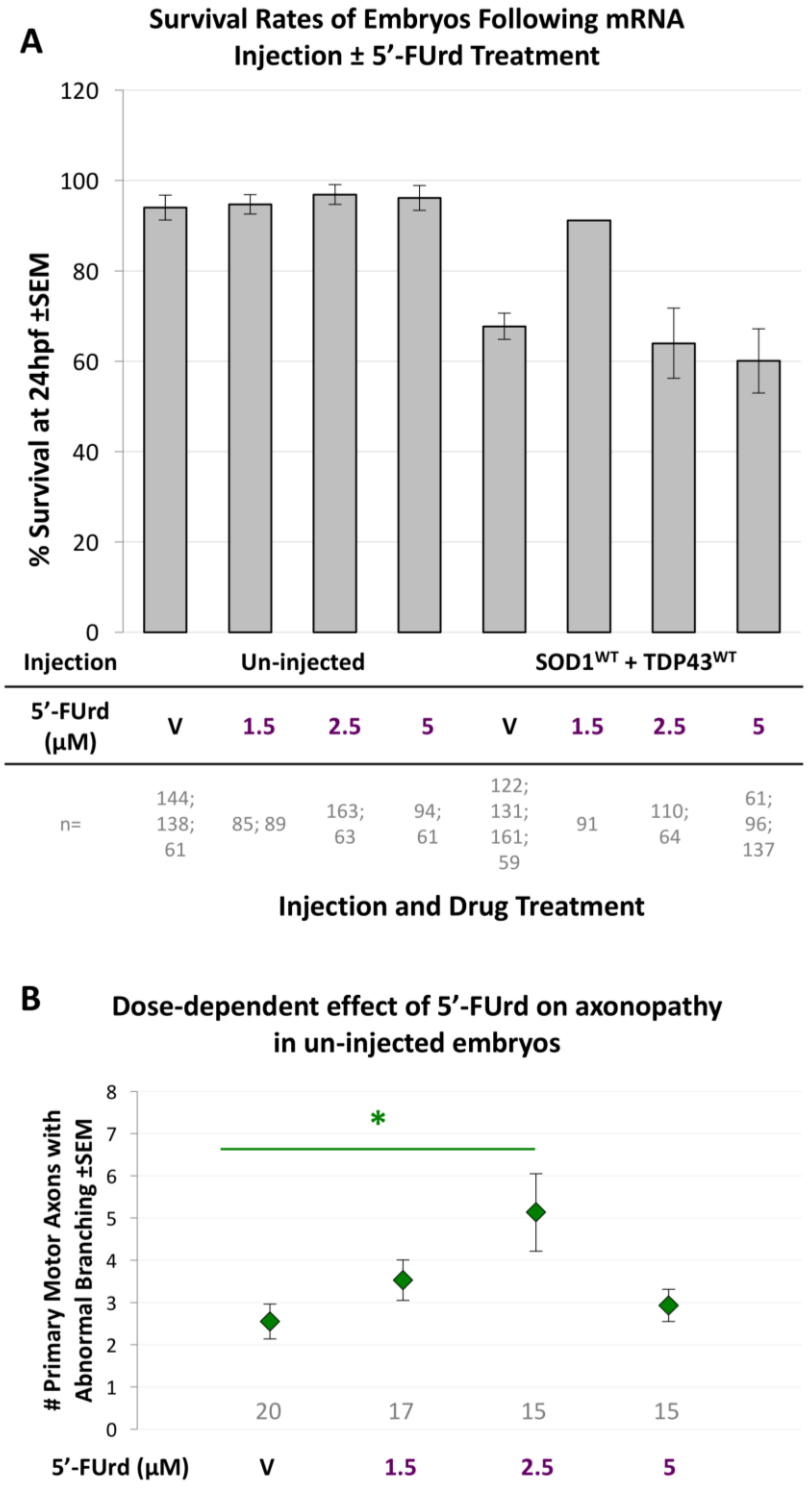

Figure A6.1. Independent effects of 5'-FUrd on survival and axonopathy.

A. Rates of survival at 24hpf among clutches of either un-injected embryos or embryos injected with SOD1WT + TDP43WT, following exposure to 5′-FU at the concentrations indicated (drug applied at 12hpf). Sample sizes (n=) of clutches noted below graph. **B.** Axonopathy among 36hpf un-injected embryos following exposure to 5′FUrd at the concentrations indicated (drug applied at 12hpf). * $p<0.05$ (Kruskall-Wallis ANOVA with Mann-Whitney pairwise comparisons).

Appendix 7. Characterization of *elovl4b* expression in the zebrafish retina

7.1. Introduction

Stargardt macular dystrophy (a.k.a. fundus flavimaculatus) is the most common juvenile macular degenerative disease, with prevalence between 1/8,000-1/10,000, accounting for approximately 7% of all retinal dystrophies. Mutations in three genes are known to be causative: *ABCA4*, *PROM1*, and *ELOVL4* (Elongase of very long-chain fatty acids-like 4). Mutation in ELOVL4 causes Stargardt Disease 3 (STGD3, OMIM# 600110). All documented mutations in ELOVL4 are located in exon 6, involving nucleotide deletion (790-794delAACTT (Griesinger et al., 2000; Zhang et al., 2001) and 789delT; 794delT (Bernstein et al., 2001)) or introduction of a premature stop codon (Y270X (Maugeri et al., 2004)), leading to C-terminal truncation and loss of a putative endoplasmic reticulum retention signal.

The protein encoded by *ELOVL4* is a multispan membrane protein located in the endoplasmic reticulum (inner segment), where it elongates very long chain polyunstaturated fatty acids (VLC-PUFAs). VLC-PUFAs are thought to contribute to the fluidity of the photoreceptor cell membrane, and are also components of lipids in the brain, testis and skin (Hopiavuori et al., 2018; Mandal et al., 2004). It has been proposed that loss of ELOVL4 function leads to reduced VLC-PUFA levels, which contributes to PhR loss. The true role of VLC-PUFAs is not known, but there is speculation that their extremely chains can span double membranes and may provide stability in highly curved membranes (such as photoreceptor outer segment membrane disks) (Agbaga, 2016; Agbaga et al., 2008). Another proposed purpose of VLC-PUFAs suggestion is to increase synaptic vesicle size, as VLC-PUFAs are found at the photoreceptor synapses, and in mouse Elovl4 conditional knockouts, the photoreceptor synaptic vesicles appeared smaller and mislocalized (Bennett et al., 2014).

Transgenic mouse models expressing clinical mutants of ELOVL4 exhibit accumulation of undigested phagosomes in the retinal pigment epithelium followed by photoreceptor degeneration. Thus pathology in the retinal pigment epithelium contributes to loss of photoreceptors.

Because mutation in *ELOVL4* results in an early-onset degeneration affecting the macula, which is populated by cones exclusively, we wanted to examine how mutation in ELOVL4 leads to cone photoreceptor death. Zebrafish have two paralogues, *elovl4a* and *elovl4b*, so we documented their expression with *in situ* hybridization. *Elovl4b* showed expression more specific to the retina and putatively the photoreceptor layer in larvae. In adult retinas, we tested a commercial ELOVL4 antibody and found consistent signal in the inner segments of photoreceptors, which is where we predict Elovl4b protein to be located based on its function at the endoplasmic reticulum. Subsequently we performed morpholino knock down in an attempt to assess the effects of *elovl4b* loss of function on developing photoreceptors, but preliminary results did not show a phenotype. Alternatively, photoreceptor degeneration in STGD3 may be caused by the protein product of mutant *ELOVL4*, and not simply loss of function. To test this, we designed transgenic constructs to express either wildtype human ELOVL4 or the clinical mutant ELOVL4^{794delAACTT} under photoreceptor specific promoters. Validation of the transgenic fish is ongoing and will not be presented here.

7.2. Methods

In situ hybridization was performed using PCR-based antisense riboprobes. Template for riboprobe synthesis was created from larval cDNA for *elovl4a* and adult retinal cDNA for *elovl4b* using the Qiagen one-step RT-PCR and the following primers and parameters:

Table A7.1. PCR-based riboprobe synthesis for *elovl4a* and *elovl4b*

RNA Target (approx. probe size)	Forward Primer	Reverse Primer + T7/T3 sequence	PCR Cycling parameters
elovl4a (1370bp)	5'- CGA CTG TGA GGA TCT GAG TCC C -3'	5'- TAA TAC GAC TCA CTA TAG GGC CTA AAA TGA AGA AAA AGG GTA TCT GC-3' *(T7)*	94°C x 2mins 94°C x 30s 54°C x 30s 72°C x 1min 70°C x 10mins
elovl4b (1767bp)	5'- ATA GCA GAC AAG CGT GTG GAG -3'	5'- AAT TAA CCC TCA CTA AAG GGA TGG TTT ACA AGG ACA TAC ACT GT-3' *(T3)*	94°C x 2mins 94°C x 15s 54°C x 30s 72°C x 1min 70°C x 10mins

PCR products were purified with a Qiagen PCR Purification kit and used in riboprobe synthesis. The riborobe transcription reaction was run with Roche FLR-tagged dNTPs, 10X transcription buffer, RNAse inhibitor, and T3 enzyme. Riboprobe products were purified, checked for degradation by running a gel, then aliquoted and stored at -80°C until use.

The *in situ* hybridization protocol was performed as follows: 4dpf larval samples were fixed in 4% PFA overnight at 4°C. Larvae were then permeabilized with an acetone wash (7 minutes) and Proteinase K digest at 37°C for 30 minutes, followed by fixation in PFA for 20 minutes. Larvae were then washed 3 x 30 minutes in PBSTw and incubated in Hauptmann's hybridization solution for 2 hours at 65°C and then incubated in 1:250 riboprobe/ Hauptmann's hybridization solution overnight at 65°C. Post-hybridization washes were done at 65°C and consisted of 50% formamide/ 2x SSCTw 2 x 30 mins; 2x SSCTw x 15 mins; then 0.2x SSCTw 2 x 30 mins. Samples were blocked in 2% RMB/ 1% Tw/ 1% DMSO/ Maleate buffer for 3 hours, then incubated in 1:5000 anti-FLR-AP/ 2% RMB/ 1% Tw/ 1% DMSO/ Maleate buffer overnight at 4°C. Following 4 x 30 minute

washes in 1% Tw/ 1% DMSO/ Maleate buffer, samples were incubated in Genius buffer for 15 minutes, then in NBT/BCIP/Genius buffer reaction mix for 10-20 minutes for colour development. Reaction was stopped by washing larvae in alkaline substrate wash x 30 minutes, followed by PBSTw x 5 mins, 4% PFA x 30 mins, and PBSTw x 5 mins. Samples were imaged in glycerol.

Commercial rabbit anti-human ELOVL4 antibody ELOVL4 (Abcam, ab14922) was tested on Western blot against adult zebrafish retina protein extract by Dr. Richard Kanyo, using the protocol described in Chapter 6.

To test ELOVL4 antibody staining on cryosectioned adult retinas, we performed a citric acid antigen retrieval (Evers and Uylings, 1994; Ino, 2003) on whole fixed adult eyes prior to cryopreservation. Briefly, eyes were fixed overnight in 4% PFA, then incubated in citrate buffer (10mM citric acid, 0.05%Tw, pH 6.0) overnight at 4°C. Eyes were immersed in boiling citrate buffer for 5 minutes, then transferred to chilled 20% sucrose/ 0.1MPO_4 and washed overnight at 4°C. Eyes were then embedded in 20% sucrose/ 0.1MPO_4/ OCT media and frozen for sectioning as described in Chapter 3. Immunocytochemistry was performed as described for cryosections in Chapter 3, incubating slides in 1:50 rabbit anti-ELOVL4 (Abcam, ab14922) for 6 days at 4°C followed by incubation in 1:1000 Alexafluor 488 anti-rabbit secondary antibody (Invitrogen A-21441) overnight at 4°C. To label cone photoreceptors, rat 10C9.1 antibody against UV opsin and mouse 1D4 antibody against red cones were used as previously described.

The *elovl4b* knockdown experiment was performed by injecting 10ng of elovl4b translation-blocking MO (5'- TGC AGC CCA GGT AAA ATA TGC GAG T- 3') into 1-2 cell stage embryos from incrosses of were *Tg(-5.5opn1sw1:EGFP)*^{kj9} (ZDB-ALT-080227); *Tg(-3.5opn1sw2:mCherry)*^{ua3011} (ZDB-TGCONSTRCT-130819-1) (Duval et al., 2013; DuVal et al., 2014b; Takechi et al., 2003; Takechi et al., 2008) fish. Larvae were raised to 4dpf and prepared for cryosectioning as previously described in Chapter 3. Double cones were labeled with 1:500 mouse zpr-1 (ZDB-ATB-081002-43) and 1:1000 Alexafluor 647 chicken anti-mouse secondary antibody (Invitrogen A-21463).

7.3. Results

In situ hybridization on 4dpf whole embryos showed expression of both *elovl4a* and *elovl4b* RNA in the brain and spinal cord, and *elovl4b* expression in the retina (Fig. A7.1A). Based on this spatial expression, we hypothesize that *elovl4b* is more closely related to human *ELOVL4* in terms of retinal expression and function.

We next tested a commercial antibody for human ELOVL4 on adult zebrafish retina in both Western blot and on cryosections for cross-reactivity. Preliminary Western blot results show a single clear band at approximately 45kDa; the expected size of Elovl4b protein is 35kDa. A citric acid antigen retrieval step was required for successful antibody labeling; this antibody distinctly labels the inner segments of the photoreceptors, including UV cones, red cones, and blue cones (Fig. A7.1B-E), in a donut pattern visible in tangential sections (Fig. A7.1F, G). The inner segment contains the endoplasmic reticulum, which is where ELOVL4 is located, so these results are promising that this antibody successfully cross-reacts with a zebrafish Elovl4 protein, and possibly Elovl4b specifically. These results are promising indicators that *elovl4b* is expressed in the retina from 4dpf through adulthood, and that it likely has a similar function to *ELOVL4* in the photoreceptors.

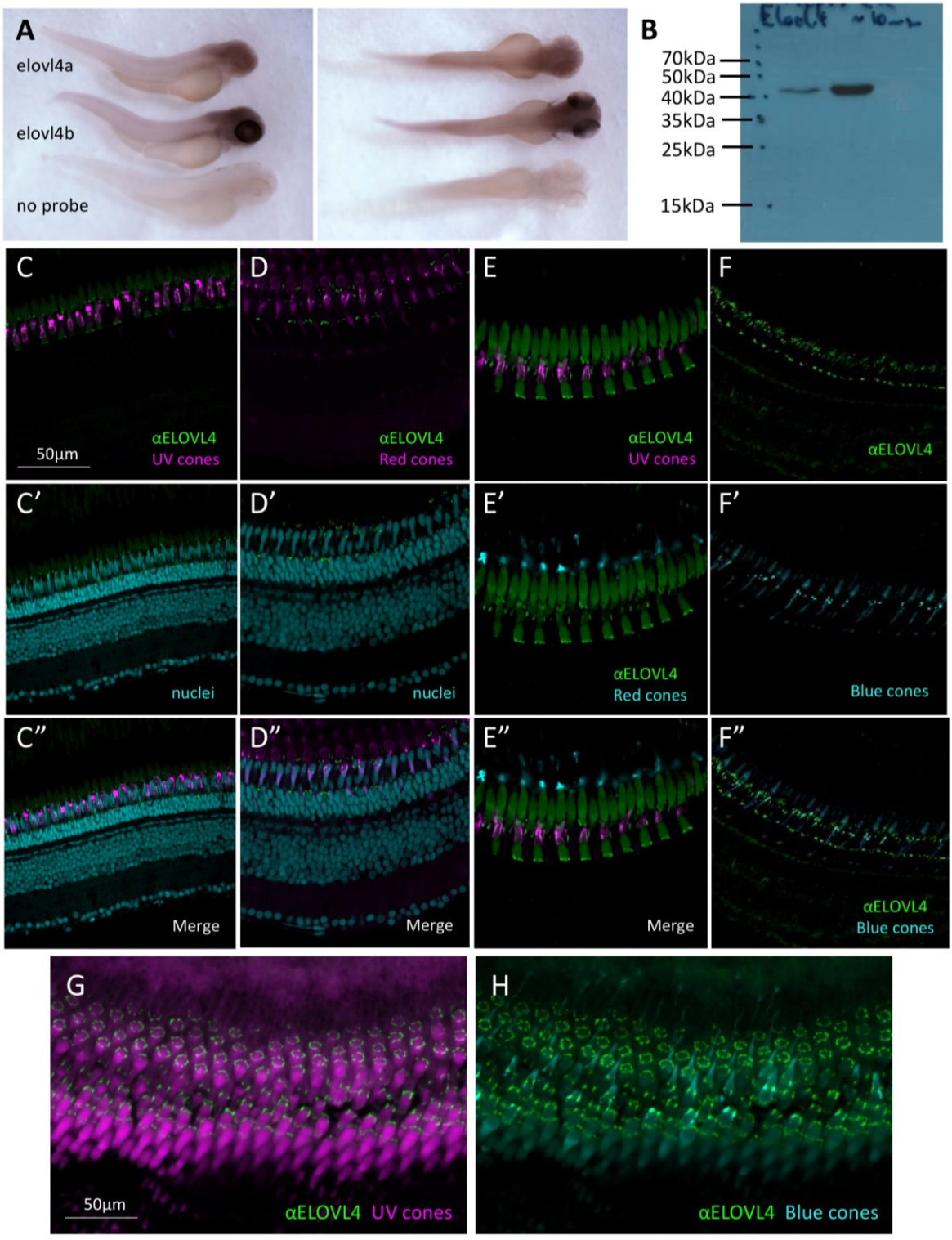

Figure A7.1 Expression of elovl4a and elovl4b in larvae and ELOVL4 antibody cross-reactivity in adult zebrafish retinas.

A. In situ hybridization of 4dpf larvae for *elovl4a* and *elovl4b* show some expression in the brain and spinal cord; *elovl4b* is expressed more strongly in the retina. **B.** Preliminary Western blot of anti-human ELOVL4 antibody detection in adult zebrafish retina protein extract shows a single band at approx. 45kDa. Expected size of Elovl4b protein is 35kDa. **C-F.** Cross-reactivity to ELOVL4 antibody is successful in adult sections, where labeling colocalizes with UV cones (C-C″), red cones (D-D″, E-E″), and blue cones (F-F″). **G, H.** Labeling occurs in the inner segment, in a donut-shaped pattern visible in tangential sections that cut through photoreceptors transversely.

Next, we tried to knock down *elvol4b* in embryos to determine if *elovl4b* is necessary for proper photoreceptor development. Sections of 4dpf morphant retinas showed no disruption to abundance or morphology of UV, blue, or double cones (Fig. A7.2). The morpholino may not have effectively disrupted *elovl4b* expression, but further work needs to be done to determine this.

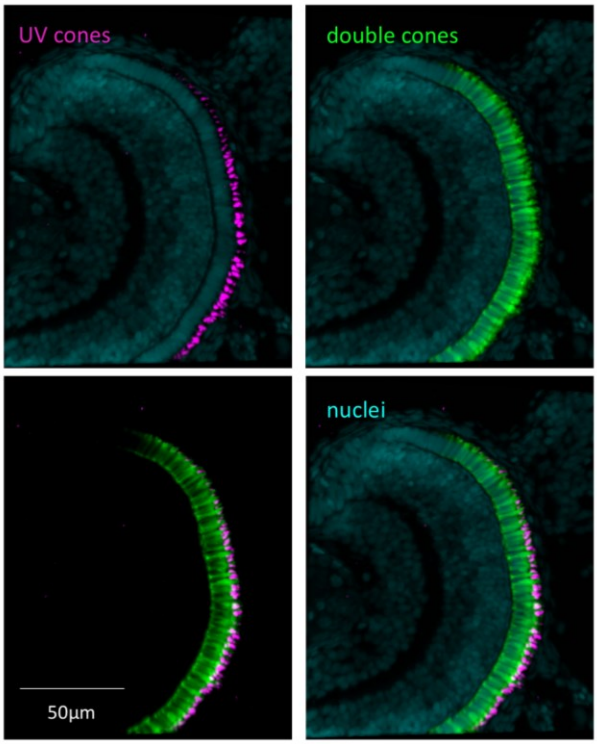

Figure A7.2. Photoreceptor morphology of elovl4b MO-injected larvae appears normal.

Embryos were injected with 10ng of MO and raised to 4dpf.